Doctoral Dissertation
博 士 論 文

Development of Seismic Site Coefficient Maps for Java, Indonesia

(インドネシア・ジャワ島における地震動のサイト増幅係数地図の開発)

Yunalia Muntafi

Gifu University
Graduate School of Engineering
Department of Engineering Science
2022

Abstract

Soil amplification at the specific site, known as site coefficient, is one of the essential parameters in earthquake-resistant building design. However, due to several reasons and limitations, site response analysis cannot always be conducted. The Indonesian Earthquake Resistant Building Design Code has been published in 2019 (SNI 1726-2019) as the completion of the previous code in 2012 (SNI 1726-2012), but the site coefficient presented are still general which followed the Pacific Earthquake Engineering Research (PEER) 2013 document. Due to the importance of seismic site coefficient for earthquake resistant building design, this study aims to develop the seismic site coefficient maps both short period (0.2s) Fa and long period (1.0s) Fv for Java, Indonesia using the probabilistic seismic hazard analysis (PSHA) which considered earthquakes as random phenomena. The site coefficients are then derived from the ratio of hazard at the ground surface (H_S) relative to hazard at bedrock (H_R). By applying PSHA, this study considered the seismic sources zone, both subduction and new identified faults data published by National Center for Earthquake Studies (PuSGeN) 2017.

The study begins with the earthquake data compilation from the national and international databanks, e.g., Indonesia's Meteorological, Climatological, and Geophysical Agency (BMKG), the National Earthquake Information Center-United States Geological Survey (NEIC-USGS), and the relocated earthquake catalog from International Seismological Center-Engdahl Hills Bullen (ISC-EHB). To obtain a better result, we proposed new empirical seismic magnitude conversion formulas for body-wave magnitude, mb, and surface-wave magnitude, Ms to moment magnitude, Mw, as the most common and reliable magnitude scale in seismicity studies, which were generated based on statistically forecast accuracy. The subduction zone was modelled into twelve segments (six interplate and six intraplate segments) based on cross-sectional Java trench and coupling model data. The seismic parameters such as a-b value were calculated based on Gutenberg-Richter Law (1994), while the magnitude maximum estimation was determined using Hanks-Kanamori (1979) and Wells-Coppersmith (1994).

This study applied the Ground motion prediction equations (GMPEs) formula of Youngs et al. (1997), Atkinson-Boore (2003), and Gregor (2006) for subduction mechanisms. Meanwhile, the GMPE of Boore et al. 1997, Chiou and Youngs NGA 2006 and Boore-Atkinson NGA 2006 were selected for the shallow crustal fault mechanisms. The Epistemic uncertainty was considered in PSHA using logic tree by including alternative interpretations, models, and parameters that are weighted according to their significance. PSHA has been conducted to obtain the spectral acceleration (Sa) values for short periods Fa (0.2 seconds) and long periods Fv (1.0 seconds) at bedrock and ground surface for 2% probability of exceedance (PE) over a period of 50 years. The values of Fa and Fv were estimated through the ratio of spectral acceleration at the ground surface relative to spectral acceleration at bedrock. Results of Fa and Fv values displayed on seismic site coefficient maps created using ArcGIS Pro 2.8.

As an initial investigation for seismic cite coefficient in Java, Malang and Yogyakarta region were chosen based on the effect of subduction and fault earthquake mechanisms. The results show that the spectral acceleration (S_a) values of Malang region are dominantly influenced by the subduction earthquake sources. Meanwhile, the Sa values of Yogyakarta region follows the Opak fault pattern, the farther, the Sa value will be lower. The Fa and Fv value for Malang and Yogyakarta region are varied. The results indicate that the harder the soil conditions (higher shear wave velocity value) and higher acceleration values at bedrock, the seismic site coefficient values are relatively lower.

The analysis was then continued for the entire Java region. Based on the PSHA, spectral acceleration value at bedrock for Java region with the PE of 2% in 50 years varies from 0.35-3.0g and 0.2-2.5g for period T=0.2s and T=1.0s, respectively. The minimum values of S_S and S_1 at bedrock are almost equal to the S_S and S_1 values in Seismic Building Code SNI 1726:2019. Meanwhile, the maximum values of S_S and S_1 in this study are relatively higher in some regions, especially in areas close to the earthquake sources. It is clearly seen from the map that the distribution of S_a value at bedrock and ground surface follows the pattern of the seismic sources (crustal fault and subduction source). The southwest part of Java region relatively has a high Sa value. The higher value of Sa is also seen along the southern part of Java. This result indicates that the subduction earthquake sources have a great influence for the higher value of S_a. In addition, some areas near the fault line also have higher S_a values.

The seismic site coefficient values, Fa and Fv were calculated from the ratio of hazard at surface and hazard at bedrock. The result showed that Fa and Fv values are not only greatly influenced by the Vs30 value, which describes the local soil type, but the values of Fa and Fv will also increase as the spectral acceleration values of S_S and S_1 at the base soil layer (bedrock) decrease. Since earthquake is random phenomena, this study considered the uncertainties of some main seismic parameters (magnitude, distance from the potential earthquake sources, and random nature of ground motion). The results of the Fa and Fv values in this study are spatially more varied than those in SNI 1726:2019, which adopts the Fa and Fv values from the PEER document. The magnitude correlation formula, subduction earthquake source modeling, Fa and Fv maps for Java proposed in this study can contribute to future seismic hazard studies and be directly used in generating the design response spectra for earthquake-resistant building design.

Keywords: *Earthquake, spectral acceleration, seismic site coefficient, probabilistic seismic hazard, ground motion attenuation.*

Acknowledgements

Alhamdulillah, all praises and thanks to Allah SWT, the Almighty, the Most Gracious, the Most Merciful for His blessing given to me during my study and dissertation completion.

I would like to express my deepest gratitude to my supervisor, Professor Nobuoto NOJIMA for his greatly continuous support of my doctoral study and research, for his guidance, motivation, encouragements, and immense knowledge. I am very thankful for his kind guidance and advice during the research work. In addition, I really appreciate all opportunities given, such as: participating the HIRAKU 3MT competition for doctoral student in Hiroshima 2019, join seminar in Kanazawa and Fukui Prefecture in 2019, International Conference on Earthquake Engineering and Disaster Mitigation (ICEEDM) 2019 in Padang, Indonesia, and International conference collaboration ICSBE 2021 hosted by Universitas Islam Indonesia (UII) in collaboration with Gifu University, Japan, and other overseas universities. Those opportunities enlarge my knowledge and experiences.

I would like to acknowledge Assoc. Prof. Matsumitsu KUSE for supporting and giving me technical support while run the program and software in some high-performance personal computers, also for the insightful discussion related to ground motion model worldwide. Also, I would like to thank Professor Tomoyuki OHTANI for his kind support, all the valuable suggestions, advice, and discussions on my research. I have benefited from his technical insights, reviews, and suggestions on my research.

I am very grateful to Assoc. Prof. Maki Koyama for all the support, advice, hospitality, and warm discussion during my study. Also, I would like to thank Professor Sugito Masata, Professor Lee Wah Liem for their kind support and hospitality during my doctoral study.

Besides, I would like to express my special thanks to Professor Fusheng Li, who gave kind support, recommendation, and advice since I decided to continue my study in Gifu University.

I would like to extend my deepest gratitude to Professor Widodo as the Head of the Civil Engineering Department, Faculty of Civil Engineering, Universitas Islam Indonesia, Yogyakarta and the Chairman of Disaster Risk Reduction Center (DiRReC) for all the kind support, guidance, insightful idea and discussions related to my PhD study.

I would like to express my special thanks to Universitas Islam Indonesia for all the great continuous support. I am very grateful to Prof. Fathul Wahid as the Rector of the Indonesian Islamic University, Yogyakarta, for all kind support and motivation given during my study. Also, I am very grateful to Assoc. Prof. Miftahul Fauziah as the Head of Faculty of Civil Engineering and Planning, Universitas Islam Indonesia for all kind support and motivation.

I also would like to thank Assoc. Prof. Lalu Makrup as the author of the book of Seismic Hazard for Indonesia who had given his time to discuss the ground motion models for Java,

Indonesia and seismic hazard analysis calculations and also for his suggestion to use the SRModel calculation program.

I am very grateful to Prof. Sri Widiyantoro as the Head of the Seismology and Instrumentation Working Group in the preparation of Indonesia Seismic Hazard Map who has provided the information and data and provided time to discuss seismicity in Indonesia. Also, many thanks to Dr. Pepen Supendi and Bambang Sunardi, MT from the Indonesia's Meteorological, Climatological, and Geophysical Agency (BMKG) for the data information and discussions related to seismicity in Indonesia.

I am grateful to Mr. Takahashi Yukihiro and Mr. Hiroki Kato for their kind discussions, hospitality, and assistance during my study at Gifu University. Also, many thanks to my friends and my Lab-mate, for their support and gracious company during my years of study at Gifu University.

Finally, and most importantly, I would like to express my deepest and greatest gratitude for the full loyal support and love I received from my lovely husband (Dr. Istiyanto), my two lovely daughters (Naila Aprisna Maulida and Nisrina Hanin Arifah), my lovely Moms (Ibu Sri Wahyuni and Ibu Sumiyem) and Dads (Ir. Ali Asroni, MT., and Bp. Dirdjo) and all my family members.

Table of Contents

List of Figure

List of Table

Chapter 1
Introduction

1.1 Background

The significant changes have taken place in the seismic design provisions of Indonesia, as one of the most seismically active countries in the world. In 2010, the hazard maps of Indonesia were published as Summary of Study Team for Revision of Seismic Hazard Maps of Indonesia (TRSHMI). Six year later, the Indonesian Ministry of Public Works and Housing established a team of earthquake scientists and engineers tasked with improving the input data available for revising the national seismic hazard map. The new seismic hazard map for Indonesia was launched in 2017 containing the importance of new identified active faults and subduction seismicity in determining the seismic hazard level. As a continuation of the previous building code document, the Indonesian Earthquake Resistant Building Design Code has been launched in 2019 (SNI 1726-2019) which is the completion of the previous code in 2012 (SNI 1726-2012). The recent development of Indonesia seismic hazard maps and Indonesia Building design code are presented in Figure 1.1.

Summary of study "Revision of Seismic Hazard Maps of Indonesia" 2010

National Earthquake Resistance Building Design Code SNI 1726:2012

Indonesian Seismic Sources and Seismic Hazard Maps 2017

National Earthquake Resistance Building Design Code SNI 1726:2019

Figure 1. 1 Development of Indonesia seismic hazard maps and building design code document

One of the essential points presented in the New Indonesia Building Code SNI 1726:2019 is the response spectra design should be performed based on the site coefficient in period of 0.2s (short period, Fa) and 1.0s (long period, Fv) as shown in Figure 1.2.

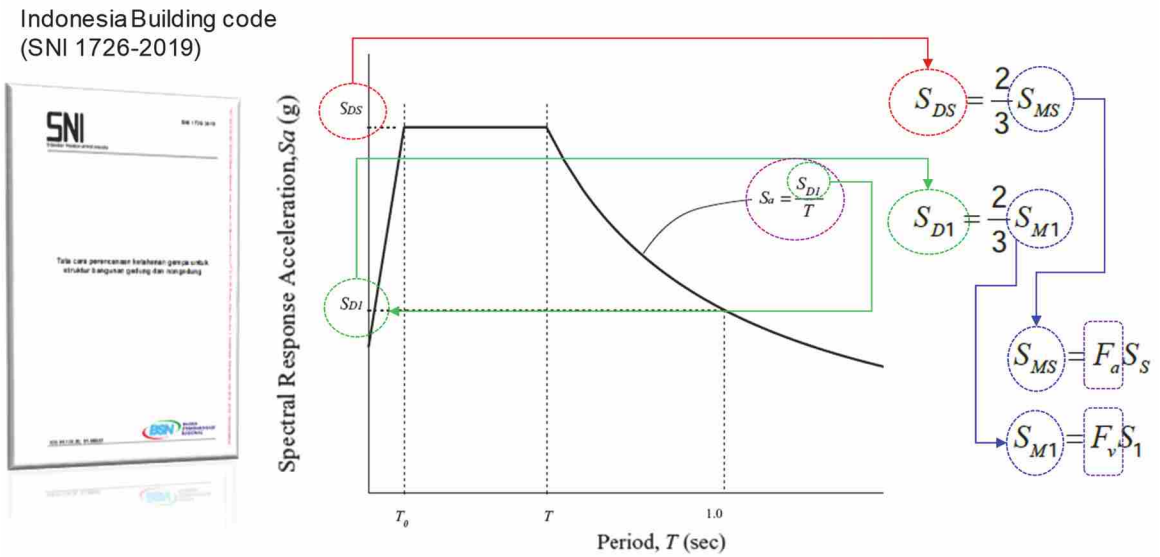

Figure 1. 2 Design spectral acceleration model of SNI 1726-2019

Where:

F_a : seismic site coefficient for short period (0.2s)

F_v : seismic site coefficient for long period (1.0s)

S_{DS} : spectral response acceleration parameter at short period (0.2s) ;

S_{D1} : spectral response acceleration parameter at long period (1.0 s) ;

S_{MS} : the MCER, 5 percent damped, spectral response acceleration parameter at short period (0.2s)

S_{M1} : the MCER, 5 percent damped, spectral response acceleration parameter at long period (1.0 s)

Several studies have highlighted the potential of soil amplification in thick sedimentary layers due to earthquake shaking. The motions of ground surface caused by earthquake which have the potential to cause structural damage are significantly influenced by the condition of local site (Kramer, 1996). The fault rupture triggers the wave propagation from the earth to the base soil layers or bedrock, then they travel to the ground surface through the soil sedimentary layers as presented in Figure 1.3. The figure illustrates the earthquake motion propagating from the source and becoming amplified as they travel through the sediments to the site at the ground surface. The mechanism of rupture and the effects of wave passage based on the soil conditions are modeled in general seismic hazard analysis studies. Site response analysis as quantification of site effects involving the earthquake propagation from the bedrock to the ground surface through the overlying soil layers.

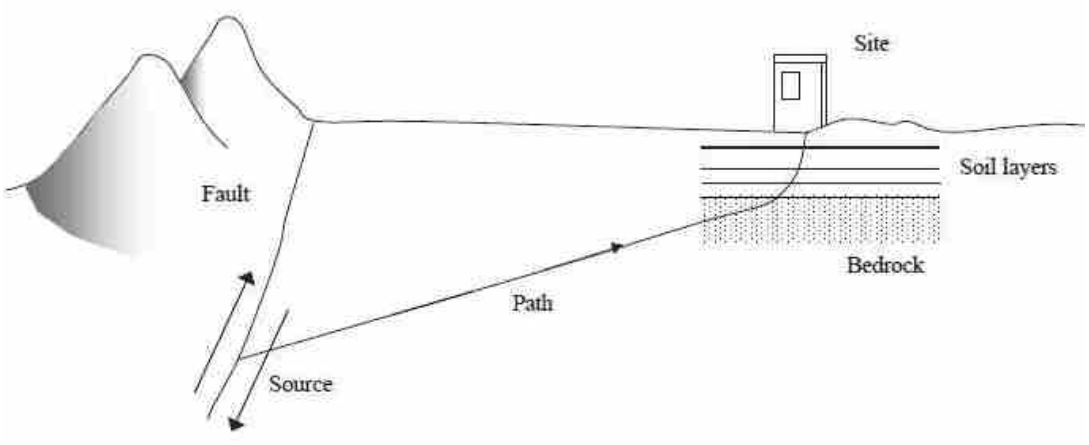

Figure 1. 3 Schematic ground motion propagation from source to site (Kramer, 1996)

Some researchers shed light on the shear wave velocity or shear modulus which represents the small-strain stiffness on the dynamic behavior (Idriss 1990, Boore et al. 1994, and Borcherdt 1994). For seismic site classification, the average shear wave velocity in the top 30 m soil layer (Vs30) has been applied due to the ineffectiveness of the costs involved in conducting site-specific soil response analysis and obtaining small-strain shear wave velocity (Vs) values (Seed et al. 1994, Borcherdt 1994, and Dobry et al. 2000). The V_{S30} value can calculated using the following formula:

$$V_{s30} = \frac{30}{\sum_{i=1}^{m} \frac{H_i}{V_{si}}} \tag{1.1}$$

where H_i is the thickness of layer i (meters); V_{si} represents the shear wave velocity (m/s) of layer i; and m is the number of layers in the top 30 m.

Based on the National Hazard Reduction Program (NEHRP) document, the site classes are usually divided into six classifications; A (hard rock), B (rock), C (hard soil or very dense soil), D (medium soil), and E (soft soil), which are represented by profiles with Vs30 > 1,500 m/s, 760 < Vs30 1,500 m/s, 360 < Vs30 760 m/s, 180 < Vs30 360 m/s and Vs30 180 m/s, respectively, while the special conditions are designated as F site class. The F site class means soils requiring geo-engineering investigation and site response analysis. The site response analysis yields the site acceleration response spectrum which typically with 5% damping for a given base motion.

Soil amplification at the specific site, known as site coefficient, is one of the essential parameters in earthquake-resistant building design. However, due to several reasons and

limitations, site response analysis cannot always be conducted. Since the amplification characterization requires detailed mapping of the soil and its properties, the Building code only provides an approximate value for the site coefficient. In general, the site coefficient (F) can be formulated from the ratio of site response spectrum and the input rock outcrop response spectrum as follows:

$$F = \frac{S_{site}}{S_{outcrop}} \tag{1.2}$$

where S_{site} represents the site spectral acceleration at a selected period; and $S_{outcrop}$ *is* the soft-rock outcrop spectral acceleration at the same period.

Several studies related to the site coefficient in the last five years have been carried out, including by Pallav et al. (2015), Partono et al. (2017), and Widodo et al. (2019). They used the estimation method for generating the site coefficient by dividing the ground surface spectral acceleration to bedrock response. In the case of some cities in Indonesia, both Partono et al. (2017) and Widodo et al. (2019) used the probabilistic approach which considered the seismic sources mechanism, that was subduction earthquakes and shallow crustal earthquakes based on the activity of faults at a radius 500 km from the site investigated. Unfortunately, the new identified faults data have not been used in these studies. The value of site coefficient provided in SNI 1726:2019 are still general (macro-scale), which directly followed the Pacific Earthquake Engineering Research (PEER) 2013 document.

1.2 Research Objective

The main purpose of this study is to develop the site coefficient both short Fa (0.2s) and long period Fv (1.0s) maps for Java region, Indonesia, as an essential parameter for earthquake resistant building design as one of disaster mitigation efforts. Since earthquake is a random phenomenon, this study applied the Probabilistic Seismic Hazard Analysis (PSHA), which considered the seismic sources zone both subduction and new identified faults data published by PuSGeN, 2017. To achieve the better result, we proposed the new empirical seismic magnitude conversion formulas from body magnitude, mb, and surface magnitude, Ms to moment magnitude, Mw, as the most common and reliable magnitude scale in seismicity studies, which were selected based on statistically forecast accuracy.

1.3 Thesis Outline

This thesis is divided into 6 chapter. The outline of all chapters is shown in Figure 1.4.

Chapter 1 presents the background and aims of this thesis. The soil amplification or known as site coefficient is essential parameter needed in seismic resistant building design. Due to several reasons and limitations, site response analysis cannot always be conducted. The main purpose of this study is to develop the site coefficient both short Fa (0.2s) and long period Fv (1.0s) maps for Java region, Indonesia, as an essential parameter for earthquake resistant building design as one of disaster mitigation efforts.

Chapter 2 reviews the seismic site coefficient and several studies related to seismic site coefficient. Past earthquakes have presented that the local soil plays a significant role in the characteristic of ground motions. Several studies in determining the soil amplification factor which is known as site coefficient has been conducted with several different methods. This chapter presented the probabilistic seismic hazard analysis as the method used for this study.

Chapter 3 reports the result of seismic properties of Java region and its vicinity. The spatial variation in a-value and b-value presented in this chapter. It is observed that there is a similar pattern of a-values and b-values. The regions with low b-values relatively fit the large earthquake locations. Based on the subduction zone modeling analysis, the low a-values and b-values are in the south coast of West Java and south coast of Central-East Java. The most significant earthquakes in subduction zone were consistent with relatively high fractal dimension (D values) and low b-values. However, further research is needed to investigate these correlations more appropriately.

Chapter 4 presents the seismic site coefficient maps for Malang and Yogyakarta region. The Fa and Fv values for Malang and Yogyakarta region are displayed in this chapter. The results indicate that the area with the lower shear wave velocity (soft to medium soil condition) has the relatively higher value of Fa and Fv. Moreover, the area with the lower value of spectral acceleration (Ss and S_1) at bedrock and lower value of shear wave velocity has the higher value of seismic site coefficient (Fa and Fv). These study findings are essential to be considered in earthquake resistant building design for Malang and Yogyakarta region.

Chapter 5 proposes the seismic site coefficient maps for entire Java. The maps describe that Fa and Fv value are not only greatly influenced by the Vs30 value, which describes the local soil type, the values of Fa and Fv will increase as the spectral acceleration values of S_S and S_1 at base soil layer (bedrock) decrease. Since earthquake is random phenomena, this study considered the uncertainties of some main seismic parameters (magnitude, distance from the potential earthquake sources, and random nature of ground motion).

Chapter 6 presents the main findings of each overall thesis result and gives some recommendations for future study.

The structure flow of this study per chapter is shown in Figure 1.4.

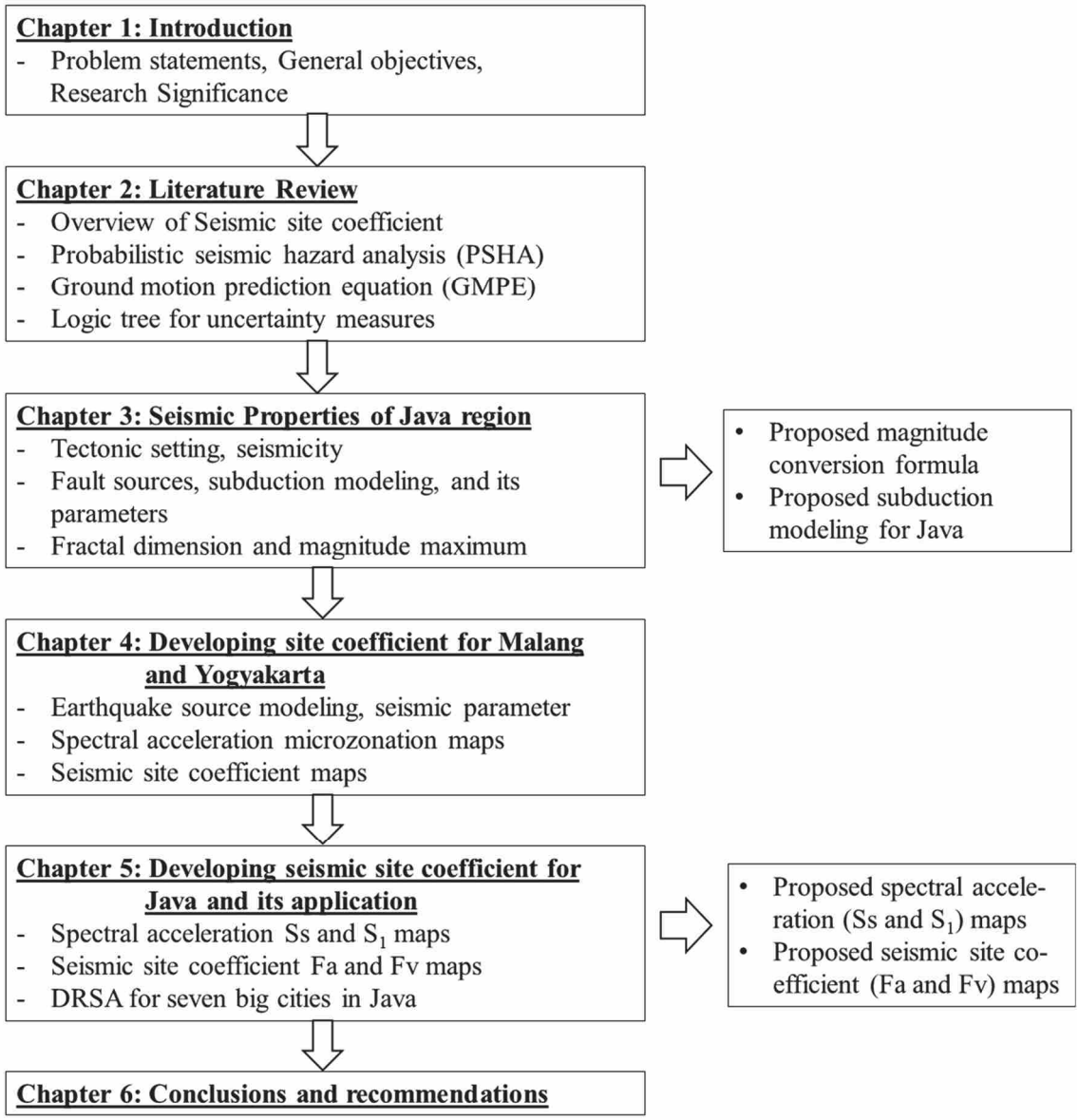

Figure 1. 4 The flow of thesis in each chapter

In order to obtain the final target of research, the steps and its specific references and methods are presented in Figure 1.5.

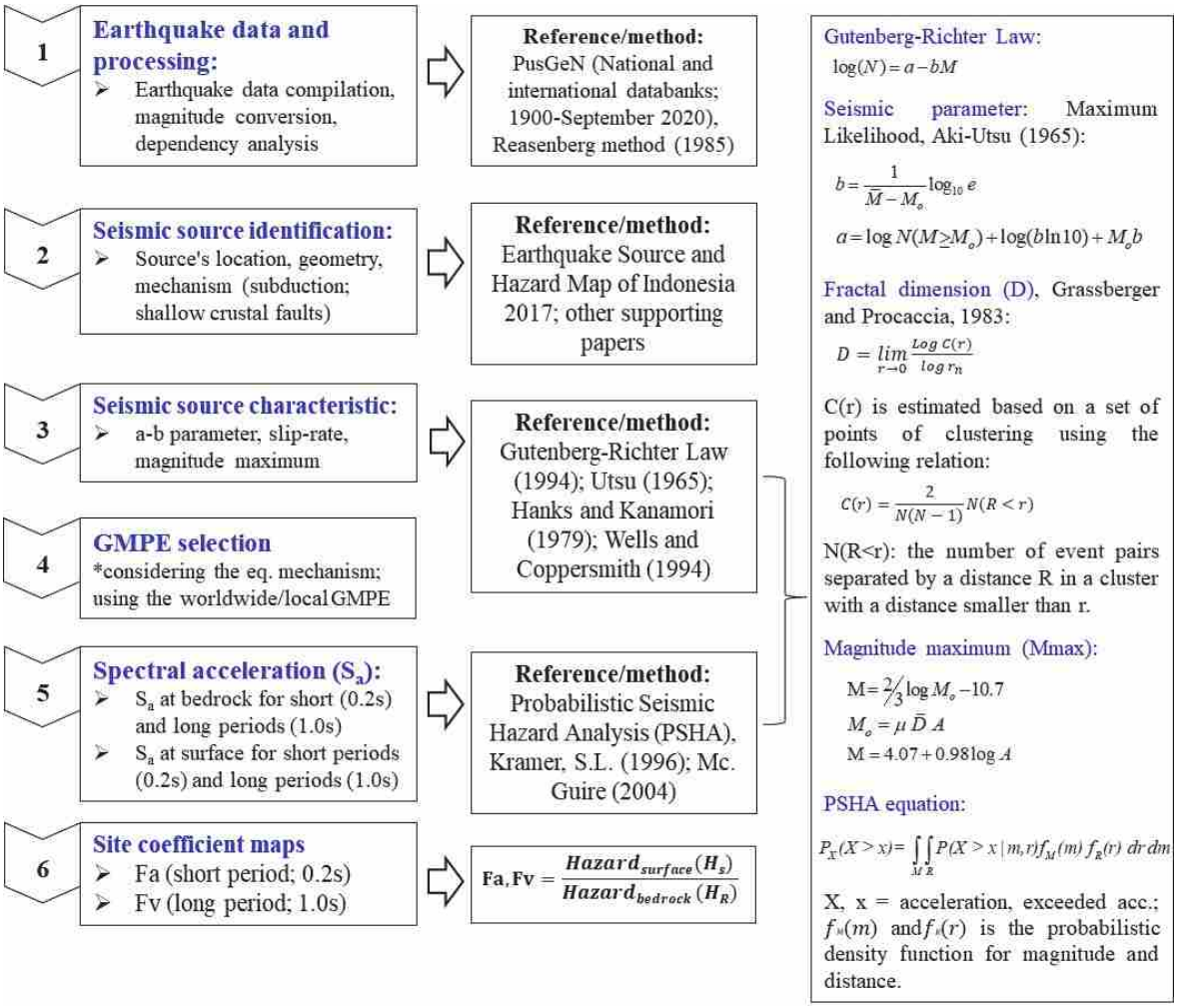

Figure 1. 5 The research flow and its specific references and methods

1.4 Research Significance

This study addresses important problems in the field of seismology and response spectral acceleration parameter for earthquake resistant building design. The three important results of this study and its contribution are as follows:

1. Magnitude conversion formula for global Indonesian earthquake catalog 2020

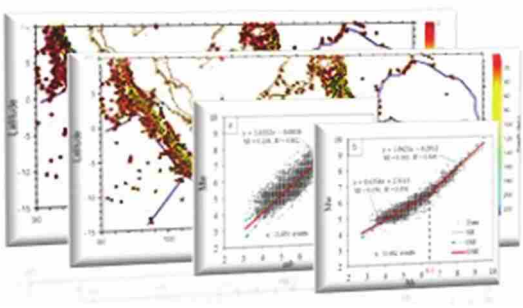

This study proposed the formula for magnitude conversion (surface-wave magnitude, Ms; body-wave magnitude, mb; and moment magnitude, Mw) for generating the comprehensive uniform earthquake catalog for Indonesia as a basis of seismic hazard studies.

2. Subduction earthquake source modeling and seismic parameters of Java region

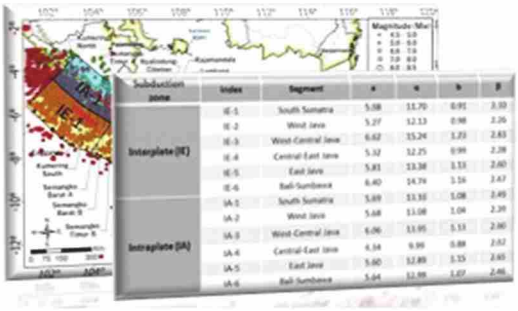

This study proposed the model of subduction segmentation, seismic parameters, including the estimated maximum magnitude (M_{max}) of each segment, which can be used as a reference for the tsunami and seismic hazard probabilistic modeling influenced by the subduction earthquake source in Java and its vicinity. This study also presented the seismic gaps areas and fault geometry complexity that can be considered in the earthquake and tsunami disaster mitigation plan.

3. Spectral acceleration (S_S and S_1) maps and site coefficient (Fa and Fv) maps

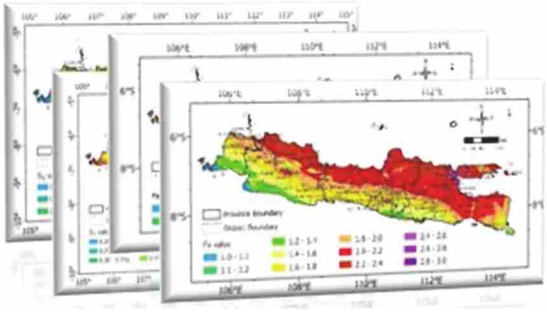

This study proposed the spectral acceleration (S_S and S_1) maps and seismic site coefficient (Fa and Fv) maps for Java region for generating the Design Response Spectral Acceleration (DRSA) in designing seismic resistant buildings. This study also presented the application of these maps on creating the DRSA for seven big cities in Java region. In addition, these maps can also be used for building damage and vulnerability assessment.

Chapter 2
Literature Review

2.1 General Overview

The significant effect of soil amplification in structural building damage caused by earthquakes has been known for many years. Past earthquakes have presented that the local soil plays a significant role in the characteristic of ground motions. Several studies in determining the soil amplification factor which is known as site coefficient presented in Indonesia Earthquake Resistant Building Code (SNI 1726-2019) [1] has been conducted with several different methods. In general, the seismic site coefficient is defined as the ratio of spectral acceleration (Sa) value at the ground surface with the reference rock outcrop at the same period [2].

2.2 Review on Seismic Site Coefficient Studies

In 1994, Borcherdt R. D., [3] measured the seismic site coefficient empirical formula as a function of Vs30 and amplitude using 35 strong-motions data from the 1989 Loma Prieta earthquake. He determined the site coefficients for short-period (T = 0.2s), Fa and mid-period (T = 1.0s), Fv by dividing the recorded Fourier amplitude spectra at soil sites and rock sites. For the rock site, he used shear wave velocity reference which is Vs30 = 795 m/s. The arithmetic averages were used to compute the Fa and Fv over a short-period and a mid-period band, which is 0.1-0.5s and 0.4-2.0s, respectively. Meanwhile, in 2005, Park D., et al. used the site response analyses (nonlinear one-dimension) to compute the site coefficients in the Mississippi Embayment. The soil-hysteretic behavior due to the seismic load was represented by using the modification of hyperbolic model. The study used Vs profile 100m/s - 1000m/s. The result of this study recommends taking into account the depth parameter in determining the site coefficient.

Another study related to the seismic soil factor has been conducted by [5] by using the analysis of frequency domain (FD) equivalent linear (EQL) and time domain (TD) non-linear (NL) for performing one-dimensional seismic ground response analysis. Some assumption for soil layer thickness taken in this study were 30, 100, 300, 500 and 1000m.

The seismic site coefficient was computed by dividing the spectrum acceleration at the ground surface and the spectrum acceleration at bedrock.

In 2015, Pallav K., et al. [6] conducted the seismic site coefficient (Fs) for Imphal City, India. He applied the probabilistic theorem to get the coefficient based on 700 synthetically generated time histories of earthquakes using the stochastic method. Some studies related to the determination of site coefficient in some cities in Indonesia have been conducted. Partono, W., et al. (2017) [7] and Pawirodikromo, W., et al. (2019) [8] applied the PSHA method for deriving the spectral acceleration to get the site coefficient values for Semarang city and Yogyakarta region, respectively by dividing the Sa at ground surface and at bedrock. They used the Probabilistic Seismic Hazard Analysis (PSHA) models which involved the shear wave velocity at bedrock with Vs reference = 760 m/s and the value of shear wave velocity at the uppermost 30m soil layer (Vs30) at ground surface. The calculation considered the subduction earthquake sources and shallow crustal faults within a radius of 500km from Semarang and Yogyakarta, respectively. The result of [7] shows the Fa and Fv values from the study were relatively similar to Fa and Fv values provided in Building Code. On the contrary, the result of [8] reveals the Fa and Fv values from the study were relatively higher than what were written in Indonesia Building Code.

This study develops the site coefficient maps for the entire Java, Indonesia by applying the combination of the method used by [6], [7], and [8]. Because earthquake is a random phenomena, the analysis of this study takes into account the seismic sources potential, random nature of earthquake occurrences, and ground motion parameter which consider the uncertainties at all levels of analysis. The PSHA applied in this study with the earthquake data from national and international databanks. The site coefficients are then derived from the ratio of hazard at surface (H_S) relative to hazard at bedrock (H_R). By applying PSHA, this study considered the seismic sources zone both subduction and new identified faults data published by National Center for Earthquake Studies (PuSGeN) 2017 [9].

2.3 Seismic Site Coefficient using Probabilistic Approach

The decision for seismic disaster mitigation requires a logical and consistent approach in assessing the future effects of earthquakes on people live and structures and the uncertainty of these effects. The uncertainty referred is the uncertainty inherent in random

phenomena and the uncertainty due to lack of knowledge about some model or parameter [10]. Assessment of the future earthquakes' effects can be carried out in two ways; by taking a specific earthquake scenario (Deterministic Seismic Hazard Analysis, DSHA) and taking all earthquakes along with their probability of recurrence in the future through a certain method (Probabilistic Seismic Hazard Analysis, PSHA). As stated in [11], in principle, probabilistic hazard analysis is a deterministic method that involves many scenarios, not only based on the seismic parameters from the largest ground motion. Moreover, this method is used based on the definition of a probability distribution function that uses the uncertainty of the magnitude size, location, and earthquake events frequency to obtain the level of earthquake risk at the site location. From PSHA, the spectral acceleration at the ground surface and at bedrock can be obtained. The ratio between them was then calculated to represent the seismic site coefficient.

2.4 Probabilistic Seismic Hazard Analysis (PSHA)

PSHA for a particular site is a way to determine the frequency of certain values that will be exceeded by an earthquake characteristic in a specified period of time (t). The variable t is the length of time in the future (e.g., t = 50 years). Here the earthquake characteristics are quantified by the variable X, and the value to be exceeded by X is quantified by x. Characteristic X can be described as the form of peak acceleration of earthquake ground motion at the site, or the form of earthquake strength with a certain level in MMI (Modified Mercalli Intensity). Rather than that, it can also be represented in the form of seismic shaking duration or displacement caused by faults under the building foundation [12]. The general step of the PSHA is presented in Figure 2.1.

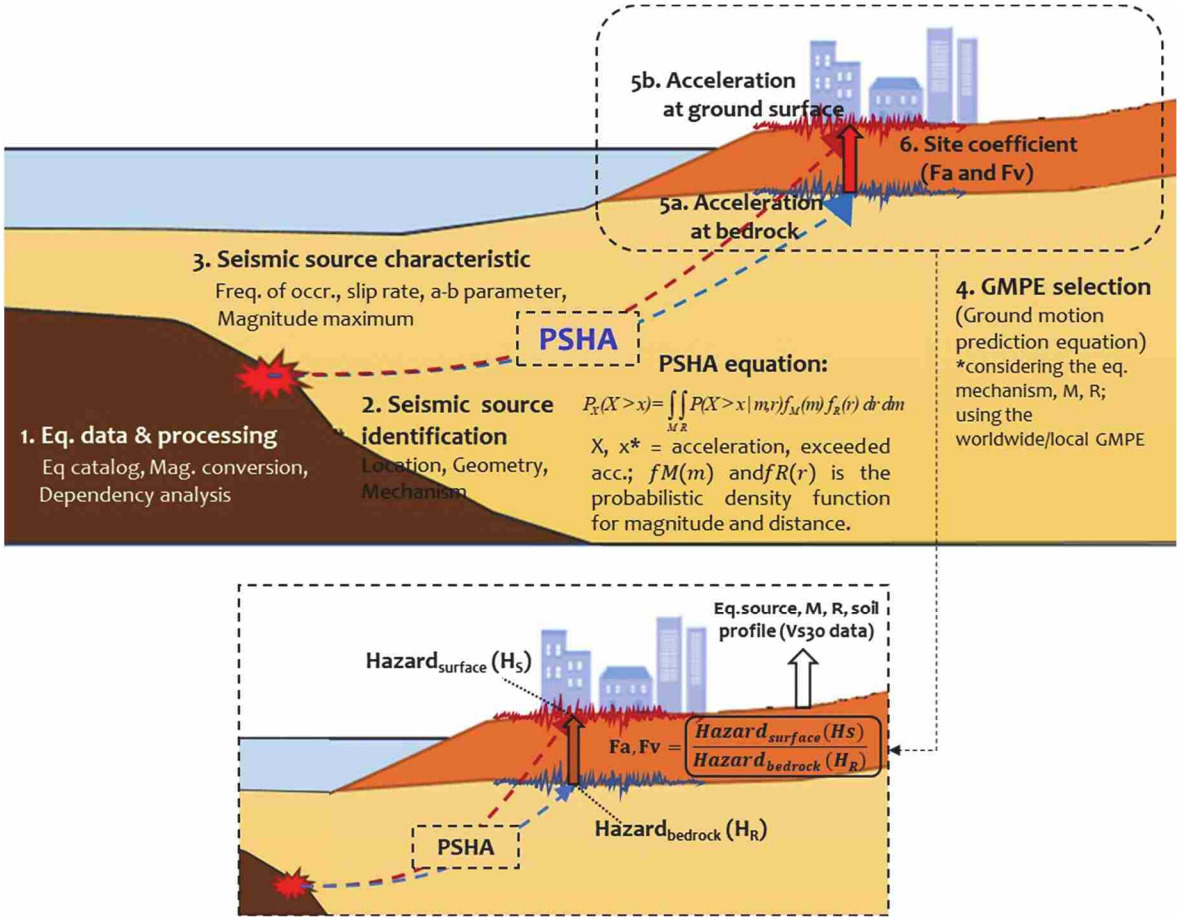

Figure 2. 1 The schematic flow for generating seismic site coefficient using PSHA (Redrawn and modification from Masyhur I. et al., 2010)

In performing the PSHA for each site, this study used the shear wave velocity data (Vs30). The reference rock site used was characterized by Vs30 = 760 m/s, while the Vs at ground surface for each site were derived from the United States Geological Survey (USGS). The site coefficients are then derived from the ratio of hazard at surface (H_S) relative to hazard at bedrock (H_R), which represents the spectral acceleration at the ground surface relative to spectral acceleration at bedrock by using the formula as follows:

$$\text{Fa, Fv} = \frac{Hazard_{surface}(H_S)}{Hazard_{bedrock}(H_R)} \tag{2.1}$$

The mathematical basis can be used for seismic hazard calculations is the earthquake recurrence model developed by Gutenberg-Richter (1944) [13] known as the Gutenberg-Richter law and the theorem developed by Cornell (1968) [14] known as the total probability

theorem. This theorem complements the earthquake recurrence model developed by [13] so that the overall mathematical model that reflects the frequency of a certain x value will be exceeded by a certain earthquake characteristic X is as follows:

$$\lambda(X > x) = \nu \int_M \int_R P(X > x \mid m, r) f_M(m) f_R(r) dr dm \tag{2.2}$$

The probabilistic approach for seismic hazard analysis was conducted by calculating the probability of a particular value of x will be exceeded an earthquake event X [15]. Considering the magnitude m and distance R of earthquake event, the formula of total probabilistic model [10], [12], and [16] is written as follows:

$$P_X(X > x) = \int_M \int_R P(X > x \mid m, r) f_M(m) f_R(r)\ dm\ dr \tag{2.3}$$

with the earthquake recurrence formula is presented as follows:

$$\nu f_M(m) = \nu \frac{\beta e^{-\beta(m - m_{\min})}}{1 - e^{-\beta(m_{\max} - m_{\min})}} \tag{2.4}$$

where M, m is magnitude, R, r is distance, f_M and f_R are probabilistic density function for magnitude and distance, respectively. ν is the rate of earthquake occurrence above the minimum magnitude ($m_{\min}$). In performing the PSHA, McGuire R. K. [10] described the procedure schematically in 4 steps as presented in Figure 2.2.

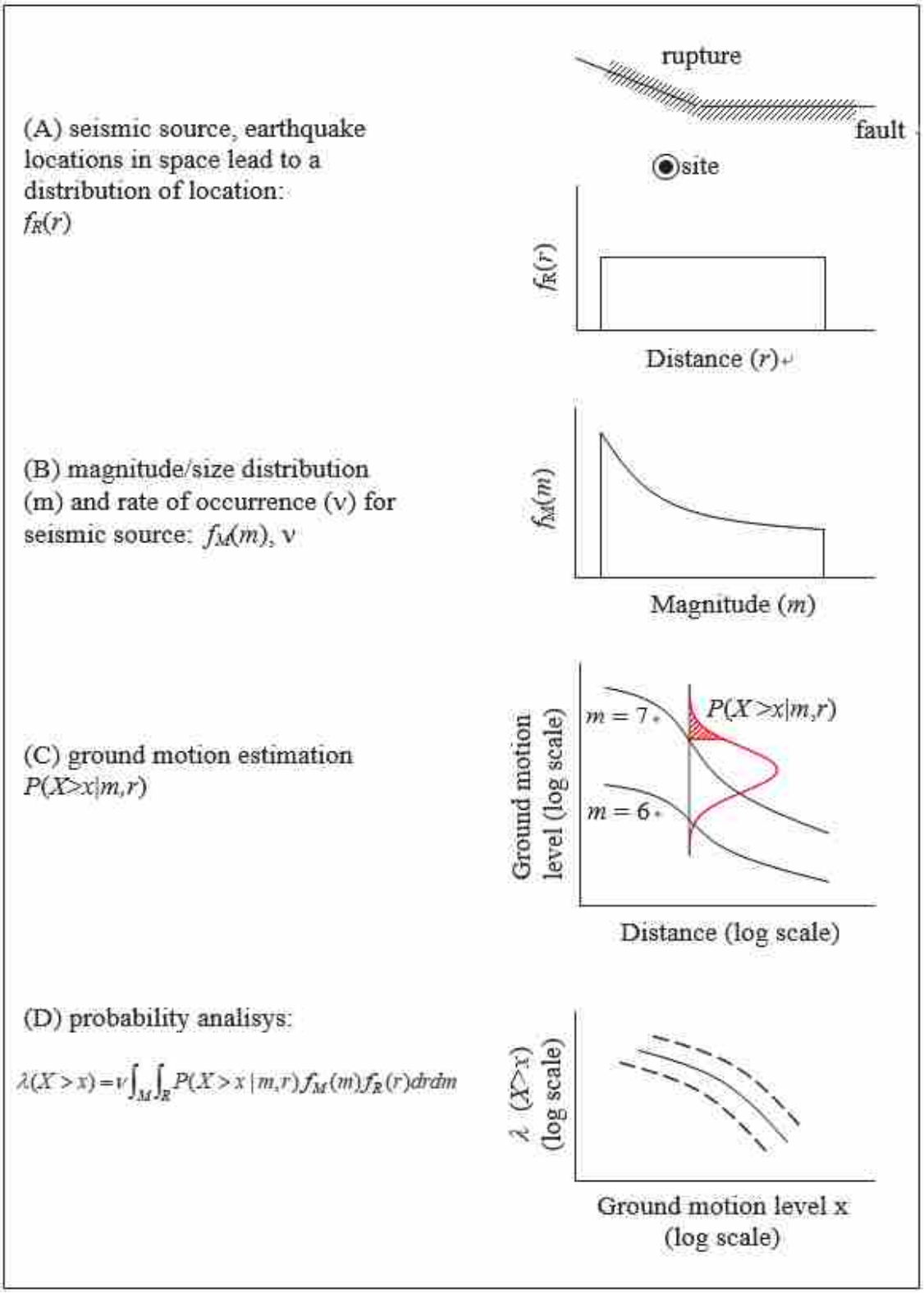

Figure 2. 2 General steps for conducting PSHA [10]

A. Magnitude Probability Distribution

Earthquake events can be described as the distribution of earthquake magnitude. Probabilistic distribution for magnitude $f_M(m)$ is follows the Gutenberg-Richter's law [13]. The cumulative distribution function $F_M(m)$ of the random variable M is defined as the probability of magnitude M which is smaller than m [17]. Magnitude m is any magnitude greater than or equal to m_o. In mostly hazard analysis, m_o ranges between 3 and 5 [18]. The formula for the cumulative distribution function is presented below:

$$F_M(m) = 1 - e^{-\beta (m - m_o)} \tag{2.5}$$

Thus, referring the equation (2.2), the probability density function can be performed as function of:

$$f_M(m) = \frac{dF_M(m)}{dm} = \beta e^{-\beta (m - m_o)} \tag{2.6}$$

The distribution density function $f_M(m)$ for the magnitude range between m_o and m_u can be expressed in the form of the following equation:

$$f_M(m) = \frac{\beta e^{-\beta (m - m_o)}}{1 - e^{-\beta (m - m_o)}}, \; m_o < m < m_u \tag{2.7}$$

B. Distance Probability Distribution

One of the factors that influence the probability of seismic hazard analysis is the rupture-to-site distance or location. A rupture and its size has the possibility to occur everywhere on a fault plane and at different times. The probability of rupture can be described in three dimensional model on the fault plane as shown in Figure 2.3a. The rupture can be occurred at the corner of the fault, in the middle, or even random and overlap. In PSHA calculations, there are several definitions of distance, depending on the GMPE used. The schematic model of various rupture-to-site distances definition are presented in Figure 2.3b. In computing the distance probability distribution $f_R(r)$, we have to considered the rupture area and total rupture area. The formula of $f_R(r)$ is presented below:

$$f_R(r) = \frac{a \; rupture \; area}{total \; rupture \; area} \tag{2.8}$$

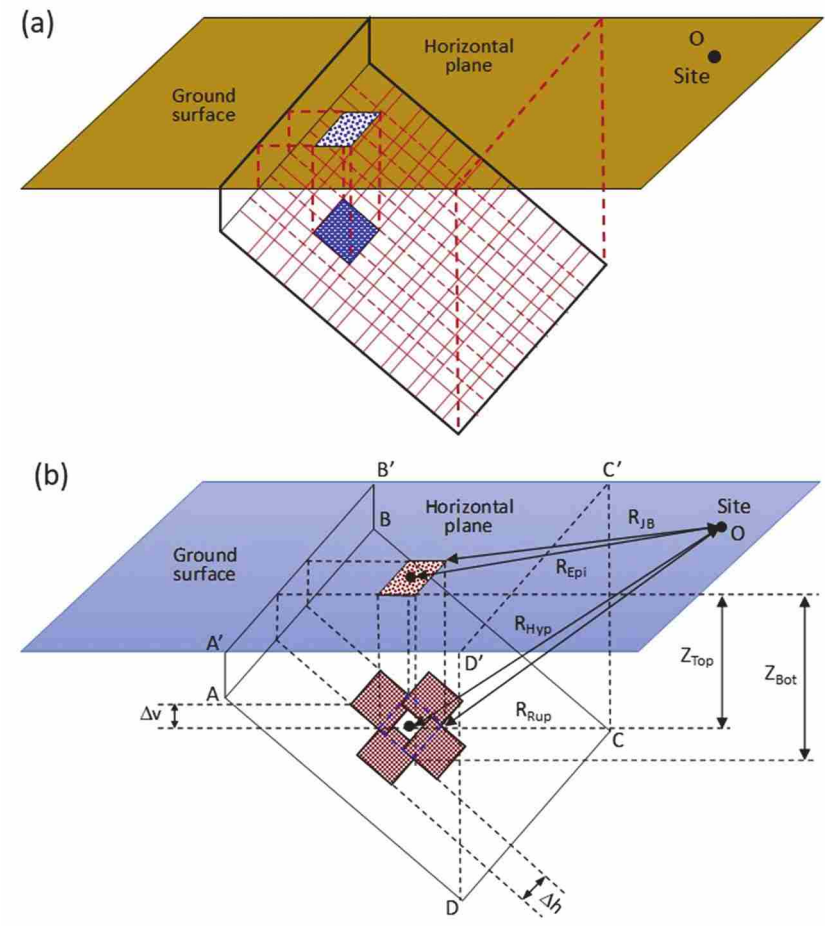

Figure 2. 3 Likely occurrence of rupture on a fault plane (a) and definition of distance (b) (redrawn from [19])

where:

R_{HIPO} = the hypocenter distance

R_{JB} = Joyner-Boore distance

R_{EPI} = Epicenter distance

R_{RUP} = Rupture distance.

2.4.1 Ground Motion Prediction Equation (GMPE)

Some researchers introduced how to select and adjust the GMPE models properly [20-22]. The GMPE selected in this study was based on the seismotectonic conditions classified due to the earthquake source mechanisms. This study applied the GMPE formula of Youngs et al. 1997, Atkinson-Boore 2003 and Gregor 2006 [23-25] for subduction mechanisms. Meanwhile, the GMPE of Boore et al. 1997, Chiou and Youngs NGA 2006 and Boore-Atkinson NGA 2006 [26-28] were selected for the shallow crustal fault mechanisms.

1) GMPE of Youngs et al (1997)

The attenuation function Youngs et al. (1997) is an empirical attenuation function that can be used to predict the peak ground acceleration and response acceleration spectra in interface and intraslab subduction zone earthquakes with the distance from the site to the earthquake source in the form of rupture distance of 10-500 km [23]. This attenuation relationship was developed using regression analysis with the formula for rock and soil as follows:

For *rock*:

$$\ln y = 0.2148 + 1.414\,M + C_1 + C_2\,(10 + M)^3 - C_3 \ln (r_{rup} + 1.7818\,e^{0.554M}) + 0.00607\,H + 0.3846\,Z_T \quad (2.9)$$

For soil:

$$\ln y = -0.6687 + 1.438\,M + C_1 + C_2\,(10 + M)^3 - C_3 \ln (r_{rup} + 1.097\,e^{0.617M}) + 0.00648\,H + 0.3643\,Z_T \quad (2.10)$$

$$\sigma_{\ln y} = C_4 + C_5 M \quad (2.11)$$

where:

y = spectral acceleration (g)

M = moment magnitude (Mw)

r_{rup} = closest distance to rupture zone (km) ; (10 km $\leq r_{rup} \leq$ 500 km)

H = depth (km)

Z_T = earthquake source type, 0 for interface and 1 for intraslab.

2) GMPE of Atkinson-Boore (2003)

Atkinson-Boore (2003) [24] proposed the ground motion attenuation relationship for earthquakes occurring in subduction zones which is an important input for seismic hazard analysis worldwide. This attenuation relationship is derived based on the results of the compilation of response spectra databases from hundreds of strong motion records of earthquake events with moment magnitude Mw 5 to 8.3 that occur in subduction zones around the world, including interface and intraslab events. The database used is four times larger than that provided for the previous empirical regression in determining the relationship of ground motion due to earthquakes from subduction zones. The large amount of data can

improve the results of decreasing attenuation parameters and magnitude scaling. The form of the Atkinson-Boore (2003) attenuation function is as follows:

$$\log y = fn(M) + c_3\, h + c_4\, R - g \log R + c_5\, sl\, S_C + c_6\, sl\, S_D + c_7\, sl\, S_E \qquad (2.12)$$

where:

M = moment magnitude (Mw),

M = 8.5 for interface events with M>8.5

M = 8.0 for intraslab events with M≥8.0

$fn(M) = c_1 + c_2\, M$

h = focal depth in km, h=100 km for event with a depth > 100 km.

$R = \sqrt{(D_{fault}{}^2 + \Delta^2)}$

D_{fault} = closest distance to the fault surface (km)

$\Delta = 0.00724 \times 10^{0.507M}$

S_C = 1 for C soil type of NEHRP (360<β≤760 m/sec), S_C=0 for other

S_D = 1 for D soil type of NEHRP (180<β≤360 m/sec), S_D=0 for other

S_E = 1 for E soil type of NEHRP (β<180 m/sec), S_E=0 for other

$g = 10^{(1.2-0.13M)}$ for interface event; $10^{(0.301-0.01M)}$ for intraslab event

$$sl = \begin{cases} 1 & for\ PGA_{TX} \le 100cm/s^2\ or\ freq \le 1Hz \\ 1-(f-1)(PGA_{TX}-100)/400 & for\ 100 \le PGA_{TX} \le 500cm/s^2\ or\ 1Hz \le f \le 2Hz \\ 1-(f-1) & for\ PGA_{TX} \le 100cm/s^2\ or\ freq \le 1Hz \\ 1-(PGATN-100)/400 & for\ 100 \le PGA_{TX} \le 500cm/s^2\ or\ 1Hz \le f \le 2Hz \\ 0 & for\ PGA_{TX} \le 100cm/s^2\ or\ frek \le 1Hz \end{cases}$$

PGA_{rX} = estimated PGA for rock (B soil type of NEHRP) in cm/s.

3) GMPE of Gregor (2006)

The ground motion prediction equation proposed by Gregor (2006) is an updated form of Gregor (2002). The attenuation coefficients for soil and rock sites in Gregor (2002) have different tables, while for Gregor (2006), soil and rock sites have the same attenuation tables. However, the soil and rock sites are determined based on the value of the soil shear wave velocity which is included in the calculation. For example, based on UBC 1997, a site with

a soil shear wave velocity of Vs30 < 760 m/s is considered as soil site, while for Vs30 ≥ 760 m/s it is considered as rock site. The ground motion prediction formula of Gregor (2006) is equal to Gregor (2002) as follows:

$$\ln y = C_1 + C_2 M + (C_3 + C_4 M) \ln[R + \exp(C_5)] + C_6(M - 10)^3 \quad (2.13)$$

where:
M = magnitude
R = closest distance to rupture zone (km)
y = peak ground motion parameter

4) GMPE of Boore et al. (1997)

The attenuation relationship provided by Boore-Joyner-Fumal (1997) can be used to estimate the peak acceleration and horizontal response spectra for shallow earthquakes in western North America [26]. For calculation purposes, a table of attenuation coefficients for peak horizontal components and pseudo-response acceleration spectra is given with 5% damping of the ground motion parameters in logarithm of natural numbers. This equation provides ground motion values in relation to moment magnitude, distance and site conditions for strike-slip, reverse-slip or unspecified fault mechanisms. Site conditions are represented by an average shear velocity in the range of 30 meters of soil depth. The recommended soil shear velocity values for rock and soil type sites correspond to the site categories used in the National Earthquake Hazards Reduction Program recommended in the national building codes. In addition, the magnitude and distance range limits have been set to match the data used in the previous equation. The attenuation relationship is written as follows:

$$\log y = b_1 + b_2 (M\text{-}6) + b_3 (M\text{-}6)^2 + b_5 \ln r + b_V \ln (V_s / V_A) \quad (2.14)$$

where:
y = ground motion parameter

$$b_1 = \begin{cases} b_{1SS} & for\ strike-slip \\ b_{1RS} & for\ reverse-slip \\ b_{1AL} & other\ mechanism \end{cases}$$

M = moment magnitude ($5.5 \leq Mw \leq 7.5$)

$r = \sqrt{r_{jb}^2 + h^2}$

r_{jb} = Joyner-Boore distance (km) ($r_{jb} \leq 80$ km)

h = depth (km)

V_s = shear wave velocity (m/s)

5) GMPE of Chiou-Youngs NGA (2006)

Chiou-Youngs (2006) proposed the next generation attenuation which provides an empirical model of ground motion to determine the horizontal component of ground motion developed as part of the PEER-NGA study [27]. This model is derived for peak ground acceleration (PGA) and pseudo-acceleration spectra with 5% attenuation with a period range from 0.01 to 10 seconds. The form of the NGA Chiou-Youngs (2006) attenuation model is as follows:

$$\ln(SA_{1130ij}) = c_1 + c_{1a} F_{RVi} + c_{1b} F_{NMi} + c_7(Z_{TORi} - 4) + c_2(M_i - 6)$$
$$+ [(c_2 - c_3)/ c_n]\ln[1 + \exp\{c_n(c_M - M_i)\}] + c_4 \ln[R_{RUPij} + c_5 \cosh\{c_6(M_i - c_{HM}, 0)_{max}\}]$$
$$(c_{4a} - c_4) \ln\sqrt{R_{RUPij}^2 + c_{RB}^2} + [c_{\gamma 1} + c_{\gamma 2}/\cosh\{(M_i - c_{\gamma 3}, 0)_{max})]R_{RUPij}$$
$$+ c_9 \cos^2\delta_i \tanh(R_{RUPij}/2) \tan^{-1}[W_i \cos \delta_i/2((Z_{TORi}$$
$$+1)] 1/(\pi/2) [1- R_{JBij}/(R_{JBij}-0.001)] + \tau z_i \quad (2.15)$$

$$\ln(SA_{ij}) = \ln(SA_{1130ij}) + \phi_1 [\ln(V_{S30ij}/1130), 0]\min$$
$$+ \phi_2 [\exp\{\phi_2 ((V_{S30ij}, 1130)_{min} - 360)\}$$
$$- \exp\{\phi_2(1130-360)\}] \ln[(SA_{1130ij}) + \phi_4)/ \phi_4] + \sigma z_{ij} \quad (2.16)$$

where:

SA = spectral acceleration (g)

R_{RUP} = closest distance to rupture zone (km)

R_{JB} = distance of Joyner-Boor (km)

δ = dip angle of rupture

$0W$ = width of rupture (km)

Z_{TOR} = rupture depth (km)

F_{RV} = 1 for $30^o \leq \lambda \leq 150^o$ and F_{RV} = 0 for others (reverse and reverse-oblique)

F_{NM} = 1 for $-120^o \leq \lambda \leq -60^o$ and F_{NM} = 0 for others (normal and normal-oblique)

λ = rake angle

V_{S30} = shear wave velocity for the uppermost of 30m top soil layer (m/s)

τ = error standard for inter-event

σ = error standard for intra-event

The 2006 Chiou-Youngs - NGA empirical ground motion model should only be used according to the predictor variables in the following ranges:

$4 \leq M \leq 8.5$ for strike-slip event

$4 \leq M \leq 8.0$ for reverse slip and normal slip

$0 \leq R_{RUP} \leq 200$ km

$150 \text{ m/s} \leq V_{S30} \leq 1500$ m/s

6) GMPE of Boore-Atkinson NGA (2006)

Boor-Atkinson (2007) provided the next generation attenuation model containing an equation for predicting a certain size ground motion in terms of the horizontal component of the ground motion as a function of the earthquake mechanism, the site distance to the earthquake source, the average shear-wave velocity and the fault type [28]. This equation was used to determine the peak ground acceleration (PGA), and pseudo-absolute acceleration spectra with 5% attenuation for the period from 0.01 s to 5.0s. The Boor-Atkinson (2006) NGA equation is derived based on empirical regression with the database used is strong ground motion data from PEER NGA. The form of the NGA Boor-Atkinson (2006) attenuation model is as follows:

$$\ln y = F_M(M) + F_D(R_{jb},M) + F_S(V_{S30},R_{jb},M) + \varepsilon\sigma_T \quad (2.17)$$

where:

$F_D(R_{jb},M)$ (distance effect function)

$F_D(R_{jb},M) = [c_1 + c_2(M - M_{ref})] \ln R/R_{ref} + c_3(R - R_{ref})$

$$R = \sqrt{r_{jb}^2 + h^2}$$

c_1, c_2, c_3, M_{ref}, R_{ref} and h is a coefficient that can be taken from the table

$F_M(M)$ (magnitude effect function)

For $M \leq M_h$

$F_M(M) = a_1U + a_2S + a_3N + a_4R + a_5(M - M_h) + a_6(M - M_h)^2$

For $M > M_h$

$F_M(M) = a_1U + a_2S + a_3N + a_4R + a_7(M - M_h)$

U, S_S, N_S and R_S are dummy variables used to specify the fault type, where U *(unspecified* fault), S_S (strike slip fault), S_S (normal slip fault) and S_S (reverse slip fault).

F_S (site amplification)

$F_S = F_{LIN} + F_{NL}$

where the linear term F_{LIN} :

$F_{LIN} = b_{lin} \ln (V_{S30}/V_{ref})$

and nonlinear F_{NL}:

for pga4$nl \leq a_1$

$F_{NL} = b_{nl} \ln(pga\_low/0.1)$

for pga4$nl \leq a_1$

$F_{NL} = b_{nl} \ln(pga\_low/0.1) + c[\ln(pga4nl/a_1)]^2 + d[\ln(pga4nl/a_1)]^3$

for $pga4nl < a_2$

$F_{NL} = b_{nl} \ln(pga4nl/0.1)$

a_1 and a_2 are determined for the lower limit levels of linear and nonlinear amplification.

pga_low is a variable that indicates a transition between linear and nonlinear behavior.

*pga*4*nl* is the initial estimate for the predicted PGA value for Vs30 = 760 m/s which can be calculated by equation (2.17) by taking $F_S = 0.0$ and $\varepsilon = 0.0$

The nonlinear slope function (b_{nl}) is a function of the period and V_{S30}.

for $V_{S30} \leq V_1$

$b_{nl} = b_1$

for $V_1 < V_{S30} \leq V_2$

$b_{nl} = (b_1 - b_2) \ln(V_{S30}/V_2)/ \ln(V_1/V_2) + b_2$

for $V_2 < V_{S30} < V_{ref}$

$b_{nl} = b_2 \ln(V_{S30}/V_{ref})/ \ln(V_2/V_{ref})$

for $V_{ref} \leq V_{S30}$

$b_{nl} = 0.0$

$c = (3\Delta y - b_{nl} \Delta x)/ \Delta x^2$

$d = -(2\Delta y - b_{nl} \Delta x)/ \Delta x^3$

$\Delta x = \ln(a_2/a_1)$

$\Delta y = b_{nl} \ln(a_2/pga\_low)$

2.4.2 Uncertainty in Seismic Hazard Analysis

Calculations with a probability approach do not provide systematic consideration of the uncertainty of parameters in a particular seismic hazard model. The uncertainty probability in the integral function provided in equation (2.2) is an aleatory uncertainty which essentially describes a random variation that cannot be reduced by additional data or new theories [29]. The selection of certain seismic hazard elements may be considered inappropriate in some cases, the uncertainty of this parameter value is a form of epistemic uncertainty. To obtain a suitable framework, some researchers [30-32] considered the uncertainty model for seismic hazard analysis.

Logic tree is one of the methods which take into account all uncertainties in determining parameters in PSHA, such as the selection of recurrence model, attenuation function, recurrence rate, and maximum magnitude. By using this method, the freedom to use various models will be more controlled for the level of accuracy because the logic tree provides different weighting factors for each model so that accuracy comparisons can be made between one model and another. Each alternative chosen in determining the parameters is given a weight that describes the level of confidence in the parameters used. The sum of the weighting factors of all alternative methods for the same parameter must be equal to one.

2.5 References

[1] National Standardization Agency (BSN) (2019) SNI 1726: 2019 Procedures for earthquake resistance structural buildings and non-buildings Jakarta

[2] Borcherdt, R., A Review of Empirical Evidance for Site Coefficient in Building Code Provision, United States Geological Survey (USGS), (2006)

[3] Borcherdt, R. D., (1994), Estimates of site-dependent response spectra for design (Methodology and Justification), Earthquake Spectra, 10, 617-653.

[4] D. Park, Y.M.A. Hashash, Evaluation of seismic site factor in the Mississippi Embayment I, Estimation of dynam.ic properties, Soil Dynamics and Earthquake Engineering, 25, pp.133-144, (2005)

[5] C.C. Tsai, Chen C.W, A comparison of site response analysis method and its impact on earthquake engineeing practice, The 2nd Europen Conference on Earthquake Engineering and Seimology, Istanbul, (2014).

[6] Pallav, K., Raghukanth, S., and Singh, K. (2015). Estimation of Seismic site coefficient and seisimic microzonation of Imphal city, India, using the probabilistic approach. Acta Geophysica, vol.36 (5), pp.1339-1367.

[7] W.Partono, M. Irsyam, S.P.R Wardani, Development of site class and site coefficient maps of Semarang, Indonesia, using field shear wave velocity data, MATEC Web of Conference, 101, 05010, (2017), pp.1-5.

[8] Pawirodikromo, W., Makrup, L., Teguh, M., Suryo, B., and Hartyanto, E. Site Coefficient of short Fa and long period Fv maps constructed from the probabilistic seismic hazard analysis in Yogyakarta Special Province. MATEC Web of Conference, 280, 01001 (2019), pp.1-17.

[9] National Center for Earthquake Studies (PuSGeN) 2017 Indonesian Seismic Sources and Seismic Hazard Maps 2017. Center for Research and Development of Housing and Resettlement, Ministry of Public Works and Human Settlements, (Peta Sumber dan Bahaya Gempa Indonesia Tahun 2017. Pusat Litbang Perumahan dan Pemukiman, Kementerian Pekerjaan Umum dan Perumahan Rakyat) 1–377.

[10] McGuire R K 2004 *Seismic Hazard and Risk Analysis* Earthquake Engineering Research Institute MNO-10 221p

[11] Susilo, A. and Adnan, Z. 2013. Probabilistic seismic hazard analysis of East Java region, Indonesia. International Journal of Computer and Electrical Engineering, Vol.5 (3), pp.341-344.

[12] Kramer S L 1996 *Geotechnical Earthquake Engineering* Prentice Hall New Jersey 653p

[13] Gutenberg B. and Richter C., Frequency of earthquakes in California. Bulletin of the Seismological Society of America, Vol. 34, Issue 4, 1944, pp.185–188.

[14] Cornell, C Allin. 1968. Engineering Seismic Risk Analysis. Bulletin of the Seismological Society of America, 58(5), 1583–1606.

[15] Baker J W 2008 *Introduction to probabilistic seismic hazard analysis (PSHA)* Stanford University version 1.3 72p

[16] Kijko A 2011 *Introduction to Probabilistic Seismic Hazard Analysis* Natural Hazard Centre University of Pretoria South Africa 26p

[17] Soong, T. T., 1981. Probabilistic modeling and analysis in Science and Engineering, John Wiley and Sons.

[18] Electric Power Research Institute (1986): "Seismic Hazard Methodology for the Central and Eastern United States", *EPRI*, Palo Alto, EPRI, NP-4726

[19] Makrup L., Irsyam M., Sengara W. I., and Hendriyawan. Numerical solution of the total probability theorem in a three dimensional earthquake source domain for developing seismic hazard map and hazard spectrum, American Journal of Civil Engineering and Architecture, Vol. 3, no. 5, 2015, pp.158-164.

[20] Cotton F, Scherbaum F, Bommer J J and Bungum H 2006 *J. Seismol.* Criteria for selecting and adjusting ground-motion models for specific target regions: Application to central Europe and rock sites 10 (2) 137–156

[21] Bommer J J, Douglas J, Scherbaum F, Cotton F, Bungum H and Fah D 2010 *Seismol. Res. Lett.* On the selection of ground-motion prediction equations for seismic hazard analysis 81 (5) 783–793

[22] Stewart J P, Douglas J, Javanbarg M, Bozorgnia Y, Abrahamson N A, Boore D M, Campbell K W, Delavaud E, Erdik M and Stafford P J 2015 *Earthq. Spectra* Selection of ground motion prediction equations for the global earthquake model 31 19-45

[23] Youngs R R, Chiou S J, Silva W J and Humphrey J R 1997 *Geophys. Res. Lett.* Strong ground motion attenuation relationships for subduction zone earthquake 68

[24] Atkinson G M and Boore D M 2003 *Bull. Seismol. Soc. Am*. Empirical ground motion relations for Subduction-Zone Earthquakes and their application to Cascadia and other region 93 (4) 1703-1729

[25] Gregor N J 2006 Applied by Steve Harmsen in USGS Software Fortran Code.

[26] Boore D M, Joyner W B and Fumal T E 1997 *Seismol. Res. Lett.* Equations for estimating horizontal response spectra and peak acceleration from western north American earthquakes: A Summary of Recent Work 68

[27] Chiou B S J and Youngs R R NGA (Next Generation Attenuation) 2006 Empirical Ground Motion Model for the Average Horizontal Component of Peak Acceleration and Pseudo-Spectral Acceleration for Spectral Periods 0.01 to 10 second1, Interim Report for USGS Review, Revised Editorially, July 10, 2006, California, USA

[28] Boore D M and Atkinson G M 2006 *Earthq. Spec.* Ground Motion Prediction Equations for the Average Horizontal Component of PGA, PGV, and 5% Damped PSA at Spectral Periods between 0.01 s and 10.0 s 24 (1)

[29] Makrup, L.2013. Seismic Hazard untuk Indonesia. Yogyakarta: Indonesia. Graha Ilmu.

[30] Kulkani, R.B., R.R. Youngs, K.J. Coppersmith, *Assesment of confidence intervals for result of seismic hazard analysis,* "Proceedings" 8th World Conference on Earthquake Engineering, San Francisco, Vol. 1, pp. 263-270, 1984.

[31] Coppersmith, K.J. and Youngs, R.R., *Capturing uncertainty in probabilistic seismic hazard assessments within intraplate tectonic environments*, Proceedings of the Third U.S. National Conference on Earthquake Engineering, Charleston, South Carolina, Vol. 1, pp. 301 – 302, 1986.

[32] Foulser-Piggott R 2014 *Soil Dyn. Earthq. Eng.* Quantifying the epistemic uncertainty in ground motion models and prediction 65 256–268

Chapter 3
Seismic Properties of Java Region

3.1 Tectonic Setting of Java, Indonesia

Indonesia is one of the earthquake prone countries, located where the Ring of Fire around the Pacific Ocean meets the Alpide belt. As a meeting point of several active tectonic plates, two continental plates (the Indo-Australian Plate and the Eurasian Plate) and two oceanic plates (the Pacific Plate and the Philippine Sea Plate) as shown in Figure 3.1, the tectonic setting of Indonesia is very complex. The Indo-Australian plate moves northward and sinks under the Eurasian tectonic plate, forming a subduction zone in the south of Java Island. The plate motion speed in the western region of northern and central Sumatra ranges from 52 to 57 mm/yr and the movement in the western region of South Sumatra is around 60 mm/yr. Meanwhile, the speed of plate movement in the south of Java is around 80 mm/yr [1]. At the Central Java trench, the subduction zone strike is relatively perpendicular with the plate motion direction [2].

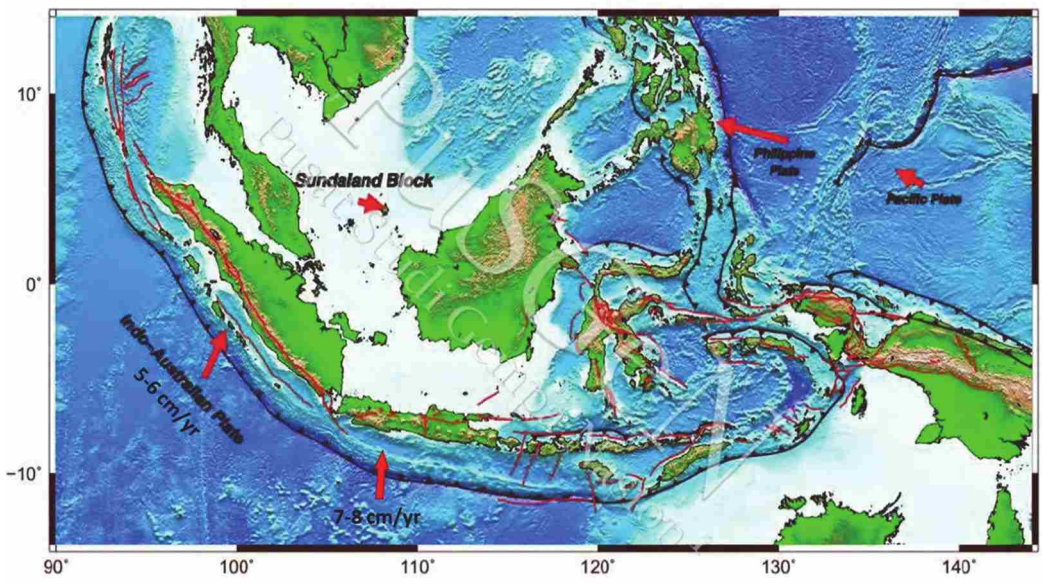

Figure 3. 1 Tectonic map of Indonesia
(Source: PuSGeN, 2017 [3])

The Java Island, which is located in the north of the two plates confluence has several tectonic faults as a form of stress accommodation generated by subduction in the south. Some of the faults identified in Java and surrounding areas and the subduction zone beneath

Java-Bali-Lombok and beneath south of Sumatra are presented in Figure 3.2.

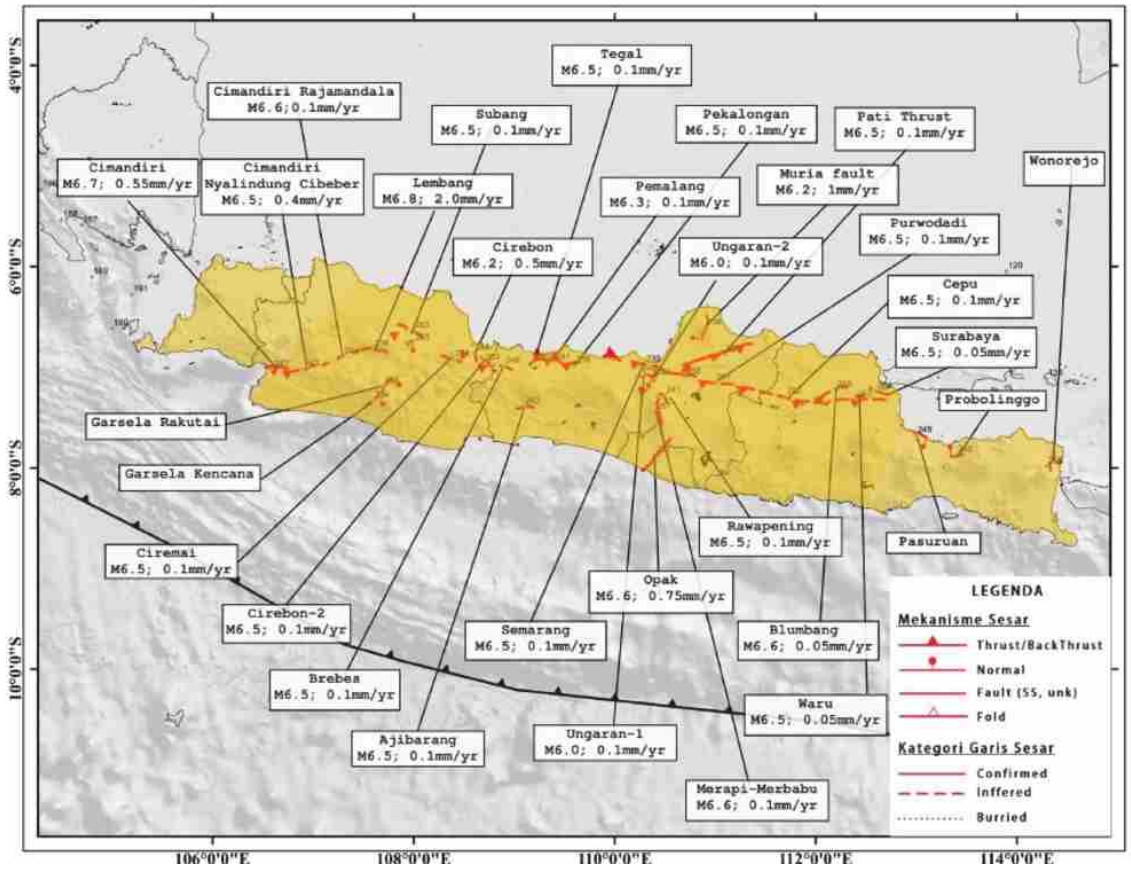

a). Identified faults in Java and its surrounding [3]

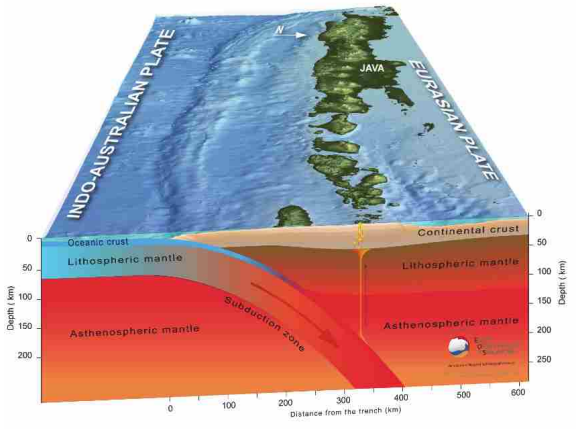

b). Subduction zone beneath Java-Bali-Lombok [4]

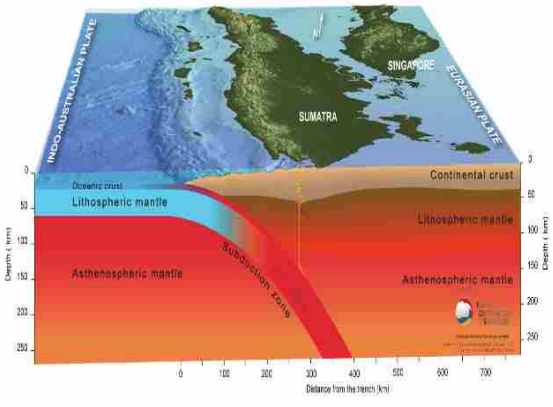

c) Subduction zone beneath south of Sumatra [4]

Figure 3. 2 Identified faults and subduction zone in Java and its surroundings

The length of Sunda trench along Sumatra and Java Island, the high rate of plate convergence, and the high deficit rate in several areas in the south of Java that trigger energy accumulation underlies many scientists to argue that potentially powerful earthquake and tsunami would affect this region. Becoming one of the world's most densely populated areas, Java Island and its surroundings face a threat of seismic activities which can cause significant losses. The large earthquakes with magnitude greater than Mw 7.0, including tsunami-earthquakes in 1921 (Mw 7.6), 1994 (Mw 7.6), 2006 (Mw 7.7), and 2009 (Mw 7.3) that have occurred along the Java subduction are presented in Table 3.1.

Table 3. 1 Earthquake in Java with magnitude of Mw > 7.0 and its impact [5-9]

Year	Magnitude (Mw)	Impact				Tsunami (height)
		killed	missing	injured	building damage	
2009	7.3	111	27	1,297	25,000	1 m
2006	7.7	637	164	9,245	1,623	5-8 m
1994	7.6	429	30	723	2,025	13.9 m
1943	7.1	213	-	2,096	2,800	-
1926	7.1	*NA*	*NA*	*NA*	*NA*	-
1921	7.6	*NA*	*NA*	*NA*	*NA*	10 cm

**NA: Not Available*

Learning from the major earthquake experienced by Japan in 2011, the seafloor of eastern Japan (B area) which is slightly older than that of southern Java (A area) shown in Figure 3.3 [10, 11] was able to produce an earthquake with magnitude of M9.0 on March 11, 2011, in the Tohuku region. The surface energy of the earthquake was two times higher than the energy of the 2004 tsunami in Aceh, Indonesia, which reached $1.9 \pm 0.5 \times 10^{17}$J [12]. The terrible tsunami attacking Tohuku reached a height of more than 39 m and left more than 24 thousand people missing or dead [13].

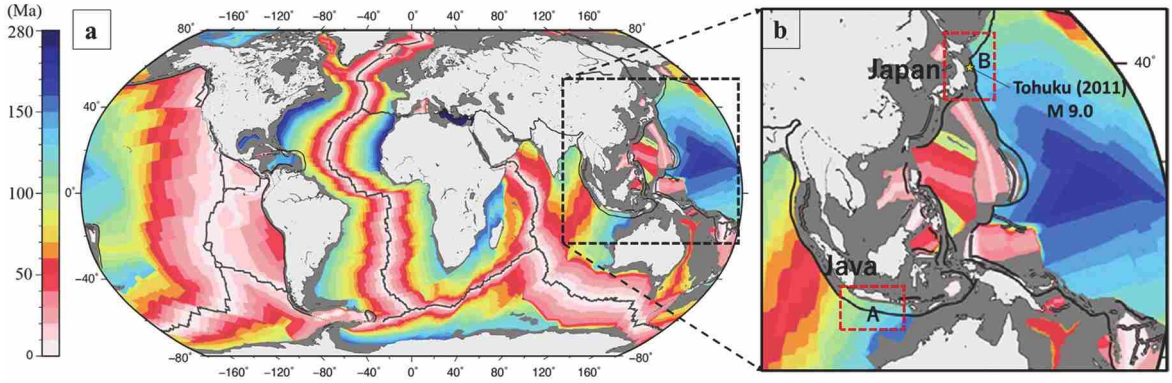

Figure 3. 3 The oceanic crustal age [10, 11]. (a) Seafloor age global map generated using the Generic Mapping Tools; (b) Seafloor age in south of Java and east-north side of Japan (zoomed-in)

Several studies related to tsunami wave modeling with the certain earthquake scenarios for the south Java coastal area have been created. Hartoko et al. [14] generated spatial tsunami wave modeling with earthquake scenarios of M8.4, M7.9, and M7.0 for the south of West Java (Serang), south of Central Java (Bantul), and south of East Java (Banyuwangi), respectively. Based on the model constructed for the three coastal areas in south of Java, two tsunami waves can reach a height of 2 to 8 m with an interval of about 30 minutes. In addition, the result also stated that a 2-m wave will hit the coastal area after 60 minutes of travel time. Meanwhile, Widiyantoro et al. [15] modeled tsunami waves using the worst-case scenario of subduction earthquakes, in which two segments of megathrust along the Java region simultaneously rupture. The results show that the earthquake scenario can trigger ~ 20 m and ~ 12 m tsunami waves on the south coast of West and East Java, respectively. In the previous studies, the essential seismic parameters have not been explicitly identified, and data on earthquake return periods remain limited. This chapter addresses such gaps by identifying the seismic properties, including the seismic activity (a-value), size distribution (b-value), fractal dimension (D), and maximum magnitude (M_{max}) of the subduction zone along the Java Island as an effort to conduct earthquake and tsunami disaster mitigation.

3.2 Seismicity of Java Region

3.2.1 Earthquake data

The earthquake data were compiled from the Agency of Meteorology, Climatology, and Geophysics (BMKG) Indonesia with relocated hypocenter data using TeletomoDD

method [16]. In addition, earthquake data from the International Seismological Center (ISC) [17] for historical earthquakes occurring in and around Java Island were also collected, including the EHB (Engdahl, van der Hilst, and Buland) improved earthquake data set [18]. From these data sources, a catalog of earthquakes from 1906 to September 2020 with magnitude of $Mw \geq 4.5$ was obtained. The earthquake data were then converted into moment magnitude (Mw) scale.

3.2.2 Magnitude Homogenization

Different magnitude scales have been considered by several researchers. In the 1960s, the Mb was introduced to be reported in the ISC and NEIC bulletins by the USGS and the National Oceanic and Atmospheric Administration (NOAA), in conjunction with the establishment of the World-Wide Standard Seismograph Network (WWSSN). Later, the Ms was introduced by the NEIC bulletin, and it was accepted later to be used by the ISC bulletin. [19]. The main problem in the application of these scales is that they saturate for large earthquakes, which leads to the underestimation of magnitude for large earthquake events. In addition to this question, their behaviors are different over the whole magnitude range [20, 21]. To overcome such problems, a new non-saturating magnitude scale (Mw) was proposed by Hanks and Kanamori 1979 [22]. This scale is based on the total scalar seismic moment released during the rupture of an earthquake. Seismic moment, and thus the Mw, is mainly controlled by both the fault/rupture area, the average dislocation, and the rigidity of the medium.

A homogeneity earthquake magnitude scale is paramount for performing seismic hazard analysis and other seismic engineering applications. For this purpose, all available earthquake dataset of the Indonesia region (1906 to September 2020) were collected to get the correlation of body-wave magnitude (m_b) and surface-wave magnitude (M_s) into M_w. The m_b-M_w dataset (21,853 events) and M_s-M_w dataset (13,402 events) compiled were then plotted into the graphs, which are presented in Figure 3.4.

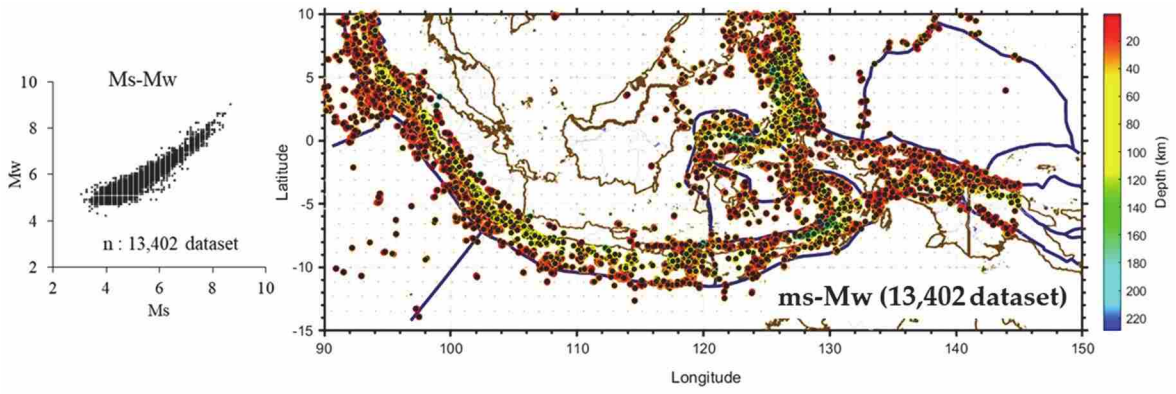

Figure 3. 4 The mb-Mw and Ms-Mw dataset map and relationship

A homogenous earthquake catalog for a seismic region needs regressed relations for conversion of several magnitude types to the most reliable and useful scale of magnitude, moment magnitude, Mw. The conversion for body-wave magnitude (mb) and surface-wave magnitude (Ms) of all earthquake events in the Indonesian region were determined based on three regression models, namely Standard Regression (SR), Inverted Standard Regression (ISR), and Orthogonal Standard Regression (OSR).

a. Standard Regression (SR)

The usual procedure while employing regression analysis is the standard regression (standard least squares regression; ordinary standard least square), SR, because of its simplicity.

- the independent (predictor) variable (each magnitude scale to be converted) is free from measurement error
- the random error on the dependent variable (Mw) is normally distributed and have a constant standard deviation in the whole regression domain

However, error is also present on the predictor variables.

b. Inverted Standard Regression (ISR)

ISR is similar to the SR but minimizes the horizontal offsets to the best fit line.

- the role of the two variables gets reversed
- My is taken as independent variable without error and Mx is the dependent variable having some error

c. Orthogonal Regression (OSR)

OSR is a standard regression method which is used to account for the effects of measurement

error in both variables (response and predictor).

The schematic relationship for each type of regression is presented in Figure 3.5.

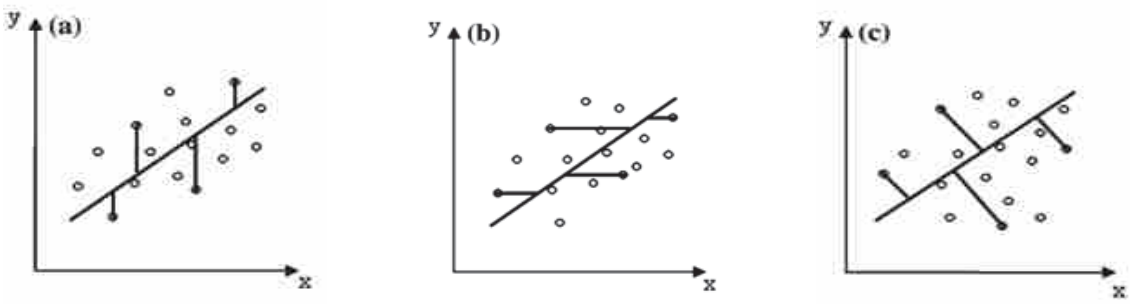

a) Standard Regression (SR)

b) Inverted Standard Regression (ISR)

c) Orthogonal Standard Regression (OSR)

Figure 3. 5 Schematic diagram for SR, ISR and OSR

The accuracy tests for magnitude correlation were performed including the R^2 test and standard error (SE) test. The result of earthquake dataset relationship for mb-Mw and Ms-Mw are shown in Figure 3.6.

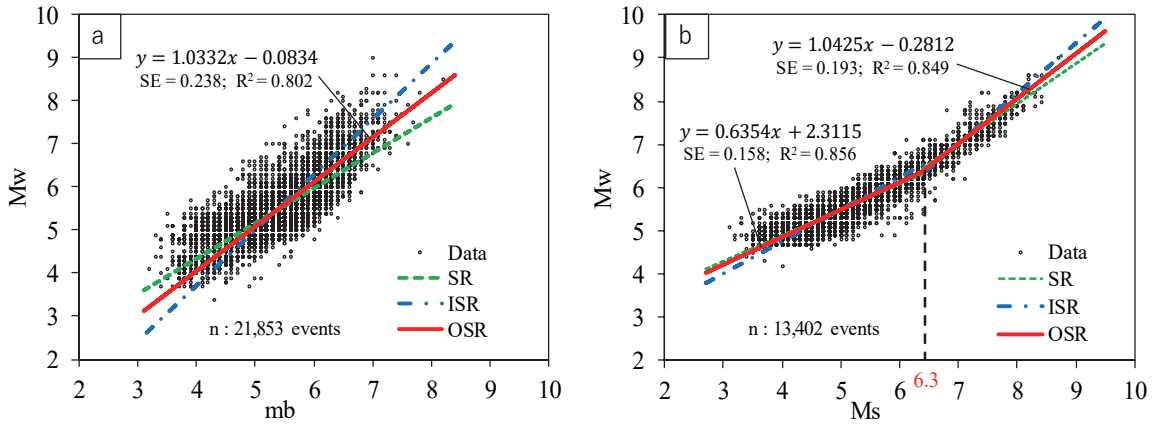

Figure 3. 6 Magnitude scale relationships of Indonesia earthquake events dataset

a) mb-Mw ; b) Ms-Mw

The OSR shows the best-fit relationship for the magnitude correlation for mb-Mw and Ms-Mw to be used in this study. The magnitude conversion formula is as follows:

$$M_w = 1.0332 m_b - 0.0834 \quad (3.1)$$

for the magnitude range of $3.2 \leq mb \leq 8.2$; SE = 0.238 and $R^2 = 0.802$

$$M_w = 0.6354 M_s + 2.3115 \quad (3.2)$$

for the magnitude range of $3.1 \leq M_s \leq 6.3$; SE = 0.158 and $R^2 = 0.856$

$$M_w = 1.0425 M_s - 0.2812 \quad (3.3)$$

for the magnitude range of $6.4 \leq M_s \leq 8.7$; SE = 0.193 and $R^2 = 0.849$

In order to observe the magnitude relations conducted on other previous studies, the comparison of magnitude conversion results is displayed in Figure 3.7.

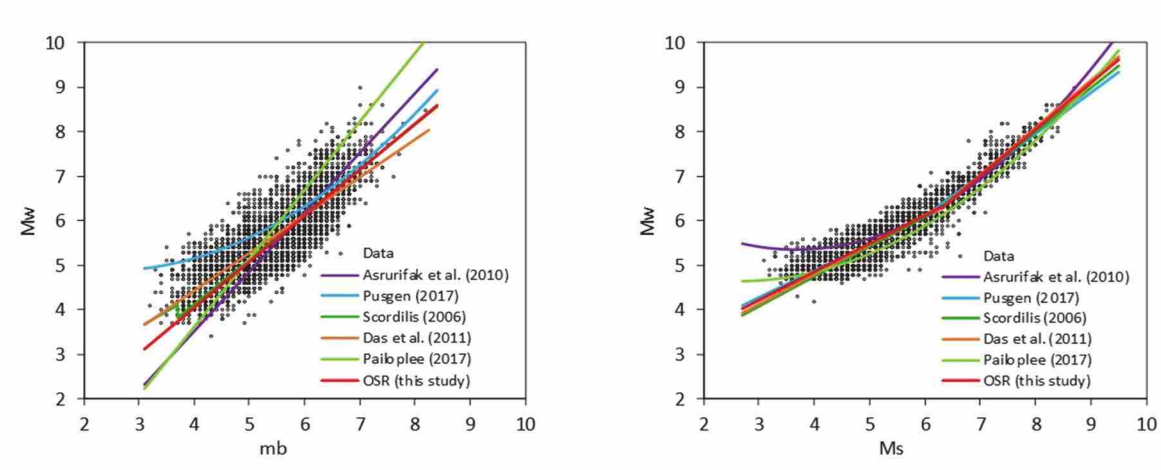

Figure 3. 7 Comparison with some previous research for magnitude correlation a) mb-Mw ; b) Ms-Mw

3.2.3 Declustering Analysis

A number of declustering algorithms were developed based on different assumptions and recorded data. Five of the most well-known declustering algorithms are provided in [23-27]. In 2019, Teng and Baker [28] evaluated several declustering algorithm models for earthquake data and applied it to a seismic hazard analysis in two cities in the USA. The results show that the Gardner and Knopoff and Zhuang methods using the epidemic type of aftershock sequence (ETAS) [29, 30] potentially result in a negligible likelihood of massive earthquakes being mainshocks and overestimate the effects of foreshock. Their observations shed light on both Reasenberg and Zaliapin and Ben-Zion declustering algorithms provide better results for a seismic hazard analysis.

In this study, the Reasenberg method was applied for declustering the earthquake data which was also carried out by [31] for an earthquake analysis in East Java, Indonesia. The earthquake catalog of Java between 1906 to 2020 is shown in Figure 3.8, while the comparison of original data and declustered data were presented in Figure 3.9.

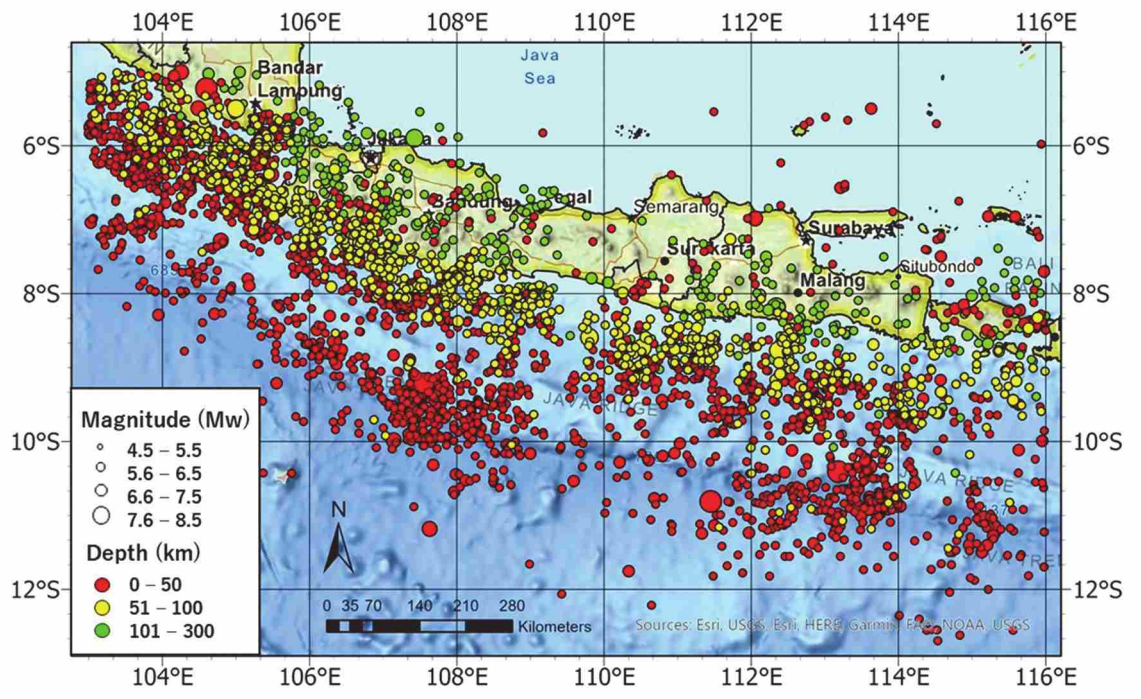

Figure 3. 8 Earthquake epicenter of Java and its vicinity (1906-2020)

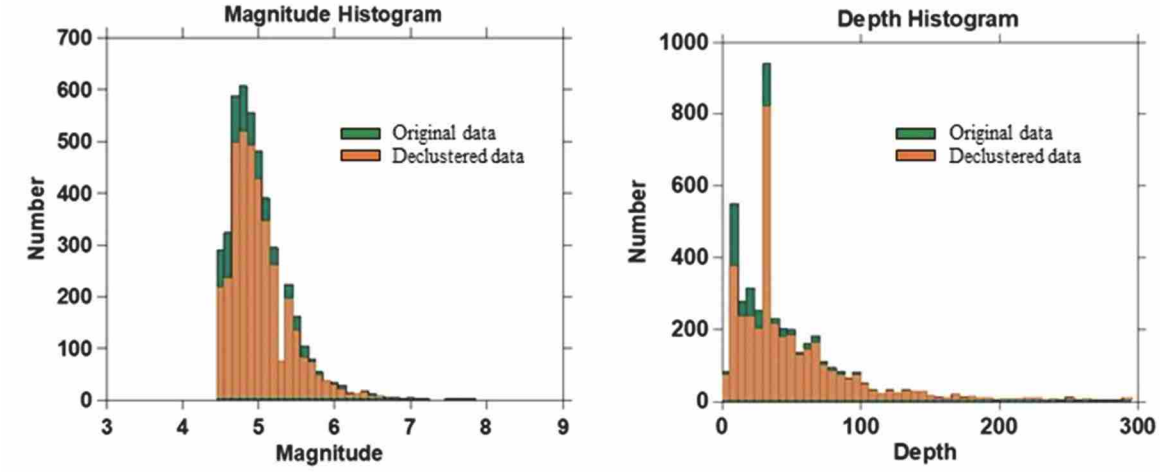

Figure 3. 9 Comparison of original and declustered earthquake data

3.2.4 The FMD and a-b Parameter

The frequency-magnitude distribution (FMD) for each group of earthquakes was conducted by using the equation first acknowledged in Japan by Ishimoto and Lida in 1939 [32] then in California by Gutenberg and Richter, 1994 [33] which is commonly known as the Gutenberg-Richter (G-R) power law. In this study, we followed the FMD provided by Gutenberg and Richter that has been verified for global and regional seismicity. The Gutenberg-Richter relationship is shown in Figure 3.10.

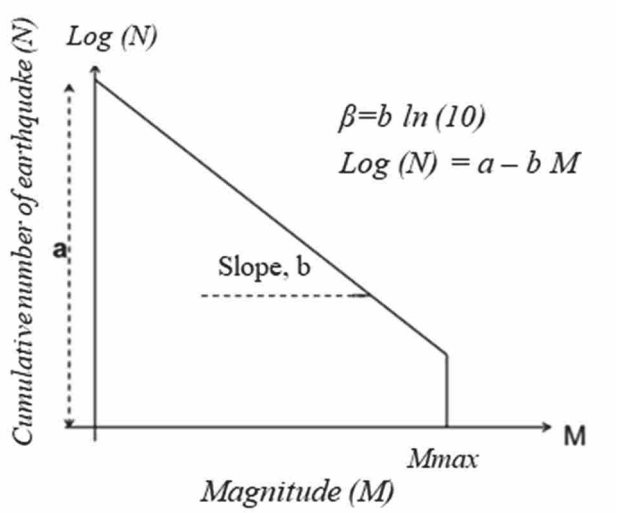

Figure 3. 10 Frequency magnitude distribution of earthquake (Gutenberg-Richter Law)

The empirical formula of Gutenberg-Richter Law is as follows:

$$\log(N) = a - bM \qquad \text{or} \qquad N = e^{\alpha - \beta M} \tag{3.4}$$

where *N* describes the cumulative number of earthquakes with magnitude equal to or greater than *M*, a and b are constants, commonly known as *a*-values and *b*-values, indicating the seismicity activity and the log-linear relation's slope, respectively, and *e* is a natural number. The *a* and *b* parameters become an essential parameter in the seismic hazard analysis. The parameter *b*, of the Gutenberg-Richter frequency-magnitude relationship has been the subject of many studies since it is associated with the intensity of seismic activity investigated in the certain observed region. The Maximum Likelihood Method (MLM) as the most widely accepted method to calculate the b-value given by Aki-Utsu [34, 35] was used in this study, the equation is:

$$b = \frac{1}{\bar{M} - M_o} \log_{10} e \tag{3.5}$$

The a-value was estimated using the formula of Wekner, 1965 in [36] as follows:

$$a = \log N(M \geq M_o) + \log(b \ln 10) + M_o b \tag{3.6}$$

where $\bar{M}$ denotes the average magnitude and M_o is the minimum threshold for the earthquake data magnitude considered, in which we used the magnitude completeness, Mc parameter.

3.3 Fractal Dimension and Maximum Magnitude Estimation

The fractal dimension (D) in a seismicity study can be determined based on the relationship of the linear regression slope between the logarithm of the fracture distance (r_n) from the earthquake source and the logarithm of the integral correlation constant C(r) [37]. The fractal dimension of each subduction segment was calculated using the correlation which was also used in [7] and [38] as follows:

$$D = \lim_{r \to 0} \frac{Log\ C(r)}{\log r_n} \tag{3.7}$$

C(r) is estimated based on a set of points of clustering using the following relation:

$$\mathrm{C(r)} = \frac{2}{N(N-1)} N(R < r) \tag{3.8}$$

N(R<r) represents the number of event pairs separated by a distance R in a cluster with a distance smaller than r.

Earthquakes occur because of the accumulation of pressure, and the process of releasing energy is related to time. Consequently, to conduct the seismic hazard analysis, the estimation of maximum earthquake magnitude must be considered. The maximum magnitude (M_{max}) for each segment was calculated using the following magnitude equation of Hanks and Kanamori [39] and Wells and Coppersmith [40]:

$$\mathrm{M} = \tfrac{2}{3} \log M_o - 10.7 \tag{3.9}$$

$$\mathrm{M} = 4.07 + 0.98 \log \mathrm{A} \tag{3.10}$$

where A is the area of each segment, and the seismic moment, M_o represents the meaningful physical relationship between the size of earthquake and rupture parameters which is defined as:

$$M_o = \mu\, \bar{D}\, A \tag{3.11}$$

where μ is the shear modulus (3 x 10^{11} dyne/cm^2) assumed to be the same for all segments, and $\bar{D}$ is the average displacement determined from the slip rate ($\dot{D}$) and return period, (Tr) so then the formula becomes:

$$\mathrm{M} = \tfrac{2}{3} \log\ (\mu\, \dot{D}\, Tr\, A) - 10.7 \tag{3.12}$$

3.4 Results and Discussion

3.4.1 Seismicity of Java Region

The earthquake data from the sources mentioned in the methods section consist of 8,269 events and were converted into a magnitude moment scale (Mw) using equation (3.1), (3.2), or (3.3). In this study, the declustering process employed the Reasenberg method using Zmap software [41]. The declustering removed 1,226 earthquake events, resulting in a total of 7,043 events. This new compiled catalog is then plotted in Figure 3.11 based on the depth and magnitude of each earthquake event.

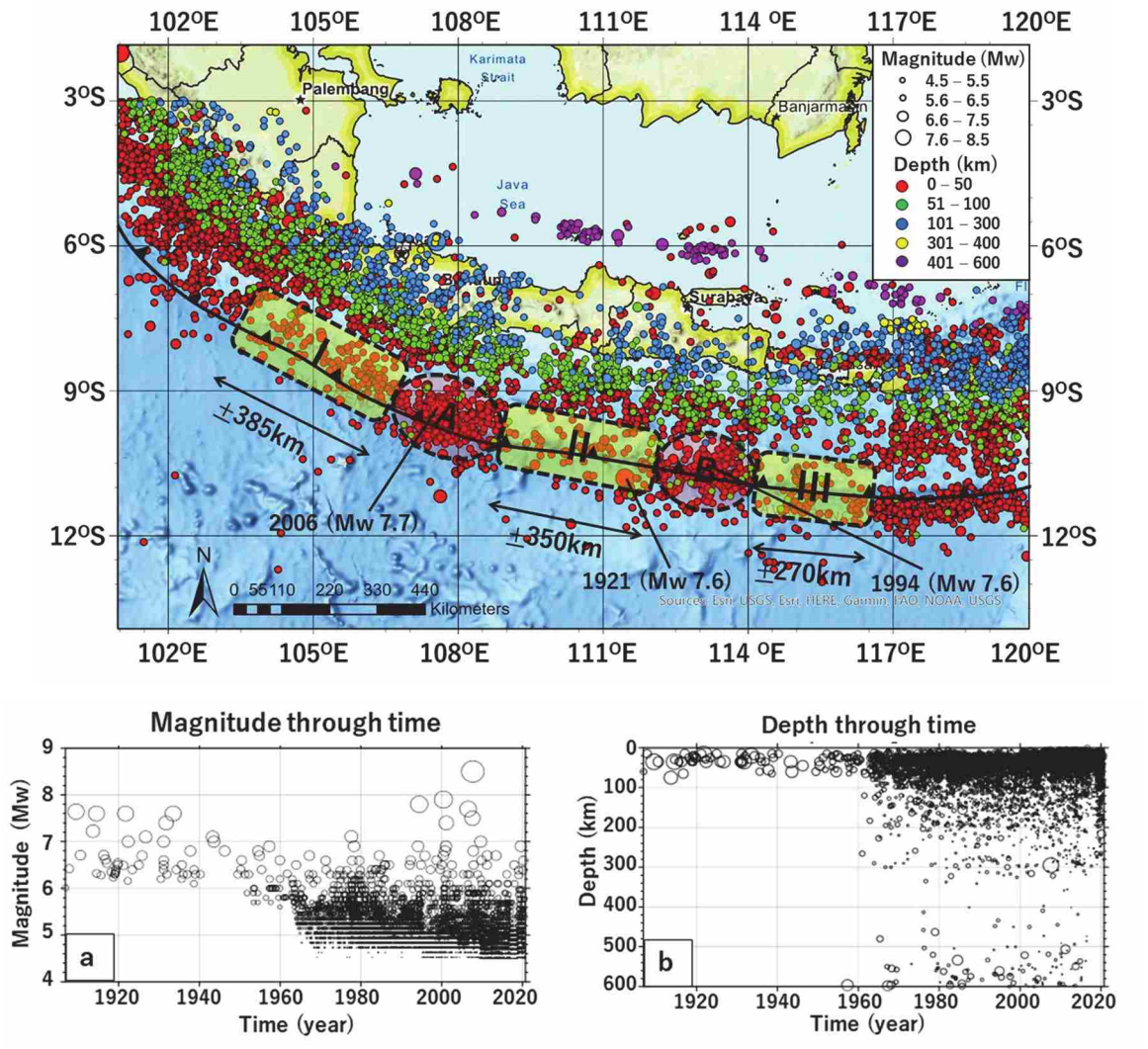

(a) Earthquake depth by time; (b) Earthquake magnitude by time

Figure 3. 11 Earthquake catalog of Java Island and adjacent region period 1906 to September 2020 with magnitude Mw≥4.5

The earthquakes distribute along plate junctions had decreased within the year of 2011-2016 but it risen again after 2017, even until 2020 the trend remained significantly upward up to magnitude of 7.0. Meanwhile, earthquake data obtained before year of 1965 were large earthquakes with a magnitude of Mw $\geq$ 5.5. This was because of the limited instrument capability to record the earthquake data with a smaller magnitude. Even before 1950, the recorded earthquakes were those with a magnitude greater than Mw 6.0. Moreover, the history of the earthquakes with a depth of > 100 km can only be recorded after 1960. Based on these earthquake distribution data, it can be said that the recording of earthquake events is getting better after 1965. It can also be seen from the figure that shallow earthquakes dominated with a depth of $\leq$100 km. However, there are only a few earthquakes that occur at a depth of 300-500km. Besides, several earthquakes recorded up to a depth of 600 km. The earthquake event plot presented in Figure 3.11 also reveals the two densely inhabited earthquake epicenter locations (A and B area). In the A area, there was an experience of major earthquake in 2006 with a magnitude of Mw 7.7, while in the B area, an earthquake occurred in 1994 (Mw 7.6), both of which were followed by a tsunami. On the contrary, there are seismic gap areas in the south coast of Java and its adjacent regions, which are indicated by yellow shaded areas (I, II, and III) extending about 385km, 350km, and 270km long, respectively.

In the seismic gap zone II, there is a large earthquake occurred in 1921 (Mw 7.6). The earthquake in 1921 was in the outer-rise zone, which was also followed by a tsunami recorded at Cilacap. Some earthquakes occurred in the immediate vicinity of the Java trench or commonly known as outer-rise earthquakes. Almost all the outer-rise earthquakes took place along the uppermost part of the subduction interface are shallow earthquakes with a depth of not more than 50km; only a few of them are up to 100km. Seismic gap zones I and III, which are 385km and 270km long are also essential to be considered, especially in the modeling of earthquake and tsunami analysis. The existence of these seismic gaps indicates the accumulation of earthquake energy, thus providing the possibility of large earthquakes in the future. Some simulations using the worst-case scenarios will be beneficial for disaster mitigation efforts.

3.4.2 Dip Angle of Subduction Zone

In order to obtain more detailed information about the mechanism and characteristics of the Indo-Australian plate subduction, which forces the Eurasian plate and affects the geological conditions of Java Island, we carried out a seismicity cross-section. A total of 18 cross-sections (CS) were created along the Java trench and adjacent regions based on the epicenter data mapped to a depth of 600km. Each cross-section describes the distribution of earthquake events, subduction dip angle, and earthquake depth per segment, which is presented in Figure 3.12 and Figure 3.13

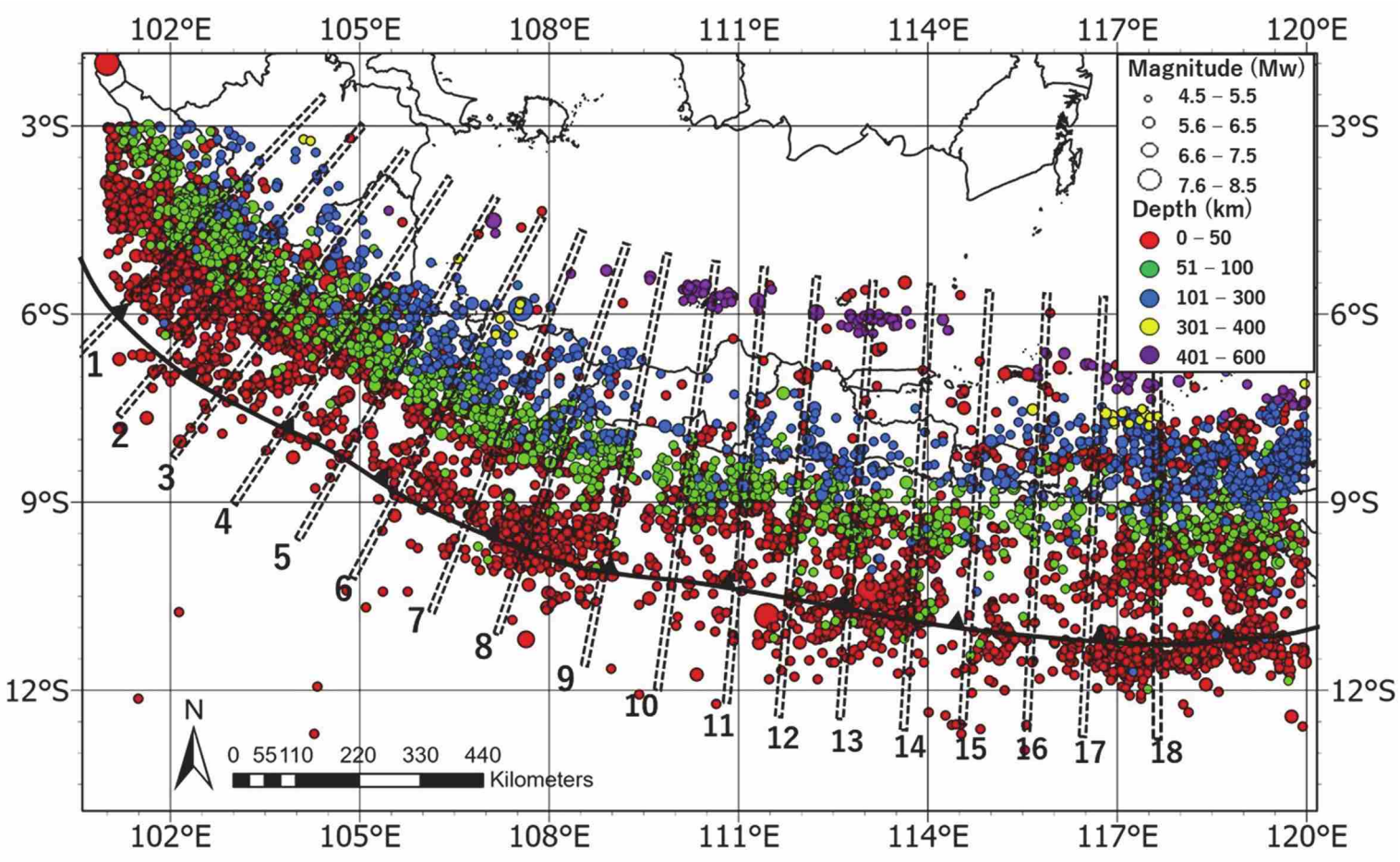

Figure 3. 12 Earthquake epicenter distribution and cross-section along Java trench

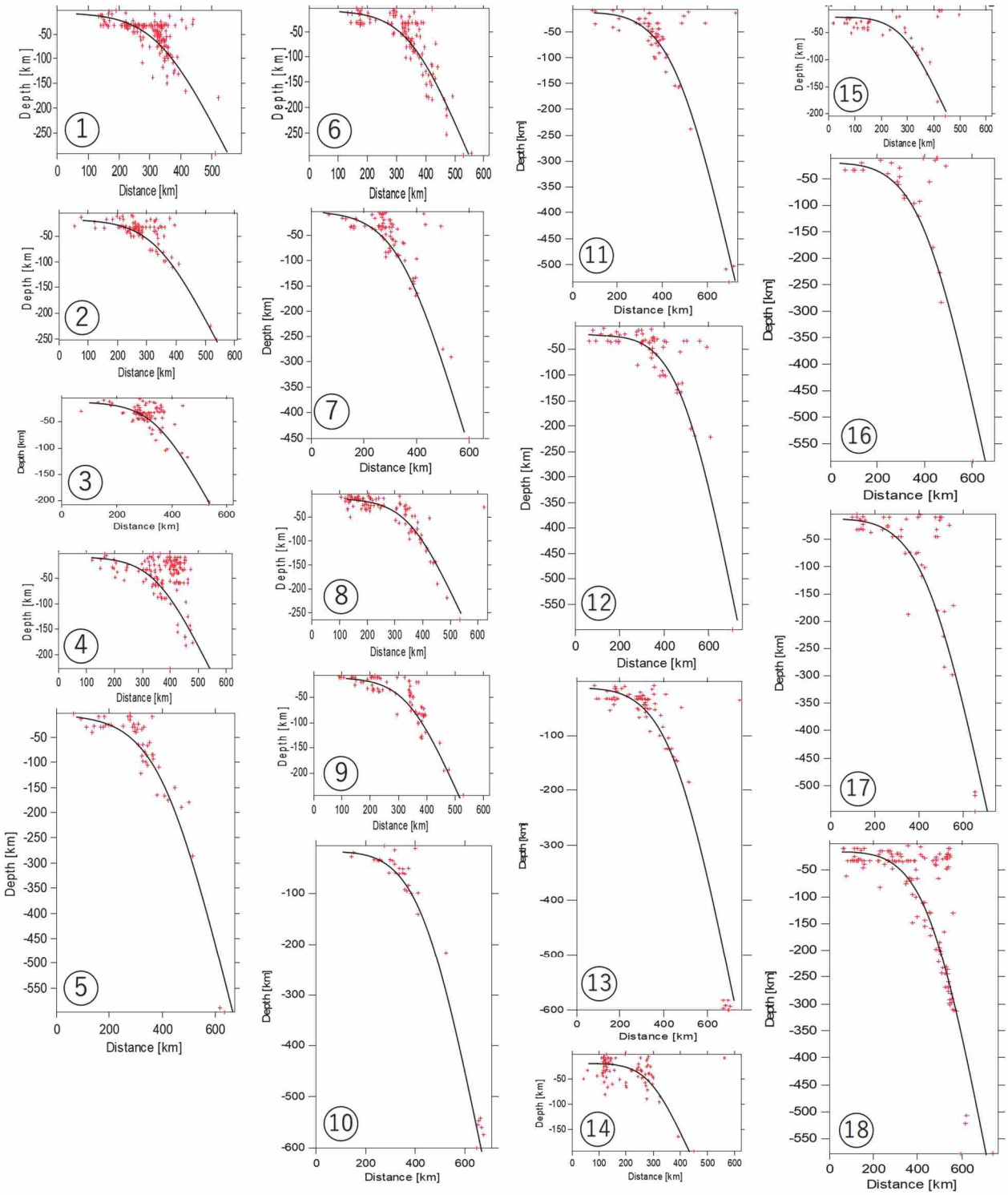

Figure 3. 13 Result of earthquake distribution cross-sectional along Java and its vicinity

Based on the cross-section results, it is found that the subduction dip angle on the southern side of South Sumatra (CS 1-4) is more gentle than the southern subduction angle in Java Island, which is around 12º-13º for the interplate zone and 40º-42º for the intraplate zone. It can also be seen in CS 1-4 that the earthquakes occurring in the southern part of

Sumatra are less than 300 km deep. Meanwhile, the subduction angle under the island of Java ranges from 13° to 14° for the interplate zone and from 43° to 47° for the intraplate zone. It can also be seen from CS 5-14 that the earthquakes in Java reached a depth of up to about 600 km. Deep earthquakes began to occur at the location of the Sunda strait to the east. This is related to the age of the submerged crust under southern Sumatra, which is younger than Java (Figure 3.3). In addition, the seafloor age is correspondingly older to the east, leading to a larger dipping angle of subduction. This result ties well with previous studies wherein the oceanic crust under Java is heavier, making it sinks more easily [42], indicating that the dip angle of subduction in this area is larger than that in the Sumatra trench. For Bali and Sumbawa regions, the dip angle of the subduction zone is relatively smaller than Java but greater than the southern side of South Sumatra, which is 42-44° (CS 15-18). Moreover, the depth of earthquakes reached up to 600km. The earthquakes with a depth of up to 600 km are in the northern regions of Central Java, East Java, and Bali-Sumbawa.

3.4.3 Spatial Variations of a-b Value for Java Region

In investigating the seismic activity rate and frequency-magnitude distribution of Gutenberg-Richter relation, we conducted the calculation of a-values and b-values in detail using grid cell of 0.1°x 0.1° using equation (3.4), (3.5), and (3.6). These a-values and b-values were calculated based on the earthquake data from the earthquake catalog between 1906 and September 2020. This study used Zmap software to compute the spatial variation of a-value and b-value for the study area with a constant radius of 100km. The spatial variation of a-value and b-value are displayed in Figure 3.14.

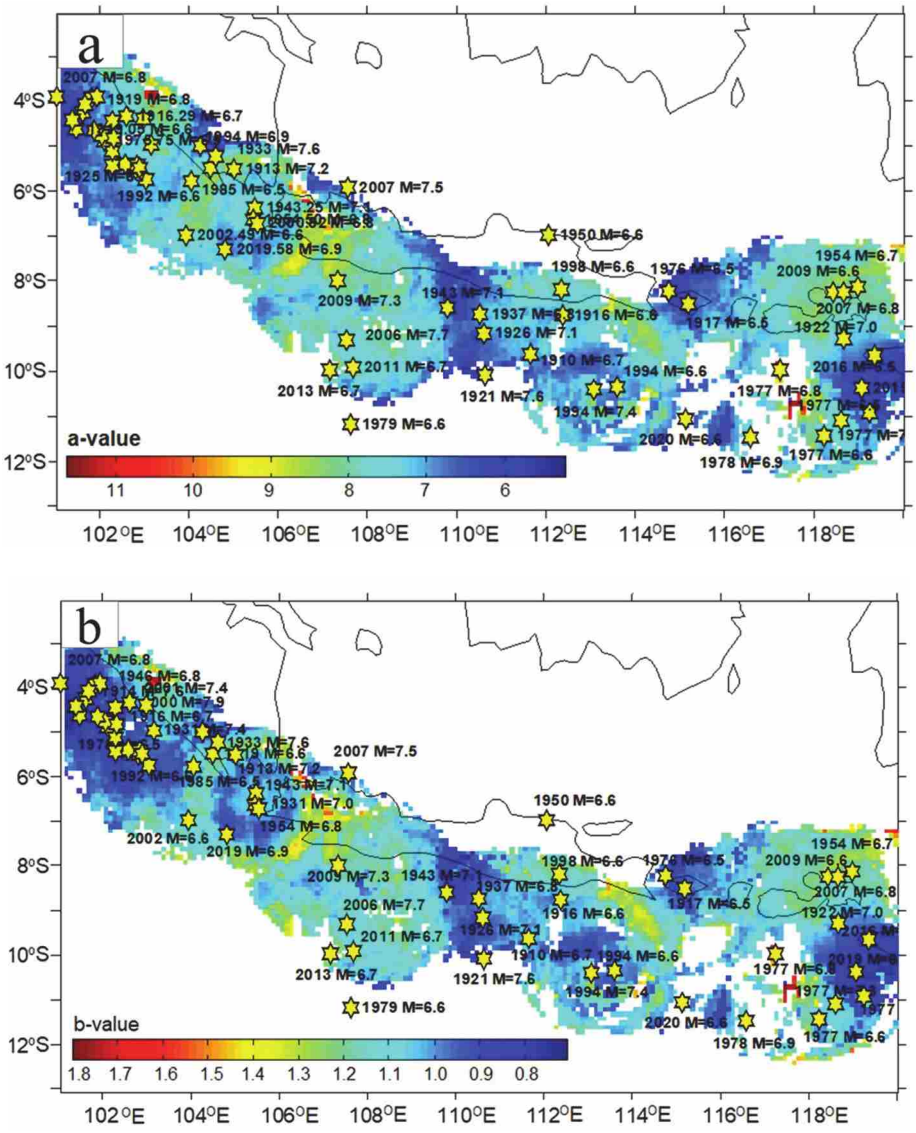

Figure 3. 14 Spatial a-value and b-value variation of Java and adjacent region
(a) a-value (b) b-value

The picture reveals a similar pattern of a-value and b-value along the Java trench and the surrounding area. The region with a low a-value corresponds to a low b-value region. The spatial variation of a-value ranges from 5 to 12, while the b-values range from 0.7 to 1.8. In general, the a-values and b-values in the southern part of Sumatra are dominated by dark blue color, indicating low a-values and b-values. In the western part of Java, the b-value is around 0.8 to 1.3. There are several points with b-value of up to 1.5 in the north-west of Java, which is correspondingly smaller to the center region and larger to the southern part of Bali-Sumbawa. The yellow stars marking the large earthquakes of Mw > 6.5 are predominantly located in relatively low a- and b-value regions. The lower b-value indicates the higher stress in an earthquake source zone.

3.4.4 Subduction segmentation

To identify the seismicity of the subduction zone in more detail, we developed the segmentation model from previous research [43]. In the previous research, the subduction zone considered was only in the southern part of southern Sumatra to the south of Central Java and parts of East Java because the research area was taken up to a radius of 500 km from the Special Capital Region of Jakarta. In this study, the subduction zone along the Java trench and adjacent regions was considered. In addition to the cross-sectional Java subduction results with more complete earthquake data which a relocation process using a teletomo-3D model, the modeling of the subduction segmentations is based on the coupling model of the GPS inversion by Widiyantoro et al. 2020 [15] for the central and eastern part of Java and GPS inversion by Hanifa et al. 2014 [44] for western part of Java as shown in Figure 3.15 and Figure 3.16.

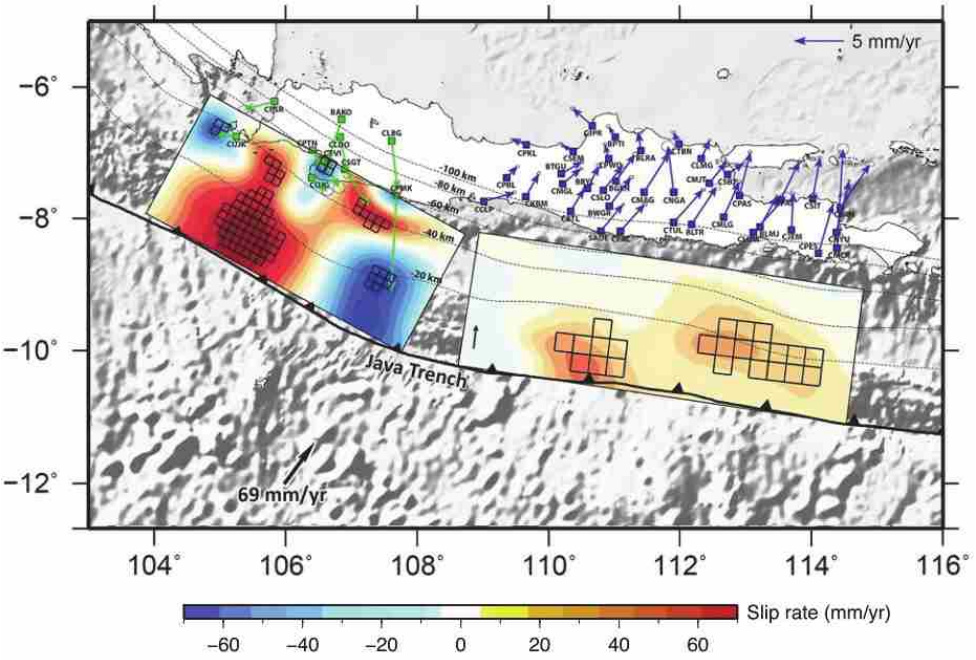

Figure 3. 15 Interplate coupling model and slip deficit/excess rate based on GPS data for the southwest and southeast coast of Java [15, 44]

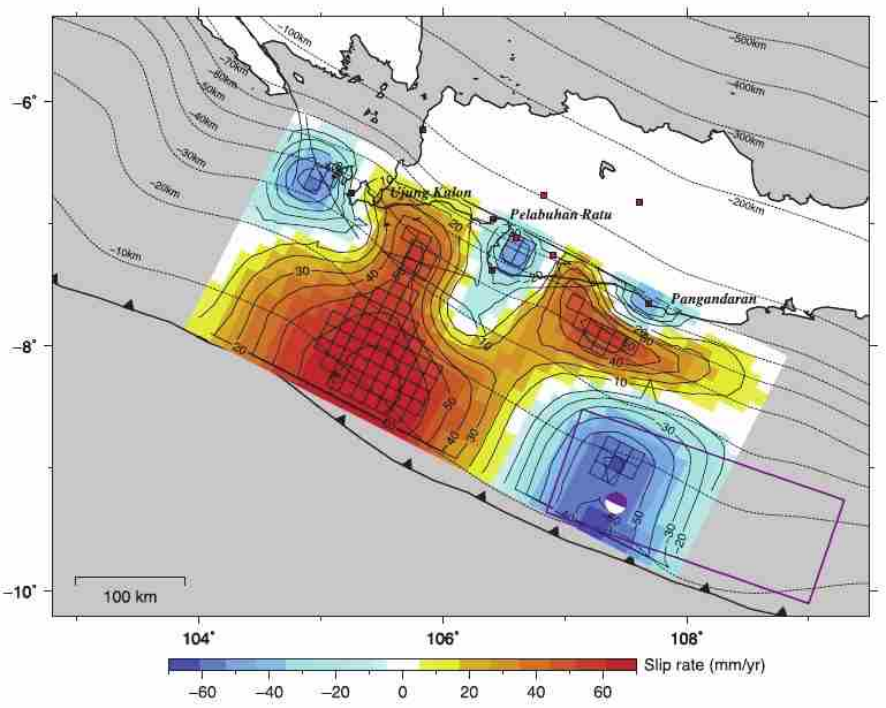

Figure 3. 16 Interplate coupling model and slip deficit/excess rate based on GPS data for the southwest coast of Java [44]

Figure 3.15 and Figure 3.16 show the result of the slip deficit/rate estimation distribution based on the GPS baseline change rates and vertical components. The estimated slip deficit/excess rate ranges from −63 to 75 mm/yr, with uncertainty from 40 to 80 mm/yr. Positive and negative values (shown by red and blue colors, respectively) indicate slip deficit and slip excess, respectively. The result clearly shows a heterogeneous distribution of slip deficit/excess in both the strike and dip directions.

Due to the limited number of GPS sites, the estimated error of the slip is rather large. However, the significant slip (slip magnitude larger than the estimation error) as is marked by thick black lines were obtained. The earthquake epicenter distribution of Java and its surrounding were plotted on the slip deficit/excess map as shown in Figure 3.17. It is found that the pattern of slip deficit/excess zone is well match with the earthquake distribution.

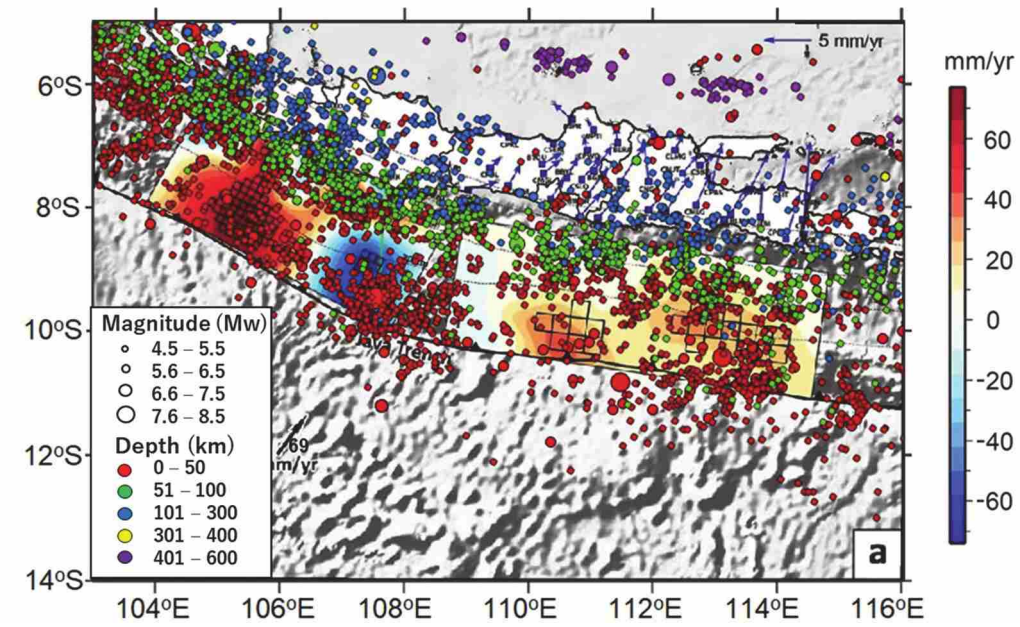

Figure 3. 17 Slip deficit/excess rate along the Java Trench generated using GPS data with the epicenter distribution of this study. Left model provided in [44]; Right model created by [15]

The red areas of slip deficit correspond to the segment's location of a-value and b-value of this study that is associated with a low seismic activity and a high stress level in that tectonic zone. Meanwhile, the IE-4 region has the lowest a and b value, while the IE-5 region has a slightly higher a and b value. Although the result for IE-4 region tends to be nearly correlated with the slip deficit map as in [15] (Figure 3.17, right model), the result for IE-5 region is somewhat different. Therefore, further research is required to determine the correlation between earthquake data and GPS data analysis during the same period. Six segments for each interplate and intraplate zone were proposed in this study: eight segments for Java subduction, two segments for the subduction in the south of southern Sumatra, and two segments for Bali-Sumbawa. The frequency-magnitude distribution (FMD) diagram for each segment is shown in Figure 3.18.

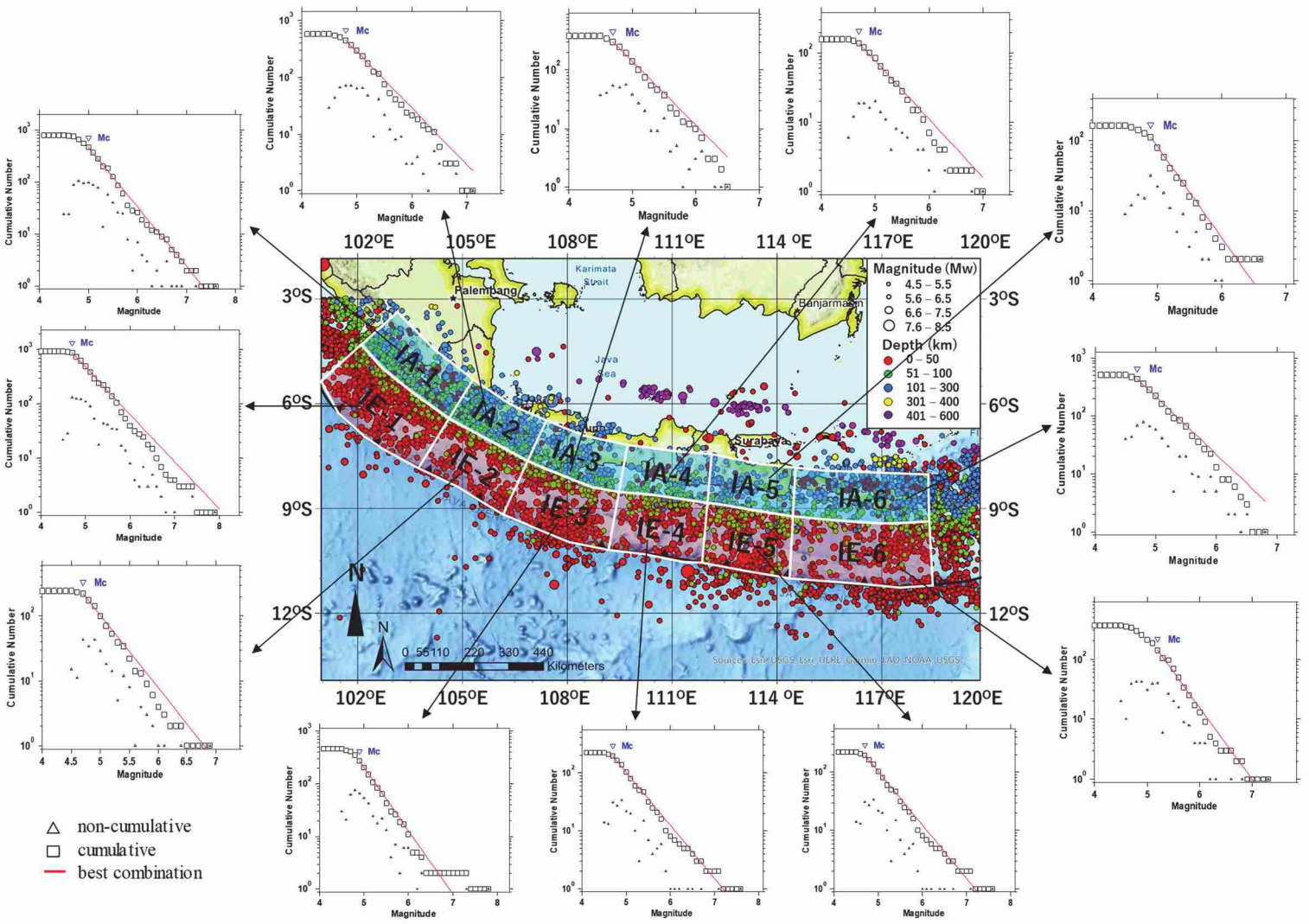

Figure 3. 18 FMD each subduction segments. Earthquake subduction segment modeling are drawn with Arc.GIS Pro, while FMD charts are computed with Zmap. The slope of the line represents the Gutenberg-Richter Law.

The figure shows the variation of cumulative and noncumulative frequency with earthquake magnitude for each subduction segment. The complete recording is indicated by magnitude completeness, Mc. Most of the segments have a value of Mc = 4.7, while the largest Mc value is in the IE-6 segment with Mc = 5.1. It is found in the figures that all the slopes in the FMD diagram are constant after the Mc value, indicating the level of completeness for the instrumental part of the compiled catalog. The slopes of segments IA-4 and IE-1 are relatively gentler, while IA-5, IE-3, and IE-6 have a steeper slope as shown in the FMD diagram. We can observe from the red line that the higher proportion of smaller magnitude events, the steeper the slope of FMD, indicating relatively few numbers of large magnitude events. These patterns follow the Gutenberg-Richter Law as in equation (3.4), which provides the a and b relationship. The a-value and b-value of each subduction segment were computed using equation (3.5) and (3.6). The results of a-value and b-value are provided in Table 3.2.

Table 3. 2 The a-value and b-value of each subduction segment

Subduction zone	Index	Segment	a	α	b	β
Interplate (IE)	IE-1	South Sumatra	4.99	11.49	0.87	2.01
	IE-2	West Java	5.14	11.84	0.94	2.16
	IE-3	West-Central Java	6.52	15.02	1.20	2.76
	IE-4	Central-East Java	4.55	10.48	0.92	2.11
	IE-5	East Java	5.57	12.83	1.06	2.44
	IE-6	Bali-Sumbawa	6.61	15.22	1.20	2.76
Intraplate (IA)	IA-1	South Sumatra	6.32	14.55	1.14	2.63
	IA-2	West Java	5.46	12.57	0.99	2.29
	IA-3	West-Central Java	5.81	13.38	1.09	2.51
	IA-4	Central-East Java	4.18	9.63	0.84	1.94
	IA-5	East Java	6.46	14.88	1.31	3.02
	IA-6	Bali-Sumbawa	5.33	12.27	1.00	2.30

The results clearly show that the a-values for twelve subduction segments vary from 4.18 to 6.61 and b-values are between 0.84 and 1.31. These findings are somewhat different from those of [45], which stated that the a-value and b-value for the subduction zone of Java Island are 7.39 and 1.28, respectively. However, these results are in agreement with the research conducted in the last 5 years by [46, 47] although globally the b-value is ~ 1 for a seismically active region [48]. In more detail, the highest a-value and b-value of Java subduction interplate segment is in the IE-3 region, which has a steep slope of FMD diagram. It is evident that the steeper the slope, the higher b-value obtained. In contrast, the IE-2 region has a lower a-value and b-value, thus shedding light on the increasing potential for moderate to large earthquakes in this region. To clarify the fault geometry of each segment, we estimated the fractal dimension using the equation (3.7) and (3.8) with the results presented in Table 3.3.

Table 3. 3 Fractal dimension for interplate and intraplate segments

Subduction zone	Index	N (events)	D
Interplate (IE)	IE-1	1,079	2.32 ± 0.03
	IE-2	397	2.24 ± 0.03
	IE-3	606	2.07 ± 0.02
	IE-4	373	2.37 ± 0.02
	IE-5	569	2.13 ± 0.02
	IE-6	517	2.05 ± 0.02
Intraplate (IA)	IA-1	953	2.07 ± 0.02
	IA-2	731	2.25 ± 0.02
	IA-3	527	1.96 ± 0.01
	IA-4	308	2.27 ± 0.02
	IA-5	316	1.54 ± 0.01
	IA-6	667	1.96 ± 0.03

The fractal dimension for six 50enioff50ate segments obtained from $D = 2.05 \pm 0.02$ to 2.37 ± 0.02, while those for intraplate segments are 1.54 ± 0.01 to 2.27 ± 0.02. The D values of 50enioff50ate segments are relatively higher than those of the intraplate ones, indicating that the 50enioff50ate zone has a more complex or irregular fault geometry. In general, the fractal dimensions and b-values of Java subduction segments show a negative

correlation. The highest D value is in the Central-East Java segment (IE-4 and IA-4) which also has the lowest b-value. These values are relatively higher than the results from [1], but smaller than the results stated in [49].

3.4.5 Maximum Magnitude

In estimating the maximum earthquake magnitude, the equation (3.9) and (3.10) were applied using the return period from 100 years to 500 years with a calculation per 100 years for equation (3.11) and (3.12). The slip rate of the southern subduction segment of Java used is 4cm/yr [3]. The M_{max} result is presented in Table 3.4, while the comparison graph for each its return period is graphically displayed in Figure 3.19.

Table 3. 4 The maximum magnitude (M_{max}) estimation for interplate and intraplate segments

Subduction zone	Index	Area (m^2)	Mw (Hanks and Kanamori, 1979)					Mw (Wells and Coppersmith, 1994)
			T=100yr	T=200yr	T=300yr	T=400yr	T=500yr	
Interplate (IE)	IE-1	8.09.E+10	8.59	8.83	8.94	9.03	9.09	8.88
	IE-2	5.29.E+10	8.47	8.70	8.82	8.90	8.97	8.70
	IE-3	6.00.E+10	8.50	8.74	8.86	8.94	9.00	8.75
	IE-4	5.48.E+10	8.48	8.71	8.83	8.91	8.98	8.71
	IE-5	5.52.E+10	8.48	8.71	8.83	8.92	8.98	8.72
	IE-6	9.66.E+10	8.64	8.88	8.99	9.08	9.14	8.96
Intraplate (IA)	IA-1	5.92.E+10	8.50	8.74	8.85	8.94	9.00	8.75
	IA-2	4.02.E+10	8.39	8.62	8.74	8.82	8.89	8.58
	IA-3	4.29.E+10	8.40	8.64	8.76	8.84	8.91	8.61
	IA-4	4.28.E+10	8.40	8.64	8.76	8.84	8.91	8.61
	IA-5	4.36.E+10	8.41	8.65	8.76	8.85	8.91	8.62
	IA-6	7.65.E+10	8.57	8.81	8.93	9.01	9.07	8.86

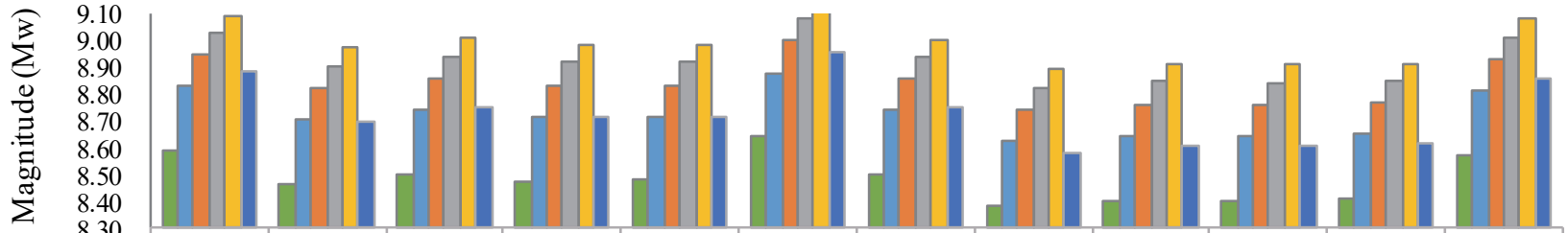

	IE-1	IE-2	IE-3	IE-4	IE-5	IE-6	IA-1	IA-2	IA-3	IA-4	IA-5	IA-6
HK-1979 (100yr)	8.59	8.47	8.50	8.48	8.48	8.64	8.50	8.39	8.40	8.40	8.41	8.57
HK-1979 (200yr)	8.83	8.70	8.74	8.71	8.71	8.88	8.74	8.62	8.64	8.64	8.65	8.81
HK-1979 (300yr)	8.94	8.82	8.86	8.83	8.83	8.99	8.85	8.74	8.76	8.76	8.76	8.93
HK-1979 (400yr)	9.03	8.90	8.94	8.91	8.92	9.08	8.94	8.82	8.84	8.84	8.85	9.01
HK-1979 (500yr)	9.09	8.97	9.00	8.98	8.98	9.14	9.00	8.89	8.91	8.91	8.91	9.07
WC-1994	8.88	8.70	8.75	8.71	8.72	8.96	8.75	8.58	8.61	8.61	8.62	8.86

Figure 3. 19 The comparison between maximum magnitude of two methods

*HK means Hanks and Kanamori method (1979); WC means Wells and Coppersmith method (1994)

Based on the calculation using some scenarios, the Java 54enioff54ate segments have the potential to trigger earthquakes up to magnitude of Mw 8.47-9.00, while the Java intraplate can trigger an earthquake up to magnitude of Mw 8.39-8.91, assuming that all the tectonic energies in those areas were released seismically. The 54enioff54ate segments in southern Sumatra and the southern part of Bali-Sumbawa have higher potential of earthquake magnitude than Java, which are up to Mw 8.59-9.09 and Mw 8.64-9.14, respectively. The results were calculated based on the assumption that all the tectonic energies in the Java trench were released seismically. For the Hanks and Kanamori method, apart from the segment area, the maximum magnitude is influenced by the return period; however, the Wells and Coppersmith formula is more influenced by dimension.

The results of estimated maximum earthquake magnitude using Wells and Coppersmith equation are between the result for a return period of 200 years and 300 years of Hanks and Kanamori method. Referring to the return period used in Indonesian Seismic Sources and Seismic Hazard Maps 2017 (Tr = 400 years) [3], the 54enioff54ate segment in southern Java has the potential to trigger an earthquake with magnitude of Mw 8.90-8.94. Meanwhile, the Bali-Sumbawa subduction segment has potential to trigger earthquake with maximum magnitude of Mw 9.08. Although there has been no earthquake with a magnitude greater than Mw 8.0 occurring along the Java trench, with the mechanism and seafloor age being similar to those in the east-north side of Japan, which triggered the 2011 Tohoku earthquake of Mw 9.0, these results are worth considering. Such findings can also become one of the references for future seismic hazard studies, earthquake and tsunami disaster mitigation plans in Java and its surroundings. All the results of the estimated maximum earthquake magnitude presented can be considered in seismic hazard modeling for subduction earthquake sources based on which scenario will be selected as the earthquake and tsunami simulation approach.

3.5 Conclusion

Located near the confluence of Indo-Australian and Eurasian plates, Java Island and its surroundings are prone to earthquakes. Subduction zones that are long enough with different velocities and seafloor ages show variations in the seismic properties of each segment. This study observed that the dipping angle of the Java subduction zones is steeper than that of Sumatra. This phenomenon is associated with the oceanic crust age submerged

beneath southern Java, which is older than Sumatra.

The spatial variation in a-value and b-value have been mapped. Moreover, these a-b parameters for each subduction segment have been comprehensively presented. It is observed that there is a similar pattern of a-values and b-values. The regions with low b-values relatively fit the large earthquake locations. Based on the subduction zone modeling analysis, the low a-values and b-values are in the south coast of West Java and south coast of Central-East Java. We found that the most significant earthquakes in subduction zone were consistent with relatively high fractal dimension (D values) and low b-values. However, further research is needed to investigate these correlations more appropriately.

For the return period of 100 to 500 years, the Java 55enioff55ate segments have the estimated maximum earthquake magnitude of Mw 8.47-9.00, assuming that all the tectonic energies in those areas were released seismically. Although there has been no earthquake with a magnitude greater than Mw 8.0 occurring along the Java trench, with the mechanism and seafloor age being similar to those in the east-north side of Japan, which triggered the 2011 Tohuku earthquake of Mw 9.0, these results are worth considering. Such findings can also become one of the references for future seismic hazard studies, earthquake and tsunami disaster mitigation plans in Java and its surroundings.

3.6 References

[1] Roy S., Ghosh U., Hazra S., and Kayal J. R., Fractal Dimension and b-value Mapping in the Andaman-Sumatra Subduction Zone, Nat Hazards, Vol. 57, 2011, pp.27–37.

[2] Sieh K. and Natawidjaja D., Neotectonics of the Sumatran Fault, Indonesia, Journal of Geophysical Research: Solid Earth, Vol. 105, Issue B12, 2000, pp.28295-28326.

[3] National Center for Earthquake Studies (PuSGeN) 2017 Indonesian Seismic Sources and Seismic Hazard Maps 2017. Center for Research and Development of Housing and Resettlement, Ministry of Public Works and Human Settlements, (Peta Sumber dan Bahaya Gempa Indonesia Tahun 2017. Pusat Litbang Perumahan dan Pemukiman, Kementerian Pekerjaan Umum dan Perumahan Rakyat) 1–377.

[4] Earth Observatory of Singapore, Nanyang Technological University, Singapore. https://earthobservatory.sg/, accessed 25 March 2020.

[5] Ammon C. J., Kanamori H., Lay, T. and Velasco A. A., The 17 July 2006 Java Tsunami Earthquake. Geophysical Research Letters, Vol. 33, Issue 24, 2006, pp.1-5.

[6] Tsuji Y., Imamura F., Matsutomi H., Synolakis C. E., Nanang P. T., Jumadi, Harada S., Han S. S., Arai K., and Cook B., Field Survey of the East Java Earthquake and Tsunami of June 3, 1994., Pure and Applied Geophysics, Vol. 144, Issue 3, 1995, pp.839-854.

[7] Abercrombie R. E., Antolik M., Felzer K., and Ekström G., The 1994 Java Tsunami Earthquake: Slip Over a Subducting Seamount, Journal of Geophysical Research, Vol. 106, Issue B4, 2001, pp.6595-6607.

[8] Okal E., The south of Java earthquake of 1921 September 11: A negative search for a large 56enioff56ate thrust event at the Java Trench, Geophysical Journal International, Vol. 190, Issue 3, 2012, pp.1657-1672.

[9] Setiyono U., Gunawan I., Priyobudi, Yatimantoro T., Imananta R.T., Ramadhan M., Hidayanti, Anggraini S., Rahayu R.H., Hawati P., Yogaswara D.S., Julius A.M., Apriani M., Harvan M., Simangunsong G., and Kriswinarso T., Catalog of Significant and Destructive Earthquakes 1821-2018, Earthquake and Tsunami Center of BMKG Indonesia., (Katalog Gempabumi Signifikan dan Merusak tahun 1821-2018, Pusat Gempabumi dan Tsunami BMKG Indonesia), 2019, pp.1-278.

[10] Diaz L. P., Regional Geology and Tectonics (Second Edition), Vol. 1: Principle of Geologic Analysis, Chapter 3 – Age of the Oceans, 2020, pp.21-40.

[11] Müller R. D., Sdrolias M., Gaina C., and Roest W. R., Age, Spreading Rates and Spreading Symmetry of the World's Ocean Crust, Geochemistry, Geophysics, Geosystems, Vol. 9, Issue 4, 2008, pp.1-19.

[12] Norio O., Ye T., Kajitani Y., Shi P., and Tatano H., The 2011 Eastern Japan Great Earthquake Disaster: Overview and Comments, International Journal of Disaster Risk Science, Vol. 2, Issue 1, 2011, pp.34-42.

[13] Mimura N., Yasuhara K, and Kawagoe S., Damage from the Great East Japan Earthquake and Tsunami – A quick report, Mitigation and Adaptation Strategies for Global Change, Vol. 16, Issues 7, 2001, pp.803-818.

[14] Hartoko A., Helmi M., Sukarno M., and Hariyadi, Spatial Tsunami Wave Modelling for The South Java Coastal Area, Indonesia. International Journal of Geomate, Vol. 11, Issue 25, 2016, pp.2455-2460.

[15] Widiyantoro S., Gunawan E., Muhari A., Rawlinson N., Mori J., Hanifa N. R., Susilo S, Supendi P, Shiddiqi H. A., Nugraha A. D., and Putra H. E., Implications for Megathrust Earthquakes and Tsunamis from Seismic Gaps South of Java Indonesia. Scientific Reports, 10, 15274, 2020.

[16] Nugraha A. D., Shiddiqi H. A., Widiyantoro S., Thurber C. H., Pesicek J. D., Zhang H., Wiyono S. H., Ramdhan M., and Irsyam M., Hypocenter Relocation along the Sunda Arc in Indonesia, Using a 3D Seismic-Velocity Model, Seismological Research Letters, Vol. 89, Issue 2A, 2018, pp.603–612.

[17] International Seismological Centre, http://www.isc.ac.uk, ISC-EHB data set, International Seismological Centre, 2020, Thatcham, United Kingdom.

[18] Engdahl E. R., Di Giacomo D., Sakarya B., Gkarlaouni C. G., Harris J., and Storchak D. A., ISC- EHB1964–2016, an Improved Data Set for Studies of Earth Structure and Global Seismicity, Earth and Space Science, Vol. 7, Issue 1, 2020, pp.1-13.

[19] Bormann, P., 2002. Magnitude calibration functions and complementary data. In Bormann, P. (ed.), IASPEI New Manual of Seismological Observatory Practice. Potsdam: GeoForschungs Zentrum Potsdam, Vol. 2, DS3.1, pp. 1–7.

[20] Kanamori, H. (1983) Magnitude Scale and Quantification of Earthquakes. Tectonophysics, 93, 185-199.

[21] Utsu, T, (2002), Relationship between magnitude scales, in International Handbook of Earthquake & Engineering Seismology Part A, Eds. W. H. K. Lee, H. Kanamori, P.C.Jennings, and C. Kisslinger (Academic Press, San Diego), 733-746.

[22] Hanks T. C. and Kanamori H., A Moment Magnitude Scale, Journal of Geophysical Research, Vol. 84, Issue B5, 1979, pp.2348–2350.

[23] Gardner J. K, and Knopoff, L., Is the Sequence of Earthquakes in Southern California, with Aftershocks Removed, Poissonian?, Bulletin of the Seismological Society of America, Vol. 64, Issue 5, 1974, pp.1363–1367.

[24] Reasenberg P., Second-order Moment of Central California Seismicity, 1969–1982, Journal of Geophysical Research: Solid Earth, Vol. 90, Issue B7, 1985, pp.5479–5495.

[25] Uhrhammer R. A., Characteristics of northern and central California seismicity, Earthquake Notes, Vol. 57, Issue 21, 1986 (abstract).

[26] Zaliapin I., and Ben-Zion Y., Earthquake Clusters in Southern California I: Identification and Stability, Journal of Geophysical Research: Solid Earth, Vol. 118, Issue 6, 2013, pp.2847–2864.

[27] Zhuang J., Ogata Y., and Vere-Jones D., Stochastic Declustering of Space-time Earthquake Occurrences, Journal of the American Statistical Association, Vol. 97, Issue 458, 2002, pp.369–380.

[28] Teng G. and Baker J. W., Seismicity Declustering and Hazard Analysis of the Oklahoma-Kansas Region, Bulletin of the Seismological Society of America, Vol. 109, Issue 6, 2019, pp.2356-2366.

[29] Ogata Y., Statistical Models for Earthquake Occurrences and Residual Analysis for Point Processes, Journal of the American Statistical Association, Vol. 83, Issue 401, 1988, pp.9–27.

[30] Ogata Y., Space-time Point-process Models for Earthquake Occurrences, Annals of the Institute of Statistical Mathematics, Vol. 50, Issue 2, 1998, pp.379–402.

[31] Susilo A., Hisyam F., and Wasis, Earthquake Analysis in East Java, Indonesia between 1960-2017 using Markov Chain Model, International Journal of Geomate, Vol. 17, Issue 63, 2019, pp.149-156.

[32] Ishimoto, M. and Lida, K. (1939), "Observations sur les seismes enregistres par le microsismographe construit dermement", Bull. Earthquake Res. Inst., Tokyo Univ., 17, 443-478.

[33] Gutenberg B. and Richter C., Frequency of earthquakes in California. Bulletin of the Seismological Society of America, Vol. 34, Issue 4, 1944, pp.185–188.

[34] Aki K 1965 *Bull. Earthquake Res Inst.* Maximum likelihood estimate of b in the formula log N=a-bM and its confidence limits Tokyo Univ. 43 237-239

[35] Utsu T., A method for Determining the Value of b in a Formula log n = a – bM Showing the Magnitude-Frequency Relation for Earthquakes. Geophys. Bull. Hokkaido Univ., Vol. 13, 1965, pp.99–103.

[36] Rohadi S., Grandis H., and Ratag M. A., Studi Variasi Spasial Seismisitas Zona Subduksi Jawa (Study of the Spatial Variation for Java Subduction Zone Seismicity), Jurnal Meteorologi dan Geofisika, Vol. 8, Issue 1, 2007, pp.42-47.

[37] Grassberger P. and Procaccia I., Characterization of Strange Attractors, Physical Review Letters, Vol. 50, Issue 5, 1983, pp.346-349.

[38] Kumar A., Rai S. S., Joshi A., Mittal H., Sachdeva R., Kumar R., and Ghangas, V., The b-value and Fractal Dimension of Local Seismicity around Koyna Dam (India), Earthquake Science, Vol. 26, Issue 2, 2013, pp.99-105.

[39] Hanks T. C. and Kanamori H., A Moment Magnitude Scale, Journal of Geophysical Research, Vol. 84, Issue B5, 1979, pp.2348–2350.

[40] Wells D. L. and Coppersmith K. J., New Empirical Relationships among Magnitude, Rupture Length, Rupture Width, Rupture Area, and Surface Displacement, Bulletin of the Seismological Society of America, Vol. 84, Issue 4, 1994, pp.974-1002.

[41] Wiemer S., A Software Package to Analyze Seismicity: ZMAP, Seismological Research Letters, Vol 72, Issue 3, 2001, pp.373-382.

[42] Berggren W. A., Kent D. V., Flynn J. J., and Van Couvering J. A., Cenozoic Geochronology, Geological Society of America Bulletin., Vol. 96, Issue 11, 1985, pp.1407-1418

[43] Muntafi Y., Widodo, and Makrup L., Analisis Hazard Gempa DKI Jakarta Metode Probabilistik dengan Pemodelan Sumber Gempa 3 Dimensi (Seismic Hazard Analysis of Jakarta Special Region using Probabilistic Method with 3-Dimensional Earthquake Sources Modeling), Teknisia, Vol. XX, Issue 2, 2015, pp.85-95.

[44] Hanifa N. R., Sagiya T., Kimata F., Efendi J., Abidin H. Z., and Meilano I., Interplate Coupling Model off The Southwestern Coast of Java, Indonesia, based on Continuous GPS data in 2008-2010. Earth and Planetary Science Letters, Vol. 401, 2014, pp.159-171.

[45] Ashadi A. L., Harmoko U., Yuliyanto G., and Kaka S. I., Bulletin of the Seismological Society of America, Vol. 105, Issue 3, 2015, pp.1711–1720.

[46] Nugraha A. D., Shiddiqi H.A., Widiyantoro S., Sutiyono., and Handayani T., Analysis of Spatiotemporal Variation in b-value for the Sunda Arc using High Precision Earthquake Location, AIP Conference Proceedings, Vol. 1730, Issue 1, 2016, pp.1-6.

[47] Suananda Y. I. B., Aufa I., and Harlianti U. Identifying Intraplate Mechanism by b-value calculations in the South of Java Island, IOP Conferences Series: Earth and Environmental Science, Vol. 132, 012032, 2018, pp.1-7.

[48] Stein S. and Wysession M., An Introduction to Seismology, Earthquakes, and Earth Structure, Geological Magazine, Vol. 140, Issue 6, 2003, pp. 733-734.

[49] Nugroho H. A., Joelianto E., and Puspito N. T., Characteristic of Earthquake Occurrences based on Chaotic Analysis and Fractal Dimension, Conference proceedings, IEEE Conference on Control, Systems and Industrial Informatics, 2012, pp. 208-213.

Chapter 4
Seismic Site Coefficient for Malang and Yogyakarta Region

4.1 Introduction

Malang and Yogyakarta are big cities in Java Island which prone to earthquake. Malang is one of the most densely populated areas in East Java after Surabaya with a population density of 752 people/km^2 [1]. The devastated earthquake hit the Malang region on April 10, 2021, with a magnitude of Mw 6.1 at coordinates 8.84°E and 112.47°S and a depth of 86km. The earthquake caused by the subduction activity showed a thrust fault mechanism which resulted in fatalities and severe building damage [2]. This earthquake was also felt in several areas of East Java with the intensity between II and VII MMI scale. The isoseismal map of the Malang earthquake is depicted in Figure 4.1.

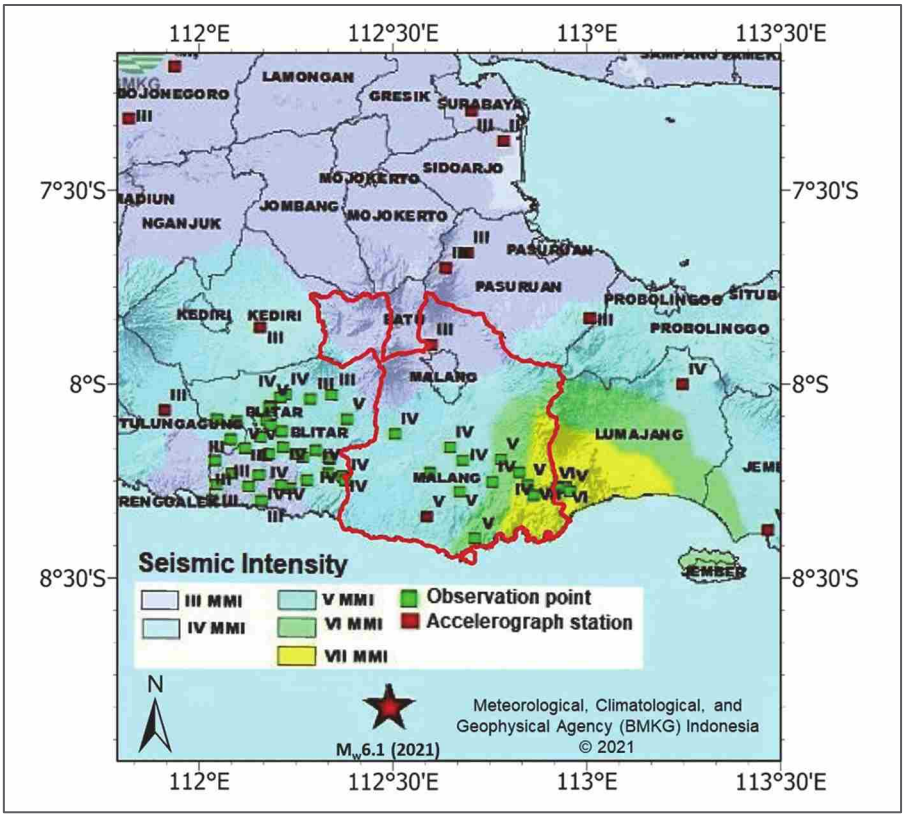

Figure 4. 1 Isoseismal map of the 10 April 2021 Malang earthquake based on MMI scale [3]

The seismic intensity map conducted by BMKG [3] showed that the Malang region felt the earthquake with an intensity of V MMI scale, which means that the earthquake was almost felt by all residents. Lumajang region has the highest earthquake intensity compared to other regions, with an intensity scale of VII MMI. Based on data from the Regional Disaster Management Agency (BPBD) [4], the earthquake resulted in 4 deaths and 110 injuries, more than 10,400 houses were damaged, and over 640 public facilities were destroyed. The number of fatalities and building damages in more detail are presented in Figure 4.2.

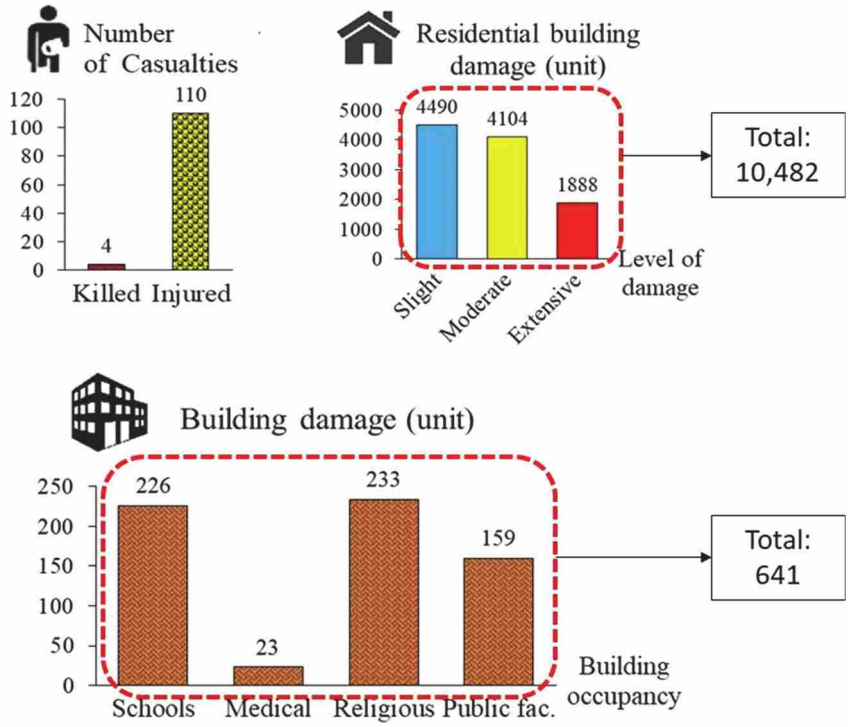

Figure 4. 2 Losses and casualties due to the 2021 Mw6.1 Malang earthquake

The mitigation effort is crucial to minimize the earthquake disaster risk. Several studies related to seismicity in the Malang region have been carried out, such as the research conducted by [5-7]. However, the study related to the evaluation of tectonic parameters (b-value) and specific earthquake analysis involving the 2021 M6.1 Malang earthquake has not been available yet. Whereas the spatial and temporal variation of the b-value is regarded as crucial clues for the future major earthquake precursors [8]. Similar to Malang, Yogyakarta is one of the regions in Java Island with a high populated density observed to have suffered a severe devastating earthquake on May 27, 2006, with a magnitude of Mw6.3. The tectonic

setting of Yogyakarta is quite similar to that of Semarang, Indonesia, which has an active fault near that city. The Opak fault is located around Bantul and Gunung Kidul district with a length of 45km and strike-slip 60E. In the northern part of Yogyakarta there is Mt. Merapi, while in the southern part of Yogyakarta region is the Indian Ocean where the Australian Plate moves towards the north and subduction occur approximately 250 km south of the coastal region as presented in Figure 4.3.

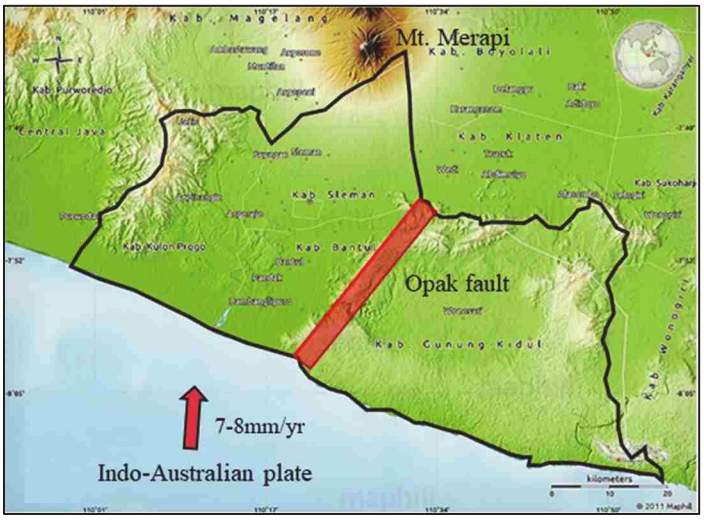

Figure 4. 3 Opak fault and physical map of Yogyakarta region

The 2006 Yogyakarta earthquake with 6.3 Mw or 5.9 Mb was a destructive earthquake that caused thousands of casualties in Yogyakarta Province. Elnashai et al. [9] provided data that more than 5,700 people were killed, whilst the injury list exceeded 37,000. Over 156,000 houses and other structures were extensively destroyed. Total published economic losses were estimated to be over $3B; it is highly likely that this number considerably under-estimates the economic impact. Based on the focal mechanism data from USGS, the 2006 Yogyakarta earthquake was caused by a strike-slip fault earthquake with the dip of 87^{o} and slip of 3^{o}. The seismotectonic analysis showed that this fault is a horizontal fault to the left (sinistral strike-slip fault). As a preliminary study, the damage probability assessment of hospital buildings as essential facility in Yogyakarta region was conducted using the 2006 Yogyakarta earthquake scenario using the deterministic method. The location of each building is presented in Figure 4.4. The building investigated categorized based on the 36 model types following the HAZUS-99 methodology described in FEMA 178 classification system, NEHRP Handbook for the Seismic Evaluation of Existing Buildings [10].

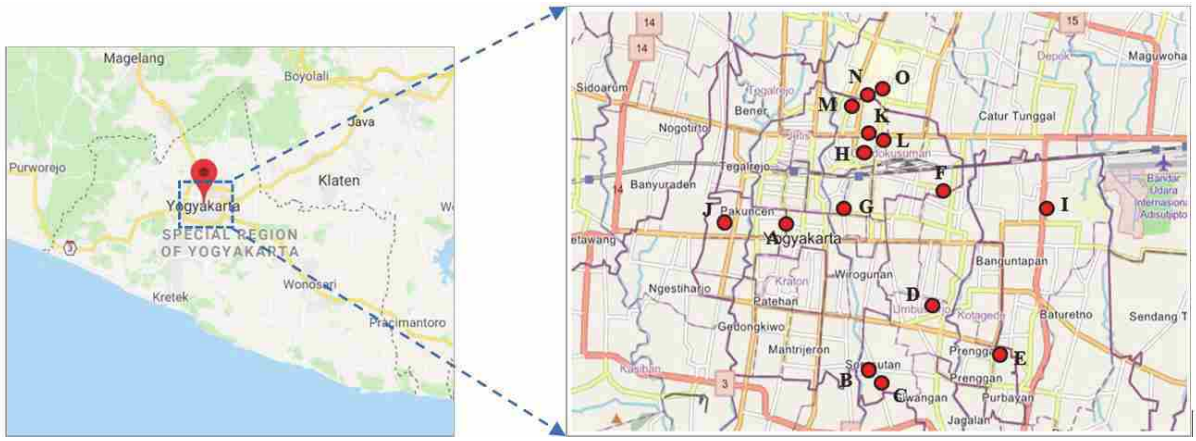

Figure 4. 4 Location of each investigated building

Based on the evaluation using the 2006 Yogyakarta earthquake scenario, the closest distance to the epicenter for buildings with the same model type was determined to have the highest damage values. In addition, other major parameters involved in this appraisal include the height of the building story and the seismic or construction design standards used. Particularly, the fragility curves show a combination of low seismic design level, high building story, proximity to the epicenter and high damage possibility. Considering the new Indonesian Seismic Design Building code (SNI 1726:2019) [11] and the new identified faults presented in Indonesian Seismic Sources and Seismic Hazard Maps 2017 [12], it is essential to develop the seismic site coefficient maps for the specific Yogyakarta region in order to obtain the more appropriate seismic resistant building design.

This study addresses these gaps by investigating the b-value of Gutenberg-Richter Law relating to the tectonic condition of the study area and generating a microzonation of spectral acceleration maps for the Malang and Yogyakarta region and creating the seismic coefficient map for short period, Fa (0.2s) and long period, Fv (1.0s). The findings of this study are expected to be one of the references in earthquake disaster mitigation efforts, spatial-building planning and building design in Malang and surrounding areas.

4.2 Data and Method

This study begins with the earthquake data collection from the national and international earthquake catalogs, continued by converting the magnitude to a uniform magnitude (Mw) and processing dependency analysis using Reasenberg (1985) method [13]. The seismic activity and magnitude distribution are then observed. The seismic sources were

then investigated and modeled into the appropriate subduction segmentation and faults. The next step is characterizing the seismic source parameter and selecting the suitable GMPE models considering the earthquake mechanism. The seismic hazard analysis used the Logic tree model in considering the epistemic uncertainty to obtain the spectral acceleration value at each bedrock and ground surface. The seismic site coefficient in each site location can be derived from the ratio of the hazard at ground surface (H_S) and the hazard at bedrock (H_R). All methods and stages of analysis used in this study are described in more detail in the following sub-chapters.

4.2.1 Earthquake data

The data used in this study is earthquake data for the Malang specific region covering coordinates of 7.5 – 10°S and 112-113.5°E from January 1962 to July 2021. Meanwhile, for generating the microzonation maps, earthquake data was taken covering an area within 500km radius from the Malang region with magnitude Mw≥4.5 and a maximum focal depth of 300km. The earthquake data were obtained from the national earthquake catalog (the Meteorological, Climatological, and Geophysical Agency, BMKG) and international earthquake catalogs such as the International Seismological Center – Engdahl, van der Hilst and Buland (ISC-EHB) and the United States Geological Survey (USGS). The earthquake data compilation was then homogenized into the Moment magnitude (M_w) scale, which is commonly used in the seismology field. Conversion from body-wave magnitude (m_b) and surface-wave magnitude (M_s) to M_w scale was carried out using the equations in Table 4.1.

Table 4. 1 Conversion relation for mb, Ms, and Mw [14]

Conversion relation	Magnitude range	Standard Error (SE)	Consistency (R^2)
$M_w = 1.0332m_b - 0.0834$	$3.2 \leq m_b \leq 8.2$	0.238	0.802
$M_w = 0.6354M_s + 2.3115$	$3.1 \leq M_s \leq 6.3$	0.158	0.856
$M_w = 1.0425M_s - 0.2812$	$6.4 \leq M_s \leq 8.7$	0.193	0.849

4.2.2 Earthquake Source Modeling and Seismic parameter

The earthquake sources used in this study are subduction earthquakes sources and shallow crustal faults within a radius of 500km from Malang and Yogyakarta,

respectively. The earthquake fault sources used for Yogyakarta region were 14 faults (Cimandiri, Nyalindung-Cibeber, Rajamandala, Lembang, Subang, Ciremai, Cirebon, Brebes, Semarang, Pati trust, Opak, Cepu, Waru, and RMKS-East). Meanwhile, the source of subduction earthquakes divided into four 66enioff66ate and four intraplate segments followed the previous research [14] is shown in Figure 4.5. For Malang region, the subduction zone was divided into five 66enioff66ate segments and five intraplate segments, while the fault sources used were 12 faults (Ciremai, Cirebon, Brebes, Semarang, Pati trust, Opak, Cepu, Waru, RMKS East, Bali, Lombok Central and Lombok North fault) which are presented in Figure 4.6. The parameter for each fault sources followed the data from National Research for Earthquake Studies (PuSGeN) and some related research, which are shown in Table 4.2, while the parameter for subduction segment is presented in Table 4.3.

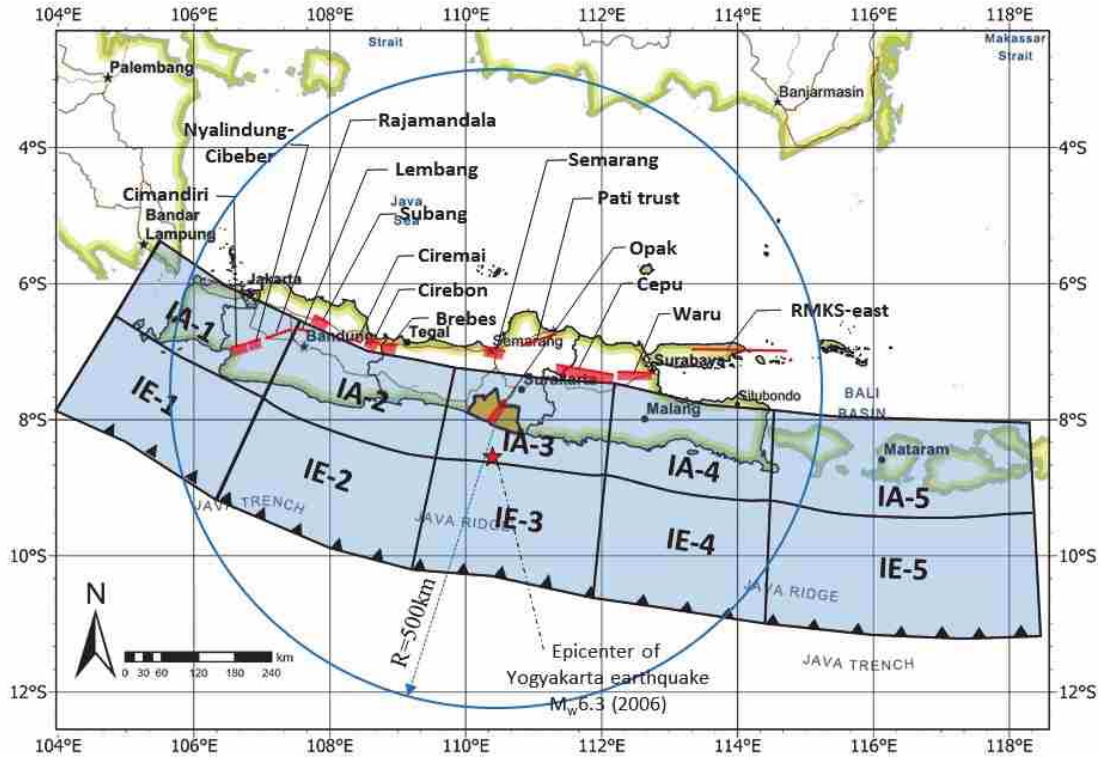

Figure 4. 5 Shallow crustal faults and subduction segmentation for Yogyakarta region

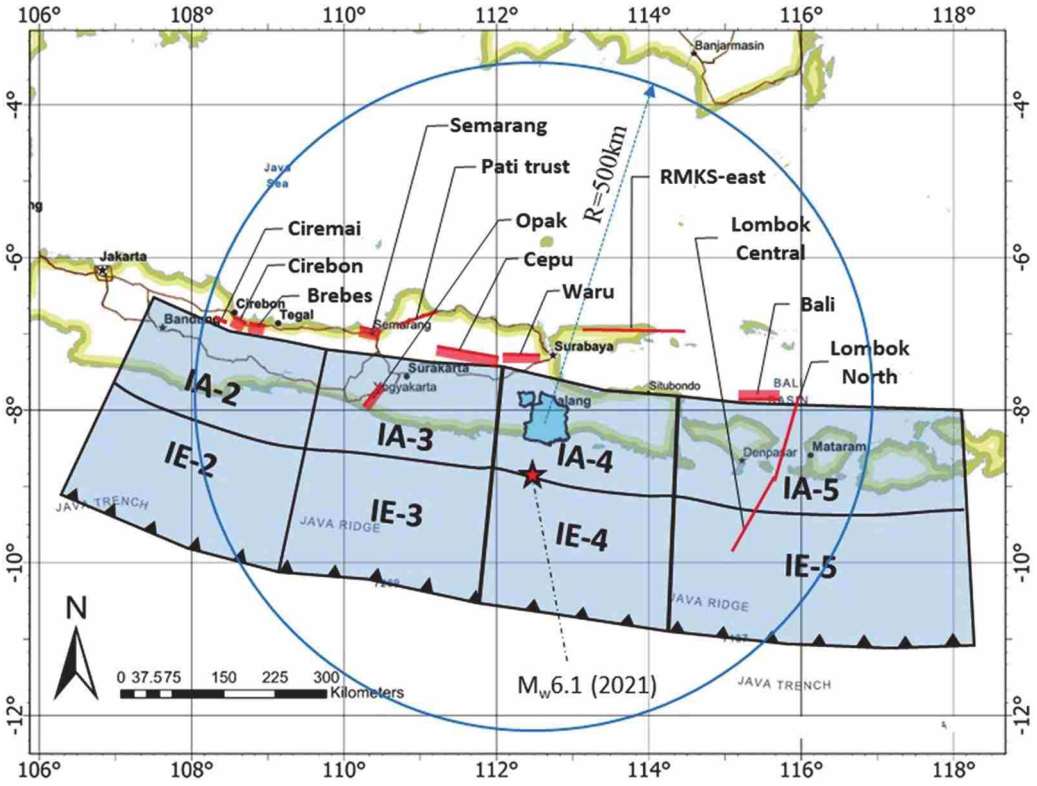

Figure 4. 6 Shallow crustal faults and subduction segmentation for Malang region

Table 4. 2 The shallow crustal fault and its parameters

No.	Fault	Source mechanism	Length (km)	Dip	Slip rate (mm/yr)	M_{max}
1	Cimandiri	Reverse-slip	23	45S	0.55	6.7
2	Nyalindung-Cibeber	Reverse-slip	30	45S	0.4	6.5
3	Rajamandala	Strike-slip	45	90	0.1	6.6
4	Lembang	Strike-slip	29.5	90	2	6.8
5	Subang	Reverse-slip	33	45S	0.1	6.5
6	Ciremai	Strike-slip	20	90	0.1	6.5
7	Cirebon-2	Reverse-slip	18	45S	0.1	6.5
8	Brebes	Reverse-slip	22	45S	0.1	6.5
9	Semarang	Reverse-slip	34	45S	0.1	6.5
10	Pati Trust	Strike-slip	69	90	0.1	6.5
11	Opak	Strike-slip	45	60E	0.75	6.6
12	Cepu	Reverse-slip	100	45S	0.1	6.5
13	Waru	Reverse-slip	64	45S	0.05	6.5
14	RMKS East	Strike-slip	230	90	1.5	7.8

Table 4. 3 The subduction segment and its parameters

Subduction zone	Index	Segment	a	b	M_{max}
Interplate (IE)	IE-1	West Java	5.29	0.94	8.9
	IE-2	West-Central Java	5.87	1.06	8.94
	IE-3	Central-East Java	5.01	1.02	8.91
	IE-4	East Java	6.91	1.26	8.92
	IE-5	Bali-Sumbawa	6.35	1.11	9.08
Intraplate (IA)	IA-1	West Java	5.62	1.02	8.82
	IA-2	West-Central Java	6.02	1.12	8.84
	IA-3	Central-East Java	4.28	0.87	8.84
	IA-4	East Java	6.26	1.27	8.85
	IA-5	Bali-Sumbawa	5.35	0.98	9.01

The stress level related to the tectonic condition or rock fragility in seismology field is expressed by the b-value parameter. The seismicity pattern of an area can be determined by analysing the relationship between frequency and magnitude is described in the Gutenberg-Richter equation [15]:

$$log\ N = a - b\ M \qquad \text{or} \qquad N = e^{\alpha - \beta M} \tag{3.6}$$

where N is the number of earthquakes with magnitude $M \geq M_o$, a and b are constants. The a-value express the seismic activity, while b-value represents the earthquake distribution related to tectonic condition. The b-value shows the gradient of the linear equation of the frequency and magnitude relationship. This constant is related to tectonic conditions and rock properties that can describe local stress activity. The b-value is an earthquake parameter that measures the accumulation of stress in rocks. The low b-value is associated with the high shear stress, and vice versa [16]. The estimated b-value is calculated using the simple form provided by Aki-Utsu [17, 18] with the following equation:

$$b = \frac{1}{\bar{M} - M_o} log_{10} e \tag{3.7}$$

The a-value was estimated using the formula of Wekner, 1965 in [19] as follows:

$$a = \log N(M \geq M_o) + \log(b \ln 10) + M_o\, b \tag{3.8}$$

where $\bar{M}$ denotes the average magnitude and M_o is the minimum threshold for the earthquake data magnitude considered, in which we used the magnitude completeness, *Mc* parameter.

4.2.3 Soil Condition

The local soil conditions of Malang and Yogyakarta region are varied. In this study, the shear wave velocity (Vs30) data were used to determine the soil classification in Malang and Yogyakarta region. The Vs30 data were obtained from USGS document covered the entire Malang and Yogyakarta region in each one kilometer grid. The Vs30 data were then displayed to the Vs30 map using ArcGIS Pro 2.8 as shown in Figure 4.7 and Figure 4.8.

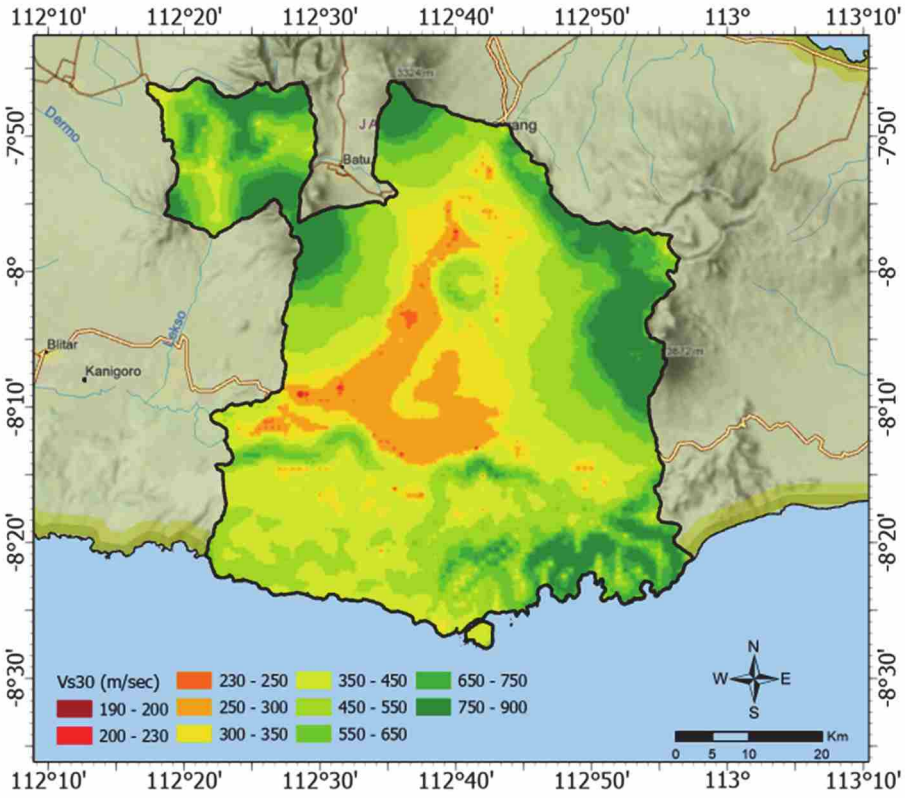

Figure 4. 7 Vs30 map of Malang region

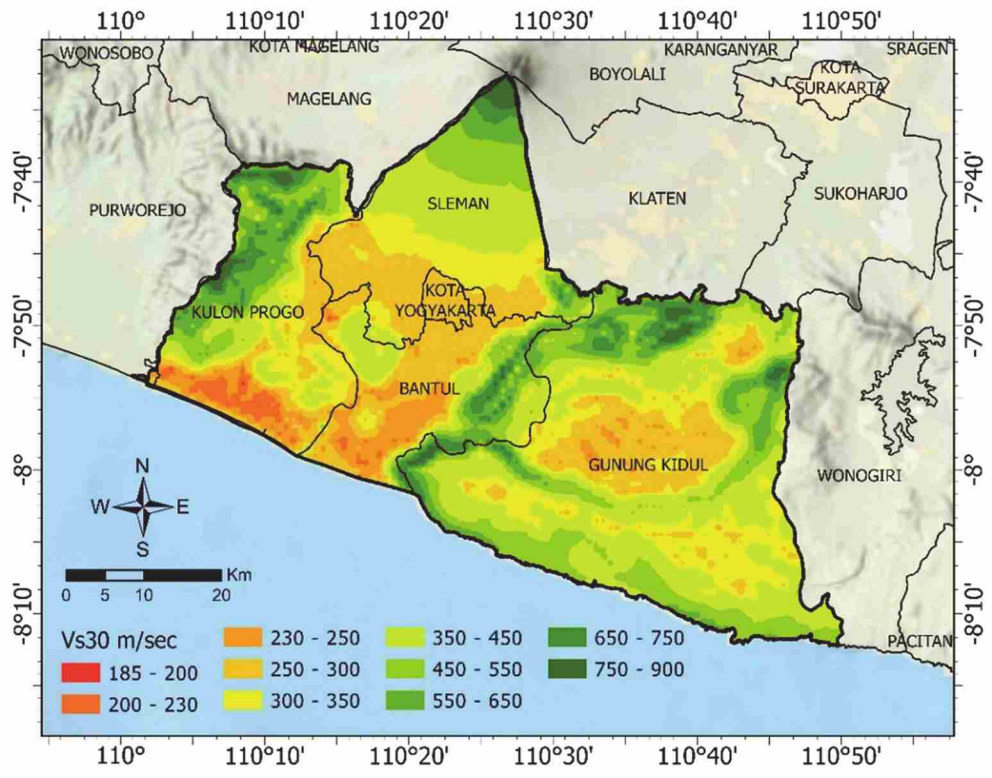

Figure 4. 8 Shear wave velocity (Vs30) map of Yogyakarta region

The figures depict Vs30 value of Malang region are between 190m/s to 900m/s, while the Vs30 values of Yogyakarta region are ranging from 185m/s to 900m/s. The level of damage due to an earthquake is not only influenced by the level of magnitude but also influenced by the geological conditions at the site. Areas that are prone to damage due to earthquakes are areas of thick-soft sediment that are on top of hard bedrock [20]. The more unstable (soft) the constituent rocks in an area, the greater the effects of earthquakes that will occur in the area. This is because unstable rock areas are generally not compact, easy to decompose, and if an earthquake occurs, the damage caused by the earthquake will be even greater [21].

Based on the physical maps of Malang and Yogyakarta presented in Figure 4.9, the lowest Vs30 values are located in the middle of Malang region indicating the soil condition on that area are relatively soft (soft soil). Meanwhile, the highest Vs30 values are located in the relatively highland area, such as around Mt. Arjuna (northern side of Malang), Mt. Kawi (western side of Malang), and Mt. Bromo (eastern side of Malang). Similar to Malang, the region near the Mt. Merapi, Yogyakarta has the higher value of Vs30. The lower value of Vs30 is located in Bantul, Gunungkidul and Yogyakarta city. The low value of Vs30 is well

correlated with the volcanic sedimentary basin which is located in the southern part of Merapi flank, on the western side of the Opak Fault [22].

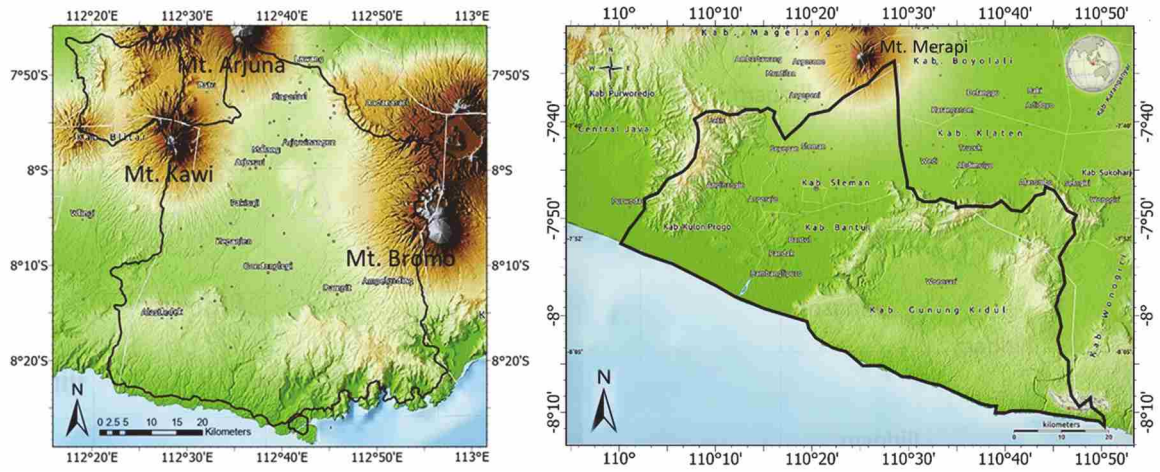

a. Malang region b. Yogyakarta region

Figure 4. 9 Physical map of Malang and Yogyakarta region

4.2.4 GMPE and Logic Tree Analysis

Several GMPE models proposed worldwide with several specific approaches. Some researchers introduced how to select and adjust the GMPE models properly [23-25]. The GMPE selected in this study was based on the seismotectonic conditions classified due to the earthquake source mechanisms. This study applied the GMPE formula of Youngs et al. 1997, Atkinson-Boore 2003 and Gregor 2006 [26-28] for subduction mechanisms. Meanwhile, the GMPE of Boore et al. 1997, Chiou and Youngs NGA 2006 and Boore-Atkinson NGA 2006 [29-31] were selected for the shallow crustal fault mechanisms.

In order to consider the epistemic uncertainty, this study used the Logic tree model with the same weighting in each GMPE as shown in Figure 4.10. The magnitude relative distribution for each earthquake source was modelled using the exponential model of Gutenberg-Richter and characteristic with weights of 0.34 and 0.66, respectively.

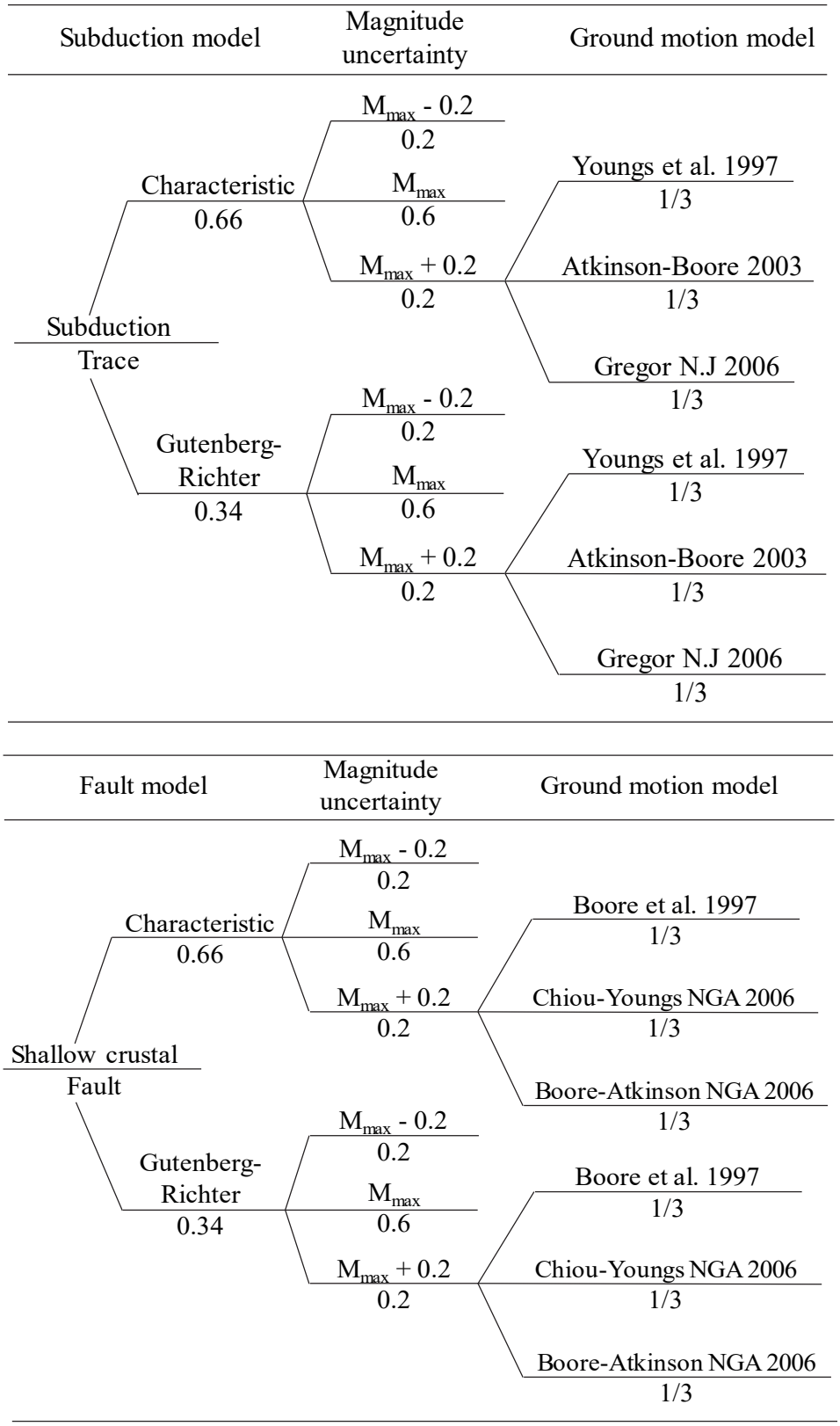

Figure 4. 10 The logic tree model for subduction and shallow crustal fault

4.3 Result and Discussion

4.3.1 Seismicity of Malang and Yogyakarta region

Earthquake data from various earthquake catalogs previously mentioned in the method section were obtained from 1962 to July 2021 with magnitude Mw≥4.5 and depth D≤300km. This earthquake data is then homogenized into a Mw scale with the equation provided in Table 4.1. The earthquake epicenter distribution map is presented in Figure 4.11.

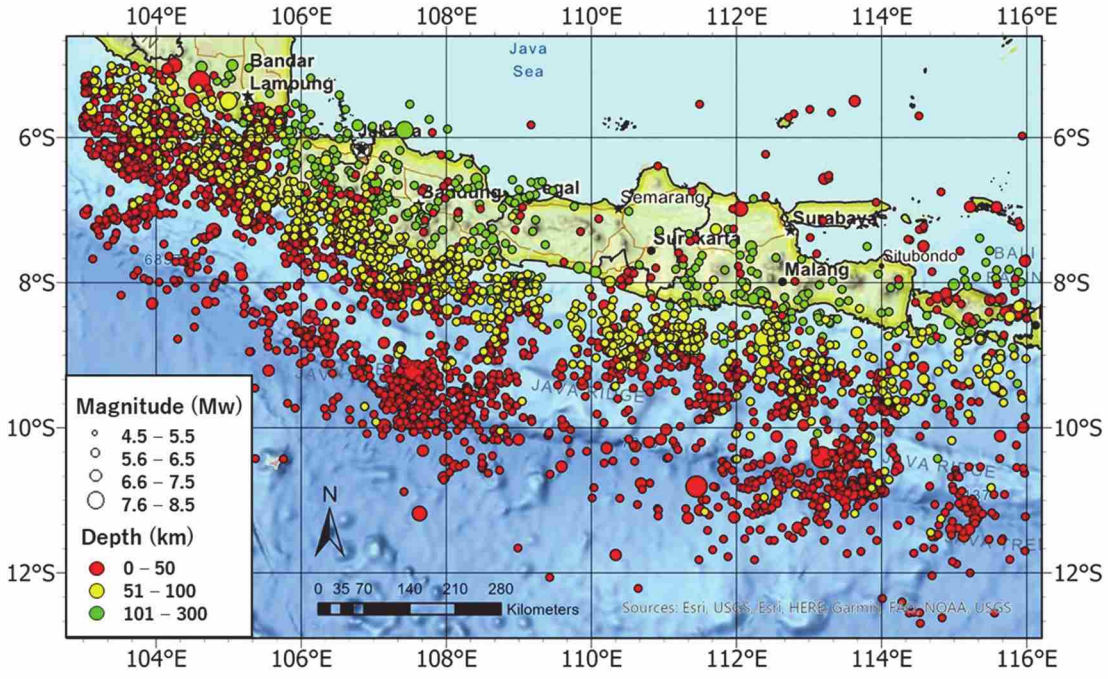

Figure 4. 11 Earthquake epicenter distribution between 1906 to July 2021 with magnitude of Mw≥4.5 and depth ≤300km

In order to investigate the influence of the 2021 M6.1 Malang earthquake, the Earthquake catalog for the specific Malang region and its surrounding are presented in Figure 4.12, while the Frequency-Magnitude Distribution (FMD) based on the Gutenberg-Richter is shown in Figure 4.13.

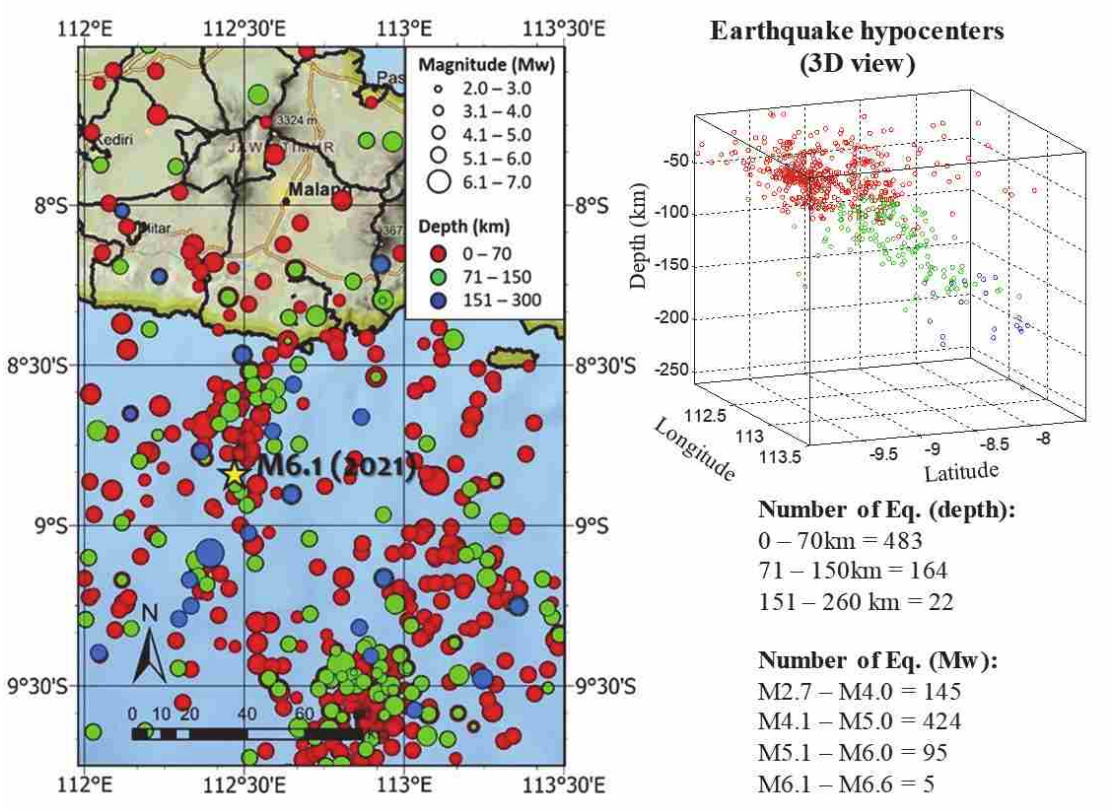

Figure 4. 12 Earthquake Epicenters of the Specific Malang Region and Its Surroundings (January 1962 to July 2021)

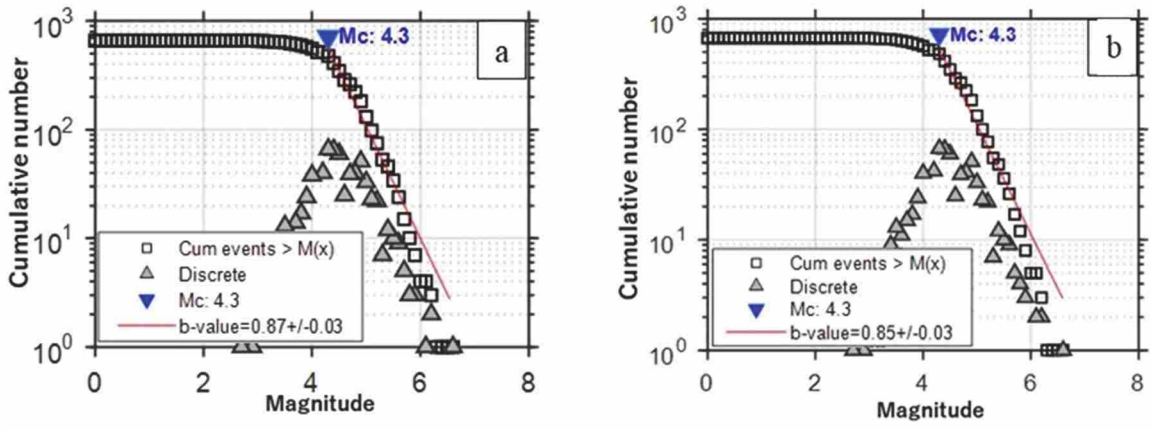

(a) FMD before the Malang earthquake (1962 to 9th April 2021)

(b) FMD after the Malang earthquake (10th April to 31st July 2021)

Figure 4. 13 The FMD of Gutenberg-Richter Law for Malang Earthquake

The figure shows that the earthquake tends to occur in the southern Malang region. Earthquakes that occurred in the 74enioff zone around Malang have a depth of 50-200km, but the distance to the Malang region is closer than the megathrust earthquakes zone, which

are hundreds of kilometers further away. However, megathrust earthquakes have a history of large magnitudes and some of them trigger tsunamis, so they are important to consider in seismic analysis. The FMD model after the M6.1 Malang earthquake is slightly steeper than the one before the large earthquake occurred. The b-value decreased from 0.87 $\pm$ 0.03 to 0.85 $\pm$ 0.03. In order to get more detailed information about the seismic activity pattern in this region, observations of magnitude and the cumulative number of earthquakes through time were conducted. The correlation between them is displayed in Figure 4.14.

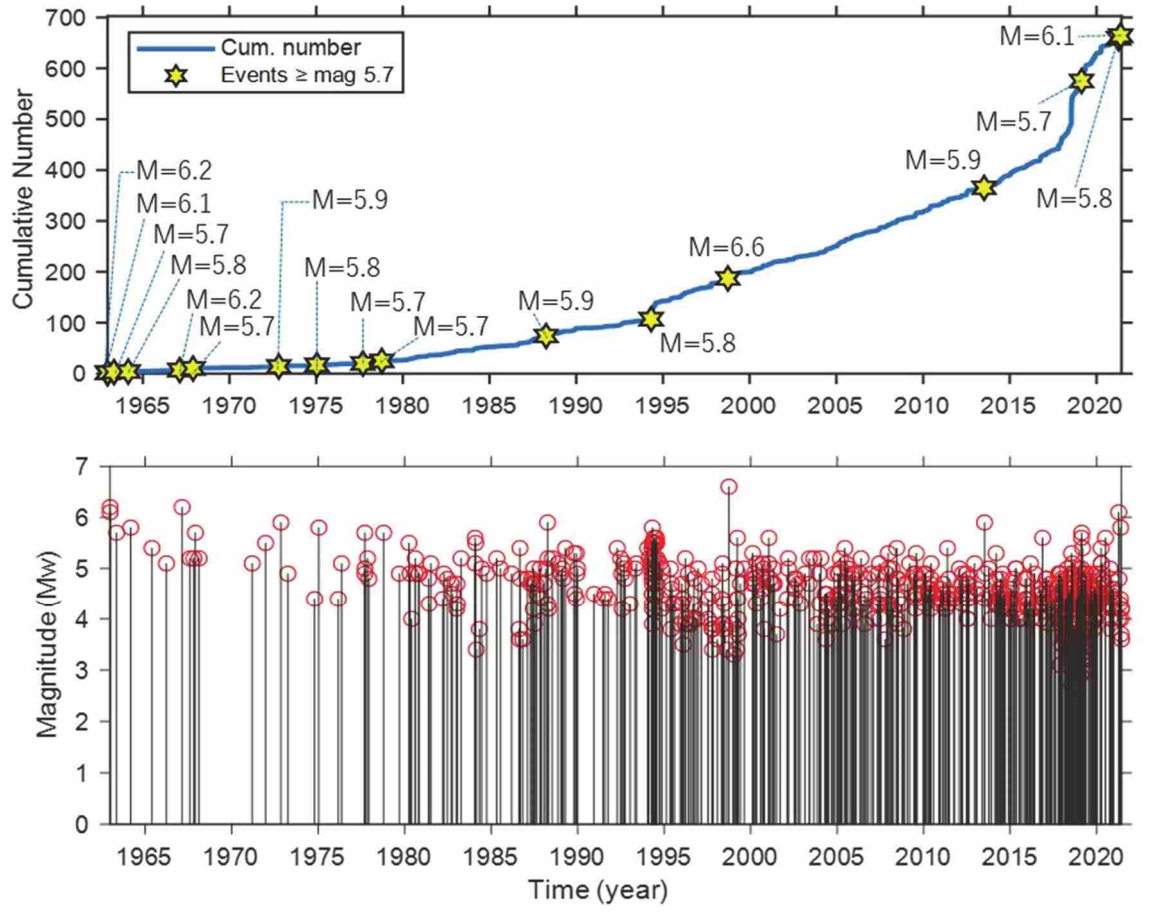

Figure 4. 14 Distribution of earthquake magnitude and their cumulative

The figure reveals that the earthquakes recorded before 1980 were large earthquakes due to the limited earthquake instrument ability. The yellow stars present the events with magnitude M$\geq$5.7. The pattern of small earthquakes was shown in the year range of 1998 to 2012 so that then a large earthquake occurred in 2013 (M5.9) due to the accumulation of energy during that year gap. The following pattern can be seen in the year range of 2014 to 2018, where many small earthquakes appeared until then the large earthquakes occurred in

2019 and 2021. The b-value analysis through time calculated for the specific area of Malang and its surroundings was observed until April 9, 2021 (before the 2021 M6.1 Malang earthquake occurred). The b-value by time graph is presented in Figure 4.15.

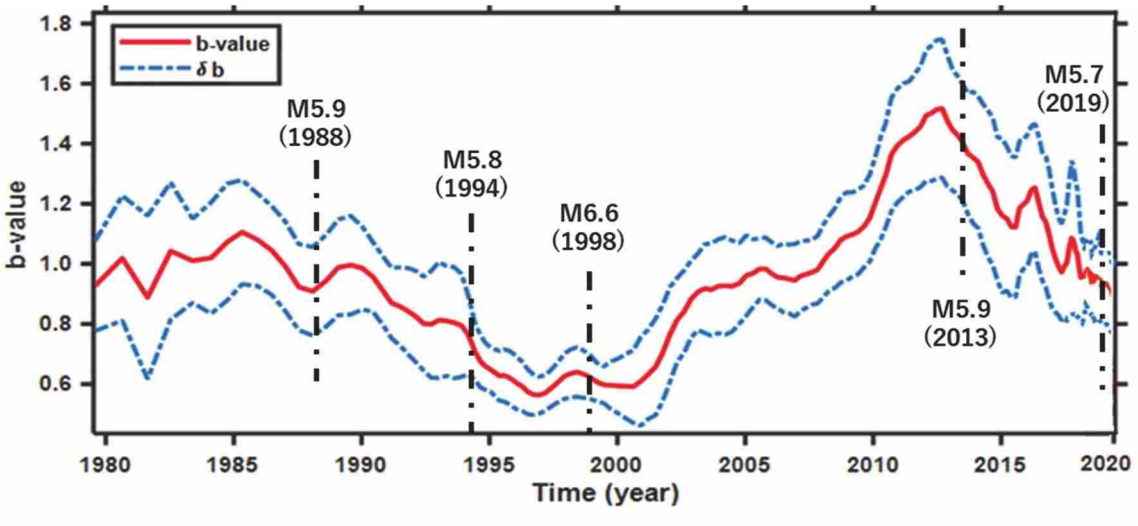

Figure 4. 15 The b-value with time before the 2021 M6.1 Malang earthquake

Based on the figure, there are some patterns of b-value related to the occurrence of large earthquakes. The significant gap of large earthquake occurred after an earthquake with a scale of M6.6 in 1998. There was no earthquake with a scale of $M \geq 5.7$ during 1999 to 2012. There is an increase of b-value before finally the large earthquake occurred in 2013. The b-value then significantly decreases, even after the large earthquake in 2019 (M5.7) until April 9, 2021 (before the Malang earthquake occurred). A lower b-value indicates an increase in seismic hazard in this period because it tends to generate large earthquakes relative to the data catalog.

In order to observe the b-value for Malang region in more detail, the spatial b-value before and after the 2021 M6.1 Malang earthquake are displayed in Figure 4.16. In general, the north and east side of Malang region tends to have the highest b-value, which is about 1.0 to 1.08, both before and after the M6.1 2021 Malang earthquake. The b-value in the epicenter area before the large earthquake occurred is smaller than the surrounding area, which is about 0.88. This condition indicates that the area has more significant pressure than the surrounding area which has a higher b-value. The existence of great pressure causes the emergence of large earthquakes to release earthquake energy.

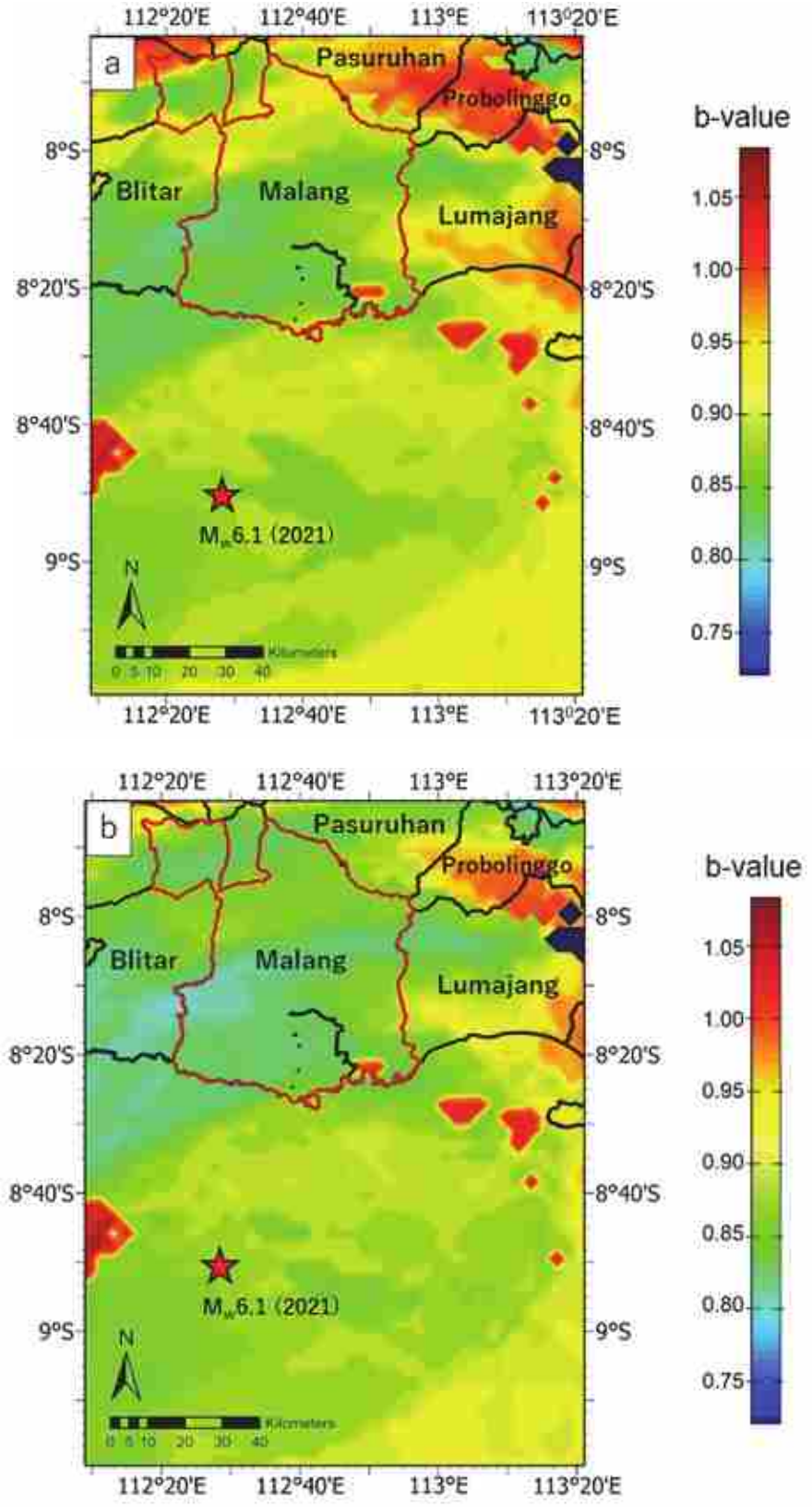

Figure 4. 16 Spatial b-value before the 2021 Malang Earthquake (left map) and after the 2021 Malang Earthquake (right map)

In the spatial b-value map after the 2021 M6.1 Malang earthquake, the area around the earthquake epicenter is still in a green zone, which means that the b-value is still low, even lower than before the Malang earthquake occurred. In addition, the area that surrounds it has a higher b-value, indicating that the area near the epicenter still has the trapped accumulated energy. In general, after the large earthquake occurred, the b-value will increase and then fall again. However, the results of observations in this study show that the b-value after the Malang earthquake still tends to decrease. This means that there is a relatively large level of stress caused by the stress of energy accumulation, which allows for the potential for forthcoming large earthquakes.

4.3.2 Spectral Acceleration for Short (S_S) and Long Period (S_1)

The PSHA for this study was conducted in each grid point of Malang region which the distance between points is about one kilometer using equation (2.3). Analysis was carried out for 4,224 points within the Malang region to obtain the value of Spectral acceleration (SA) at bedrock for period of 0.2s (S_S), and 1.0s (S_1) with 2% probability of exceedance (PE) in 50 years. All the potential earthquake sources, both shallow crustal faults and subduction sources within a radius of 500km from each Malang and Yogyakarta are taken into account in the analysis. Taking the example of spectral acceleration calculation for fault earthquake source in Malang, the steps are as follows:

1). Probability of distance, F®

The distance probability was calculated by dividing the fault into some segments which is presented in Figure 4.17. For example, one coordinate point is taken in Malang city (112.631ºE 7.961ºS) by taking into account the effect of fault, i.e., the RMKS East fault, which extends from 113.272ºE; 6,966ºS to 115,346ºE; 7,196ºS (the fault is considered straight line). If the coordinate system is changed into (x,y) in km and the point location of Malang is considered to have coordinates (0,0), then the fault corner coordinates at each are (70.65;111.76) and (299.39;86.14), respectively. The calculation results of segment faults are shown in Table 4.4 and the graph of the probability of distance is presented in Figure 4.18.

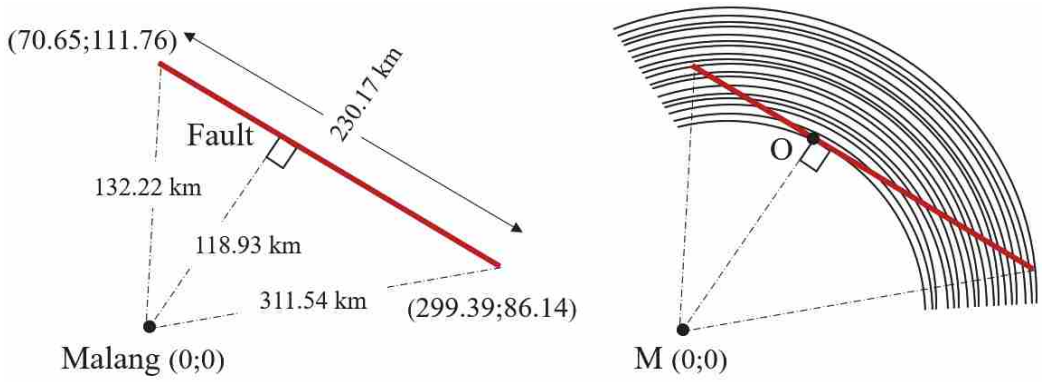

Figure 4. 17 Distance and segmentation for fault line source

Table 4. 4 The distance probability density result for fault line source

No.	R (km)	$R_{average}$ (km)	Segment (km)	Prob. dens. of Distance®*(r)*
1	118.9316			
2	121.4997	120.2156	49.6974	0.0863
3	124.0678	122.7838	20.9597	0.0364
4	126.6359	125.3519	16.3359	0.0284
5	129.2041	127.9200	13.9818	0.0243
6	131.7722	130.4881	12.5012	0.0217
7	134.3403	133.0563	11.4658	0.0199
8	136.9085	135.6244	10.6932	0.0186
9	139.4766	138.1925	10.0908	0.0175
10	142.0447	140.7606	9.6059	0.0167
11	144.6128	143.3288	9.2059	0.0160
12	147.1810	145.8969	8.8697	0.0154
13	149.7491	148.4650	8.5826	0.0149
14	152.3172	151.0332	8.3343	0.0145
15	154.8853	153.6013	8.1173	0.0141
16	157.4535	156.1694	7.9260	0.0138
17	160.0216	158.7375	7.7559	0.0135
18	162.5897	161.3057	7.6036	0.0132
19	165.1579	163.8738	7.4665	0.0130
20	167.7260	166.4419	7.3424	0.0127
21	170.2941	169.0100	7.2295	0.0126
22	172.8622	171.5782	7.1263	0.0124
23	175.4304	174.1463	7.0317	0.0122
24	177.9985	176.7144	6.9447	0.0121
25	180.5666	179.2826	6.8643	0.0119
26	183.1347	181.8507	6.7898	0.0118
27	185.7029	184.4188	6.7207	0.0117
28	188.2710	186.9869	6.6563	0.0116
29	190.8391	189.5551	6.5963	0.0115
30	193.4073	192.1232	6.5401	0.0114
31	195.9754	194.6913	6.4875	0.0113

No.	R (km)	$R_{average}$ (km)	Segment (km)	Prob. dens. of Distance®*(r)*
32	198.5435	197.2594	6.4381	0.0112
33	201.1116	199.8276	6.3917	0.0111
34	203.6798	202.3957	6.3479	0.0110
35	206.2479	204.9638	6.3066	0.0110
36	208.8160	207.5320	6.2676	0.0109
37	211.3841	210.1001	6.2307	0.0108
38	213.9523	212.6682	6.1957	0.0108
39	216.5204	215.2363	6.1626	0.0107
40	219.0885	217.8045	6.1310	0.0106
41	221.6567	220.3726	6.1011	0.0106
42	224.2248	222.9407	6.0726	0.0105
43	226.7929	225.5088	6.0454	0.0105
44	229.3610	228.0770	6.0195	0.0105
45	231.9292	230.6451	5.9947	0.0104
46	234.4973	233.2132	5.9711	0.0104
47	237.0654	235.7814	5.9485	0.0103
48	239.6335	238.3495	5.9268	0.0103
49	242.2017	240.9176	5.9061	0.0103
50	244.7698	243.4857	5.8863	0.0102
51	247.3379	246.0539	5.8672	0.0102
52	249.9061	248.6220	5.8489	0.0102
53	252.4742	251.1901	5.8313	0.0101
54	255.0423	253.7582	5.8144	0.0101
55	257.6104	256.3264	5.7982	0.0101
56	260.1786	258.8945	5.7825	0.0100
57	262.7467	261.4626	5.7675	0.0100
58	265.3148	264.0308	5.7530	0.0100
59	267.8829	266.5989	5.7390	0.0100
60	270.4511	269.1670	5.7255	0.0099
61	273.0192	271.7351	5.7125	0.0099
62	275.5873	274.3033	5.6999	0.0099
63	278.1555	276.8714	5.6878	0.0099
64	280.7236	279.4395	5.6760	0.0099
65	283.2917	282.0076	5.6647	0.0098
66	285.8598	284.5758	5.6537	0.0098
67	288.4280	287.1439	5.6431	0.0098
68	290.9961	289.7120	5.6328	0.0098
69	293.5642	292.2802	5.6228	0.0098
70	296.1323	294.8483	5.6132	0.0097
71	298.7005	297.4164	5.6038	0.0097
72	301.2686	299.9845	5.5947	0.0097
73	303.8367	302.5527	5.5859	0.0097
74	306.4049	305.1208	5.5774	0.0097
75	308.9730	307.6889	5.5691	0.0097
76	311.5411	310.2570	5.5611	0.0097
				1.0000

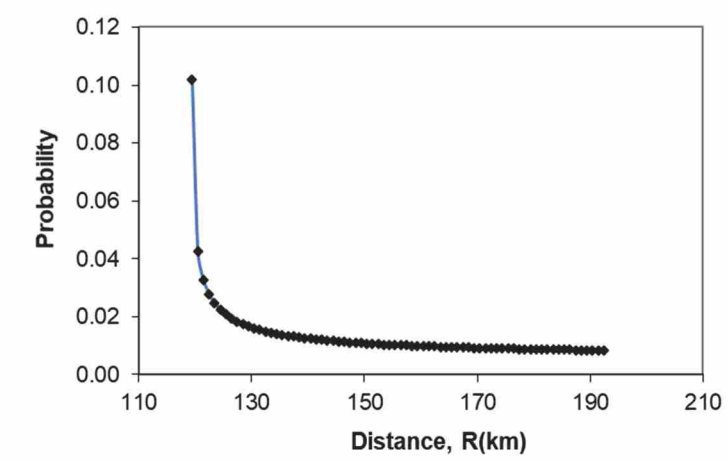

Figure 4. 18 Probability of distance for line fault source

2). Probability of magnitude, F(*m*)

The probability of magnitude was calculated based on the minimum magnitude (M_{min}), maximum magnitude (M_{max}), and magnitude distribution density function using equation (2.7). The calculation used the value of M_{min} = 4.5 and M_{max} = 7.8 based on the data for RMKS fault, with a distance between magnitude is taken for each 0.1 unit. The result for probability of magnitude is presented in Table 4.5 and Figure 4.19.

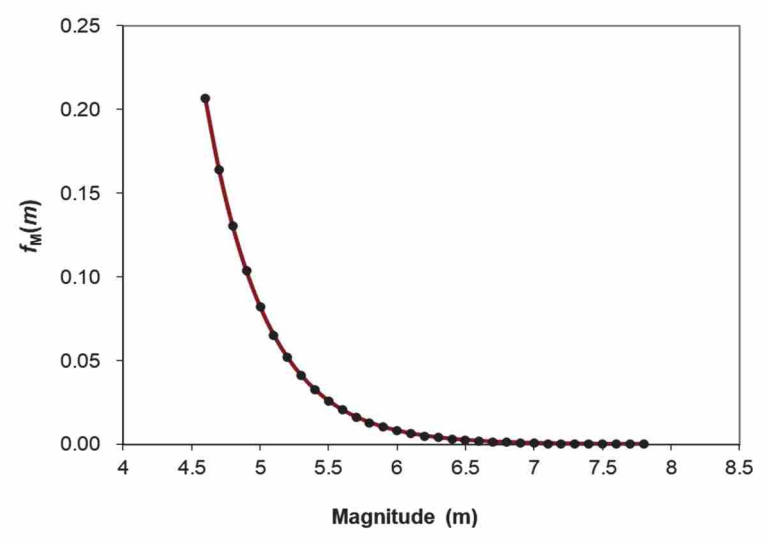

Figure 4. 19 Probability of magnitude for line fault source

Table 4. 5 The magnitude probability result for fault line source

No.	m (Mw)	$m_{average}$ (Mw)	$f(m)$	$f(m)_{average}$	Prob. Dens. Of Magnitude $f_M(m)$
1	4.500		2.304		
2	4.600	4.550	1.830	2.067	0.2067
3	4.700	4.650	1.454	1.642	0.1642
4	4.800	4.750	1.155	1.304	0.1304
5	4.900	4.850	0.917	1.036	0.1036
6	5.000	4.950	0.728	0.823	0.0823
7	5.100	5.050	0.579	0.654	0.0654
8	5.200	5.150	0.460	0.519	0.0519
9	5.300	5.250	0.365	0.412	0.0412
10	5.400	5.350	0.290	0.328	0.0328
11	5.500	5.450	0.230	0.260	0.0260
12	5.600	5.550	0.183	0.207	0.0207
13	5.700	5.650	0.145	0.164	0.0164
14	5.800	5.750	0.115	0.130	0.0130
15	5.900	5.850	0.092	0.104	0.0104
16	6.000	5.950	0.073	0.082	0.0082
17	6.100	6.050	0.058	0.065	0.0065
18	6.200	6.150	0.046	0.052	0.0052
19	6.300	6.250	0.036	0.041	0.0041
20	6.400	6.350	0.029	0.033	0.0033
21	6.500	6.450	0.023	0.026	0.0026
22	6.600	6.550	0.018	0.021	0.0021
23	6.700	6.650	0.015	0.016	0.0016
24	6.800	6.750	0.012	0.013	0.0013
25	6.900	6.850	0.009	0.010	0.0010
26	7.000	6.950	0.007	0.008	0.0008
27	7.100	7.050	0.006	0.007	0.0007
28	7.200	7.150	0.005	0.005	0.0005
29	7.300	7.250	0.004	0.004	0.0004
30	7.400	7.350	0.003	0.003	0.0003
31	7.500	7.450	0.002	0.003	0.0003
32	7.600	7.550	0.002	0.002	0.0002
33	7.700	7.650	0.001	0.002	0.0002
34	7.800	7.750	0.001	0.001	0.0001
					1.0004

3). Probability of ground motion attenuation, P(z)

The ground motion attenuation was calculated based on the GMPE models. Calculation was conducted based on the combination of average distance (Table 4.4) and average magnitude (Table 4.5). The result of calculation for ground motion attenuation using the GMPE of Boore et al. 1997 and probability of attenuation is presented in Table 4.6 and Table 4.7, respectively.

Table 4. 6 Calculation of ground motion attenuation, *ln (y)*

m (*Mw*)	$m_{average}$	R (km)											
		120.216	122.784	125.352	127.920	130.488	133.056	135.624	138.193	140.761	143.329		310.257
4.50		*ln (y)*											
4.60	4.55	-4.403	-4.422	-4.441	-4.460	-4.478	-4.496	-4.514	-4.531	-4.548	-4.565		-5.277
4.70	4.65	-4.256	-4.275	-4.294	-4.313	-4.331	-4.349	-4.367	-4.384	-4.401	-4.418		-5.131
4.80	4.75	-4.115	-4.134	-4.153	-4.172	-4.190	-4.208	-4.226	-4.243	-4.260	-4.277		-4.989
4.90	4.85	-3.979	-3.998	-4.017	-4.036	-4.054	-4.072	-4.090	-4.107	-4.124	-4.141		-4.853
5.00	4.95	-3.848	-3.868	-3.887	-3.905	-3.924	-3.942	-3.959	-3.977	-3.994	-4.010		-4.723
5.10	5.05	-3.723	-3.743	-3.762	-3.780	-3.799	-3.817	-3.834	-3.851	-3.868	-3.885		-4.598
5.20	5.15	-3.603	-3.623	-3.642	-3.661	-3.679	-3.697	-3.714	-3.732	-3.749	-3.765		-4.478
5.30	5.25	-3.489	-3.509	-3.528	-3.546	-3.565	-3.583	-3.600	-3.617	-3.634	-3.651		-4.364
5.40	5.35	-3.380	-3.400	-3.419	-3.437	-3.456	-3.474	-3.491	-3.509	-3.526	-3.542		-4.255
5.50	5.45	-3.277	-3.296	-3.315	-3.334	-3.352	-3.370	-3.388	-3.405	-3.422	-3.439		-4.151
5.60	5.55	-3.179	-3.198	-3.217	-3.236	-3.254	-3.272	-3.290	-3.307	-3.324	-3.341		-4.053
5.70	5.65	-3.086	-3.105	-3.124	-3.143	-3.161	-3.179	-3.197	-3.214	-3.231	-3.248		-3.961
5.80	5.75	-2.999	-3.018	-3.037	-3.056	-3.074	-3.092	-3.110	-3.127	-3.144	-3.161		-3.873
5.90	5.85	-2.917	-2.936	-2.955	-2.974	-2.992	-3.010	-3.028	-3.045	-3.062	-3.079		-3.791
6.00	5.95	-2.840	-2.860	-2.879	-2.897	-2.916	-2.934	-2.951	-2.969	-2.986	-3.002		-3.715
6.10	6.05	-2.769	-2.789	-2.808	-2.826	-2.845	-2.863	-2.880	-2.897	-2.914	-2.931		-3.644
6.20	6.15	-2.703	-2.723	-2.742	-2.761	-2.779	-2.797	-2.814	-2.832	-2.849	-2.865		-3.578
6.30	6.25	-2.643	-2.663	-2.682	-2.700	-2.719	-2.737	-2.754	-2.771	-2.788	-2.805		-3.518
6.40	6.35	-2.588	-2.608	-2.627	-2.645	-2.664	-2.682	-2.699	-2.717	-2.734	-2.750		-3.463
6.50	6.45	-2.539	-2.558	-2.577	-2.596	-2.614	-2.632	-2.650	-2.667	-2.684	-2.701		-3.413
6.60	6.55	-2.495	-2.514	-2.533	-2.552	-2.570	-2.588	-2.606	-2.623	-2.640	-2.657		-3.369
6.70	6.65	-2.456	-2.475	-2.494	-2.513	-2.531	-2.549	-2.567	-2.584	-2.601	-2.618		-3.331
6.80	6.75	-2.423	-2.442	-2.461	-2.480	-2.498	-2.516	-2.534	-2.551	-2.568	-2.585		-3.297
6.90	6.85	-2.395	-2.414	-2.433	-2.452	-2.470	-2.488	-2.506	-2.523	-2.540	-2.557		-3.269
7.00	6.95	-2.372	-2.392	-2.411	-2.429	-2.448	-2.466	-2.483	-2.501	-2.518	-2.534		-3.247
7.10	7.05	-2.355	-2.375	-2.394	-2.412	-2.431	-2.449	-2.466	-2.483	-2.500	-2.517		-3.230
7.20	7.15	-2.343	-2.363	-2.382	-2.401	-2.419	-2.437	-2.454	-2.472	-2.489	-2.505		-3.218
7.30	7.25	-2.337	-2.357	-2.376	-2.394	-2.413	-2.431	-2.448	-2.465	-2.482	-2.499		-3.212
7.40	7.35	-2.336	-2.356	-2.375	-2.393	-2.412	-2.430	-2.447	-2.465	-2.482	-2.498		-3.211
7.50	7.45	-2.341	-2.360	-2.379	-2.398	-2.416	-2.434	-2.452	-2.469	-2.486	-2.503		-3.215
7.60	7.55	-2.351	-2.370	-2.389	-2.408	-2.426	-2.444	-2.462	-2.479	-2.496	-2.513		-3.225
7.70	7.65	-2.366	-2.385	-2.404	-2.423	-2.441	-2.459	-2.477	-2.494	-2.511	-2.528		-3.241
7.80	7.75	-2.387	-2.406	-2.425	-2.444	-2.462	-2.480	-2.498	-2.515	-2.532	-2.549		-3.261

Table 4. 7 Probability of ground motion attenuation, P(z)

$m_{average}$ (Mw)	R (km)											
	120.216	122.784	125.352	127.920	130.488	133.056	135.624	138.193	140.761	143.329		310.257
	P(z)											
4.55	1.35E-08	1.08E-08	8.68E-09	6.99E-09	5.65E-09	4.57E-09	3.72E-09	3.03E-09	2.47E-09	2.02E-09		1.43E-13
4.65	6.90E-08	5.58E-08	4.53E-08	3.69E-08	3.01E-08	2.46E-08	2.02E-08	1.66E-08	1.37E-08	1.13E-08		1.20E-12
4.75	3.07E-07	2.51E-07	2.06E-07	1.69E-07	1.40E-07	1.15E-07	9.56E-08	7.93E-08	6.60E-08	5.51E-08		8.63E-12
4.85	1.20E-06	9.92E-07	8.22E-07	6.82E-07	5.68E-07	4.74E-07	3.96E-07	3.32E-07	2.79E-07	2.34E-07		5.34E-11
4.95	4.16E-06	3.47E-06	2.90E-06	2.43E-06	2.04E-06	1.72E-06	1.45E-06	1.23E-06	1.04E-06	8.81E-07		2.87E-10
5.05	1.29E-05	1.09E-05	9.16E-06	7.75E-06	6.56E-06	5.57E-06	4.74E-06	4.04E-06	3.45E-06	2.95E-06		1.35E-09
5.15	3.60E-05	3.06E-05	2.60E-05	2.22E-05	1.90E-05	1.62E-05	1.39E-05	1.19E-05	1.03E-05	8.86E-06		5.65E-09
5.25	9.12E-05	7.81E-05	6.70E-05	5.76E-05	4.96E-05	4.28E-05	3.70E-05	3.20E-05	2.77E-05	2.41E-05		2.10E-08
5.35	2.11E-04	1.82E-04	1.58E-04	1.37E-04	1.19E-04	1.03E-04	8.96E-05	7.81E-05	6.82E-05	5.96E-05		6.97E-08
5.45	4.51E-04	3.92E-04	3.42E-04	2.98E-04	2.60E-04	2.28E-04	2.00E-04	1.75E-04	1.54E-04	1.35E-04		2.10E-07
5.55	8.91E-04	7.80E-04	6.84E-04	6.01E-04	5.29E-04	4.66E-04	4.11E-04	3.63E-04	3.20E-04	2.84E-04		5.73E-07
5.65	1.64E-03	1.45E-03	1.28E-03	1.13E-03	1.00E-03	8.86E-04	7.86E-04	6.98E-04	6.21E-04	5.52E-04		1.43E-06
5.75	2.83E-03	2.52E-03	2.23E-03	1.99E-03	1.77E-03	1.58E-03	1.41E-03	1.26E-03	1.12E-03	1.01E-03		3.29E-06
5.85	4.62E-03	4.12E-03	3.68E-03	3.29E-03	2.95E-03	2.64E-03	2.37E-03	2.13E-03	1.91E-03	1.72E-03		7.01E-06
5.95	7.12E-03	6.39E-03	5.74E-03	5.16E-03	4.64E-03	4.18E-03	3.77E-03	3.40E-03	3.07E-03	2.77E-03		1.39E-05
6.05	1.05E-02	9.43E-03	8.51E-03	7.69E-03	6.95E-03	6.29E-03	5.69E-03	5.16E-03	4.68E-03	4.24E-03		2.56E-05
6.15	1.47E-02	1.33E-02	1.20E-02	1.09E-02	9.92E-03	9.02E-03	8.20E-03	7.46E-03	6.79E-03	6.19E-03		4.44E-05
6.25	1.98E-02	1.80E-02	1.64E-02	1.49E-02	1.36E-02	1.24E-02	1.13E-02	1.03E-02	9.43E-03	8.63E-03		7.25E-05
6.35	2.56E-02	2.34E-02	2.14E-02	1.95E-02	1.79E-02	1.64E-02	1.50E-02	1.37E-02	1.26E-02	1.15E-02		1.12E-04
6.45	3.21E-02	2.94E-02	2.69E-02	2.47E-02	2.27E-02	2.08E-02	1.91E-02	1.76E-02	1.62E-02	1.49E-02		1.64E-04
6.55	3.89E-02	3.58E-02	3.29E-02	3.03E-02	2.78E-02	2.56E-02	2.36E-02	2.18E-02	2.01E-02	1.85E-02		2.29E-04
6.65	4.59E-02	4.23E-02	3.90E-02	3.59E-02	3.31E-02	3.06E-02	2.82E-02	2.61E-02	2.41E-02	2.23E-02		3.05E-04
6.75	5.26E-02	4.86E-02	4.49E-02	4.15E-02	3.83E-02	3.55E-02	3.28E-02	3.04E-02	2.81E-02	2.60E-02		3.89E-04
6.85	5.89E-02	5.45E-02	5.04E-02	4.67E-02	4.32E-02	4.00E-02	3.71E-02	3.44E-02	3.19E-02	2.96E-02		4.75E-04
6.95	6.43E-02	5.96E-02	5.52E-02	5.12E-02	4.75E-02	4.40E-02	4.09E-02	3.79E-02	3.52E-02	3.27E-02		5.56E-04
7.05	6.87E-02	6.37E-02	5.91E-02	5.49E-02	5.09E-02	4.73E-02	4.39E-02	4.08E-02	3.80E-02	3.53E-02		6.27E-04
7.15	7.19E-02	6.67E-02	6.19E-02	5.75E-02	5.34E-02	4.97E-02	4.62E-02	4.29E-02	3.99E-02	3.72E-02		6.80E-04
7.25	7.36E-02	6.83E-02	6.35E-02	5.90E-02	5.48E-02	5.10E-02	4.74E-02	4.41E-02	4.10E-02	3.82E-02		7.10E-04
7.35	7.38E-02	6.86E-02	6.37E-02	5.92E-02	5.50E-02	5.11E-02	4.76E-02	4.42E-02	4.12E-02	3.83E-02		7.14E-04
7.45	7.26E-02	6.74E-02	6.26E-02	5.81E-02	5.40E-02	5.02E-02	4.67E-02	4.34E-02	4.04E-02	3.76E-02		6.93E-04
7.55	6.99E-02	6.49E-02	6.02E-02	5.59E-02	5.19E-02	4.82E-02	4.48E-02	4.16E-02	3.87E-02	3.60E-02		6.47E-04
7.65	6.59E-02	6.11E-02	5.66E-02	5.25E-02	4.87E-02	4.52E-02	4.20E-02	3.90E-02	3.62E-02	3.37E-02		5.81E-04
7.75	6.08E-02	5.63E-02	5.21E-02	4.83E-02	4.47E-02	4.14E-02	3.84E-02	3.56E-02	3.31E-02	3.07E-02		5.03E-04

4). Total probability, *P(x>X | m,R)*

The total probability calculated based on the attenuation probability, P(z), the magnitude probability, F(m) and the distance probability, F(r). The calculation results can be seen in Table 4.8.

Table 4. 8 Recapitulation result of total probability, *P(x>X | m,R)*

F(m)	P(r)											
	8.63E-02	3.64E-02	2.84E-02	2.43E-02	2.17E-02	1.99E-02	1.86E-02	1.75E-02	1.67E-02	1.60E-02		0.009656
	P(x>X | m,R)											
0.2067	2.41E-10	8.13E-11	5.09E-11	3.51E-11	2.53E-11	1.88E-11	1.43E-11	1.10E-11	8.52E-12	6.69E-12		2.85E-16
0.1642	9.78E-10	3.34E-10	2.11E-10	1.47E-10	1.07E-10	8.05E-11	6.16E-11	4.78E-11	3.76E-11	2.97E-11		1.91E-15
0.1304	3.46E-09	1.19E-09	7.62E-10	5.36E-10	3.95E-10	3.00E-10	2.31E-10	1.81E-10	1.44E-10	1.15E-10		1.09E-14
0.1036	1.07E-08	3.74E-09	2.41E-09	1.72E-09	1.28E-09	9.77E-10	7.62E-10	6.02E-10	4.81E-10	3.88E-10		5.34E-14
0.0823	2.96E-08	1.04E-08	6.78E-09	4.86E-09	3.65E-09	2.82E-09	2.22E-09	1.77E-09	1.42E-09	1.16E-09		2.28E-13
0.0654	7.27E-08	2.58E-08	1.70E-08	1.23E-08	9.31E-09	7.25E-09	5.75E-09	4.62E-09	3.76E-09	3.08E-09		8.55E-13
0.0519	1.61E-07	5.78E-08	3.83E-08	2.80E-08	2.14E-08	1.68E-08	1.34E-08	1.09E-08	8.90E-09	7.35E-09		2.83E-12
0.0412	3.25E-07	1.17E-07	7.84E-08	5.77E-08	4.44E-08	3.51E-08	2.83E-08	2.31E-08	1.91E-08	1.59E-08		8.34E-12
0.0328	5.97E-07	2.17E-07	1.47E-07	1.09E-07	8.43E-08	6.72E-08	5.45E-08	4.48E-08	3.72E-08	3.12E-08		2.21E-11
0.0260	1.01E-06	3.71E-07	2.52E-07	1.88E-07	1.47E-07	1.18E-07	9.64E-08	7.98E-08	6.67E-08	5.63E-08		5.27E-11
0.0207	1.59E-06	5.87E-07	4.01E-07	3.02E-07	2.37E-07	1.92E-07	1.58E-07	1.31E-07	1.10E-07	9.37E-08		1.14E-10
0.0164	2.32E-06	8.64E-07	5.95E-07	4.50E-07	3.56E-07	2.89E-07	2.40E-07	2.01E-07	1.70E-07	1.45E-07		2.27E-10
0.0130	3.19E-06	1.19E-06	8.26E-07	6.29E-07	5.01E-07	4.09E-07	3.41E-07	2.87E-07	2.44E-07	2.09E-07		4.15E-10
0.0104	4.12E-06	1.55E-06	1.08E-06	8.28E-07	6.62E-07	5.44E-07	4.55E-07	3.86E-07	3.30E-07	2.84E-07		7.01E-10
0.0082	5.05E-06	1.91E-06	1.34E-06	1.03E-06	8.29E-07	6.85E-07	5.75E-07	4.90E-07	4.21E-07	3.65E-07		1.10E-09
0.0065	5.89E-06	2.24E-06	1.58E-06	1.22E-06	9.85E-07	8.18E-07	6.90E-07	5.90E-07	5.10E-07	4.43E-07		1.62E-09
0.0052	6.57E-06	2.51E-06	1.77E-06	1.38E-06	1.12E-06	9.32E-07	7.90E-07	6.78E-07	5.88E-07	5.13E-07		2.22E-09
0.0041	7.03E-06	2.70E-06	1.91E-06	1.49E-06	1.22E-06	1.02E-06	8.65E-07	7.46E-07	6.49E-07	5.68E-07		2.89E-09
0.0033	7.24E-06	2.79E-06	1.98E-06	1.55E-06	1.27E-06	1.07E-06	9.10E-07	7.87E-07	6.87E-07	6.04E-07		3.54E-09
0.0026	7.20E-06	2.78E-06	1.99E-06	1.56E-06	1.28E-06	1.08E-06	9.23E-07	8.01E-07	7.01E-07	6.18E-07		4.13E-09
0.0021	6.94E-06	2.69E-06	1.93E-06	1.52E-06	1.25E-06	1.05E-06	9.05E-07	7.87E-07	6.91E-07	6.11E-07		4.57E-09
0.0016	6.50E-06	2.52E-06	1.81E-06	1.43E-06	1.18E-06	9.99E-07	8.60E-07	7.50E-07	6.60E-07	5.84E-07		4.84E-09
0.0013	5.92E-06	2.31E-06	1.66E-06	1.31E-06	1.08E-06	9.20E-07	7.94E-07	6.93E-07	6.11E-07	5.43E-07		4.89E-09
0.0010	5.26E-06	2.05E-06	1.48E-06	1.17E-06	9.71E-07	8.25E-07	7.13E-07	6.24E-07	5.51E-07	4.90E-07		4.74E-09
0.0008	4.56E-06	1.78E-06	1.29E-06	1.02E-06	8.47E-07	7.21E-07	6.24E-07	5.47E-07	4.83E-07	4.30E-07		4.42E-09
0.0007	3.87E-06	1.51E-06	1.10E-06	8.70E-07	7.22E-07	6.15E-07	5.33E-07	4.67E-07	4.14E-07	3.69E-07		3.95E-09
0.0005	3.22E-06	1.26E-06	9.11E-07	7.24E-07	6.02E-07	5.13E-07	4.45E-07	3.90E-07	3.45E-07	3.08E-07		3.40E-09
0.0004	2.62E-06	1.02E-06	7.42E-07	5.90E-07	4.90E-07	4.18E-07	3.62E-07	3.18E-07	2.82E-07	2.51E-07		2.82E-09
0.0003	2.09E-06	8.17E-07	5.91E-07	4.70E-07	3.91E-07	3.33E-07	2.89E-07	2.54E-07	2.25E-07	2.01E-07		2.26E-09
0.0003	1.63E-06	6.38E-07	4.61E-07	3.67E-07	3.05E-07	2.60E-07	2.25E-07	1.98E-07	1.75E-07	1.56E-07		1.74E-09
0.0002	1.25E-06	4.87E-07	3.53E-07	2.80E-07	2.33E-07	1.98E-07	1.72E-07	1.51E-07	1.33E-07	1.19E-07		1.29E-09
0.0002	9.33E-07	3.65E-07	2.63E-07	2.09E-07	1.73E-07	1.48E-07	1.28E-07	1.12E-07	9.91E-08	8.82E-08		9.21E-10
0.0001	6.83E-07	2.67E-07	1.93E-07	1.53E-07	1.26E-07	1.07E-07	9.29E-08	8.13E-08	7.18E-08	6.39E-08		6.32E-10

The final result of the calculation is the total probability *P(x>X|m,R)* which is the sum of all P(x>X|m.r) values in the table. The calculation is then continued to determine the correlation between annual rate of exceedance and acceleration amplitude to create the seismic hazard curve which is presented in Table 4.9 and Figure 4.20.

Table 4. 9 The acceleration and annual rate of exceedance

Acceleration amplitude (g)	Total probability P_{tot}	Annual rate of exceedance (λ) = 2.0 P_{tot}
0.1	8.66E-02	1.73E-01
0.2	6.15E-03	1.23E-02
0.3	5.24E-04	1.05E-03
0.4	5.45E-05	1.09E-04
0.5	5.93E-06	1.19E-05
0.6	1.05E-06	2.10E-06
0.7	2.25E-07	4.51E-07
0.8	6.35E-08	1.27E-07
0.9	1.87E-08	3.74E-08
1.0	5.68E-09	1.14E-08
1.5	7.64E-11	1.53E-10
2.0	3.82E-12	7.64E-12
2.5	2.72E-13	5.45E-13
3.0	3.51E-14	7.02E-14

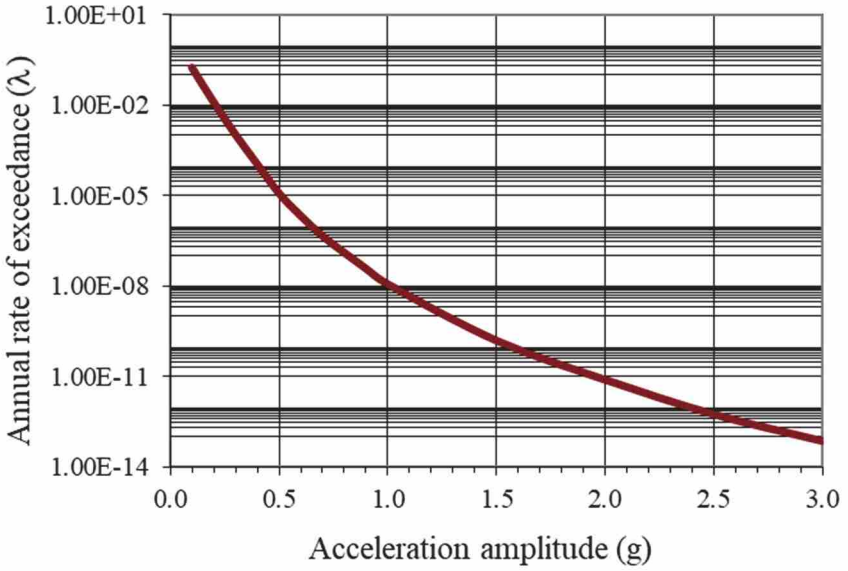

Figure 4. 20 Seismic hazard curve for the specific fault line source

The calculation is then conducted based on the logic tree model as presented in Figure 4.10 using three kinds of GMPE in each earthquake sources model to get the spectral acceleration value for each site location. Because the earthquake source model uses 3-dimensional modeling, with several GMPE and logic tree weighting, the calculations are carried out using the SRModel based on the numerical solution for the total probability theorem [33] by using the reference distance definition according to Figure 2.3.

The spectral acceleration values were calculated at bedrock and at ground surface for each short period and long period. The results of the Sa values for 4,224 points were shown in Table 4.10 then plotted and displayed on the spectral acceleration microzonation map for the periods of 0.2s (S_S) and 1.0s (S_1) at bedrock as presented in Figure 4.21 and Figure 4.22. The calculation for spectral acceleration at ground surface was conducted using the same steps for Sa bedrock. However, the parameter of soil condition including the Vs values were applied based on each condition of local site. The calculation result of Sa at ground surface (S_S S and S_1 S) is presented in Table 4.10 while the Sa surface maps are displayed in Figure 4.23 and Figure 4.24.

Table 4. 10 The calculation of spectral acceleration for bedrock and surface of Malang region

No.	Longitude	Latitude	Vs30	Soil	Ss R	Ss S	S_1 R	S_1 S
1	112.3417	-7.7667	583	SC	0.6800	0.9989	0.2951	0.6029
2	112.3500	-7.7667	597	SC	0.6788	0.9977	0.2947	0.6021
3	112.3583	-7.7667	627	SC	0.6776	0.9964	0.2943	0.6014
4	112.5917	-7.7667	614	SC	0.6348	0.9598	0.2808	0.5714
5	112.2917	-7.7750	346	SD	0.6872	1.0441	0.2974	0.6011
6	112.3000	-7.7750	377	SC	0.6860	1.0343	0.2970	0.6003
7	112.3083	-7.7750	357	SC	0.6848	1.0277	0.2967	0.6000
8	112.3333	-7.7750	558	SC	0.6837	1.0179	0.2963	0.6046
9	112.3417	-7.7750	539	SC	0.6826	1.0125	0.2960	0.6049
10	112.3500	-7.7750	559	SC	0.6813	1.0026	0.2956	0.6041
11	112.3583	-7.7750	705	SC	0.6801	0.9983	0.2952	0.6031
12	112.3667	-7.7750	895	SB	0.6788	0.9966	0.2948	0.6023
13	112.4250	-7.7750	527	SC	0.6704	0.9921	0.2926	0.6041
14	112.4333	-7.7750	696	SC	0.6670	0.9858	0.2904	0.5878
15	112.4417	-7.7750	427	SC	0.6656	0.9873	0.2900	0.5889
16	112.4583	-7.7750	490	SC	0.6628	0.9841	0.2891	0.5871
17	112.4667	-7.7750	673	SC	0.6614	0.9813	0.2887	0.5859
18	112.4750	-7.7750	840	SB	0.6600	0.9794	0.2884	0.5858
19	112.4833	-7.7750	900	SB	0.6597	0.9802	0.2886	0.5926
20	112.5917	-7.7750	900	SB	0.6375	0.9603	0.2817	0.5728
21	112.6000	-7.7750	900	SB	0.6359	0.9591	0.2815	0.5723
22	112.3000	-7.7833	355	SC	0.6887	1.0536	0.2980	0.6024
23	112.3083	-7.7833	331	SD	0.6875	1.0473	0.2976	0.6021
24	112.3167	-7.7833	427	SC	0.6863	1.0348	0.2972	0.6010
25	112.3250	-7.7833	494	SC	0.6872	1.0434	0.2974	0.6046
4224	112.7083	-8.4583	600	SC	0.9972	1.6926	0.3998	0.6803

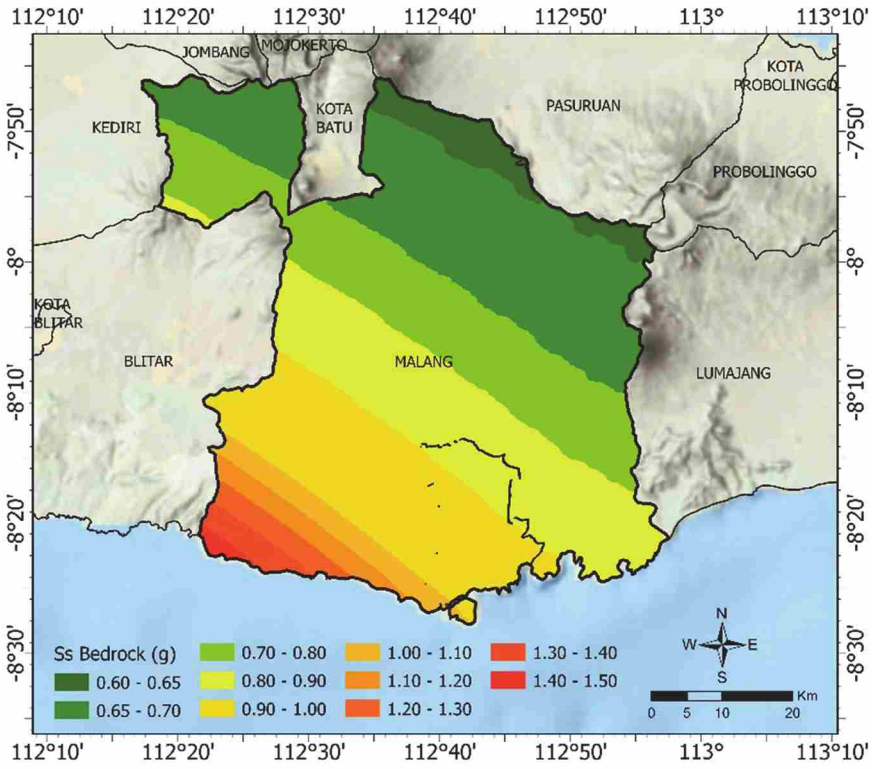

Figure 4. 21 Spectral acceleration at bedrock for short period 0.2s (S_S bedrock) of Malang region

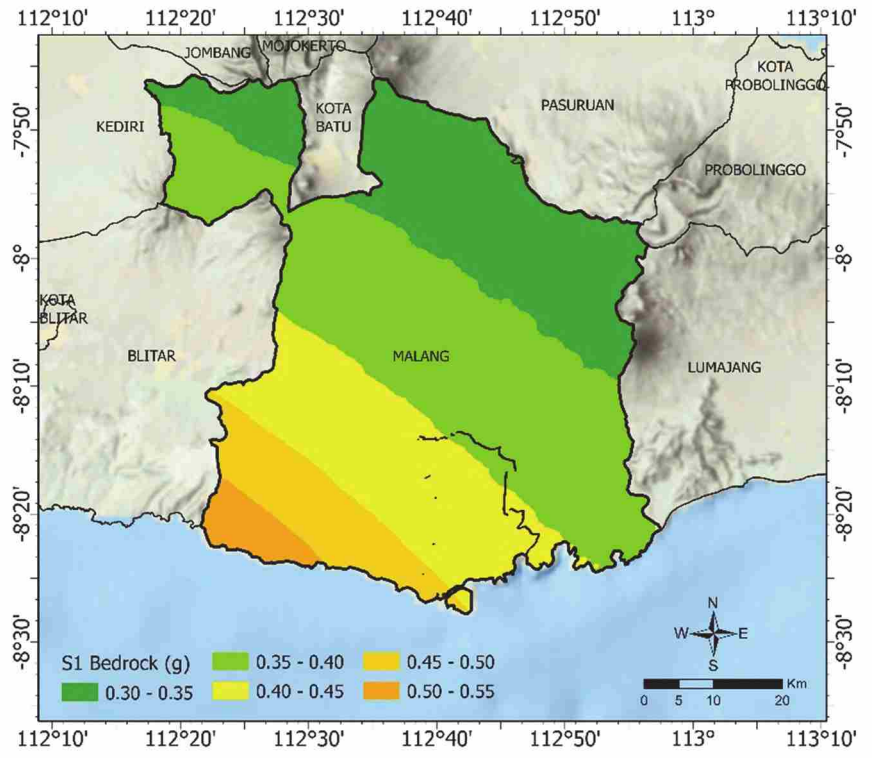

Figure 4. 22 Spectral acceleration at bedrock for long period 1.0s (S_1 bedrock) of Malang region

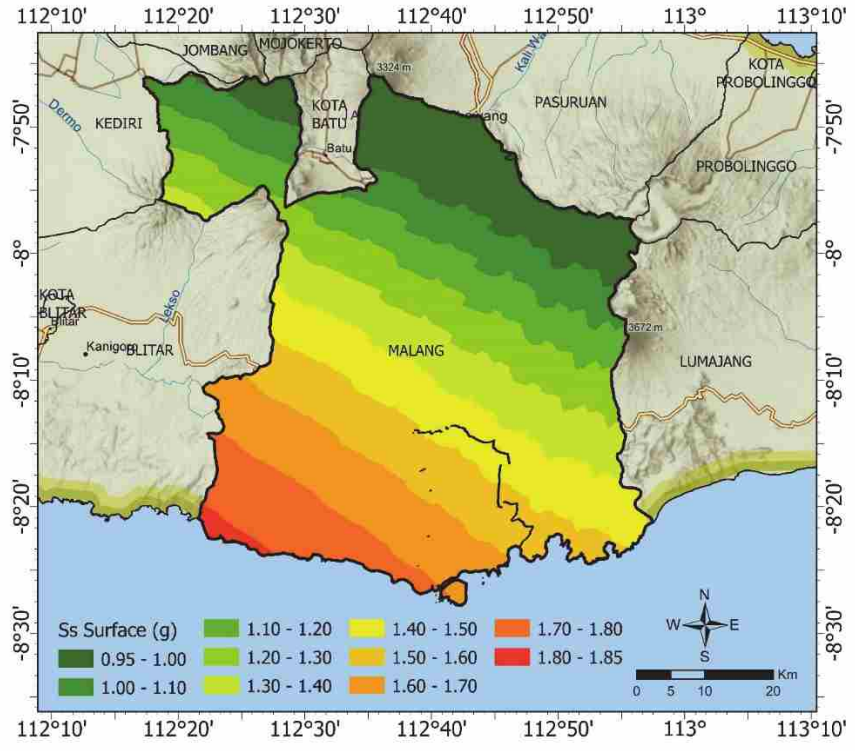

Figure 4. 23 Spectral acceleration at ground surface for short period 0.2s (S_S surface) of Malang region

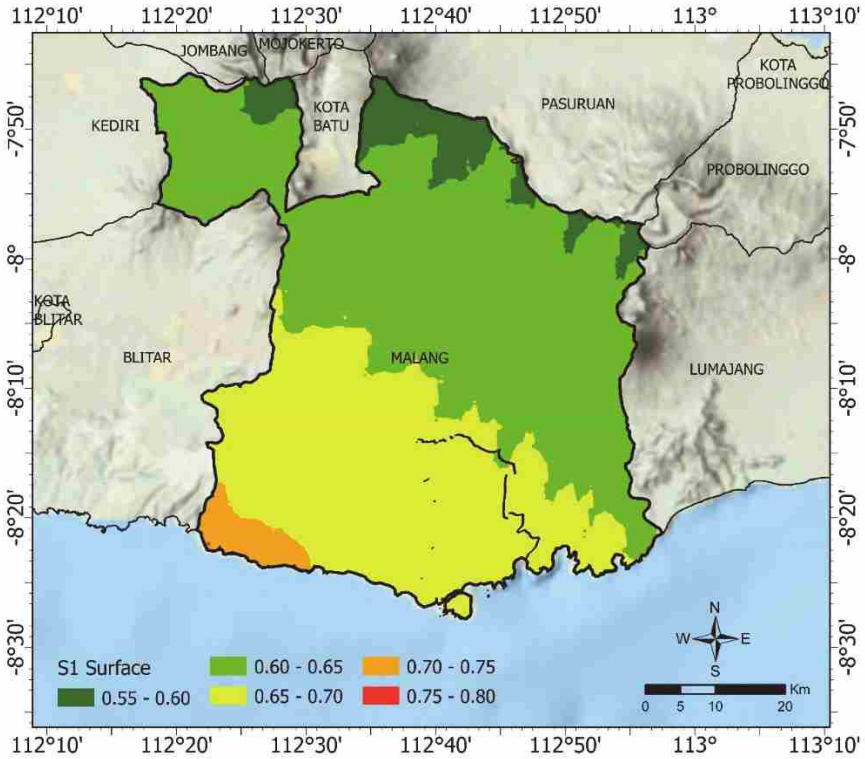

Figure 4. 24 Spectral acceleration at ground surface for long period 1.0s (S_1 surface) of Malang region

The values of spectral acceleration at bedrock in 0.2s period are higher than the S_a values in 1.0s periods, which is ranging from 0.60g to 1.50g. As for the 1.0s period, the S_a value is 0.30 – 0.55g. This result is larger than the investigation conducted by [32], which is 0.62 – 0.88g and 0.22 – 0.28g for the 0.2s and 1.0s periods, respectively. This difference is because this study has used the latest fault data sources according to the [12] and subduction earthquake source parameters with the latest earthquake catalog data up to July 2021 involving the 2021 M6.1 Malang earthquake.

The spectral acceleration for Yogyakarta region is also calculated using the steps as Malang region calculation. The map for Yogyakarta region was carried out from 3,775 points within the Yogyakarta region to obtain the value of Spectral acceleration (S_a) at bedrock and surface for period of 0.2s (S_S), and 1.0s (S_1) with 2% probability of exceedance (PE) in 50 years. The results of the S_a values for 3,775 points were shown in Table 4.11 and then plotted and displayed on the spectral acceleration microzonation map for the periods of 0.2s (S_S) and 1.0s (S_1) as presented in Figure 4.25 and Figure 4.26 for Sa at bedrock and Figure 4.27 and Figure 4.28 for Sa at ground surface, respectively.

Table 4. 11 The calculation of Spectral acceleration for bedrock and surface of Yogyakarta region

No.	Longitude	Latitude	Vs30	Soil	Ss R	Ss S	S_1 R	S_1 S
1	110.4333	-7.5500	900	SB	0.9258	1.5364	0.3777	0.6681
2	110.4417	-7.5500	900	SB	0.9297	1.5395	0.3777	0.6678
3	110.4500	-7.5500	900	SB	0.9339	1.5429	0.3725	0.6660
4	110.4250	-7.5583	900	SB	0.9290	1.5470	0.3798	0.6701
5	110.4333	-7.5583	900	SB	0.9324	1.5495	0.3798	0.6698
6	110.4417	-7.5583	900	SB	0.9361	1.5523	0.3747	0.6682
7	110.4500	-7.5583	900	SB	0.9403	1.5560	0.3748	0.6678
8	110.4167	-7.5667	745	SC	0.9324	1.5717	0.3818	0.6722
9	110.4250	-7.5667	828	SB	0.9355	1.5662	0.3819	0.6719
10	110.4333	-7.5667	900	SB	0.9389	1.5623	0.3770	0.6702
11	110.4417	-7.5667	900	SB	0.9427	1.5655	0.3771	0.6699
12	110.4500	-7.5667	900	SB	0.9466	1.5691	0.3772	0.6696
13	110.4083	-7.5750	659	SC	0.9357	1.5905	0.3839	0.6743
14	110.4167	-7.5750	709	SC	0.9386	1.5882	0.3840	0.6740
15	110.4250	-7.5750	697	SC	0.9418	1.5940	0.3840	0.6738
16	110.4333	-7.5750	772	SB	0.9452	1.5885	0.3793	0.6721
17	110.4417	-7.5750	900	SB	0.9489	1.5782	0.3794	0.6717
18	110.4500	-7.5750	900	SB	0.9529	1.5821	0.3795	0.6714
19	110.4583	-7.5750	877	SB	0.9572	1.5896	0.3797	0.6713
20	110.4083	-7.5833	615	SC	0.9417	1.6082	0.3860	0.6761
21	110.4167	-7.5833	707	SC	0.9447	1.6004	0.3860	0.6758
22	110.4250	-7.5833	737	SC	0.9478	1.6008	0.3815	0.6741
23	110.4333	-7.5833	718	SC	0.9513	1.6081	0.3816	0.6740
24	110.4417	-7.5833	748	SC	0.955	1.6092	0.3817	0.6736
25	110.4500	-7.5833	727	SC	0.9590	1.6184	0.3818	0.6734
3775	110.8000	-8.1917	500	SC	1.9452	2.2157	0.7853	0.9694

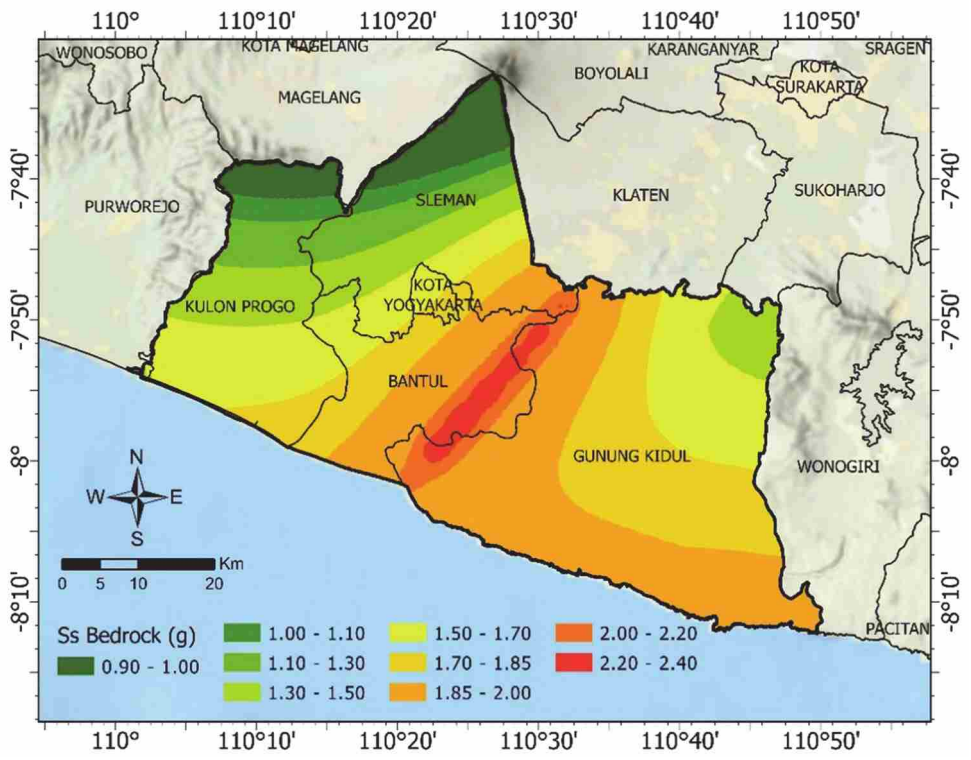

Figure 4. 25 Spectral acceleration map at bedrock for short period 0.2s (S_S bedrock) of Yogyakarta region

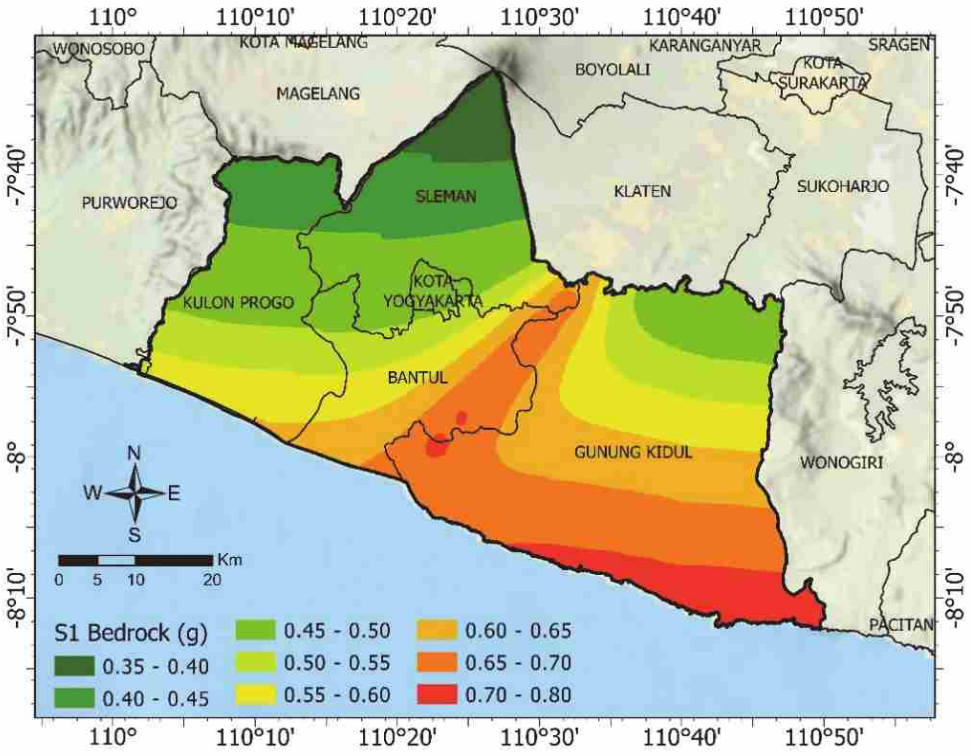

Figure 4. 26 Spectral acceleration map at bedrock for long period 1.0s (S_1 bedrock) of Yogyakarta region

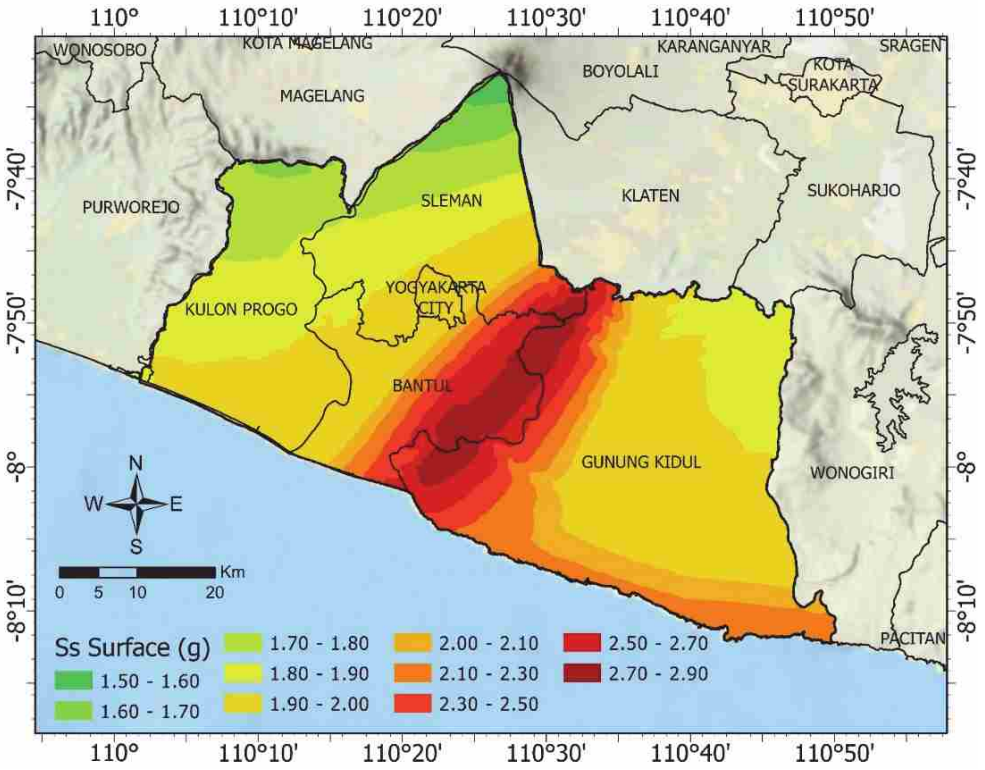

Figure 4. 27 Spectral acceleration at ground surface for short period 0.2s (S_S surface) of Yogyakarta region

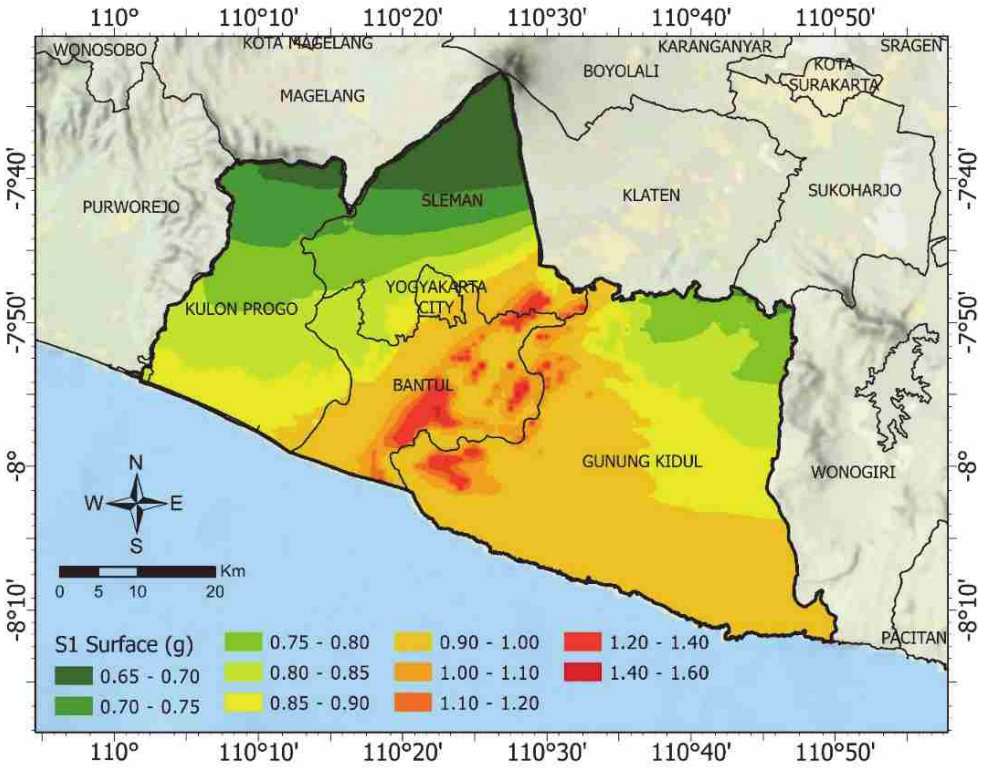

Figure 4. 28 Spectral acceleration at ground surface for long period 1.0s (S_1 surface) of Yogyakarta region

The spectral acceleration value at bedrock in 0.2s period (S_S value) for Yogyakarta region are more varied which is about 0.9g to 2.4g. On the other hand, the spectral acceleration value at bedrock for 1.0s period (S_1 value) is ranging from 0.35 to 0.80g. The picture shows that the pattern of spectral acceleration value follows the Opak fault line located near the Opak river. The highest Ss and S_1 values are marked with the red colour zone. The southeast part of Yogyakarta region also has a high S_S and S_1 value as a result of the influence of subduction earthquake sources.

4.3.3 Seismic Site Coefficient, Fa and Fv Map

The site coefficient values, Fa and Fv are obtained for each site location by dividing the spectral acceleration value at ground surface and bedrock at the same period using the equation (2.1). The result of calculation is presented in Table 4.12 for Malang region and Table 4.13 for Yogyakarta region, respectively. In order to display the more detail Fa and Fv values, the values of Fa and Fv are mapped using ArcGIS Pro 2.8. For Malang region, the Fa values are divided into 8 zones while Fv values are grouped in 9 zones as presented in Figure 4.29 and Figure 4.30. However, the Fa and Fv values for the Yogyakarta region are divided into 8 zones each as presented in Figure 4.31 and Figure 4.32.

Table 4. 12 The calculation of site coefficient for Malang region

No.	Longitude	Latitude	Ss R	Ss S	S_1 R	S_1 S	Fa	Fv
1	112.3417	-7.7667	0.6800	0.9989	0.2951	0.6029	1.469	2.043
2	112.3500	-7.7667	0.6788	0.9977	0.2947	0.6021	1.470	2.043
3	112.3583	-7.7667	0.6776	0.9964	0.2943	0.6014	1.470	2.043
4	112.5917	-7.7667	0.6348	0.9598	0.2808	0.5714	1.512	2.035
5	112.2917	-7.7750	0.6872	1.0441	0.2974	0.6011	1.519	2.021
6	112.3000	-7.7750	0.6860	1.0343	0.2970	0.6003	1.508	2.021
7	112.3083	-7.7750	0.6848	1.0277	0.2967	0.6000	1.501	2.022
8	112.3333	-7.7750	0.6837	1.0179	0.2963	0.6046	1.489	2.040
9	112.3417	-7.7750	0.6826	1.0125	0.2960	0.6049	1.483	2.044
10	112.3500	-7.7750	0.6813	1.0026	0.2956	0.6041	1.472	2.044
11	112.3583	-7.7750	0.6801	0.9983	0.2952	0.6031	1.468	2.043
12	112.3667	-7.7750	0.6788	0.9966	0.2948	0.6023	1.468	2.043
13	112.4250	-7.7750	0.6704	0.9921	0.2926	0.6041	1.480	2.065
14	112.4333	-7.7750	0.6670	0.9858	0.2904	0.5878	1.478	2.024
15	112.4417	-7.7750	0.6656	0.9873	0.2900	0.5889	1.483	2.031
16	112.4583	-7.7750	0.6628	0.9841	0.2891	0.5871	1.485	2.031
17	112.4667	-7.7750	0.6614	0.9813	0.2887	0.5859	1.484	2.029
18	112.4750	-7.7750	0.6600	0.9794	0.2884	0.5858	1.484	2.031
19	112.4833	-7.7750	0.6597	0.9802	0.2886	0.5926	1.486	2.053
20	112.5917	-7.7750	0.6375	0.9603	0.2817	0.5728	1.506	2.033
21	112.6000	-7.7750	0.6359	0.9591	0.2815	0.5723	1.508	2.033
22	112.3000	-7.7833	0.6887	1.0536	0.2980	0.6024	1.530	2.021
23	112.3083	-7.7833	0.6875	1.0473	0.2976	0.6021	1.523	2.023
24	112.3167	-7.7833	0.6863	1.0348	0.2972	0.6010	1.508	2.022
25	112.3250	-7.7833	0.6872	1.0434	0.2974	0.6046	1.518	2.033
4224	112.7083	-8.4583	0.9972	1.6926	0.3998	0.6803	1.697	1.702

Table 4. 13 The calculation of site coefficient for Yogyakarta region

No.	Longitude	Latitude	Ss R	Ss S	S_1 R	S_1 S	Fa	Fv
1	110.4333	-7.5500	0.9258	1.5364	0.3777	0.6681	1.660	1.769
2	110.4417	-7.5500	0.9297	1.5395	0.3777	0.6678	1.656	1.768
3	110.4500	-7.5500	0.9339	1.5429	0.3725	0.6660	1.652	1.788
4	110.4250	-7.5583	0.9290	1.5470	0.3798	0.6701	1.665	1.764
5	110.4333	-7.5583	0.9324	1.5495	0.3798	0.6698	1.662	1.764
6	110.4417	-7.5583	0.9361	1.5523	0.3747	0.6682	1.658	1.783
7	110.4500	-7.5583	0.9403	1.5560	0.3748	0.6678	1.655	1.782
8	110.4167	-7.5667	0.9324	1.5717	0.3818	0.6722	1.686	1.761
9	110.4250	-7.5667	0.9355	1.5662	0.3819	0.6719	1.674	1.759
10	110.4333	-7.5667	0.9389	1.5623	0.3770	0.6702	1.664	1.778
11	110.4417	-7.5667	0.9427	1.5655	0.3771	0.6699	1.661	1.776
12	110.4500	-7.5667	0.9466	1.5691	0.3772	0.6696	1.658	1.775
13	110.4083	-7.5750	0.9357	1.5905	0.3839	0.6743	1.700	1.756
14	110.4167	-7.5750	0.9386	1.5882	0.3840	0.6740	1.692	1.755
15	110.4250	-7.5750	0.9418	1.5940	0.3840	0.6738	1.693	1.755
16	110.4333	-7.5750	0.9452	1.5885	0.3793	0.6721	1.681	1.772
17	110.4417	-7.5750	0.9489	1.5782	0.3794	0.6717	1.663	1.770
18	110.4500	-7.5750	0.9529	1.5821	0.3795	0.6714	1.660	1.769
19	110.4583	-7.5750	0.9572	1.5896	0.3797	0.6713	1.661	1.768
20	110.4083	-7.5833	0.9417	1.6082	0.3860	0.6761	1.708	1.752
21	110.4167	-7.5833	0.9447	1.6004	0.3860	0.6758	1.694	1.751
22	110.4250	-7.5833	0.9478	1.6008	0.3815	0.6741	1.689	1.767
23	110.4333	-7.5833	0.9513	1.6081	0.3816	0.6740	1.690	1.766
24	110.4417	-7.5833	0.9550	1.6092	0.3817	0.6736	1.685	1.765
25	110.4500	-7.5833	0.9590	1.6184	0.3818	0.6734	1.688	1.764
				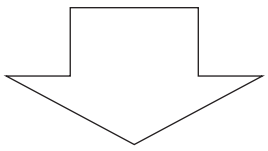				
3775	110.8000	-8.1917	1.9452	2.2157	1.1391	0.7853	0.969	1.234

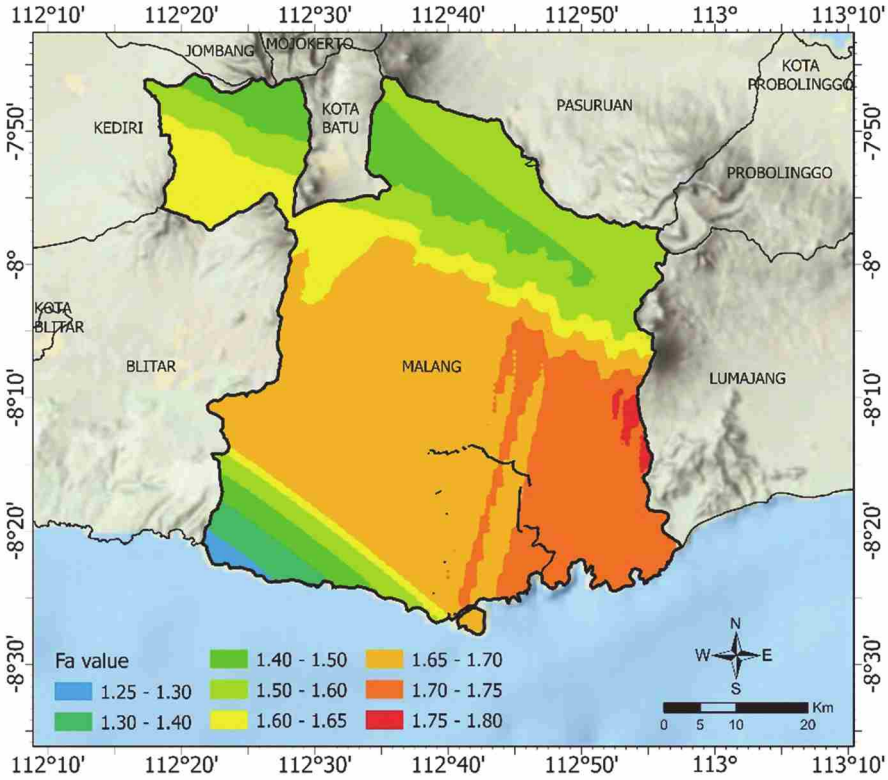

Figure 4. 29 Seismic site coefficient map for short period, Fa

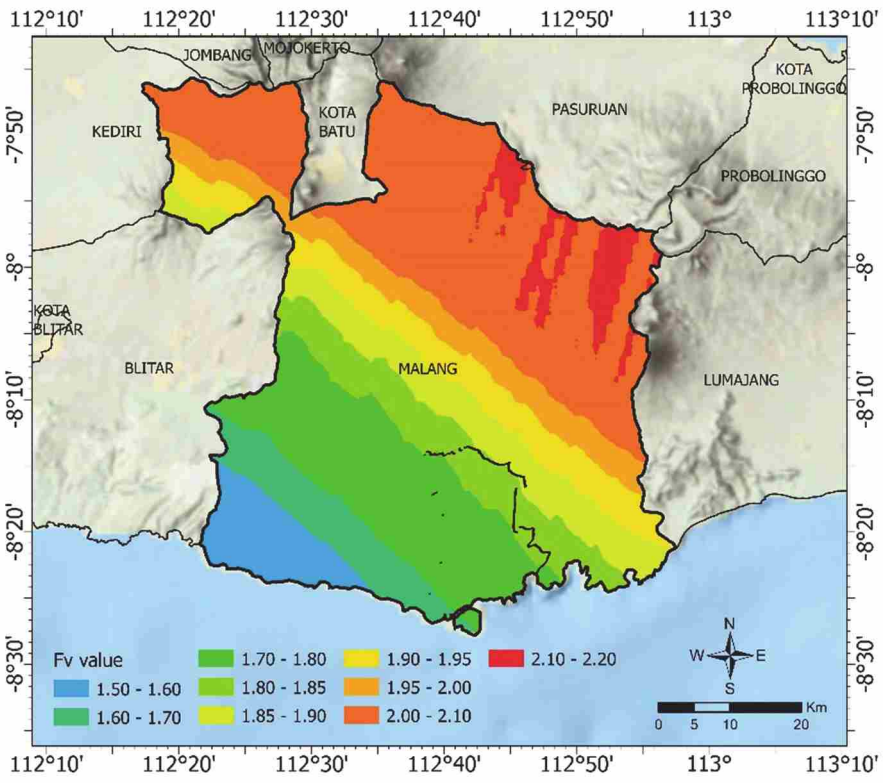

Figure 4. 30 Seismic site coefficient map for long period, Fv

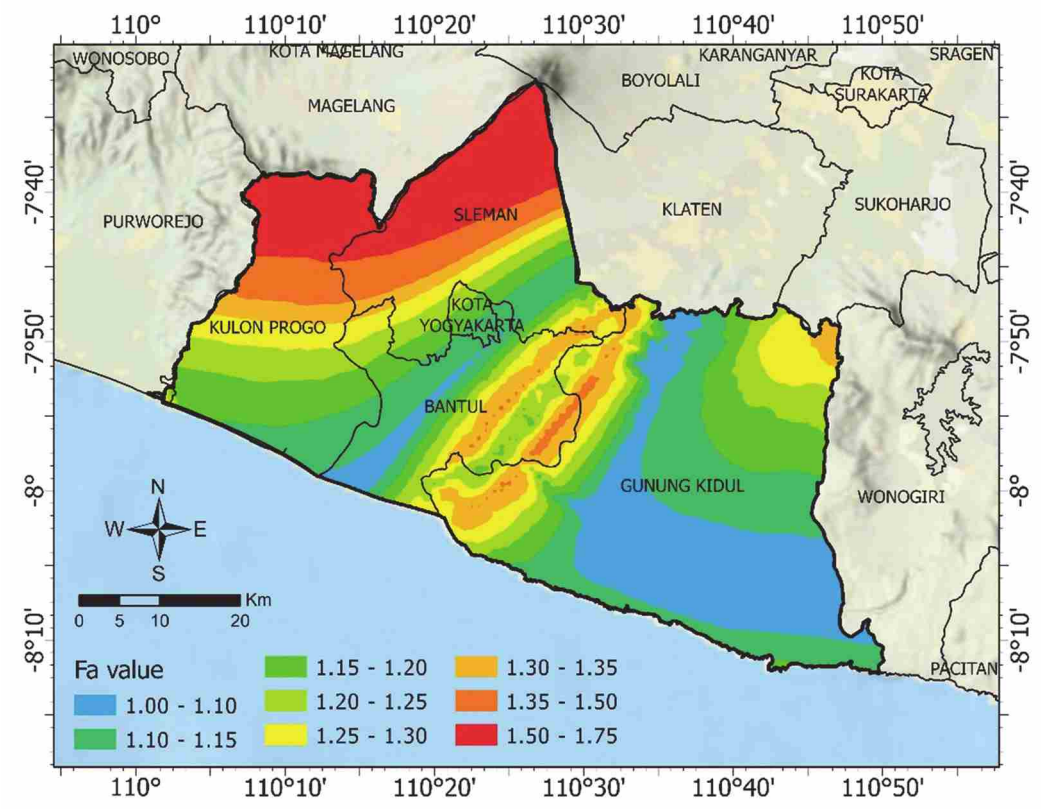

Figure 4. 31 Seismic site coefficient map for short period, Fa

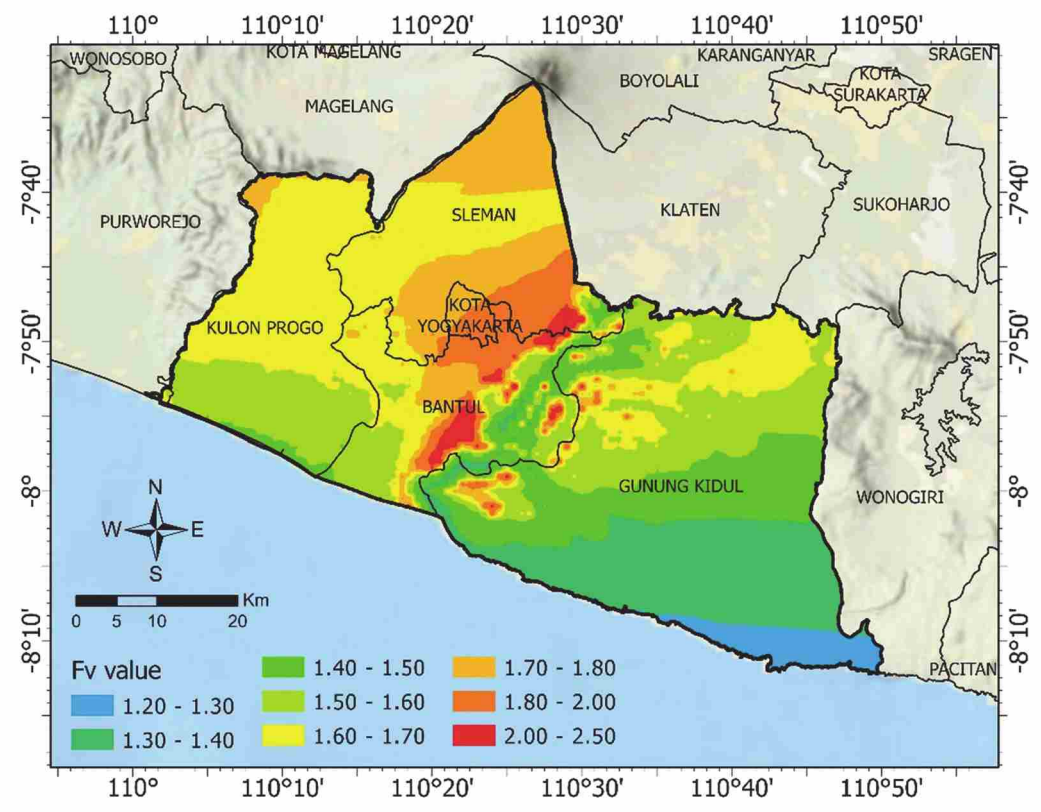

Figure 4. 32 Seismic site coefficient map for long period, Fv

Figure 4.29 depicts the values of seismic site coefficient for short period, Fa are between 1.25 and 1.80. The lowest value of Fa is in the southwest part of Malang region. The highest Fa value is in the middle and eastern part of Malang region which has relatively lower Vs30 value (soft to medium soil condition). Fa values for the northern part of Malang region are about 1.4-1.6. The northern part of Malang region has the lowest spectral acceleration values, but it has relatively high shear wave velocity since the area is a mountainous area, resulting in medium to high seismic site coefficient (Fa value). Figure 4.30 reveals the Fv values for Malang region are within 1.5 to 2.2. The highest Fv value is in the northeast part of Malang region which has relatively medium soil condition and lower spectral acceleration value at bedrock. Similar to the Fa value, the lowest Fv value is in the southwest part of Malang region marked by the blue zone. The middle part of Malang, which has the lowest shear wave velocity has the Fv value of about 1.8-2.1. These values are relatively high and essential to be considered in earthquake resistance building design. The Fa and Fv values for Yogyakarta region are varied. The site coefficient at a short period or Fa is affected by the sedimentary soil at Opak river valley or strongly affected by the activity of Opak fault as a seismic source. The results indicate that the area with the lower shear wave velocity (soft to medium soil condition) has the relatively higher value of Fa and Fv. All the result findings indicate that the value of Fa and Fv are relatively influenced by the soil condition (shear wave velocity, Vs30 value) and the spectral acceleration value at bedrock.

4.4 Conclusion

The seismic distribution related to tectonic conditions and microzonation maps for the Malang region have been conducted. The number of small earthquakes causing the energy of earthquake released more smoothly, while the less frequent earthquakes occur, the possibility of large earthquakes will be greater. The temporal b-value analysis shows a significant decrease of b-value values from 2013 until before the Malang earthquake (April 9, 2021). A relatively significant decrease in the b-value indicates an accumulation of trapped energy causing a high stress level, which triggers a large earthquake. The spatial analysis result shows the variation of b-value from 0.72 to 1.08. Thus, the b-value map shed light on the indication of a relatively decreased b-value even until the last day of observation. This phenomenon indicates the possibility for future large earthquakes in the study area.

Based on the acceleration microzonation maps at bedrock for Malang region, the range of SA values is 0.3-0.7g for PGA, 0.6-1.3g for a short period (S_S), and 0.3-0.5 for a long period (S_1). The subduction earthquake sources dominantly influence spectral acceleration values of the Malang region. The further south, the depth of the earthquake source tends to be shallower so that the spectral acceleration is relatively higher. The Fa and Fv values for Malang are varied. The results indicate that the area with the lower shear wave velocity (soft to medium soil condition) has the relatively higher value of Fa and Fv. Moreover, the area with the lower value of spectral acceleration (Ss and S_1) at bedrock and lower value of shear wave velocity has the higher value of seismic site coefficient (Fa and Fv). These study findings can be references in earthquake disaster mitigation, such as earthquake-resistant building design and spatial-building planning in Malang and its vicinity.

On the other hand, Yogyakarta region is located in earthquake prone area which the Eurasian Plate moved southward colliding with the Australian Plate which is moving northward. Thus, there is not only Opak fault line but also the subduction earthquake sources threat this region. Studies on seismic site coefficient for short period Fa and long period Fv have been conducted. Based on the acceleration microzonation maps at bedrock for Yogyakarta region, the range of S_a value is 0.9-2.4g for a short period (S_S), and 0.35-0.80 for a long period (S_1). This result is relatively higher than the S_a value for Malang region. The Opak fault line dominantly influence the spectral acceleration values of the Yogyakarta region. the pattern of spectral acceleration value follows the Opak fault line located near the Opak river. The further south, the depth of the earthquake source tends to be shallower so that the spectral acceleration is relatively higher.

The Fa and Fv values for Yogyakarta region are varied. The site coefficient at a short period or Fa is affected by the sedimentary soil at Opak river valley or strongly affected by the activity of Opak fault as a seismic source. The results indicate that the area with the lower shear wave velocity (soft to medium soil condition) has the relatively higher value of Fa and Fv. Moreover, the area with the lower value of spectral acceleration (S_S and S_1) at bedrock and lower value of shear wave velocity has the higher value of seismic site coefficient (Fa and Fv). These study findings are essential to be considered in earthquake resistant building design.

4.5 References

[1] Central Bureau of Statistics (BPS) of Malang district, 2021, *Berita Resmi Statistik* The 2020 population census No. 2/01/3507/Th. I. Malang, Indonesia.

[2] Meteorological, Climatological, and Geophysical Agency (BMKG) 2021 *Report* Earthquake Review due to Earthquake in Southwest Malang, East Java 10 April 2021

[3] Meteorological, Climatological, and Geophysical Agency (BMKG) 2021 Isoseismal map based on MMI observations of the Malang earthquake, April 10, 2021

[4] Regional Disaster Management Agency (BPBD) of Malang district 2021 *Report* Laporan kerusakan akibat Gempa Malang 2021

[5] Desmonda N I and Pamungkas A 2014 *Jurnal Teknik Pomits* Determination of vulnerability zones for tectonic earthquakes in the southern district of Malang 3 (2) 107-112 (in bahasa)

[6] Kumala S A and Wahyudi 2016 *Inersia* Analysis of PGA (Peak Ground Acceleration) value for all districts and cities in East Java XII (1) 37-43 (in bahasa)

[7] Purbandini P, Santosa B J and Sunardi B 2017 *Jurnal Sains dan Seni ITS* Seismic hazard analysis for Malang region using probabilistic approach 6 (2) 2337-3520 (in bahasa)

[8] Smith W D 1981 *Nature* The b-value as an earthquake precursor 289 136 –139

[9] Elnashai, A.S., Kim, S.J., Yun, G.J., & Sidarta, D., 2006. The Yogyakarta Earthquake of May 27th, 2006, Mid-America Earthquake Center Report No.07-02. Urbana: University of Illinois Champaign.

[10] Federal Emergency Management Agency (FEMA), 1992. NEHRP Handbook for the Seismic Evaluation of Existing Buildings. FEMA 178. Washington, D.C.: FEMA Publication.

[11] National Standardization Agency (BSN) 2019 SNI 1726:2019 Procedures for earthquake resistance structural buildings and non-buildings, Jakarta, Indonesia

[12] National Center for Earthquake Studies (PuSGeN). Indonesian Seismic Sources and Seismic Hazard Maps 2017. Center for Research and Development of Housing and Resettlement, Ministry of Public Works and Human Settlements, (Peta Sumber dan Bahaya Gempa Indonesia Tahun 2017. Pusat Litbang Perumahan dan Pemukiman, Kementerian Pekerjaan Umum dan Perumahan Rakyat), 2017, pp 1–377.

[13] Reasenberg P 1985 *Journal of Geoph. Research: Solid Earth* Second-order Moment of Central California Seismicity 1969–1982 90 (B7) 5479–5495

[14] Muntafi Y and Nojima N 2021 *Int. J. of Geomate* Seismic properties and fractal dimension of subduction zone in Java and its vicinity using data from 1906 to 2020 21 (85) 71-83

[15] Gutenberg B and Richter C F 1944 *Bull. Seismol. Soc. Am.* Frequency of earthquakes in California 34 185– 188

[16] Scholz C H 1968 *Bull. Seismol. Soc. Am.* The frequency magnitude relation of micro fracturing in rock and its relation to earthquakes 58 399–415

[17] Aki K 1965 *Bull. Earthquake Res Inst.* Maximum likelihood estimate of b in the formula log N=a-bM and its confidence limits Tokyo Univ. 43 237-239

[18] Utsu T 1965 *Geophys. Bull. Hokkaido Univ*. A method for determining the value of b in a formula Log $N = a – bM$ showing the magnitude frequency for earthquakes 13 99–103

[19] Rohadi S., Grandis H., and Ratag M. A., Studi Variasi Spasial Seismisitas Zona Subduksi Jawa (Study of the Spatial Variation for Java Subduction Zone Seismicity), Jurnal Meteorologi dan Geofisika, Vol. 8, Issue 1, 2007, pp.42-47.

[20] Wulandari, A., Suharno, S., Rustadi, R. dan Robiana, R. (2016), Microzonation mapping of earthquake prone area using the HVSR method in the Painan area of West Sumatra (Pemetaan Mikrozonasi Daerah Rawan Gempabumi menggunakan metode HVSR daerah Painan Sumatra Barat), JGE (Jurnal Geofisika Eksplorasi), Vol.4, No.1, pp.33–48.

[21] Supartoyo (2008), Catalog of destructive earthquakes in Indonesia 1629-2007 (Katalog gempabumi merusak di Indonesia tahun 1629-2007), Ministry of Energy and Mineral Resources, Geological Agency, Center for Volcanology and Geological Hazard Mitigation, Bandung.

[22] Walter TR, Wang R, Leuhr BF, Wassermann J, Behr Y, Porolai S, Anggraini A, Gunther E, Sobiesiak G, Grosser H, Wetzel HU, Milkeriet C, Sri Brotopuspito PJK, Hatjadi P, Zschau J (2008) The 26 May magnitude 6.4 Yogyakarta Earthquake south of Merapi Volcano: Did Lahar deposit amplify ground shaking and thus lead to a disaster? Geochem Geophys Geosyst Res Letter.

[23] Cotton F, Scherbaum F, Bommer J J and Bungum H 2006 *J. Seismol.* Criteria for selecting and adjusting ground-motion models for specific target regions: Application to central Europe and rock sites 10 (2) 137–156

[24] Bommer J J, Douglas J, Scherbaum F, Cotton F, Bungum H and Fah D 2010 *Seismol. Res. Lett.* On the selection of ground-motion prediction equations for seismic hazard analysis 81 (5) 783–793

[25] Stewart J P, Douglas J, Javanbarg M, Bozorgnia Y, Abrahamson N A, Boore D M, Campbell K W, Delavaud E, Erdik M and Stafford P J 2015 *Earthq. Spectra* Selection of ground motion prediction equations for the global earthquake model 31 19-45

[26] Youngs R R, Chiou S J, Silva W J and Humphrey J R 1997 *Geophys. Res. Lett.* Strong ground motion attenuation relationships for subduction zone earthquake 68

[27] Atkinson G M and Boore D M 2003 *Bull. Seismol. Soc. Am*. Empirical ground motion relations for Subduction-Zone Earthquakes and their application to Cascadia and other region 93 (4) 1703-1729

[28] Gregor N J 2006 Applied by Steve Harmsen in USGS Software Fortran Code.

[29] Boore D M, Joyner W B and Fumal T E 1997 *Seismol. Res. Lett.* Equations for estimating horizontal response spectra and peak acceleration from western north American earthquakes: A Summary of Recent Work 68

[30] Chiou B S J and Youngs R R NGA (Next Generation Attenuation) 2006 Empirical Ground Motion Model for the Average Horizontal Component of Peak Acceleration and Pseudo-Spectral Acceleration for Spectral Periods 0.01 to 10 second1, Interim Report for USGS Review, Revised Editorially, July 10, 2006, California, USA

[31] Boore D M and Atkinson G M 2006 *Earthq. Spec.* Ground Motion Prediction Equations for the Average Horizontal Component of PGA, PGV, and 5% Damped PSA at Spectral Periods between 0.01 s and 10.0 s 24 (1)

[32] Purbandini P, Santosa B J and Sunardi B 2017 Jurnal Sains dan Seni ITS Seismic hazard analysis for Malang region using probabilistic approach 6 (2) 2337-3520 (in bahasa).

[33] Makrup L., Irsyam M., Sengara W. I., and Hendriyawan. Numerical solution of the total probability theorem in a three dimensional earthquake source domain for developing seismic hazard map and hazard spectrum, American Journal of Civil Engineering and Architecture, Vol. 3, no. 5, 2015, pp.158-164.

Chapter 5
Seismic Site Coefficient Map for Java

5.1 Introduction

Indonesia has implemented the seismic design code for building and non-building structure SNI-03-1726-2012 [1]. The code contains maps which were developed by conducting 1% probability of collapse in 50 years at short-period (0.2 second) spectral response acceleration, S_S, and long period (1.0 second) spectral response acceleration, S_1, at bedrock elevation. In 2019, the new seismic design code has been published. The spectral acceleration maps on the new seismic design code are based on the probability of exceedance of 2% in 50 years. Site class and site coefficient are two parameters needed for designing response spectra at ground surface. Based on [2] site class can be estimated using average standard penetration test (N-SPT), average shear wave velocity (Vs) and average un-drained shear strength (Su) of top 30-meter soil deposit. An average shear wave velocity in the upper 30-meter soil deposit is referred to as Vs30.

This chapter is a continuation of chapter 4. The seismic site coefficient value is carried out for the entire Java. Based on several previous research, many new faults have been identified on the Java Island. Several research related to the source of earthquakes in Java, especially active inland faults has been carried out [3-5]. In addition, in 2017, the National Center for Earthquake Studies (PusGeN) [6] published the Seismic Source and Seismic Hazard Map of Indonesia. All these previous studies become the basis of reference in determining the seismic site coefficient for Java region presented in this chapter.

5.2 Data and Method

5.2.1 Earthquake Data and Processing

The earthquake data used covered the longitude of 101-120^{o}E and latitude of 2-13^{o}S during 1906 to August 2021 obtained from the Agency of Meteorology, Climatology, and Geophysics (BMKG) Indonesia with the relocated hypocenter data using TeletomoDD method [7]. In addition, earthquake data from the International Seismological Center (ISC) [8] for historical earthquakes occurring in and around Java Island were also collected,

including the EHB (Engdahl, van der Hilst, and Buland) improved earthquake data set [9]. All the earthquake data were then converted into the uniform magnitude scale (Moment magnitude, Mw) using the magnitude correlation for Indonesia region presented in Table 4.1.

After all the earthquake data have been homogenized into Mw scale, the declustering process was performed to investigate the dependent and independent earthquakes. Five of the most well-known declustering algorithms are Gardner and Knopoff (1974), Reasenberg (1985), Uhrhammer (1986), Zhuang et al. (2002), and Zaliapin and Ben-Zion (2013) [10-14]. In 1974, Gardner and Knopoff introduced a procedure for identifying aftershocks within seismicity catalogs using time and space inter-event distances. This method, known as a window method is one of the simplest forms of aftershock identification, which is not consider the secondary and higher order aftershocks. By assuming circular spatial windows, this method ignored the fault extension for larger magnitude earthquakes. In 2019, Teng and Baker [15] evaluated several declustering algorithm models for earthquake data and applied it to a seismic hazard analysis in two cities in the USA. The results show that the Gardner and Knopoff and Zhuang methods using the epidemic type of aftershock sequence (ETAS) [16,17] potentially result in a negligible likelihood of massive earthquakes being mainshocks and overestimate the effects of foreshocks.

Their observations shed light on both Reasenberg and Zaliapin and Ben-Zion declustering algorithms provide better results for a seismic hazard analysis. This study used the Reasenberg method for declustering the earthquake data which was also carried out by Susilo et al. (2019) [18] for an earthquake analysis in East Java, Indonesia. The algorithm of Reasenberg (1985) allows to link up aftershock triggering within an earthquake cluster. It assumes an interaction zone centered on each earthquake event. If A is the mainshock of B, and B the mainshock of C, then all A, B and C are considered to belong to one common cluster. When defining a cluster, only the largest earthquake is finally kept being the cluster's mainshock. From this process, a catalog of earthquakes from 1906 to August 2021 with magnitude of Mw $\geq$ 4.5 and depth $\leq$ 300km is displayed in Figure 5.1, while the distribution of earthquake hypocenter in 3D view is shown in Figure 5.2.

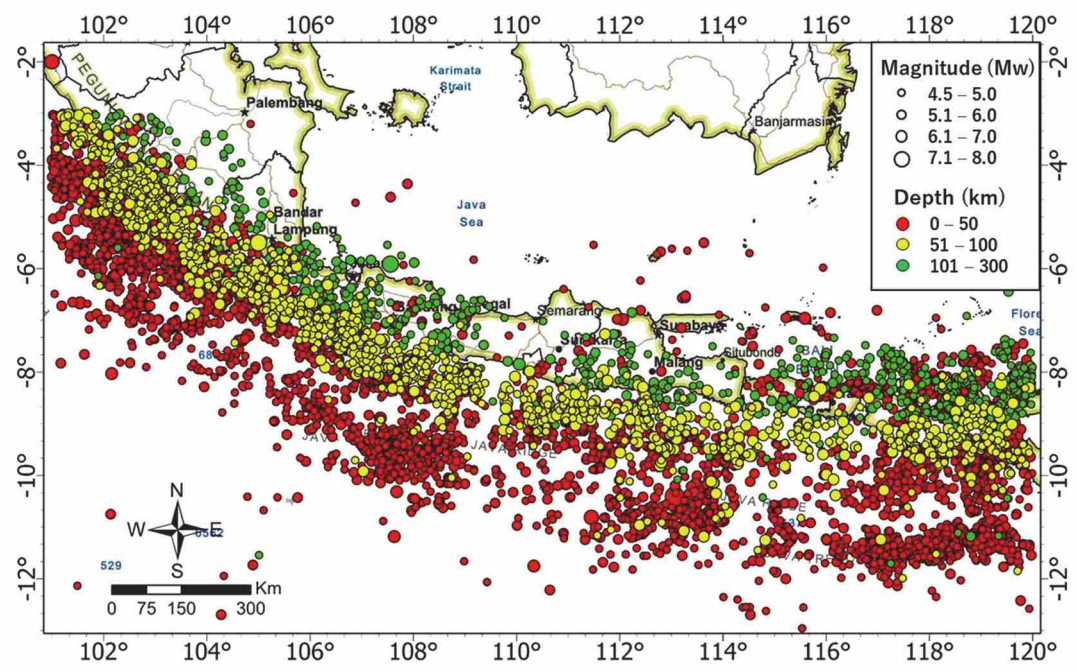

Figure 5. 1 Earthquake epicenter distribution for Java and its surrounding between 1906 and August 2021 with magnitude Mw≥4.5 and depth ≤300km

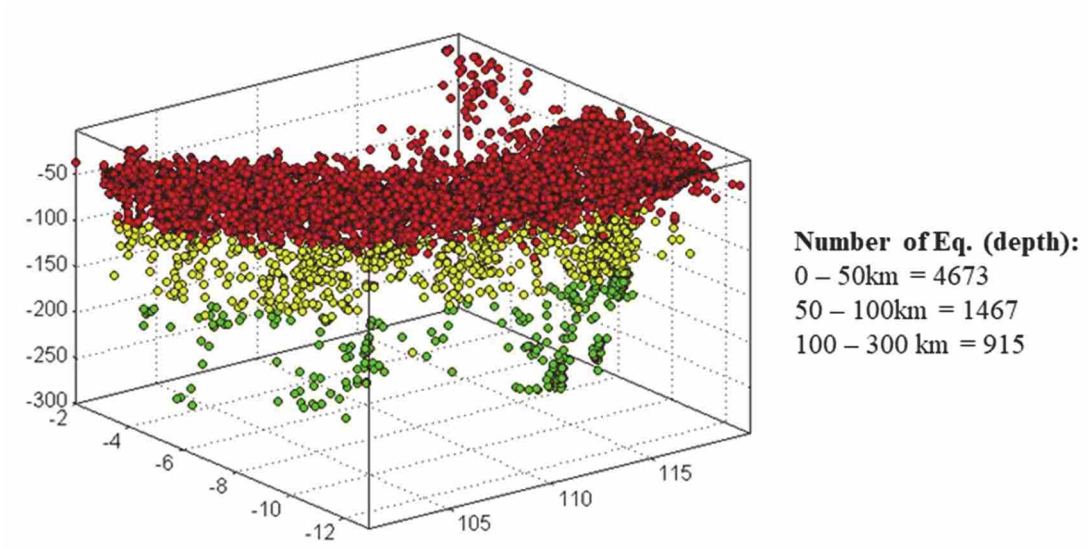

Figure 5. 2 Earthquake hypocenter distribution in 3D view with magnitude Mw≥4.5 and depth ≤300km

Historical earthquake data used in this study is the events with magnitude Mw≥4.5 occurring in and around Java, a magnitude that is considered for seismic hazard analysis and engineering practice in Indonesia. This refers to the National Center for Earthquake Studies (PuSGeN) of Indonesia, which developed the Indonesia Seismic Hazard Map. The figure

clearly shows that the earthquake events are dominantly by the events with a depth of less than 50km, which is categorized as shallow earthquakes. Meanwhile, the intermediate earthquake which is 50-300km deep are 2,382 events. In order to get more detail information of earthquake distribution based on magnitude and depth in each year, those relationships are presented in Figure 5.3.

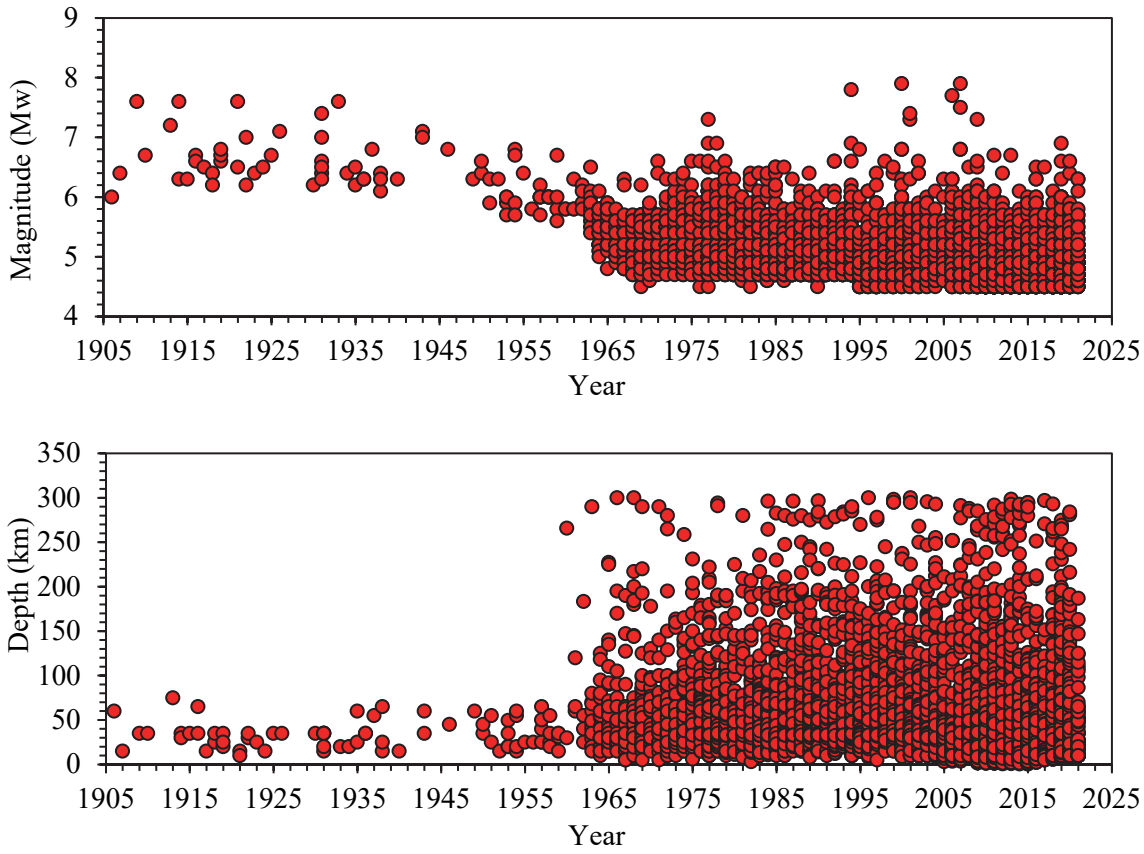

Figure 5. 3 Earthquake epicenter distribution for Java and its surrounding based on magnitude (Mw) and depth (km) in time

It can be seen on the figure that the earthquakes recorded before 1960 were only large earthquakes with magnitude above Mw5.5 due to the limitation capability of seismic record instrument. In addition, only shallow earthquakes with a depth of less than 100km were recorded before 1960. Several large earthquakes with magnitude Mw≥7.5 occurred in Java and surrounding areas are presented in the cumulative number of earthquakes graph as presented in Figure 5.4.

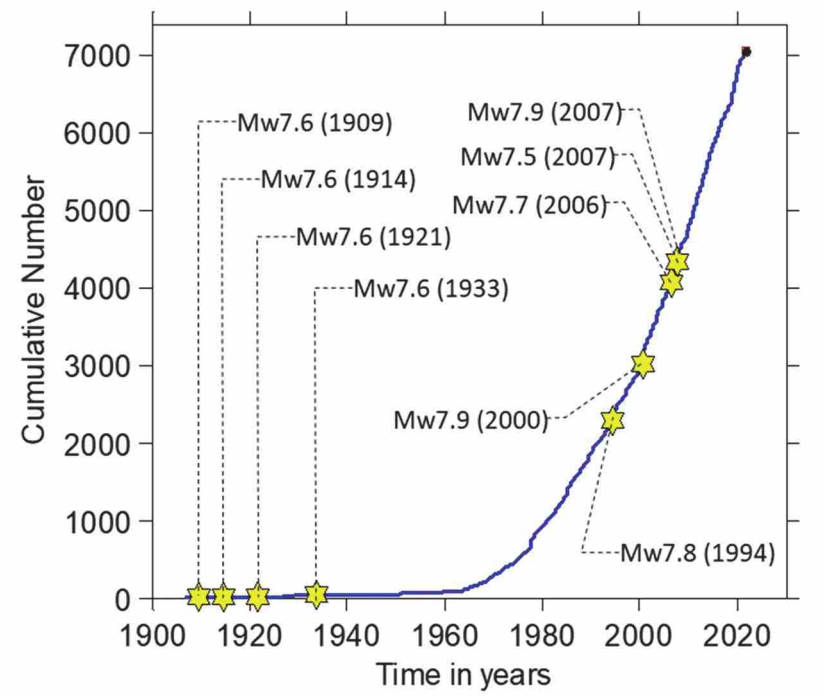

Figure 5. 4 Cumulative number of earthquakes in time and several large earthquakes with magnitude Mw>7.5

Based on the earthquake data recorded in the national and international earthquake databanks, the subduction zone in the southern part of Java only produces earthquakes with a magnitude class of Mw-7, there is no history of earthquake events with a magnitude of Mw8 or above. However, the results comprehensively described in Chapter 3 shows that there is a potential for an earthquake with a magnitude of Mw8-9 in the Java subduction zone. This result in line with the research conducted by [19, 20]. Thus, the results of the maximum magnitude estimation need to be considered in seismic hazard modeling for subduction earthquake sources. It is also essential to consider the rupture mechanism whether it may rupture separately or together during an earthquake.

5.2.2 Earthquake Source Identification

Java is located in one of the most active tectonic regions, characterized by the subduction of the Indo-Australian plate under the Eurasian plate at a present rate of 7.0-8.0 cm/yr [21]. The contact between these two plates produces large earthquakes, depths ranging between 5 and 50 km, known as interplate, thrust events. The cross-section of Java subduction has been presented in Figure 3.3 (Chapter 3). Earthquake events due to thrust faults, normal faults, reverse slips, and strike slips that occur along plate encounters can be

classified as subduction zones. The subduction zone is divided into an interplate/megathrust zone and an intraplate/benioff zone. The megathrust zone is at a depth of less than 50 km and the benioff zone covered the area at a depth of more than 50 km [22] as shown in Figure 5.5.

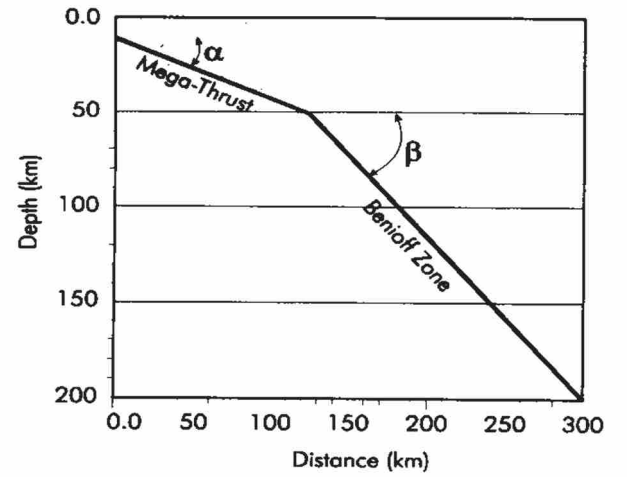

Figure 5. 5 Subduction zone model [22]

This study used the subduction model for interplate events and intraplate events along Java region. General cross-section diagram of Java subduction zone, the collision between Indo-Australian Plate and Eurasian Plate is presented in Figure 5.6.

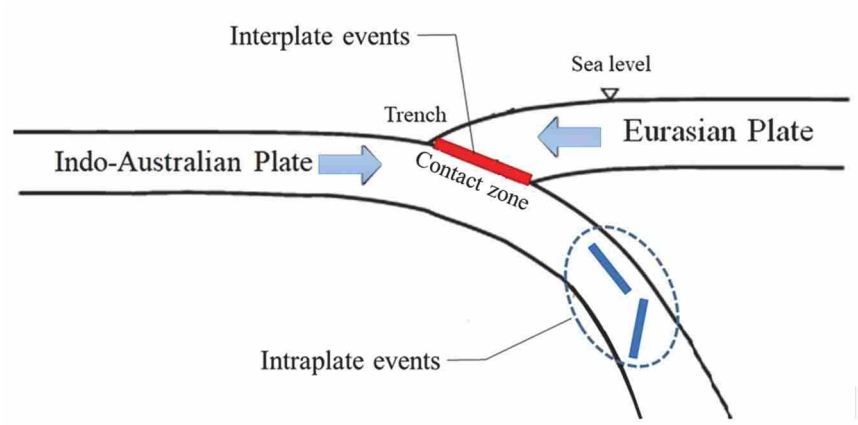

Figure 5. 6 Schematic of Java subduction cross-section

The very different behavior of subduction zones involving young and old lithosphere is also shown in the strain regime manifested behind the magmatic arc: Some subduction zones spawn back arc basins with rifting or even seafloor spreading, whereas others induce folding and thrusting behind the arc. A first-order differentiation of subduction zones

distinguishes those subducting old lithosphere (Mariana type) from those subducting young lithosphere (Chilean type) as presented in Figure 5.7.

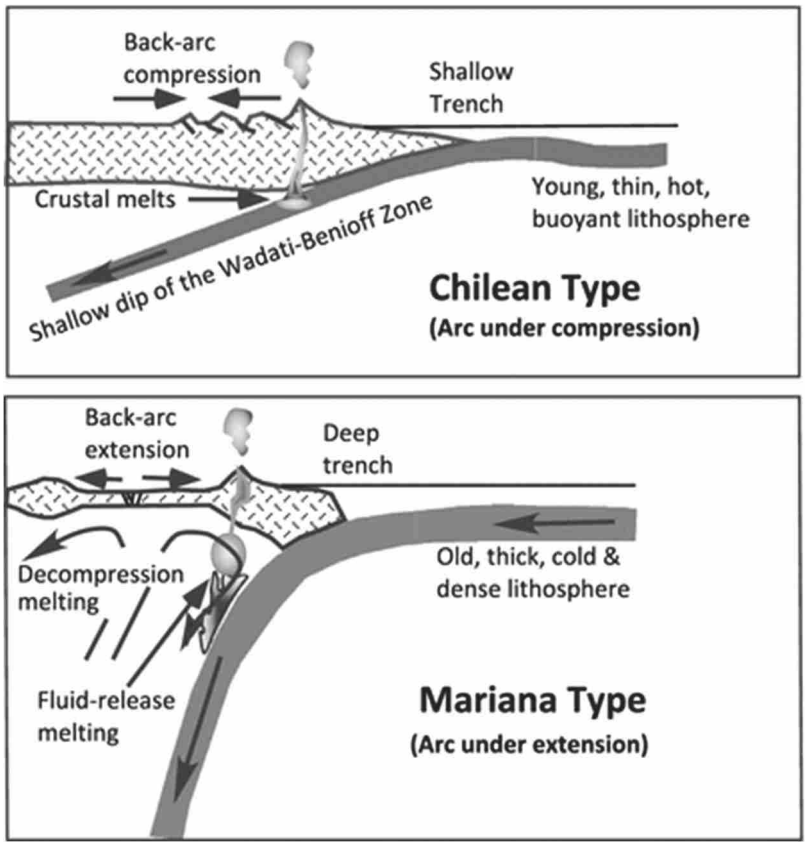

Figure 5. 7 Types of subduction zones based on the lithosphere age being subducted [23]

Mariana-type subduction zones are strongly extensional with weak coupling between the two plates, whereas Chilean-type subduction zones are strongly compressional with strong coupling between the two plates. Based on their characteristics, results of the investigation of Java and Sumatra subduction described in Chapter 3 show that the Java subduction are almost equivalent to the Mariana type while the Sumatra subduction resembles the Chilean type. However, the further studies should be conducted to confirm this phenomenon.

The modeling of the subduction segmentations in this study is based on several research related to Java coupling information conducted by [19] for western Java, [24,25] for eastern Sunda-Banda Arc and Java and [20] for the central and eastern Java using the GPS inversion data. The subduction model and fault line in and around Java region are shown in Figure 5.8.

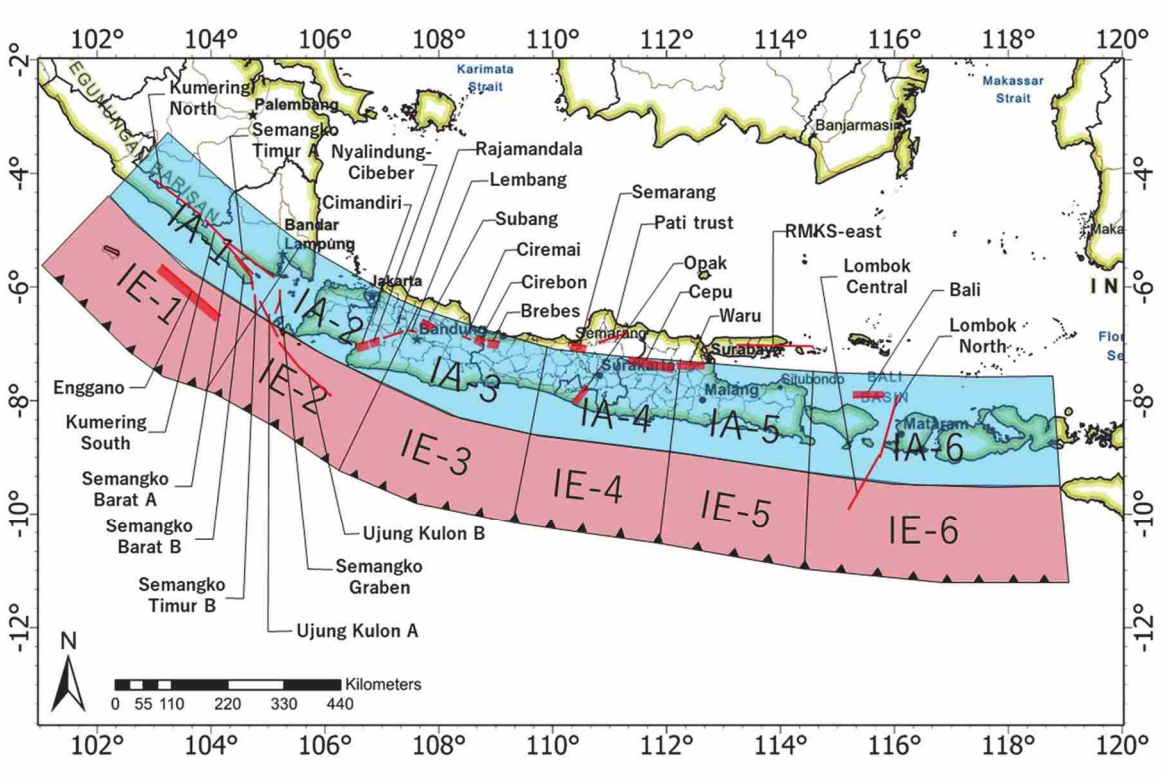

Figure 5. 8 Seismic source modeling for Java and its surrounding

The frequency-magnitude distribution (FMD) for each group of earthquakes subduction segment was conducted by using the equation first acknowledged in Japan (Ishimoto and Lida, 1939) then in California (Gutenberg and Richter, 1994) which is commonly known as the Gutenberg-Richter (G-R) power law. In this study, we followed the FMD provided by Gutenberg and Richter [26] that has been verified for global and regional seismicity. The Gutenberg-Richter relationship is shown in Figure 5.9.

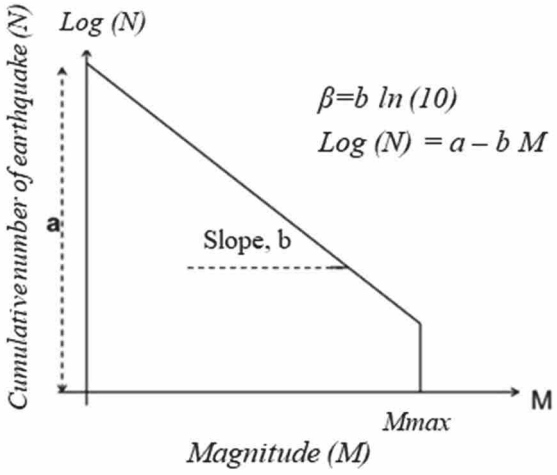

Figure 5. 9 Frequency magnitude distribution of earthquake (Gutenberg-Richter Law)

The empirical formula of Gutenberg-Richter Law is as follows:

$$log\,(N)=a - b\,M \quad \text{or} \quad N=e^{\alpha - \beta M} \tag{5.1}$$

where N describes the cumulative number of earthquakes with magnitude equal to or greater than *M, a* and *b* are constants, commonly known as a-values and b-values, indicating the seismicity activity and the log-linear relation's slope, respectively, and e is a natural number. The FMD of each interplate and intraplate subduction segment is presented in Figure 5.10 and Figure 5.11.

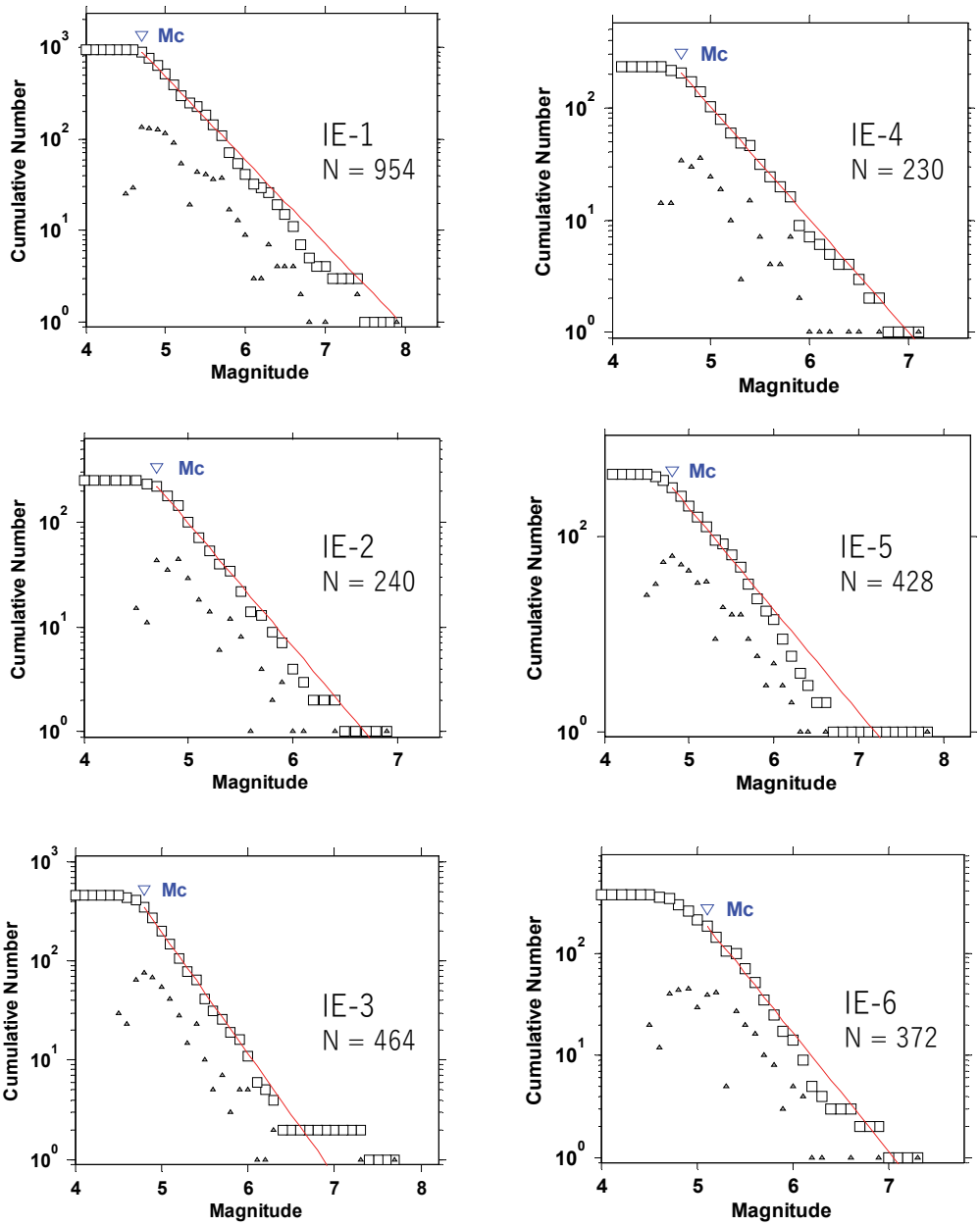

Figure 5. 10 Frequency magnitude distribution for interplate subduction segment

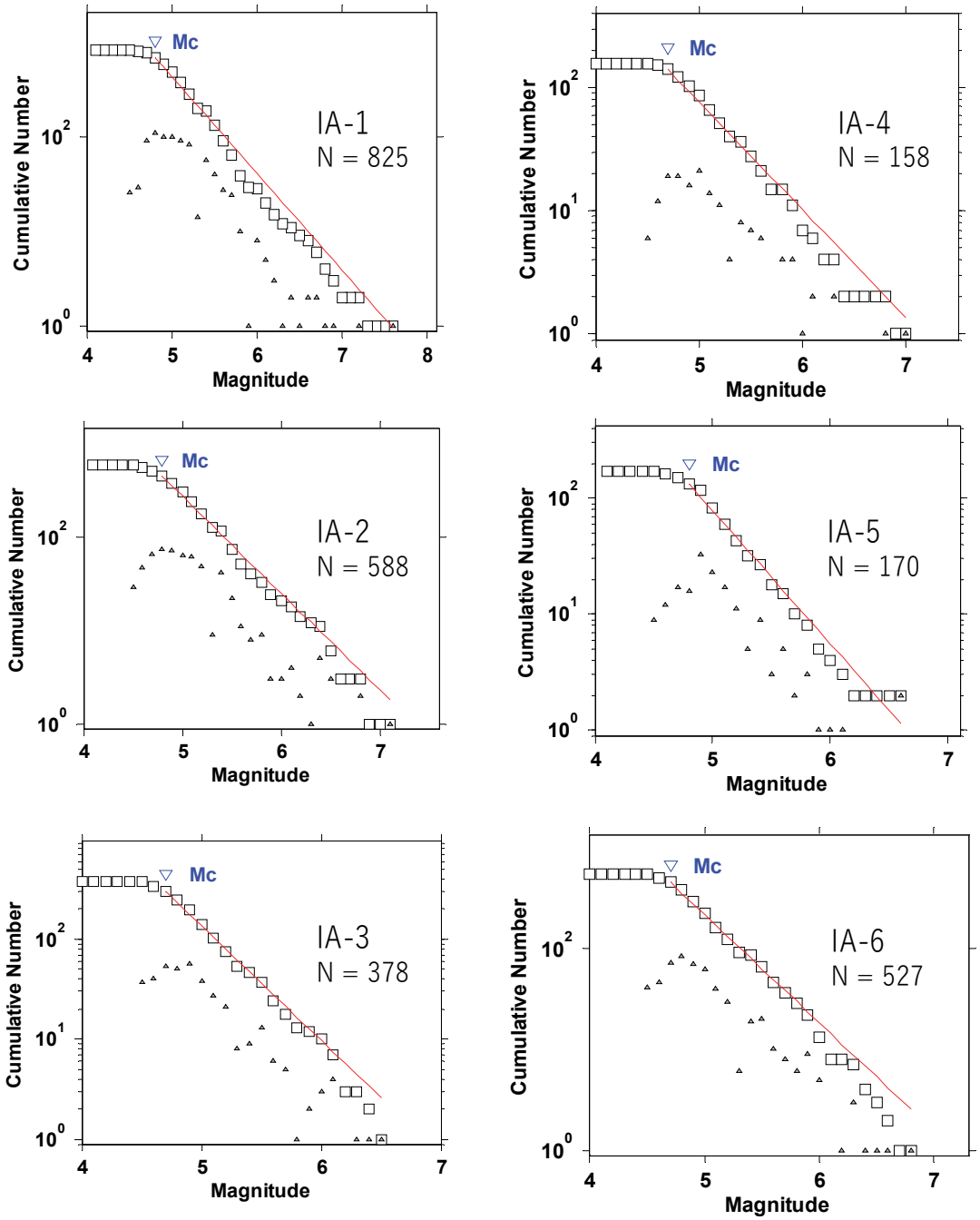

Figure 5. 11 Frequency magnitude distribution for intraplate subduction segment

The a and b parameters become an essential parameter in the seismic hazard analysis. The parameter b, of the Gutenberg-Richter frequency-magnitude relationship has been the subject of many studies since it is associated with the intensity of seismic activity investigated in the certain observed region. The Maximum Likelihood Method (MLM) as the most widely accepted method to calculate the b-value given by Aki-Utsu 1965 [27] was

used in this study, the equation is:

$$b = \frac{1}{\bar{M} - M_o} \log_{10} e \tag{5.2}$$

The a-value was estimated using the formula of Wekner, 1965 in [28] as follows:

$$a = \log N(M \geq M_o) + \log(b \ln 10) + M_o b \tag{5.3}$$

where $\bar{M}$ denotes the average magnitude and M_o is the minimum threshold for the earthquake data magnitude considered, in which we used the magnitude completeness, Mc parameter. The parameter for each subduction segment (12 subduction segments) is shown in Table 5.1.

Table 5. 1 Seismic parameter of subduction segment for Java and its surrounding

Subduction zone	Index	Segment	a	α	b	β	M_{max}
Interplate (IE)	IE-1	South Sumatra	5.08	11.70	0.91	2.10	9.03
	IE-2	West Java	5.27	12.13	0.98	2.26	8.9
	IE-3	West-Central Java	6.62	15.24	1.23	2.83	8.94
	IE-4	Central-East Java	5.32	12.25	0.99	2.28	8.91
	IE-5	East Java	5.81	13.38	1.13	2.60	8.92
	IE-6	Bali-Sumbawa	6.40	14.74	1.16	2.67	9.08
Intraplate (IA)	IA-1	South Sumatra	5.69	13.10	1.08	2.49	8.94
	IA-2	West Java	5.68	13.08	1.04	2.39	8.82
	IA-3	West-Central Java	6.06	13.95	1.13	2.60	8.84
	IA-4	Central-East Java	4.34	9.99	0.88	2.02	8.84
	IA-5	East Java	5.60	12.89	1.15	2.65	8.85
	IA-6	Bali-Sumbawa	5.64	12.99	1.07	2.46	9.01

The faults used in this study were 27 faults, both on land and at sea. The parameters data of each fault such as length, slip rate, and maximum magnitude are obtained from the Indonesian Seismic Sources and Seismic Hazard Maps 2017 (PuSGeN, 2017) and several recent studies related to new identified faults. Fault mechanisms are varied, such as strike-slip, normal, and reverse-slip with varying magnitude and direction of dip angle.

Table 5. 2 The shallow crustal fault and its parameters

No.	Fault	Source mechanism	Length (km)	Dip	Slip rate (mm/yr)	M_{max}
1	Cimandiri	Reverse-slip	23	45S	0.55	6.7
2	Nyalindung-Cibeber	Reverse-slip	30	45S	0.4	6.5
3	Rajamandala	Strike-slip	45	90	0.1	6.6
4	Lembang	Strike-slip	29.5	90	2	6.8
5	Subang	Reverse-slip	33	45S	0.1	6.5
6	Ciremai	Strike-slip	20	90	0.1	6.5
7	Cirebon-2	Reverse-slip	18	45S	0.1	6.5
8	Brebes	Reverse-slip	22	45S	0.1	6.5
9	Semarang	Reverse-slip	34	45S	0.1	6.5
10	Pati Trust	Strike-slip	69	90	0.1	6.5
11	Opak	Strike-slip	45	60E	0.75	6.6
12	Cepu	Reverse-slip	100	45S	0.1	6.5
13	Waru	Reverse-slip	64	45S	0.05	6.5
14	Enggano	Reverse-slip	160	45W	5	7.6
15	Kumering North	Strike-slip	111	90	12.5	7.5
16	Kumering South	Strike-slip	60	90	12.5	7.1
17	Semangko Barat A	Strike-slip	90	90	8	7.4
18	Semangko Barat B	Strike-slip	80	90	8	7.3
19	Semangko Timur A	Strike-slip	120	90	5	6.5
20	Semangko Timur B	Strike-slip	35	90	3	6.9
21	Semangko Graben	Normal	50	90	3	6.5
22	Ujung Kulon A	Strike-slip	80	90	10	7.3
23	Ujung Kulon B	Strike-slip	150	90	10	7.6
24	RMKS East	Strike-slip	230	90	1.5	7.8
25	Bali	Reverse-slip	84	45N	6.95	7.4
26	Lombok North	Strike-slip	156	90	0.5	7.6
27	Lombok Central	Strike-slip	133	90	0.5	7.5

**Source: Indonesian Seismic Sources and Seismic Hazard Maps 2017 (PuSGeN, 2017)* [6]

5.2.3 Site Classification

Java region has various soil condition from the west to the east which are classified according to their stability. In formulating seismic design criteria for a building at ground surface or determining the amplification of the acceleration from bedrock to ground surface in a site, the site must be classified first. A site classification is a systematic categorization of soils on the construction site into different types of soil which is usually used by the structural engineer for designing the construction. Based on Indonesia Building Code (SNI 1726:2019) [2] the site classification is defined based on soil profile for 30m depth below the surface that is represented in Table 5.3.

Table 5. 3 Site Classification based on SNI 1726:2019

Site class	Description	V_s (m/s)	N or N_{ch}	S_u (kPa)
SA	Hard rock	>1500	N/A	N/A
SB	Rock	750-1500	N/A	N/A
SC	Hard soil, very dense soil and soft rock	350-750	>50	³100
SD	Medium soil	175-350	15-50	50-100
SE	Soft soil	<175	<15	<50
SF	Soils requiring geo-engineering investigation and site response analysis			

Note:
V_s = average shear wave velocity in the upper 100ft (30m) of the soil profile
N = average field standard penetration resistance
N_{ch} = average standard penetration resistance for cohesionless soil layer
S_u = average undrained shear strength

The soil profile on the site location can be obtained from the average shear wave velocity data (Vs), average field standard penetration resistance (N-SPT), or from the average undrained shear strength (S_u). This study used the shear wave velocity (Vs30) in order to determine the soil classification in each local region. The Vs30 data were obtained from the USGS data source for each about one-kilometer distance (grid of 0.01° x 0.01°). All data (154,860 points) were then mapped by performing the Inverse Distance Weighted (IDW) interpolation method using ArcGIS Pro 2.8 as displayed in Figure 5.12.

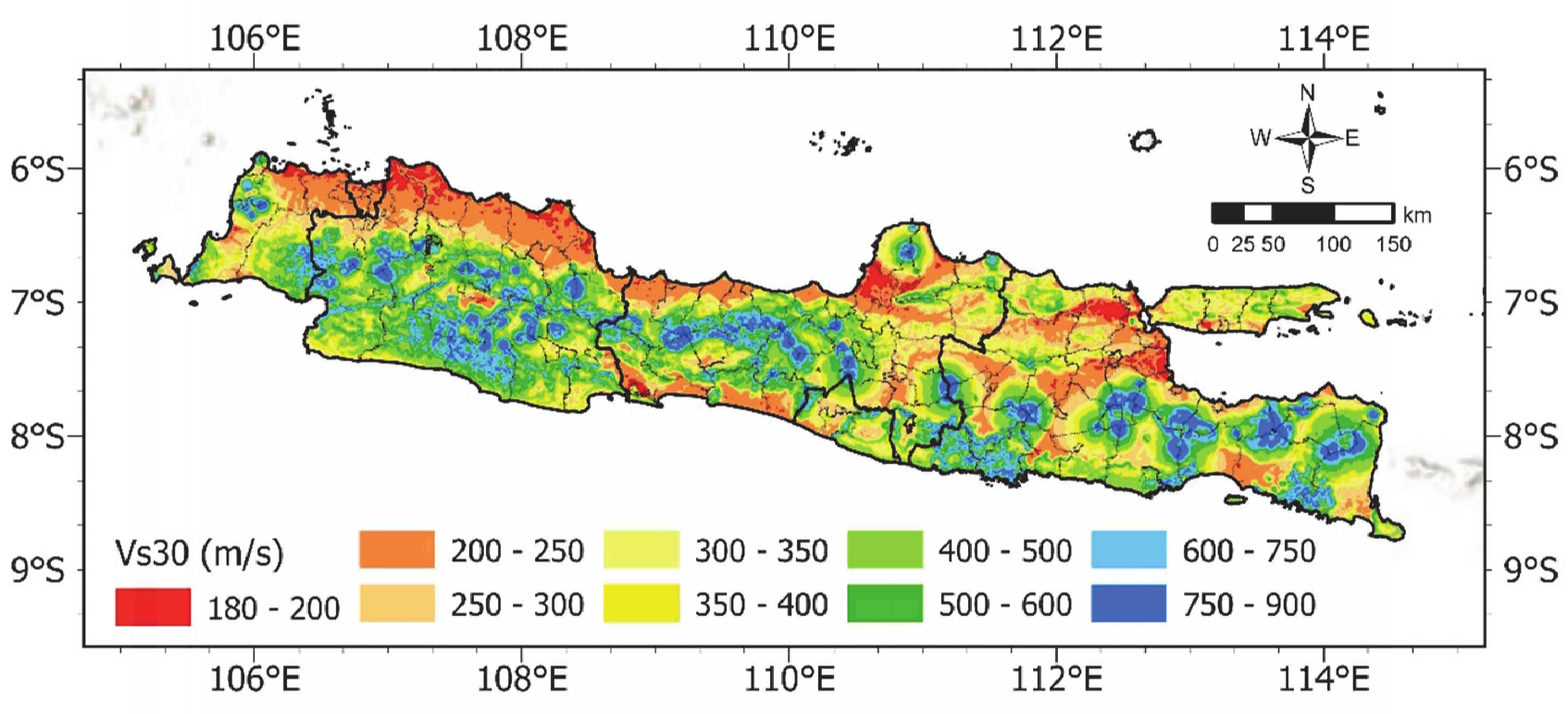

Figure 5. 12 Shear wave velocity (Vs30) map for Java region

It can be seen from the map that the Vs30 value for Java region is ranging from 180m/s to 900m/s. The lowest value of Vs30 is mostly located along the northern tip of Java and partly at the southern tip of Java near the coast. Meanwhile, the highest value of Vs30 is in the mid-Java area which is a mountainous area. The topography map of Java is presented in Figure 5.13.

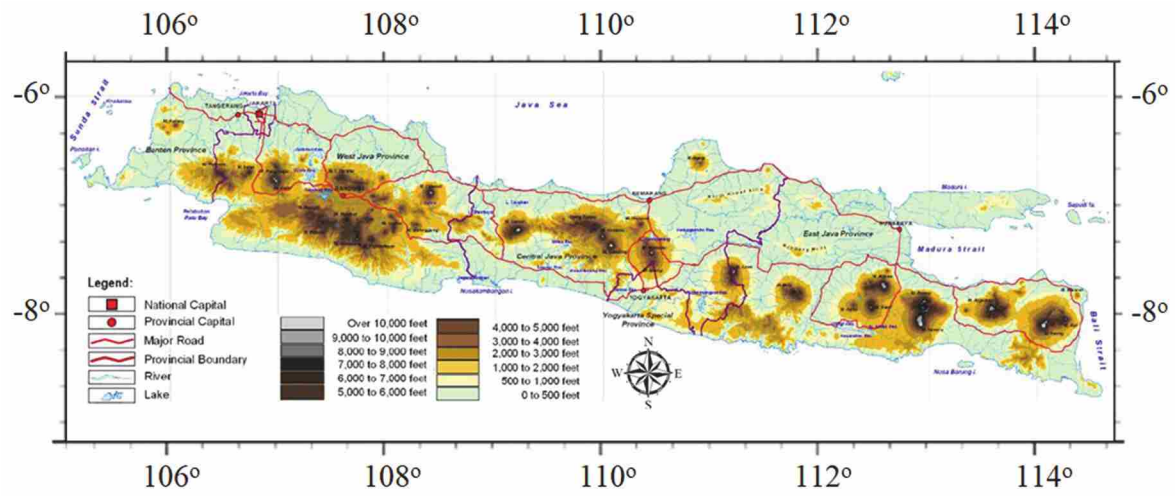

Figure 5. 13 Topography map of Java region

(Source: Bappenas, 2003 in [29]*)*

The figure shows that the higher elevation (mountain range) is in the middle of Java Island. In the East Java and West Java segments, the mountain range is divided into two ranges, while in the Central Java segment, the mountain range is only in one line. Based on those two maps, the values of Vs30 in mountainous areas tend to be higher, while those in coastal areas tend to be lower. In order to adjust the map with site class categorization according to Indonesia Building Code SNI 1726:2019, site classification for Java region is then presented in Figure 5.14.

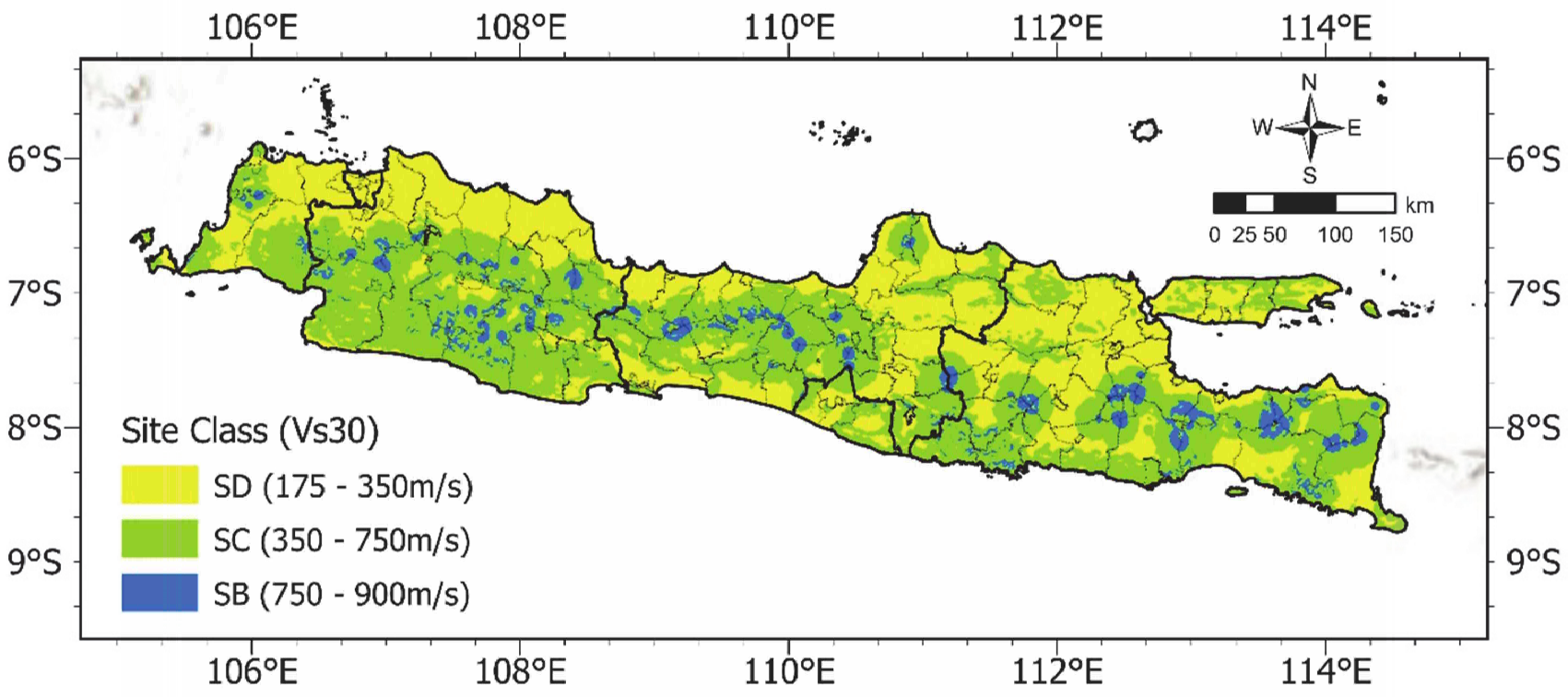

Figure 5. 14 Site classification map for Java region

Based on the category adjustment to site class in SNI 1726:2019 as presented in Table 5.3, the Java region has three types of soil, namely rock (SB), hard soil or very dense soil and soft soil (SC), and medium soil (SD). The medium soil dominates the northern part of Java and the southern part of Central Java, while the rock soil type tends to be in mountainous or highland areas.

5.2.4 GMPE and Logic Tree Analysis

The GMPE selected in this study was based on the seismotectonic conditions classified due to the earthquake source mechanisms. The GMPE models used for Java region are Youngs et al. 1997, Atkinson-Boore 2003 and Gregor 2006 [33-35] for subduction mechanisms. Meanwhile, the GMPE of Boore et al. 1997, Chiou and Youngs NGA 2006 and Boore-Atkinson NGA 2006 [36-38] were selected for the shallow crustal fault mechanisms, same as the GMPE models for Malang and Yogyakarta region. The analysis also used the Logic tree model in considering the epistemic uncertainty as shown in Figure 4.10. The magnitude relative distribution for each earthquake source was modelled using the exponential model of Gutenberg-Richter and characteristic with weights of 0.34 and 0.66, respectively.

5.3 Result and Discussion

5.3.1 Spectral Acceleration, S_S and S_1 Microzonation Map

The spectral acceleration values were calculated for the entire Java region containing 154,860 point locations. Analysis was carried out for each point within the Java region to obtain the value of Spectral acceleration (S_a) at bedrock for period of 0.2s (S_S), and 1.0s (S_1) with 2% probability of exceedance (PE) in 50 years which displayed in Table 5.4 and Table 5.5. The map for this study was conducted in each grid point using grid of 0.01^o x 0.01^o which the distance between points is about one kilometer using ArcGIS Pro 2.8.3. The results of the S_a values for 154,860 point locations were then interpolated using Inverse Distance Weighted (IDW) method and displayed on the spectral acceleration microzonation map for the periods of 0.2s (S_S) and 1.0s (S_1). The probabilistic seismic hazard analysis at bedrock (base soil layer) were calculated based on Vs = 760m/s. Meanwhile, the probabilistic seismic hazard analysis for spectral acceleration on the ground surface were computed based on the value of the near-surface shear wave velocity at the uppermost 30m soil layer (Vs30). The

result of the IDW interpolated for short period, S_S at bedrock and ground surface are displayed in Figure 5.15 and Figure 5.16, while for long period, S_1 at ground surface are presented in Figure 5.17 and Figure 5.18.

Table 5. 4 Recapitulation of spectral acceleration for short period (S_S) at bedrock and surface

ID	Longitude	Latitude	Vs30 (m/s)	Soil type	Ss Rock (g)	Ss Surface (g)
1	106.042	-5.883	424	SC	0.853	1.536
2	106.050	-5.883	359	SC	0.850	1.533
3	106.067	-5.883	367	SC	0.843	1.521
4	106.075	-5.883	600	SC	0.839	1.511
5	106.025	-5.892	390	SC	0.866	1.558
6	106.033	-5.892	477	SC	0.863	1.550
7	106.042	-5.892	565	SC	0.860	1.543
8	106.050	-5.892	558	SC	0.856	1.538
9	106.058	-5.892	476	SC	0.853	1.534
10	106.067	-5.892	448	SC	0.849	1.529
11	106.075	-5.892	400	SC	0.846	1.524
12	106.025	-5.900	525	SC	0.872	1.564
13	106.033	-5.900	579	SC	0.869	1.558
14	106.042	-5.900	604	SC	0.866	1.553
15	106.050	-5.900	690	SC	0.862	1.547
16	106.058	-5.900	542	SC	0.859	1.543
17	106.067	-5.900	492	SC	0.855	1.538
18	106.075	-5.900	522	SC	0.852	1.532
19	106.083	-5.900	432	SC	0.849	1.528
20	106.017	-5.908	528	SC	0.881	1.578
21	106.025	-5.908	661	SC	0.878	1.572
22	106.033	-5.908	698	SC	0.875	1.567
23	106.042	-5.908	678	SC	0.872	1.562
24	106.050	-5.908	570	SC	0.868	1.557
25	106.058	-5.908	607	SC	0.865	1.552
26	106.067	-5.908	635	SC	0.862	1.546
27	106.075	-5.908	598	SC	0.858	1.541
28	106.083	-5.908	572	SC	0.855	1.536
29	106.008	-5.917	460	SC	0.890	1.594
30	106.017	-5.917	662	SC	0.887	1.586
⇩	⇩	⇩	⇩	⇩	⇩	⇩
154857	114.525	-8.775	474	SC	1.701	1.907
154858	114.533	-8.775	391	SC	1.703	1.908
154859	114.542	-8.775	357	SC	1.705	1.908
154860	114.550	-8.775	368	SC	1.707	1.910

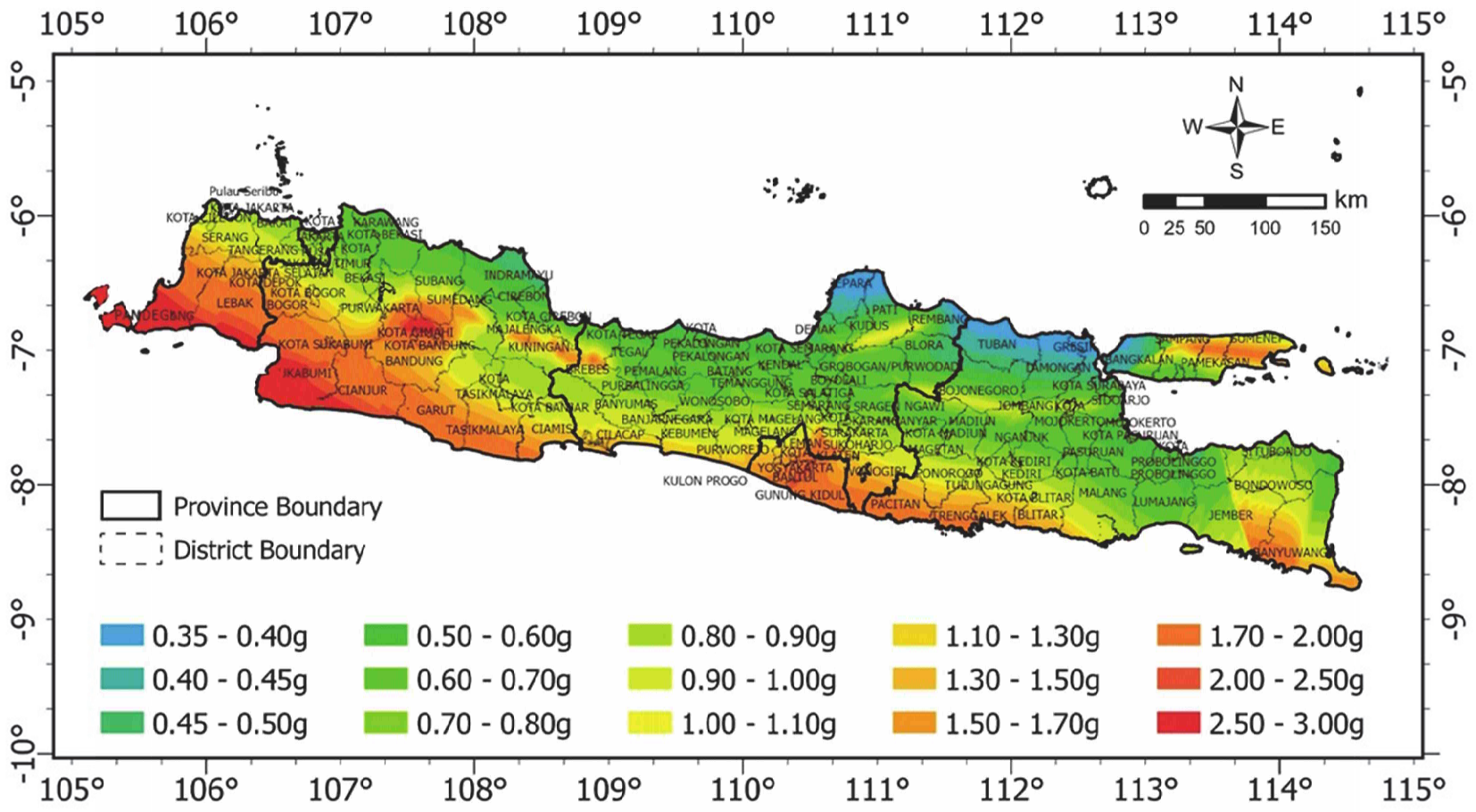

Figure 5. 15 Spectral acceleration map for short period, S_S at bedrock

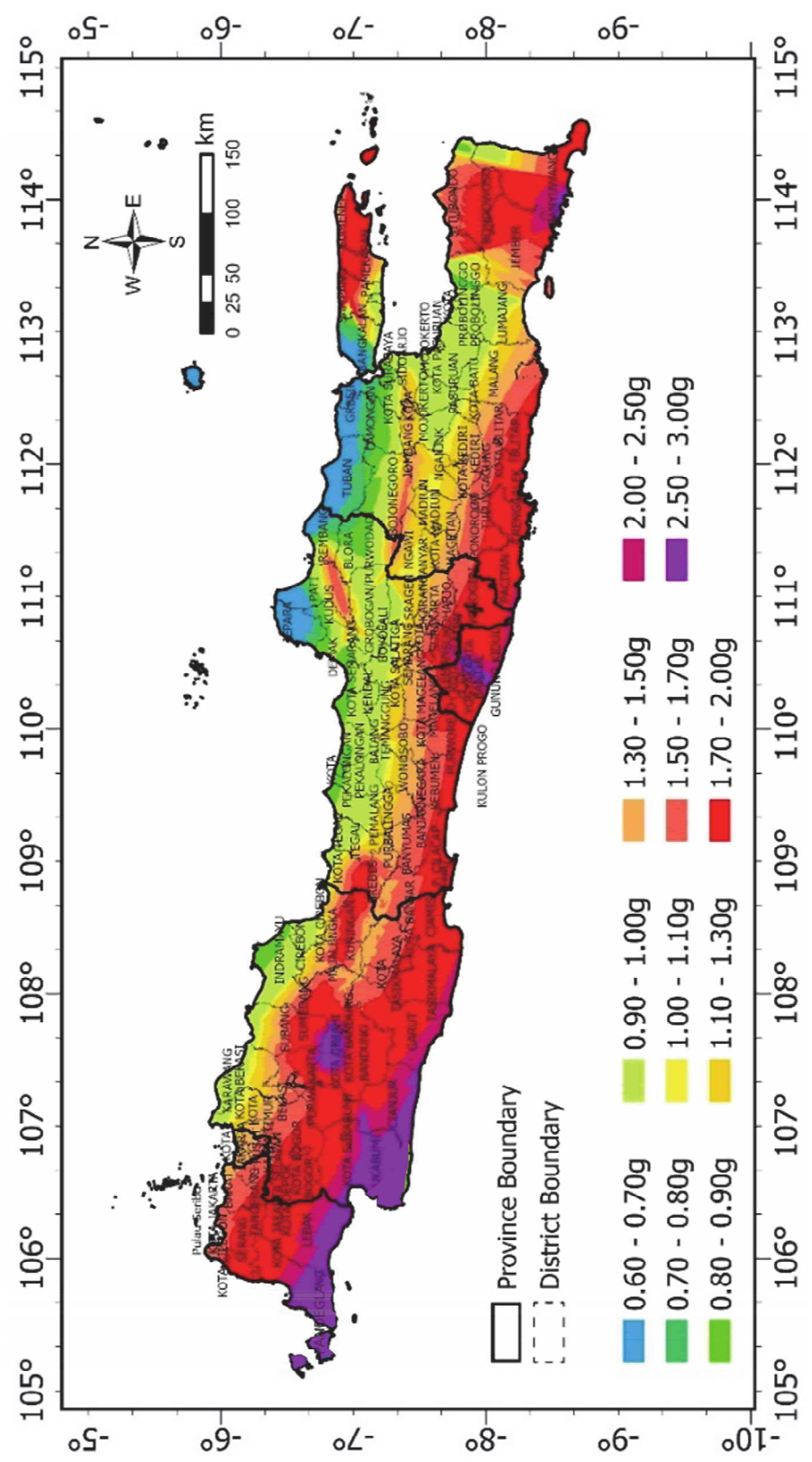

Figure 5. 16 Spectral acceleration map for short period, S_S at the ground surface

Table 5. 5 Recapitulation of spectral acceleration for long period (S_1) at

bedrock and surface

ID	Longitude	Latitude	Vs30 (m/s)	Soil type	S_1 Rock (g)	S_1 Surface (g)
1	106.042	-5.883	424	SC	0.363	0.682
2	106.050	-5.883	359	SC	0.362	0.682
3	106.067	-5.883	367	SC	0.360	0.680
4	106.075	-5.883	600	SC	0.359	0.678
5	106.025	-5.892	390	SC	0.367	0.685
6	106.033	-5.892	477	SC	0.366	0.683
7	106.042	-5.892	565	SC	0.365	0.682
8	106.050	-5.892	558	SC	0.364	0.682
9	106.058	-5.892	476	SC	0.363	0.681
10	106.067	-5.892	448	SC	0.362	0.681
11	106.075	-5.892	400	SC	0.361	0.680
12	106.025	-5.900	525	SC	0.369	0.685
13	106.033	-5.900	579	SC	0.368	0.684
14	106.042	-5.900	604	SC	0.367	0.684
15	106.050	-5.900	690	SC	0.366	0.683
16	106.058	-5.900	542	SC	0.365	0.682
17	106.067	-5.900	492	SC	0.364	0.682
18	106.075	-5.900	522	SC	0.363	0.681
19	106.083	-5.900	432	SC	0.362	0.681
20	106.017	-5.908	528	SC	0.372	0.687
21	106.025	-5.908	661	SC	0.371	0.686
22	106.033	-5.908	698	SC	0.370	0.685
23	106.042	-5.908	678	SC	0.369	0.685
24	106.050	-5.908	570	SC	0.368	0.684
25	106.058	-5.908	607	SC	0.367	0.684
26	106.067	-5.908	635	SC	0.366	0.683
27	106.075	-5.908	598	SC	0.365	0.682
28	106.083	-5.908	572	SC	0.364	0.682
29	106.008	-5.917	460	SC	0.375	0.689
30	106.017	-5.917	662	SC	0.374	0.688
⇩	⇩	⇩	⇩	⇩	⇩	⇩
154857	114.525	-8.775	474	SC	0.583	0.779
154858	114.533	-8.775	391	SC	0.584	0.780
154859	114.542	-8.775	357	SC	0.584	0.781
154860	114.550	-8.775	368	SC	0.585	0.785

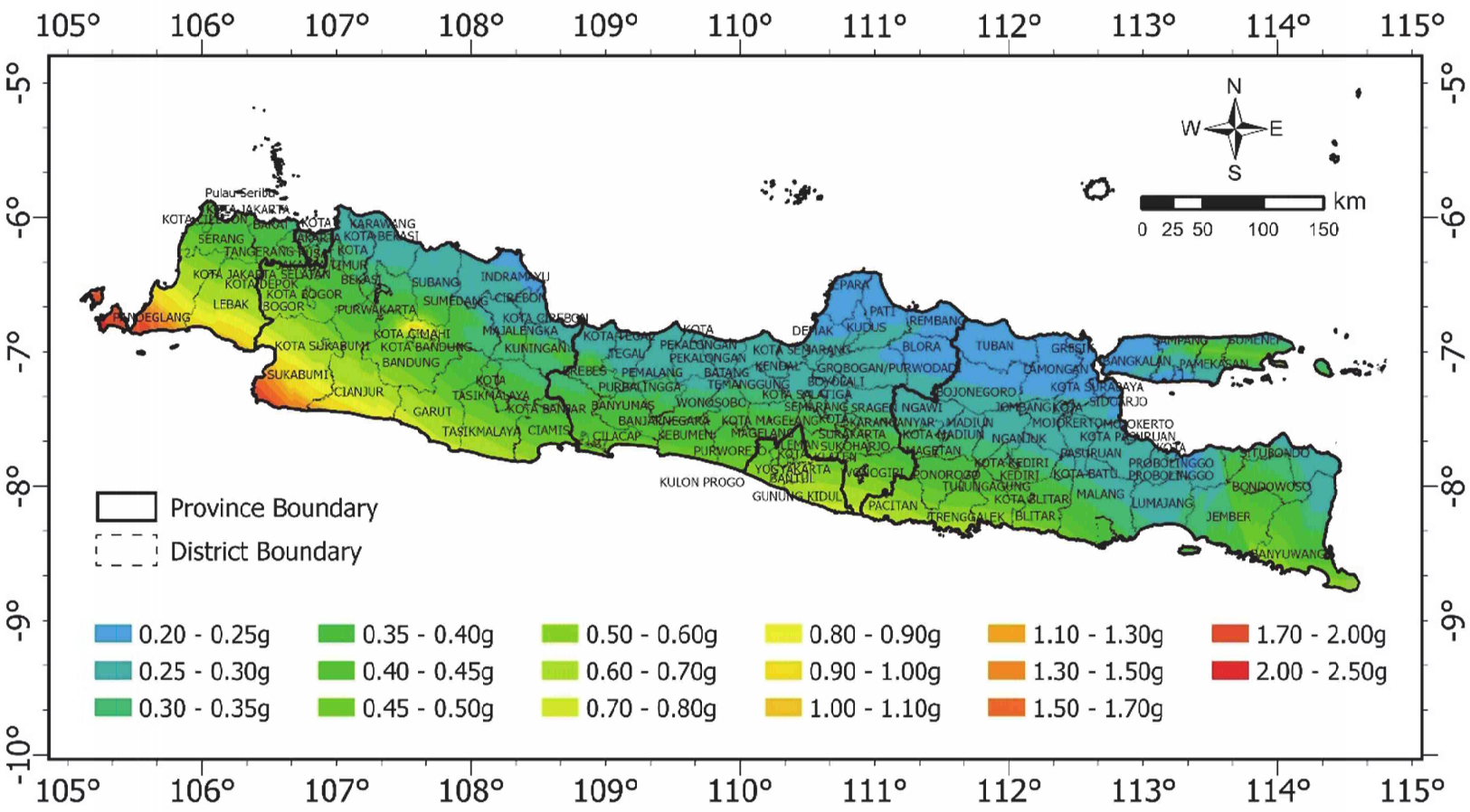

Figure 5. 17 Spectral acceleration map for long period, S_1 at bedrock

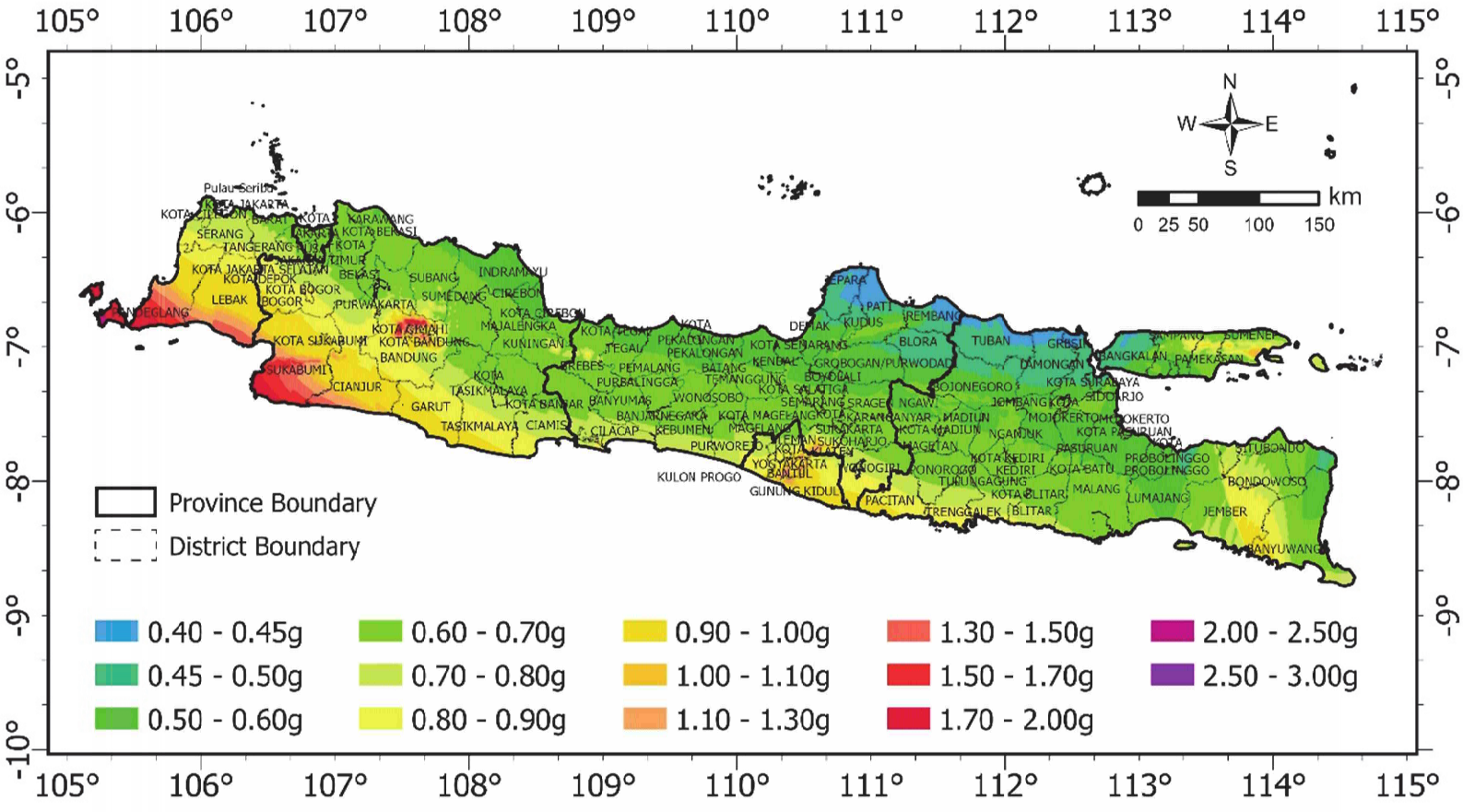

Figure 5. 18 Spectral acceleration map for long period, S_1 at the ground surface

In general, the distribution of spectral acceleration value at bedrock and ground surface follows the pattern of the seismic sources (crustal fault and subduction source). The southwest part of Java region is relatively having a high spectral acceleration value. The higher value of spectral acceleration is also seen along the southern part of Java. This result indicate that the subduction earthquake sources have a great influence for the higher value of spectral acceleration. In addition, some areas near the fault line also have higher spectral acceleration value. Interestingly, the areas with a high Vs30 value are relatively have low to medium spectral acceleration value except the area located in or near the fault line. The correlation between spectral acceleration at bedrock and ground surface in each soil type for short period and long period are shown in Figure 5.19 and Figure 5.20.

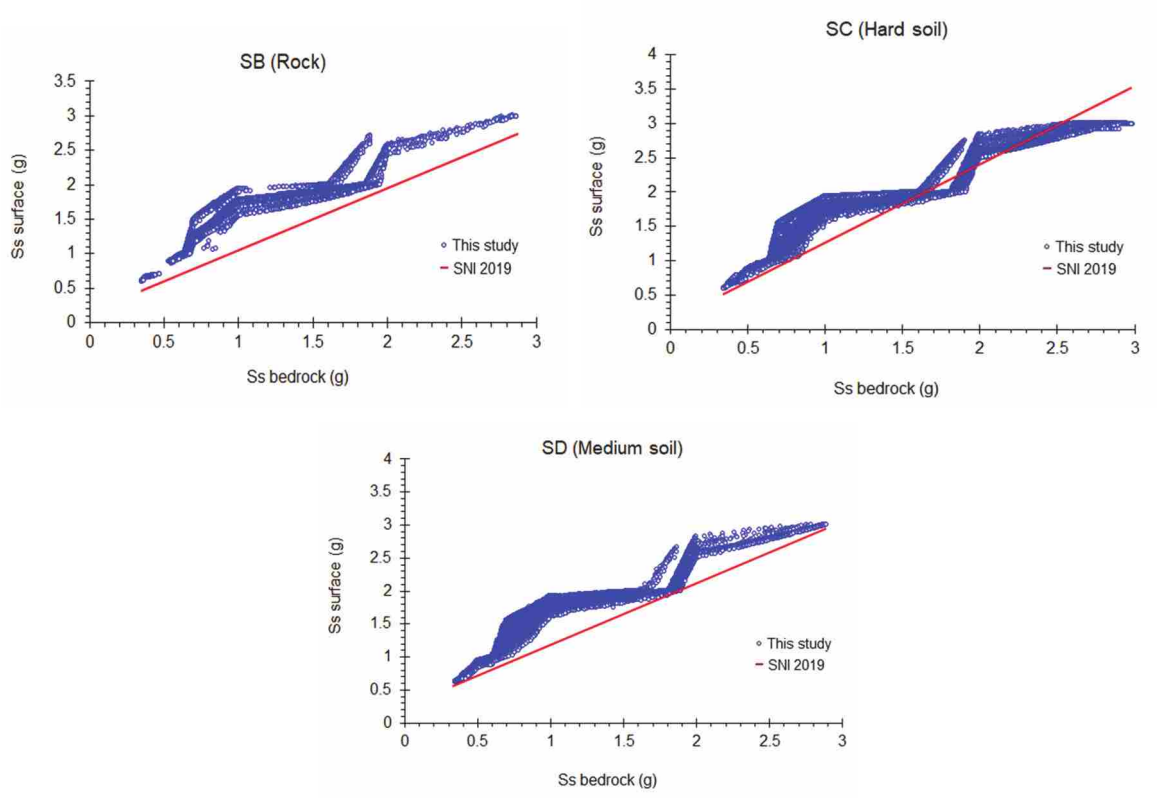

Figure 5. 19 Correlation between S_S at bedrock and S_S at ground surface

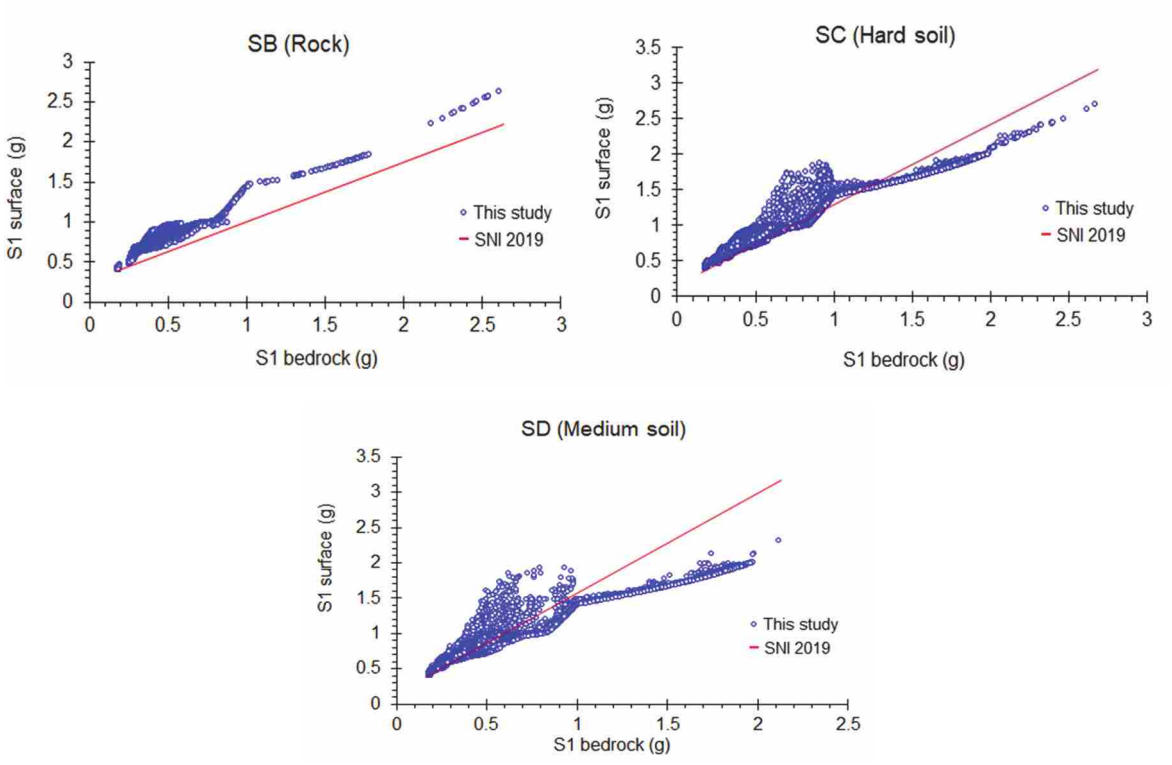

Figure 5. 20 Correlation between S_1 at bedrock and S_1 at ground surface

The relationship between spectral acceleration values of S_S and S_1 at bedrock and ground surface in this study are nonlinear, while the relationship of S_S and S_1 calculated using SNI 1726:2019 are linear. This is because in addition to considering the value of shear wave velocity, this study also considered the probability of magnitude, distance of earthquake sources, including the epistemic uncertainty of GMPE models.

5.3.2 Seismic Site Coefficient, Fa and Fv Map

The site amplification values of each location obtained from the ratio between the spectral acceleration at ground surface and the spectral acceleration value at rock outcrop were then interpolated and displayed into Fa and Fv map. Based on the calculation using equation (2.1), the Fa and Fv values were obtained. Both Fa and Fv values are divided into 11 zones marked with several colour. The areas with red to dark purple colour indicate the highest value of site coefficient. The map created using a grid of 0.01^{o}x0.01^{o} which the distance between points is about one kilometer using ArcGIS Pro 2.8. The Fa and Fv map are shown in Figure 5.21 and Figure 5.22, respectively.

Table 5. 6 Result of seismic site coefficient for short period (0.2s), Fa

ID	Longitude	Latitude	Vs30 (m/s)	Ss Rock (g)	Ss Surface (g)	Fa
1	106.042	-5.883	424	0.853	1.536	1.800
2	106.050	-5.883	359	0.850	1.533	1.803
3	106.067	-5.883	367	0.843	1.521	1.804
4	106.075	-5.883	600	0.839	1.511	1.800
5	106.025	-5.892	390	0.866	1.558	1.798
6	106.033	-5.892	477	0.863	1.550	1.796
7	106.042	-5.892	565	0.860	1.543	1.795
8	106.050	-5.892	558	0.856	1.538	1.796
9	106.058	-5.892	476	0.853	1.534	1.798
10	106.067	-5.892	448	0.849	1.529	1.800
11	106.075	-5.892	400	0.846	1.524	1.802
12	106.025	-5.900	525	0.872	1.564	1.793
13	106.033	-5.900	579	0.869	1.558	1.793
14	106.042	-5.900	604	0.866	1.553	1.794
15	106.050	-5.900	690	0.862	1.547	1.794
16	106.058	-5.900	542	0.859	1.543	1.796
17	106.067	-5.900	492	0.855	1.538	1.798
18	106.075	-5.900	522	0.852	1.532	1.798
19	106.083	-5.900	432	0.849	1.528	1.800
20	106.017	-5.908	528	0.881	1.578	1.791
21	106.025	-5.908	661	0.878	1.572	1.791
22	106.033	-5.908	698	0.875	1.567	1.791
23	106.042	-5.908	678	0.872	1.562	1.792
24	106.050	-5.908	570	0.868	1.557	1.793
25	106.058	-5.908	607	0.865	1.552	1.794
26	106.067	-5.908	635	0.862	1.546	1.795
27	106.075	-5.908	598	0.858	1.541	1.796
28	106.083	-5.908	572	0.855	1.536	1.797
29	106.008	-5.917	460	0.890	1.594	1.791
30	106.017	-5.917	662	0.887	1.586	1.789
⇩	⇩	⇩	⇩	⇩	⇩	⇩
154857	114.525	-8.775	474	1.701	1.907	1.121
154858	114.533	-8.775	391	1.703	1.908	1.120
154859	114.542	-8.775	357	1.705	1.908	1.119
154860	114.550	-8.775	368	1.707	1.910	1.119

Table 5. 7 Result of seismic site coefficient for long period (1.0s), Fv

ID	Longitude	Latitude	Vs30 (m/s)	S_1 Rock (g)	S_1 Surface (g)	Fv
1	106.042	-5.883	424	0.363	0.682	1.876
2	106.050	-5.883	359	0.362	0.682	1.882
3	106.067	-5.883	367	0.360	0.680	1.889
4	106.075	-5.883	600	0.359	0.678	1.889
5	106.025	-5.892	390	0.367	0.685	1.864
6	106.033	-5.892	477	0.366	0.683	1.865
7	106.042	-5.892	565	0.365	0.682	1.868
8	106.050	-5.892	558	0.364	0.682	1.871
9	106.058	-5.892	476	0.363	0.681	1.876
10	106.067	-5.892	448	0.362	0.681	1.880
11	106.075	-5.892	400	0.361	0.680	1.885
12	106.025	-5.900	525	0.369	0.685	1.855
13	106.033	-5.900	579	0.368	0.684	1.859
14	106.042	-5.900	604	0.367	0.684	1.861
15	106.050	-5.900	690	0.366	0.683	1.865
16	106.058	-5.900	542	0.365	0.682	1.869
17	106.067	-5.900	492	0.364	0.682	1.873
18	106.075	-5.900	522	0.363	0.681	1.877
19	106.083	-5.900	432	0.362	0.681	1.881
20	106.017	-5.908	528	0.372	0.687	1.846
21	106.025	-5.908	661	0.371	0.686	1.849
22	106.033	-5.908	698	0.370	0.685	1.852
23	106.042	-5.908	678	0.369	0.685	1.855
24	106.050	-5.908	570	0.368	0.684	1.859
25	106.058	-5.908	607	0.367	0.684	1.862
26	106.067	-5.908	635	0.366	0.683	1.866
27	106.075	-5.908	598	0.365	0.682	1.869
28	106.083	-5.908	572	0.364	0.682	1.873
29	106.008	-5.917	460	0.375	0.689	1.838
30	106.017	-5.917	662	0.374	0.688	1.840
⇩	⇩	⇩	⇩	⇩	⇩	⇩
154857	114.525	-8.775	474	0.583	0.779	1.337
154858	114.533	-8.775	391	0.584	0.780	1.337
154859	114.542	-8.775	357	0.584	0.781	1.337
154860	114.550	-8.775	368	0.585	0.785	1.342

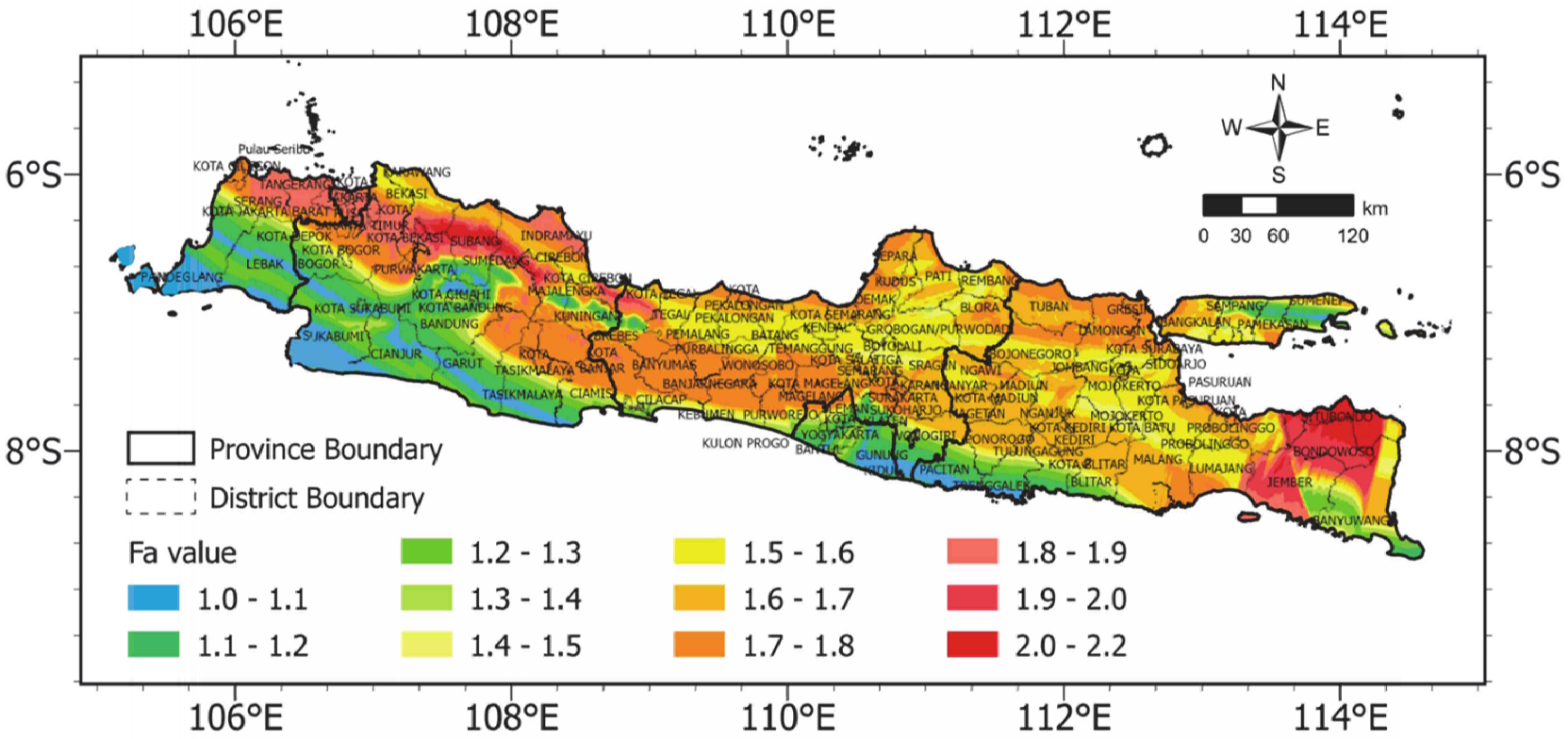

Figure 5. 21 Site coefficient map for short period (T=0.2s), Fa

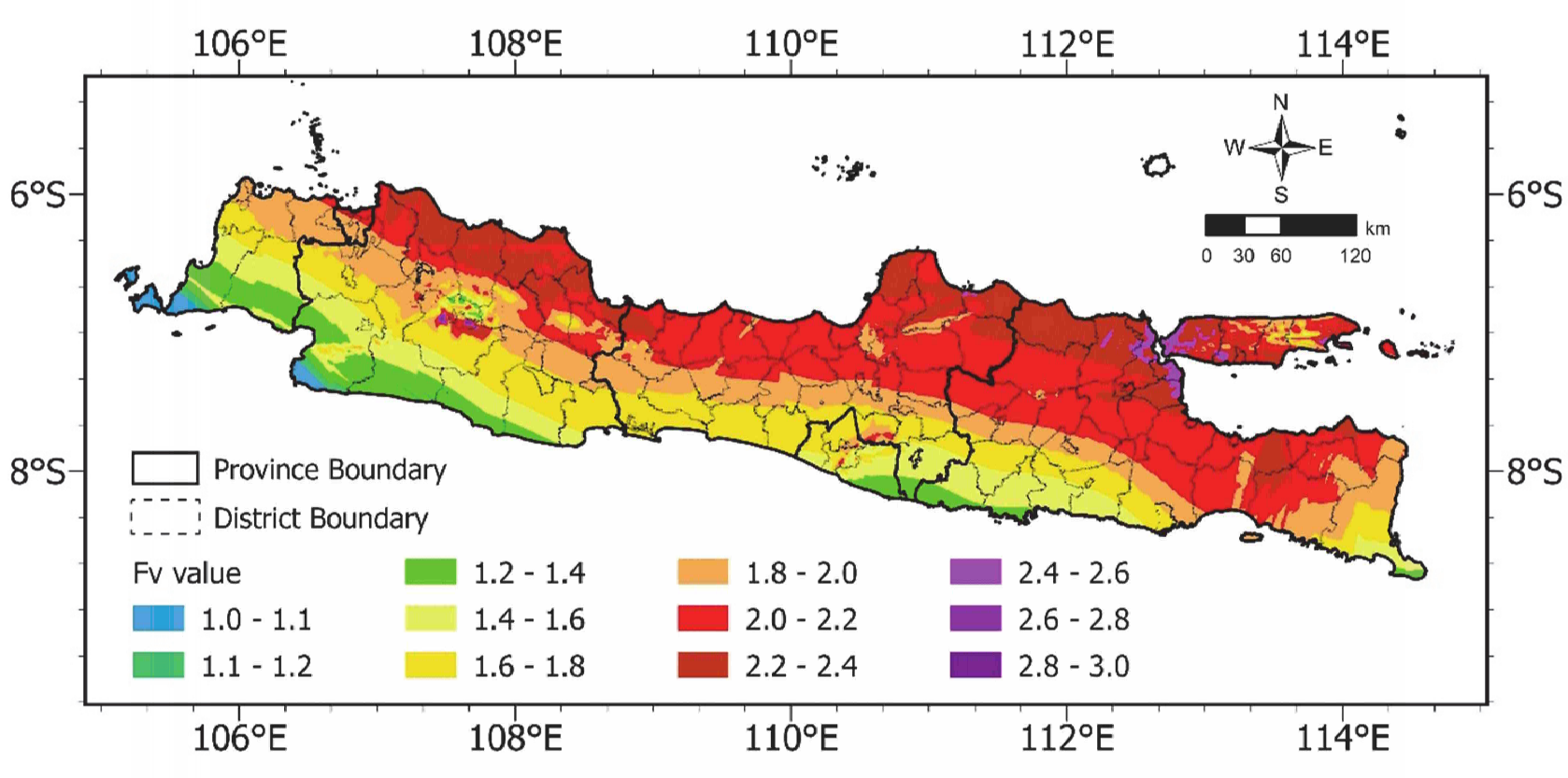

Figure 5. 22 Site coefficient map for long period (T=1.0s), Fv

The site coefficient values for short period, Fa for Java region are relatively lower than site coefficient for long period, Fv. In general, those two Fa and Fv maps show a similar pattern of amplification value trend, where the site coefficient value in southern Java is lower than in northern Java. The figures show that the Fa values are between 1.0 and 2.2, while the Fv values are ranging from 1.0 to 3.0 for three types of soil in Java region. These results are higher from the Fa and Fv value in the Indonesia Building Code SNI 1726:2019. The recapitulation for Fa and Fv values from this study versus those provided in SNI 1726:2019 for the entire Java region is presented in Table 5.8, while the detail graph for Fa and Fv values related to the shear wave velocity (Vs30) value is shown in Figure 5.23.

Table 5. 8 Fa and Fv value of this study and SNI 1726:2019

Site class			**Spectra 0.2s**		**Spectra 1.0s**	
			min	**max**	**min**	**max**
SD (Medium soil)	accel.(g) Ss, S1	this study	0.35	2.90	0.20	2.12
		SNI 2019	0.40	2.50	0.20	1.50
	site coef. Fa, Fv	this study	1.04	2.20	1.00	3.00
		SNI 2019	1.10	1.45	1.70	2.20
SC (Hard soil)	accel.(g) Ss, S1	this study	0.35	2.98	0.20	2.50
		SNI 2019	0.40	2.50	0.20	1.50
	site coef. Fa, Fv	this study	1.00	2.20	1.00	2.45
		SNI 2019	1.20	1.30	1.40	1.50
SB (Rock)	accel.(g) Ss, S1	this study	0.35	2.87	0.20	2.50
		SNI 2019	0.40	2.50	0.20	1.50
	site coef. Fa, Fv	this study	1.02	2.13	1.00	2.32
		SNI 2019	0.90	0.90	0.80	0.80

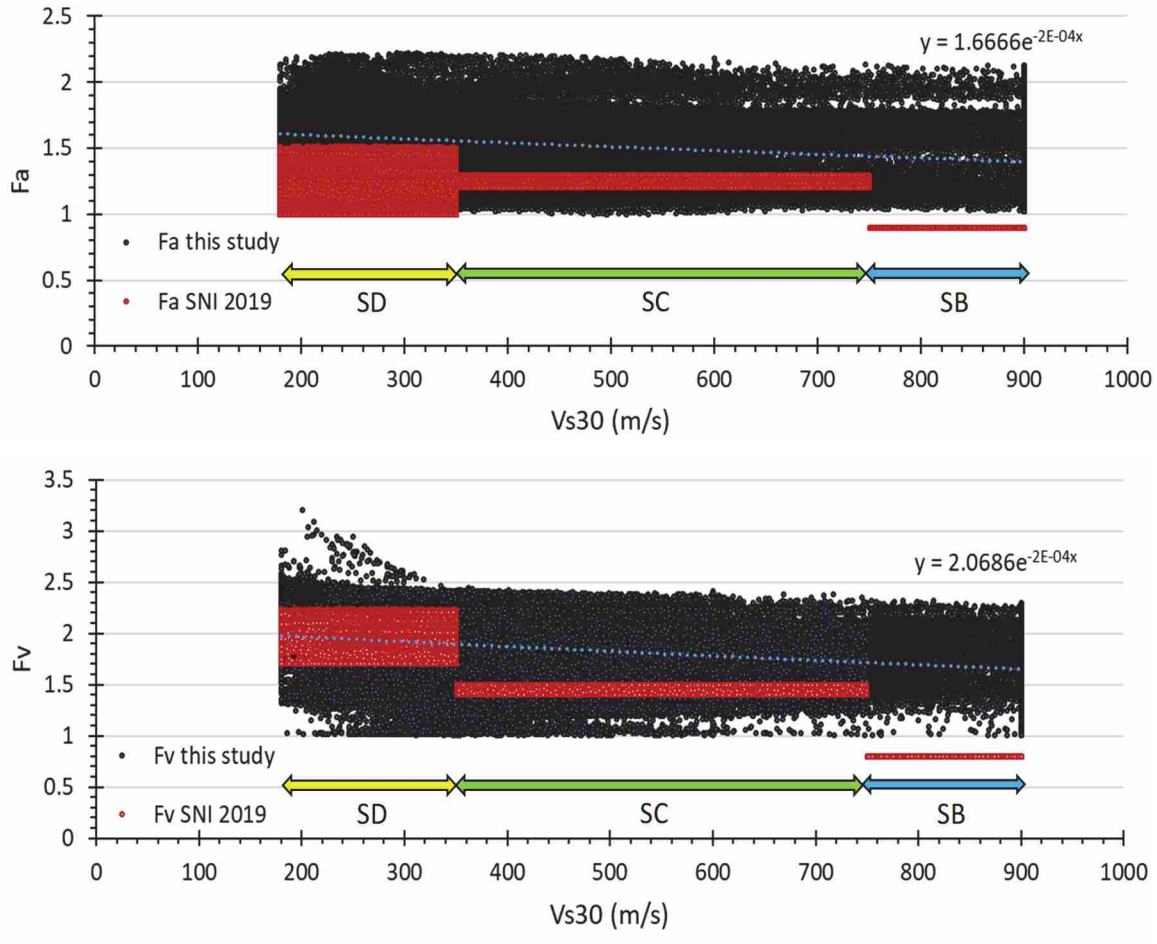

Figure 5. 23 Relationship between Vs30 and seismic site coefficient, Fa and Fv

The results of the Fa and Fv values in this study are spatially more varied than those in SNI 1726:2019 which adopts the Fa and Fv values from the PEER document. In addition, the values of Fa and Fv will increase as the spectral acceleration values of S_S and S_1 at base soil layer (bedrock) decrease. The minimum value of S_S and S_1 at bedrock are almost equal to the S_S and S_1 value in Seismic Building Code SNI 1726:2019. Meanwhile, the maximum value of S_S and S_1 in this study are relatively higher in some regions, especially in areas close to the earthquake source. Referring the site classification map (Figure 5.12 and Figure 5.14) and Ss and S_1 at bedrock map (Figure 5.15 and Figure 5.17), the Fa and Fv value will be higher in the area with lower Vs30 and lower spectral acceleration at bedrock. On the contrary, the low values of Fa and Fv are located in the area with a high value of Vs30 and high value of S_S at base soil layer. These results indicate that the softer soil conditions and the lower the spectral acceleration value, the higher the site coefficient value or vice versa.

Based on Figure 5.24, the values of Fa and Fv for SD and SC soil type based on SNI 2019 are still in the range of Fa and Fv values of this study. However, the Fa and Fv for SB soil type have a relatively large difference in values. This finding shows that the seismic site coefficient, Fa and Fv in this study is not only influenced by the value of Vs30 which represents the soil type, but also other parameters, i.e. magnitude uncertainties, distance uncertainties, and random nature of the ground motions.

5.3.3 Application of Fa and Fv in some cities

Based on the Fa and Fv from this study result, the design response spectral acceleration (DSRA) was generated for seven big cities in Java region, e.g., Serang, Jakarta, Bandung, Yogyakarta, Semarang, Surabaya, and Malang. All sites investigated accidentally have medium soil type (SD) with the value of Vs30 = 180-350 m/s. The parameter for each city is displayed in Figure 5.24 while the DSRA result is presented in Figure 5.25.

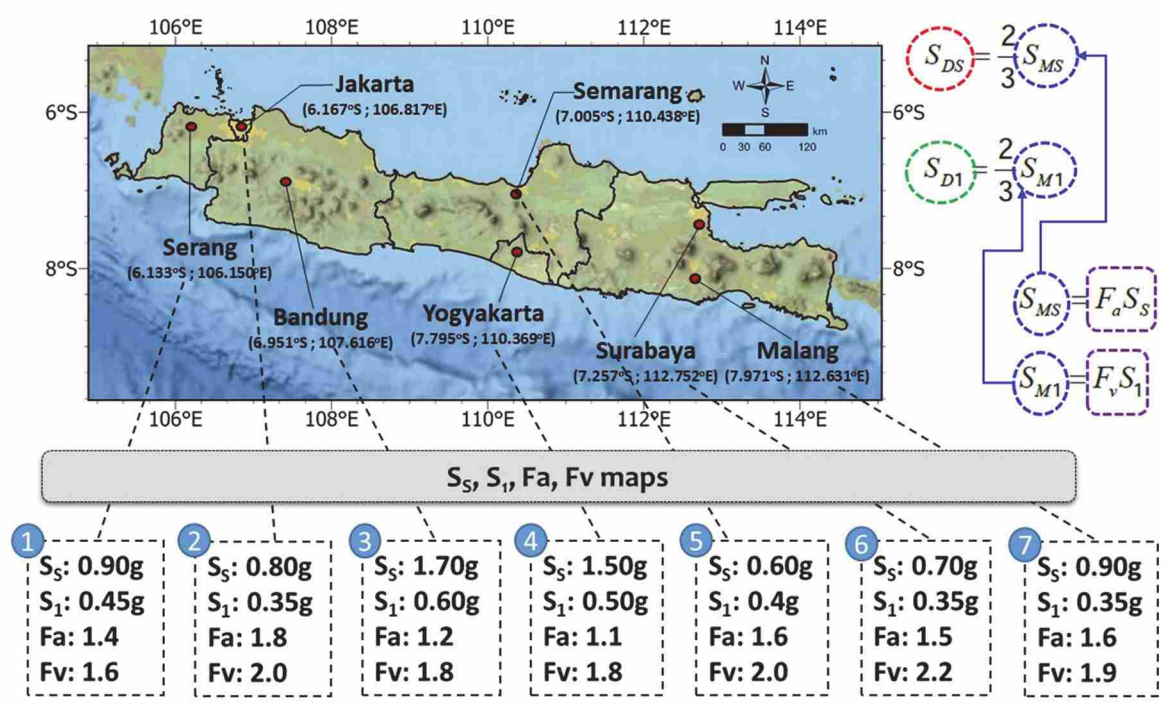

Figure 5. 24 Site location and seismic parameter for seven big cities in Java region

Table 5. 9 Spectral acceleration and site coefficient value of seven big cities in Java

No.	City	Location		Vs30	Site Class	Spectral acceleration (g)		Seismic site coefficient	
		Long	Lat	(m/s)		S_S	S_1	Fa	Fv
1	Serang	106.150	-6.133	250-300	SD	0.90	0.45	1.40	1.60
2	Jakarta	106.817	-6.167	180-200	SD	0.80	0.35	1.80	2.00
3	Bandung	107.616	-6.951	200-250	SD	1.70	0.60	1.20	1.80
4	Yogyakarta	110.369	-7.795	250-300	SD	1.50	0.50	1.10	1.80
5	Semarang	110.438	-7.005	300-350	SD	0.60	0.40	1.60	2.00
6	Surabaya	112.752	-7.257	200-250	SD	0.70	0.35	1.50	2.20
7	Malang	112.631	-7.971	250-300	SD	0.90	0.35	1.60	1.90

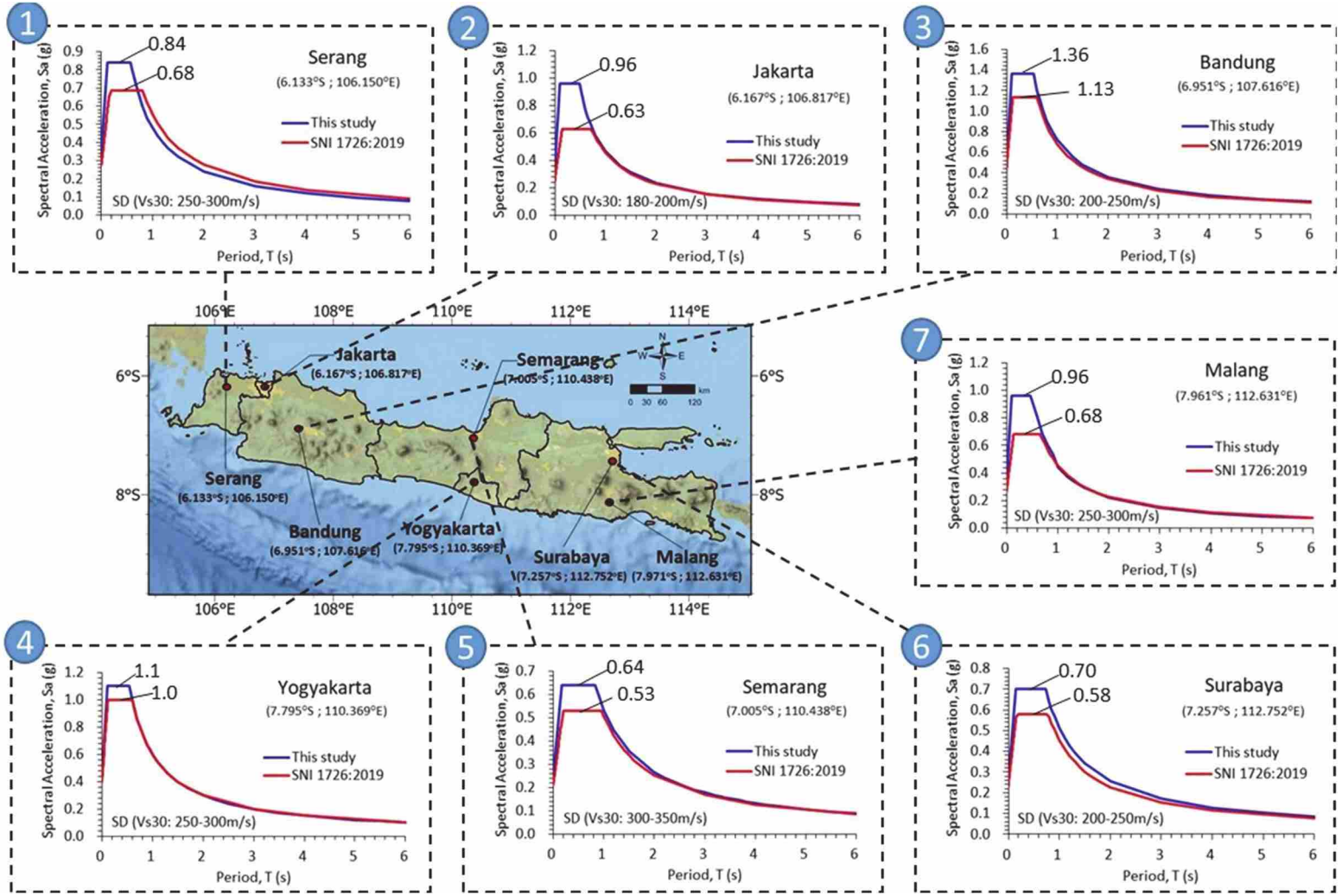

Figure 5. 25 Results of DRSA for seven big cities in Java region

5.4 Conclusion

The seismic activity in Java Island has been observed. Based on the frequency magnitude distribution following the Gutenberg-Richter method, the a and b value for the earthquake catalog within 1906 and August 2021 shows an increase compared to previous investigations using the earthquake catalog up to September 2020. The area with the smallest b value is located in the interplate area. southern part of west Java and intraplate of Central-East Java segment. This indicates the potential for a large earthquake to occur in the area. The investigation results of the subduction of the Indo-Australian plate to the Eurasian plate in the south of Java show similarities to the Mariana type while the Sumatra subduction resembles the Chilean type. However, the further studies should be conducted to observe this subduction type in more detail.

Based on the probabilistic seismic hazard analysis, spectral acceleration value at bedrock for Java region with the PE of 2% in 50 years varies from 0.35-3.00g and 0.2-2.5g for period T=0.2s and T=1.0s, respectively. The minimum value of S_S and S_1 at bedrock are almost equal to the S_S and S_1 value in Seismic Building Code SNI 1726:2019. Meanwhile, the maximum value of S_S and S_1 in this study are relatively higher in some regions, especially in areas close to the earthquake sources. It is clearly seen from the map that the distribution of spectral acceleration value at bedrock and ground surface follows the pattern of the seismic sources (crustal fault and subduction source). The southwest part of Java region is relatively having a high spectral acceleration value. The higher value of spectral acceleration is also seen along the southern part of Java. This result indicate that the subduction earthquake sources have a great influence for the higher value of spectral acceleration. In addition, some areas near the fault line also have higher spectral acceleration value.

The seismic site coefficient map, Fa and Fv have been created. The maps describe that Fa and Fv value are not only greatly influenced by the Vs30 value, which describes the local soil type, the values of Fa and Fv will increase as the spectral acceleration values of S_S and S_1 at base soil layer (bedrock) decrease. Since earthquake is random phenomena, this study considered the uncertainties of some main seismic parameters (magnitude, distance from the potential earthquake sources, and random nature of ground motion). The results of the Fa and Fv values in this study are spatially more varied than those in SNI 1726:2019 which adopts the Fa and Fv values from the PEER document. Based on the results of this study, the

values of Fa and Fv will increase along with the decrease in the value of Vs30 and the spectral acceleration value. The results of the Fa and Fv maps in this study can be used as a reference in generating the design response spectra for earthquake resistant building design in the Java region. In addition, this map can also be used as a reference in mapping areas that require high design seismic loads, as an effort of earthquake disaster mitigation.

5.5 References

[1] National Standardization Agency (BSN) 2012 SNI 1726:2012 Procedures for earthquake resistance structural buildings and non-buildings, Jakarta, Indonesia

[2] National Standardization Agency (BSN) 2019 SNI 1726:2019 Procedures for earthquake resistance structural buildings and non-buildings, Jakarta, Indonesia

[3] Marliyani, G. I., Arrowsmith J. R., and Whipple K.X., Characterization of slow slip rate faults in humid areas: Cimandiri fault zone, Indonesia. Journal of Geophysical Research: Earth Surface. 2016.

[4] Daryono M.R. Paleoseismology Tropis Indonesia: Dengan studi kasus di sesar Sumatra, sesar Palukoro-Matano, dan sesar Lembang. Disertasi Program Doktor, Institut Teknologi Bandung, 2016.

[5] Supartoyo E. T. and Djadja. Active faults and destructive earthquake epicenter distribution map of Indonesia. 2005.

[6] National Center for Earthquake Studies (PuSGeN). Indonesian Seismic Sources and Seismic Hazard Maps 2017. Center for Research and Development of Housing and Resettlement, Ministry of Public Works and Human Settlements, (Peta Sumber dan Bahaya Gempa Indonesia Tahun 2017. Pusat Litbang Perumahan dan Pemukiman, Kementerian Pekerjaan Umum dan Perumahan Rakyat), 2017, pp 1–377.

[7] Nugraha A. D., Shiddiqi H. A., Widiyantoro S., Thurber C. H., Pesicek J. D., Zhang H., Wiyono S. H., Ramdhan M., and Irsyam M., Hypocenter Relocation along the Sunda Arc in Indonesia, Using a 3D Seismic-Velocity Model, Seismological Research Letters, Vol. 89, Issue 2A, 2018, pp.603–612.

[8] International Seismological Centre, http://www.isc.ac.uk, ISC-EHB data set, International Seismological Centre, 2020, Thatcham, United Kingdom.

[9] Engdahl E. R., Di Giacomo D., Sakarya B., Gkarlaouni C. G., Harris J., and Storchak D. A., ISC- EHB1964–2016, an Improved Data Set for Studies of Earth Structure and

Global Seismicity, Earth and Space Science, Vol. 7, Issue 1, 2020, pp.1-13.

[10] Gardner J. K, and Knopoff, L., Is the Sequence of Earthquakes in Southern California, with Aftershocks Removed, Poissonian?, Bulletin of the Seismological Society of America, Vol. 64, Issue 5, 1974, pp.1363–1367.

[11] Reasenberg P., Second-order Moment of Central California Seismicity, 1969–1982, Journal of Geophysical Research: Solid Earth, Vol. 90, Issue B7, 1985, pp.5479–5495.

[12] Uhrhammer R. A., Characteristics of northern and central California seismicity, Earthquake Notes, Vol. 57, Issue 21, 1986 (abstract).

[13] Zhuang J., Ogata Y., and Vere-Jones D., Stochastic Declustering of Space-time Earthquake Occurrences, Journal of the American Statistical Association, Vol. 97, Issue 458, 2002, pp.369–380.

[14] Zaliapin I., and Ben-Zion Y., Earthquake Clusters in Southern California I: Identification and Stability, Journal of Geophysical Research: Solid Earth, Vol. 118, Issue 6, 2013, pp.2847–2864.

[15] Teng G. and Baker J. W., Seismicity Declustering and Hazard Analysis of the Oklahoma-Kansas Region, Bulletin of the Seismological Society of America, Vol. 109, Issue 6, 2019, pp.2356-2366.

[16] Ogata Y., Statistical Models for Earthquake Occurrences and Residual Analysis for Point Processes, Journal of the American Statistical Association, Vol. 83, Issue 401, 1988, pp.9–27.

[17] Ogata Y., Space-time Point-process Models for Earthquake Occurrences, Annals of the Institute of Statistical Mathematics, Vol. 50, Issue 2, 1998, pp.379–402.

[18] Susilo A., Hisyam F., and Wasis, Earthquake Analysis in East Java, Indonesia between 1960-2017 using Markov Chain Model, International Journal of Geomate, Vol. 17, Issue 63, 2019, pp.149-156.

[19] Hanifa N. R., Sagiya T., Kimata F., Efendi J., Abidin H. Z., and Meilano I., Interplate Coupling Model off The Southwestern Coast of Java, Indonesia, based on Continuous GPS data in 2008-2010. Earth and Planetary Science Letters, Vol. 401, 2014, pp.159-171.

[20] Widiyantoro S., Gunawan E., Muhari A., Rawlinson N., Mori J., Hanifa N. R., Susilo S, Supendi P, Shiddiqi H. A., Nugraha A. D., and Putra H. E., Implications for Megathrust Earthquakes and Tsunamis from Seismic Gaps South of Java Indonesia.

Scientific Reports, 10, 15274, 2020.

[21] Roy S., Ghosh U., Hazra S., and Kayal J. R., Fractal Dimension and b-value Mapping in the Andaman-Sumatra Subduction Zone, Nat Hazards, Vol. 57, 2011, pp.27–37.

[22] Crouse C.B. Ph.D., P.E. Associate, *Seismic Hazard Evaluation Offshore Northwest Java, Indonesia*, Report Maxus/ARII Offshore Area Indonesia, 1992.

[23] Stern R. J. Subduction Zones. Reviews of Geophysics, Vol.4, Issue 4, 2002, 3-1-3-38

[24] Koulali A., Susilo S., McClusky S., Crustal strain partitioning and the associated earthquake hazard in the eastern Sunda-Banda Arc, Geophysical Research Letters, vol. 43, no.5, 2016, pp.1943-1949.

[25] Koulali A., Mc.Clusky S., Susilo S., Leonard Y., Cummins P., Tregoning P., and Wijanarko A. B., The Kinematics of Crustal Deformation in Java from GPS observations: Implications for fault slip partitioning. Earth Planetary Science Letters, 458, 2016, pp.69-79.

[26] Gutenberg B. and Richter C., Frequency of earthquakes in California. Bulletin of the Seismological Society of America, Vol. 34, Issue 4, 1944, pp.185–188.

[27] Utsu T., A method for Determining the Value of b in a Formula log n = a - bM Showing the Magnitude-Frequency Relation for Earthquakes. Geophys. Bull. Hokkaido Univ., Vol. 13, 1965, pp.99–103.

[28] Rohadi S., Grandis H., and Ratag M. A., Studi Variasi Spasial Seismisitas Zona Subduksi Jawa (Study of the Spatial Variation for Java Subduction Zone Seismicity), Jurnal Meteorologi dan Geofisika, Vol. 8, Issue 1, 2007, pp.42-47.

[29] Andrea, E. P. 2015. Study on impact of urbanization and rapid urban expansion in Java and Jabodetabek Megacity, Indonesia. Ph.D. Thesis, Kyoto, Japan: Kyoto University.

[30] Cotton F, Scherbaum F, Bommer J J and Bungum H 2006 *J. Seismol.* Criteria for selecting and adjusting ground-motion models for specific target regions: Application to central Europe and rock sites 10 (2) 137–156

[31] Bommer J J, Douglas J, Scherbaum F, Cotton F, Bungum H and Fah D 2010 *Seismol. Res. Lett.* On the selection of ground-motion prediction equations for seismic hazard analysis 81 (5) 783–793

[32] Stewart J P, Douglas J, Javanbarg M, Bozorgnia Y, Abrahamson N A, Boore D M, Campbell K W, Delavaud E, Erdik M and Stafford P J 2015 *Earthq. Spectra* Selection of ground motion prediction equations for the global earthquake model 31 19-45

[33] Youngs R R, Chiou S J, Silva W J and Humphrey J R 1997 *Geophys. Res. Lett.* Strong ground motion attenuation relationships for subduction zone earthquake 68.

[34] Atkinson G M and Boore D M 2003 *Bull. Seismol. Soc. Am*. Empirical ground motion relations for Subduction-Zone Earthquakes and their application to Cascadia and other region 93 (4) 1703-1729.

[35] Gregor N J 2006 Applied by Steve Harmsen in USGS Software Fortran Code.

[36] Boore D M, Joyner W B and Fumal T E 1997 *Seismol. Res. Lett.* Equations for estimating horizontal response spectra and peak acceleration from western north American earthquakes: A Summary of Recent Work 68 .

[37] Chiou B S J and Youngs R R NGA (Next Generation Attenuation) 2006 Empirical Ground Motion Model for the Average Horizontal Component of Peak Acceleration and Pseudo-Spectral Acceleration for Spectral Periods 0.01 to 10 second1, Interim Report for USGS Review, Revised Editorially, July 10, 2006, California, USA

[38] Boore D M and Atkinson G M 2006 *Earthq. Spec.* Ground Motion Prediction Equations for the Average Horizontal Component of PGA, PGV, and 5% Damped PSA at Spectral Periods between 0.01 s and 10.0 s 24 (1).

Chapter 6
Conclusions

6.1 Conclusions

In this dissertation, the probabilistic seismic hazard analysis has been applied in computing the seismic site coefficient for short period, Fa and long period, Fv. The analysis takes into account the seismic source's potential, the random nature of earthquake occurrences (including the probability of magnitude and distance), and the ground motion model. The key findings of this dissertation are summarized in the following:

Presented in chapter 3, a homogeneity earthquake magnitude scale is paramount for performing seismic hazard analysis and other seismic engineering applications. For this purpose, all available earthquake dataset of the Indonesia region (1906 to September 2020) were collected to get the correlation of body-wave magnitude (mb) and surface-wave magnitude (Ms) into Mw. In this study, the magnitude conversion formula for mb-Mw and Ms-Mw are proposed. The accuracy tests for magnitude correlation were performed including the R^2 test and standard error (SE) test. The spatial variation in a-value and b-value have been mapped. Moreover, these a-b parameters for each subduction segment have been comprehensively presented. It is observed that there is a similar pattern of a-values and b-values. The regions with low b-values relatively fit the large earthquake locations. Based on the subduction zone modeling analysis, the low a-values and b-values are in the south coast of West Java and south coast of Central-East Java. We found that the most significant earthquakes in subduction zone were consistent with relatively high fractal dimension (D values) and low b-values. However, further research is needed to investigate these correlations more appropriately.

For the return period of 100 to 500 years, the Java interplate segments have the estimated maximum earthquake magnitude of Mw 8.47-9.00, assuming that all the tectonic energies in those areas were released seismically. Although there has been no earthquake with a magnitude greater than Mw 8.0 occurring along the Java trench, with the mechanism and seafloor age being similar to those in the east-north side of Japan, which triggered the 2011 Tohuku earthquake of Mw 9.0, these results are worth considering. Such findings can also become one of the references for future seismic hazard studies, earthquake and tsunami disaster mitigation plans in Java and its surroundings.

Presented in chapter 4, based on the acceleration microzonation maps at bedrock for Malang region, the range of S_a values is 0.3-0.7g for PGA, 0.6-1.3g for a short period (S_S), and 0.3-0.5 for a long period (S_1). The subduction earthquake sources dominantly influence spectral acceleration values of the Malang region. The further south, the depth of the earthquake source tends to be shallower so that the spectral acceleration is relatively higher. The Fa and Fv values for Malang are varied. The results indicate that the area with the lower shear wave velocity (soft to medium soil condition) has the relatively higher value of Fa and Fv. On the other hand, Yogyakarta region is located in earthquake prone area which the Eurasian Plate moved southward colliding with the Australian Plate which is moving northward. The range of S_a value is 0.9-2.4g for a short period (S_S), and 0.35-0.80 for a long period (S_1). This result is relatively higher than the S_a value for Malang region. The Opak fault line dominantly influence the spectral acceleration values of the Yogyakarta region. The Fa and Fv values for Yogyakarta region are also varied. The site coefficient at a short period or Fa is affected by the sedimentary soil at Opak river valley or strongly affected by the activity of Opak fault as a seismic source. The results indicate that the area with the lower shear wave velocity (soft to medium soil condition) has the relatively higher value of Fa and Fv. Moreover, the area with the lower value of spectral acceleration (S_S and S_1) at bedrock and lower value of shear wave velocity has the higher value of seismic site coefficient (Fa and Fv). These study findings can be references in earthquake disaster mitigation, such as earthquake-resistant building design and spatial-building planning.

Presented in chapter 5, The spectral acceleration value at bedrock for Java region with the PE of 2% in 50 years varies from 0.35-3.00g and 0.20-2.50g for period T=0.2s and T=1.0s, respectively. The minimum value of S_S and S_1 at bedrock are almost equal to the S_S and S_1 value in Seismic Building Code SNI 1726:2019. Meanwhile, the maximum value of S_S and S_1 in this study are relatively higher in some regions, especially in areas close to the earthquake source. The distribution of spectral acceleration value at bedrock and ground surface follows the pattern of the seismic sources (crustal fault and subduction source). The Fa and Fv value are not only influenced by the Vs30 value, but also the value of spectral acceleration at base soil layer. The values of Fa and Fv will increase along with the decrease in the value of Vs30 and the spectral acceleration value. In addition, the values of Fa and Fv will increase as the spectral acceleration values of S_S and S_1 at base soil layer decrease. These findings indicate that since the earthquake is a random phenomenon, some seismic

parameters uncertainties (magnitude, distance to earthquake sources, and ground motion characteristic) have to be considered in calculating the site coefficient value. The results of the Fa and Fv values in this study are spatially more varied than those in SNI 1726:2019 which adopts the Fa and Fv values from the PEER document. The Fa and Fv maps for Java proposed in this study can be contribute to the future seismic hazard studies and directly used in generating the design response spectra for earthquake resistant building design.

6.2 Recommendations for Future Research

Some recommendations for future study are presented as follows:

1) The subduction zone modeling in this study is limited based on the historical earthquake data information and referring the coupling model and slip deficit/excess rate of subduction zone from the GPS inversion data. The more detail investigation of subduction modeling is needed by using the advanced technology. Since the Sumatra and Java subduction has the different characteristic, further observation is recommended to be done considering the Mariana and Chilean subduction type.
2) The previous seismic hazard map of Indonesia was developed by applying the probability of exceedance (PE) 10% in 50 years. Meanwhile, the new seismic building code is based on 2% PE in 50 years. However, in generating the response spectra design, the acceleration value multiply by 2/3 since the building designed according to current procedures assumed to have margin of collapse of 1.5. It is said that, in general, the 10% in 50 years curve gives about 2/3 the 2% in 50 years acceleration for a particular period. As further study, it is necessary to compare the result of this study by scaling 2/3 with 10% PE in 50 years.
3) The damage probability assessment of essential buildings in Yogyakarta region has been conducted using the deterministic method. For future study, it is recommended to evaluate the response spectra of the existing buildings in each location with the response spectra generated using Fa and Fv map resulted in this study. The result of building damage assessment will be valuable for the mitigation effort.
4) The seismic site coefficient of this study used the shear wave velocity data (Vs30) from USGS document in each one-kilometer distance. It is better to develop the Fa and Fv value using several other soil characteristic data (e.g N-SPT and Su) for entire Java region and do investigation in more detail in each parameter involved.